

# **Early diagenetic processes in northwestern Black Sea sediments**



RIJKSUNIVERSITEIT GRONINGEN

# **Early diagenetic processes in northwestern Black Sea sediments**

Proefschrift

ter verkrijging van het doctoraat in de  
Wiskunde en Natuurwetenschappen  
aan de Rijksuniversiteit Groningen  
op gezag van de  
Rector Magnificus, dr. D.F.J. Bosscher,  
in het openbaar te verdedigen op  
vrijdag 12 januari 2001  
om 14.15 uur

door

Johannes Wijnandus Maria Wijsman

geboren op 17 december 1967  
te Zierikzee

Promotores: Prof. dr. P.A.W.J. de Wilde  
Prof. dr. C.H.R. Heip

Referenten: Dr. P.M.J. Herman  
Dr. J.J. Middelburg

Beoordelingscommissie: Prof. dr. C. Lancelot  
Prof. dr. ir. H.J.W. de Baar  
Prof. dr. P. van Cappellen

*'...But tell me – why is he kicking his heels around here? What is he after?'*

*'He's studying marine life.'*

*'No, no, that's not it, old man,' sighted Layevsky.*

*'From what I gathered from a passenger on the steamer, a scientist, the Black Sea's poor in fauna, and organic life can't exist in its depths owing to the excess of hydrogen sulfide. All serious students of the subject work in the biological stations of Naples or Villefrance. But Von Koren's independent and stubborn. He works on the Black Sea because no one else does.'*

Anton Chekhov, *'The Duel'*

Front cover: Subsampling from box core

Back cover: Box corer before sediment sampling

J.W.M. Wijsman  
Department of Ecosystem Studies  
Netherlands Institute of Ecology  
P.O. Box 140  
4400 AC Yerseke  
The Netherlands

Present address:  
Department of Marine and Coastal Management  
WL | Delft hydraulics  
P.O. box 177  
2600 MH Delft  
[jeroen.wijsman@wldelft.nl](mailto:jeroen.wijsman@wldelft.nl)



Koninklijke  
Nederlandse  
Akademie van  
Wetenschappen



NIOO-Thesis nr. 8 of the Netherlands Institute of Ecology, NIOO-CEMO, Yerseke, the Netherlands.

The research reported in this thesis was carried out at the Department of Ecosystem Studies of the Netherlands Institute of Ecology – Centre for Estuarine and Coastal Ecology.

Parts of the research presented in this thesis were carried out in the framework of the EROS-2000 and EROS-21 projects of the Environment and Climate Program of the European Commission (EV5V-CT94-0501 and ENV4-CT96-0286).

# Voorwoord

Na mijn studie in Wageningen ben ik in 1994 terug naar Zeeland gekomen om bij het Centrum voor Estuarine en Mariene Oecologie in Yerseke mijn promotieonderzoek uit te voeren. Als onderdeel van een Europees onderzoeksproject zou ik mij gaan bezighouden met de vroege diagenese (een woord dat ik eerst moest opzoeken in een woordenboek) in de bodem van de Zwarte Zee. Als visserijbioloog was dit een volledig nieuwe richting voor mij, maar ik zou gaan werken bij een onderzoeksgroep die tot de top behoorde op het gebied van aquatische ecosysteemmodellering. Nu 6 jaar later heb ik nog steeds geen spijt van deze keuze, en ik kijk dan ook met veel plezier naar deze periode terug.

Ik heb in de afgelopen periode heel veel geleerd van de drie-eenheid binnen onze werkgroep “Ecosysteem Studies”: Peter Herman (de filosoof), Jack Middelburg (de pragmaticus) en Karline Soetaert (de modelleur). Peter, mijn directe begeleider en initiator van dit promotieonderzoek. Jou kritische en vaak ook vernieuwende kijk op het functioneren van ecosystemen hebben aanzienlijk bijgedragen aan de kwaliteit van dit proefschrift. Jack, jou enthousiaste betrokkenheid bij dit onderzoek heeft mij ontzettend gemotiveerd. Waarschijnlijk zou zonder jou bemoeienissen dit proefschrift nooit zijn afgerond. Ik ben je hiervoor dan ook ontzettend dankbaar. Karline, jij moet echt engelengeduld met mij hebben gehad als ik het weer eens voor elkaar kreeg om een “singuliere matrix” of een “floating point error” te produceren. Van jou heb ik niet alleen de kunst van het gestructureerd en overzichtelijk programmeren geleerd, maar ook van het duidelijk en overzichtelijk presenteren van resultaten.

Mijn promotoren Peter de Wilde en Carlo Heip wil ik bedanken voor hun begeleiding van dit onderzoek. Peter, ondanks je emeritaat was je toch bereid om je tijd te steken in het lezen van de manuscripten en het structureren van de grote lijnen in dit proefschrift. Carlo, ik ben mij er terdege van bewust dat wij als promovendi bij het CEMO in een luxe positie verkeren. Door jou inzet en betrokkenheid zijn de randvoorwaarden voor het uitvoeren van wetenschappelijk onderzoek in Yerseke uitstekend. Het heeft mij in deze periode dan ook aan niets ontbroken om mijzelf als wetenschapper te ontwikkelen.

Een belangrijk aandeel in het creëren van deze randvoorwaarden komt natuurlijk ook voor rekening van mijn collega's op het CEMO. Mijn dank gaat dan ook uit naar de mensen van de ondersteunende afdelingen. Maarten Pronk, een bibliothecaris waar menig onderzoeksinstelling jaloers op zou moeten zijn, Joop Nieuwenhuize, Adri Merks, Jan Sinke, de helaas overleden Jaap van Liere, Yvonne van der Maas en Peter van Breugel van de servicelabs, voor de altijd gewillige assistentie bij de voorbereiding van de expedities en de nauwkeurigheid bij het uitvoeren van de vele analyses met de monsters die ik meenam na iedere expeditie. De administratie onder leiding van Leen Goud, voor de nodige financiële en administratieve ondersteuning. Chris Almekinders, Lowie Haazen en Ko Hoekman van de werkplaats voor de bouw van de benodigde monster apparatuur. De systeembeheerders Rini Braat en Jan Mol, de huishoudelijke dienst en natuurlijk alle andere collega's van het instituut voor hun collegialiteit en gezelligheid.

Bijzondere dank gaat ook uit naar Leon Moodley. Leon, ik heb veel geleerd van jou secure en kritische werkwijze bij de voorbereiding en uitvoering van

veldwerk. Pieter van Rijswijk, bedankt voor je gemotiveerde inzet bij de ijzer- en zwavelanalyses. De mede AIO's en OIO's, verenigd in het YAIIO (Yerseke AIO overleg) en later de "knuffels", voor de vaak nuttige, maar vooral gezellige bijeenkomsten. In het bijzonder wil ik ook Birgit Dauwe en Eric de Deckere noemen voor hun betrokkenheid en vriendschap, zowel binnen als buiten het werk. Na de verhuizing van de Vierstraat naar de Korringaweg hebben ook twee personen het aangedurfd om met mij een kamer te delen, Johan Craeymeersch en Paul van Nugteren. Johan, bedankt voor je altijd welwillende hulp en de inspirerende discussies bij het dagelijkse bakje koffie om de dag mee te beginnen. Paul, hoewel ik de laatste anderhalf jaar meer thuis achter mijn bureau dan bij jou op de kamer heb doorgebracht, heb ik jou als een zeer plezierige kamergenoot ervaren.

Special thanks go to Sabine Gerbersdorf and Filip Meijsman, who assisted me with the expeditions in August 1995 and May 1997, respectively. Nicolae Panin, Marian Gomoiu, Dan Secrieru, Silviu Radan, Stephan Reschke (I'm still sorry that I broke your rib), Peter Jöhrendt, Tim Jennerjahn, Jordi Dachs, Christina Maldonado, Gaëlle Deliat, Gabriela Friedl, Jana Friedrich, Christian Dinkel, Cecile Gieu, Frank Brodrecht and all the others that participated in the cruises on the Prof. Vodyanitsky for their friendship and collaboration. I would like to thank Christiane Lancelot and Jean-Marie Martin for the perfect organization of the EROS projects.

Naast het werk heb ik veel steun gehad aan de belangstelling en vriendschap van mijn familie (Wijnand, Anneke, Jan, Marij, Marcel, Mieke, Erik, Annette, Tonny en Debby) en vrienden. Mijn dank gaat ook uit naar de "bio's": Paul, Susan, Richard (dank voor de literatuur informatie), Maartje, Jan-Willem, Jenny, Erwin & Erwin (ik kijk uit naar de dag dat jullie ook de kennedymars uitlopen), Bartje, Henriëtte, Roland, Sylvie, Pascal, Anne, Gerard, en intussen al weer 8 "mini-biootjes". Ondanks het feit dat we over het hele land (zelfs in het buitenland) zijn uitgezworven, lukt het ons nog steeds om de vriendschap sterk te houden. Klasse!

Eric, niet zomaar een paraminf. Opvallend is de gelijkenis in onze karakters, interesses en levensloop. Allebei afkomstig uit Zeeland en voor de studie naar Wageningen getrokken om vervolgens bij het CEMO in Yerseke een promotieonderzoek te gaan doen. Hoogtepunten waren wel het EMBS in Wilhelmshaven, de nachtelijke zwempartij in de vijver van "Drakenburgh" en het feit dat wij op 4 dagen na gelijktijdig vader zijn geworden van een dochter.

Erik, broertje, paranimf en vismaat. Ik hoop dat we nog vaak kunnen ouwehoeren aan de zeedijk met een thermoskan koffie (zonder mokken), een palingdoek, een vislamp (dit keer met olie), een flesje bier, een sigaar en vishengels, wachtend tot de brug opengaat zodat we eindelijk een keer vis vangen.

Mijn ouders wil ik danken voor hun getoonde interesse en alle vormen van steun, zowel tijdens mijn studie als gedurende dit promotieonderzoek. Dit boekje is daarom ook een beetje van jullie.

Tenslotte Mano, mijn vrouw maar vooral beste vriendin. Ik weet als geen ander wat jij hebt moeten investeren in dit promotieonderzoek. Samen met Claire en Jacky heb jij altijd gezorgd voor een gezellig en plezierig leven naast het werk. Dank voor je onvoorwaardelijke steun en vriendschap door dik en dun.



# Table of contents

<b>Chapter 1</b>	Introduction and outline of the thesis	1
<b>Chapter 2</b>	Benthic mineralization in marine environments <i>Jeroen W.M. Wijsman, Jack J. Middelburg, Karline Soetaert and Peter M.J. Herman</i>	7
<b>Chapter 3</b>	Spatial distribution in sediment characteristics and benthic activity on the northwestern Black Sea shelf <i>Jeroen W.M. Wijsman, Peter M.J. Herman and Marian-Traian Gomoiu Marine Ecology Progress Series 181: 25-39 (1999)</i>	23
<b>Chapter 4</b>	A model for early diagenetic processes in sediments of the continental shelf of the Black Sea <i>Jeroen W.M. Wijsman, Peter M.J. Herman, Jack J. Middelburg and Karline Soetaert Estuarine Coastal and Shelf Science (In press)</i>	43
<b>Chapter 5</b>	Sulfur and iron speciation in surface sediments along the northwestern margin of the Black Sea <i>Jeroen W.M. Wijsman, Jack J. Middelburg, Peter M.J. Herman, Michael E. Böttcher and Carlo H.R. Heip Submitted to Marine Chemistry</i>	67
<b>Chapter 6</b>	Reactive iron in Black Sea sediments: implications for iron cycling <i>Jeroen W.M. Wijsman, Jack J. Middelburg and Carlo H.R. Heip Marine Geology (In press)</i>	85
<b>Chapter 7</b>	Summary	97
<b>Chapter 8</b>	Samenvatting	101
	References	105
	Curriculum Vitae	121
	List of publications	121



---

# CHAPTER 1

## Introduction and outline of the thesis

---

### The Black Sea, an ecosystem under human impact

The Black Sea is a large (423,000 km<sup>2</sup>) semi-enclosed basin with a maximum water depth of 2,212 m, having water exchange with the Mediterranean through the narrow and shallow Bosphorus Strait and the Sea of Marmara (Figure 1.1). The Bosphorus has a two-layer flow, carrying about 175 km<sup>3</sup> yr<sup>-1</sup> saline water (~34) from the Mediterranean to the Black Sea along the bottom and returning about 350 km<sup>3</sup> yr<sup>-1</sup> of low salinity water (~18) in the upper layer. In the Black Sea itself this low salinity water layer with a thickness of about 150 meters is overlying the high salinity, sulfide containing deep-water. Due to the sharp salinity gradient, which is maintained by the freshwater inflow in the surface layer through rain and rivers and the saline Mediterranean water flowing into the deep-sea, mixing between the two layers occurs very slowly.

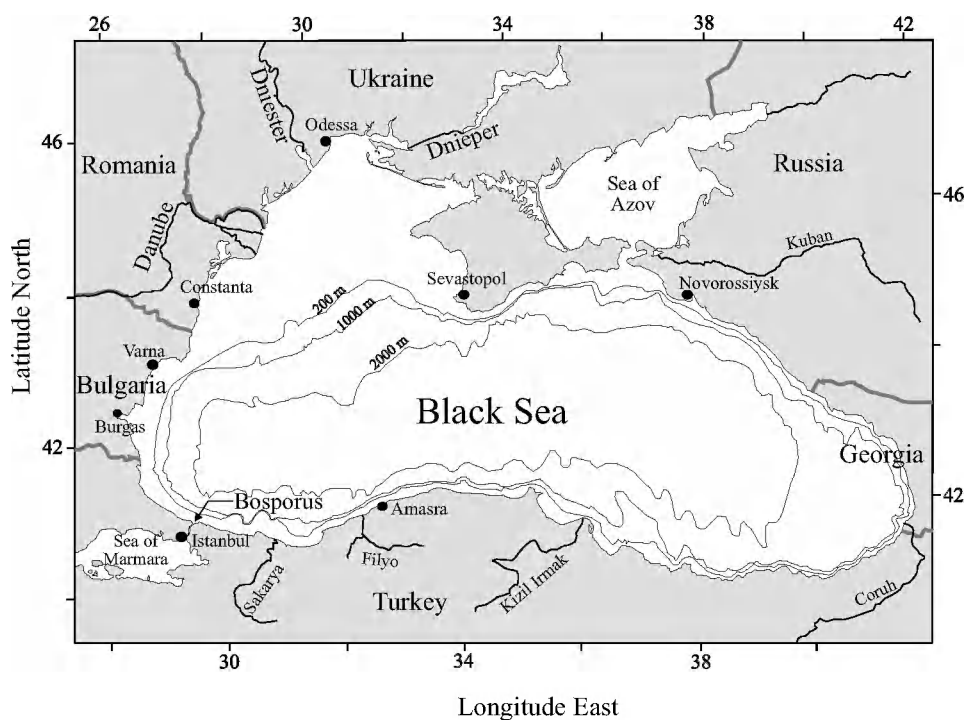


**Figure 1.1.** The Black Sea Basin

During the last glacial period (20,000 to 10,000 B.P.), the Black Sea was a low salinity lake. About 7,500 years ago (Ryan et al., 1997) saline water from the Mediterranean entered the Black Sea through the Bosphorus Strait as a result of the rise in global sea levels. The sea level of the Black Sea rose about 130 meters in only a couple of decades, and this must have caused a very rapid flooding of the plains surrounding the lake and a dramatic impact on the people inhabiting them. Ryan et al. (1997) suggested that these are the catastrophic floodings described in the epic of Gilgamesh and the Noah Flood story. The influx of saline waters has led to a density stratification of the basin and depletion of oxygen and development of sulfide in the deep-water. A gradual salinization of the Black Sea followed until some 3,000 years ago the existing salinity became established (Deuser, 1974; Glenn and Arthur, 1985). At present, nearly 87 % of the Black Sea waters are anoxic and contain high levels of hydrogen sulfide. A permanent halocline at a depth of 100 to 200 m below the surface separates the brackish, oxygenated surface waters from the saline, sulfidic deep-water (Sorokin, 1983). However, due to internal waves and long-term changes in mean circulation, the actual depth of the oxic/anoxic interface varies both spatially and temporally (Shaffer, 1986; Kempe et al., 1990; Lyons et al., 1993).

Since the early sixties dramatic and well-documented changes have been observed at various levels of the Black Sea ecosystem (Gomoiu, 1992; Mee, 1992; Zaitsev, 1993; Bologa et al., 1995; Leppäkoski and Mihnea, 1996). In less than 30 years the Black Sea ecosystem has evolved from a highly biodiverse ecosystem, rich in biological resources, to a low biodiversity ecosystem (Zaitsev and Mamaev, 1997). Many species that used to be common in the Black Sea, such as the macroalgae *Phyllophora* spp., the mussel *Mytilus galloprovincialis* (Zaitsev, 1993) and fish species such as sturgeons (Acipenseridae) and turbot (*Psetta maotica*) (Gomoiu, 1985a) were greatly reduced or have even disappeared. Other species increased rapidly in biomass, e.g. *Mya arenaria* (bivalve) (Gomoiu, 1985b), the flagellate *Noctiluca scintillans* (Porumb, 1992), the jellyfish *Aurelia aurita* (Gomoiu, 1980) and the comb jelly *Mnemiopsis leidyi*, which were inadvertently introduced in the early eighties (Mutlu et al., 1994). In the late eighties, commercial fisheries in the Black Sea collapsed (Zaitsev, 1993).

The changes in the Black Sea ecosystem have been related to a combination of man-induced perturbations that occurred almost synchronously in the Black Sea waters and the drainage basins of its major supplying rivers (Mee, 1992; Leppäkoski and Mihnea, 1996; Van Eeckhout and Lancelot, 1997). Urban and industrial expansion and intensive use of agricultural fertilizers have increased the nutrient load to the Black Sea, which stimulated the development of phytoplankton blooms in the coastal areas. Changes in nutrient composition of the Danube discharges due to the construction of dams for hydropower plants in the early seventies may have changed the composition of the phytoplankton community (Humborg et al., 1997). As an immediate response to the increased primary production, herbivorous copepods and fish populations developed well in the Black Sea. The higher fish availability led to an increase in fish catches, but also stimulated the fishing effort in the Black Sea (Zaitsev, 1993). The collapse of the commercial fisheries in 1989 due to overfishing coincided with the explosive development of the carnivorous ctenophore *Mnemiopsis leidyi*, which not only competes with fish for copepods but also feeds on fish eggs and larvae. The absence of natural predators for *Mnemiopsis* in the Black Sea accelerated this expansion. The enhanced level of primary production has led to increased benthic mineralization rates in the sediments of the northwestern continental shelf of the Black Sea. As a result of these higher mineralization rates, the frequency of

occurrence of anoxic conditions of the near-bottom waters of the northwestern shelf increased (Zaitsev, 1993). The EC supported projects EROS–2000 (EV5V–CT94–0501) and EROS–21 (ENV4–CT96–0286) were initiated to study the effect of enhanced levels of eutrophication on the ecosystem of the Black Sea. As part of these projects, this study deals with benthic processes.

## Early diagenetic processes

Early diagenesis refers to the combination of biological, chemical, and physical processes that occur during burial in the upper several hundred meters of marine sediments (Berner, 1980b). This thesis is restricted to the early diagenetic processes in the upper decimeters of the sediments, since these are generally most important in benthic-pelagic coupling and consequently changes in pelagic processes will be reflected in the early diagenetic processes in these upper sediment layers. Benthic mineralization of organic matter is the driving force for many of the early diagenetic reactions. In shallow waters such as the northwestern continental shelf of the Black Sea, a substantial part of the organic matter production in the water column is deposited on the sea floor where it is available to the benthic community. This benthic community decomposes the organic matter through a complex of reactions including hydrolysis, fermentation and oxidation into inorganic components. The nutrients resulting from benthic mineralization can diffuse back into the water column, where they can be used for primary production. Consequently benthic mineralization is a key factor for benthic-pelagic coupling in marine ecosystems (Graf, 1992).

Sedimentary organic matter is composed of many different size fractions with different degradability. Due to the depletion of the degradable organic matter with depth and the preferential degradation of the labile compounds, benthic mineralization rate usually decreases rapidly with depth in the sediment. Consequently, most of the biological activity is restricted to the upper decimeters of the sediment column. Benthic macrofauna plays an important role in early diagenesis. Filter feeding organisms, for example, can selectively filter food particles from the water column and thus increase the flux of high quality organic matter to the sediment (e.g. Heip et al., 1995). Additionally, bioturbating and bio-irrigating activity of the macrofauna can increase the transport processes within the sediment. Conversely, the carbon loading and the effects of benthic mineralization, such as the production of reduced substances and depletion of oxygen, can influence the activity and composition of the benthic community (e.g. Pearson and Rosenberg, 1978).

The products of the mineralization reactions are involved in a complex of secondary reactions including oxidation, sorption and precipitation reactions. Due to this complexity, mathematical models have become important tools to study early diagenetic processes in marine sediments. In general the variables in these models are described by the Advection–Diffusion–Reaction equation (Berner, 1980b; Boudreau, 1997).

$$\frac{\partial \xi C_i}{\partial t} = -\frac{\partial}{\partial x} \left[ -\xi D \frac{\partial C_i}{\partial x} + \omega \xi C_i \right] + \sum \xi REAC_i, \quad (1.1)$$

where  $x$  is sediment depth,  $t$  is time and  $\xi C_i$  is the concentration of species  $i$  (in mol volume<sup>-1</sup> of bulk sediment). Parameter  $\xi$  stands for the sediment porosity ( $\phi$ ) for the solute components and  $(1 - \phi)$  for the solid components.  $D$  is the total dispersion-diffusion coefficient,  $\omega$  is the advection rate and  $\sum \xi REAC_i$  is the net production (in mol volume<sup>-1</sup> of bulk sediment time<sup>-1</sup>) of species  $i$  by all biogeochemical reactions. In the mid-nineties, an evolution occurred in diagenetic modeling through the publication of non-linear, uncoupled and numerically solved models (Boudreau, 1996a; Dhakar and Burdige, 1996; Soetaert et al., 1996a; Soetaert et al. 1996b; Van Cappellen and Wang, 1996). This has not only increased our knowledge of early diagenesis, but also resulted in an extension and improvement of the parameter estimations for the various reaction kinetics (e.g. Soetaert et al., 1996a; Van Cappellen and Wang, 1996). With these early diagenetic models it is possible to generate depth profiles and to calculate fluxes across the sediment-water interface of the various components, which can be related to field observations. Additionally these models allow to study specific diagenetic processes and to predict the effect of changes in boundary conditions.

## Study area and sampling

This study is mainly focused on the northwestern part of the Black Sea, where a large continental shelf is located. This continental shelf is defined as the area with a water depth of less than 200 meter, north of Varna and west of Sevastopol, and covers a total area of 70,000 km<sup>2</sup>. Three major rivers (Danube, Dnieper and Dniester), together accounting for more than 75 % of the total river input into the Black Sea, discharge in this continental shelf area, which comprises only 0.5 % of the total volume of the Black Sea. Consequently, this area is expected to be the most vulnerable to changes in nutrient input via rivers.

The data presented in chapters 3 to 6 of this study were obtained in the northwestern part of the Black Sea during cruises in August 1995 and May 1997 with the RV “Prof. Vodyanitsky” (Figure 1.2). In total 58 stations were sampled. The majority of the stations were located on the oxygenated continental shelf, but also stations were sampled in the permanently anoxic deep-sea (1995: 2 and 27; 1997: 20, 21 and 22). Sediment was sampled with a Reineck box corer (60 × 30 × 30 cm) and sub-sampled with Plexiglass cores. Data obtained include depth profiles of various solid phase and pore water components, oxygen fluxes across the sediment water interface measured by deck incubations and abundance and biomass of the macrofauna species.

## Outline of this thesis

The general purpose of this thesis was to study the response of early diagenetic processes and the macrofauna community to changes in sedimentation and nutrient composition of the overlying water. In **chapter 2**, we investigate the factors that determine benthic degradation rates in marine sediments. A compilation of literature data on sediment community oxygen consumption (SCOC) rates is presented that includes data from various marine systems from all over the world, ranging from

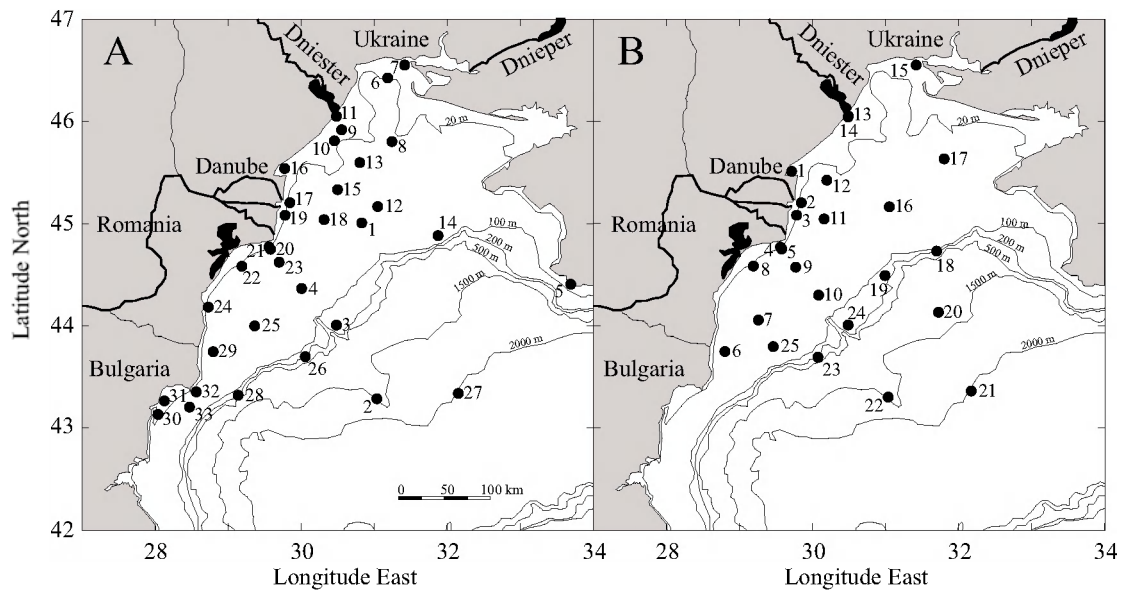


**Figure 1.2.** Location of the stations sampled in August 1995 (A) and May 1997 (B) in the northwestern part of the Black Sea

shallow estuaries and coastal systems to deep-seas. When assuming that nitrification can be neglected and that no reduced components are lost by burial or diffusion into the water column, SCOC rates provide an estimate for the total, depth-integrated rate of benthic mineralization and thus the flux of reactive organic matter to the sediment (Heip et al., 1995). Consequently, the sea floor can be regarded as the ultimate sediment trap for degradable organic matter (Jahnke et al., 1990; Herman et al., 2000). The effect of environmental parameters such as water depth, macrofauna biomass and temperature and oxygen concentration in the overlying water on the SCOC is investigated by means of multiple and non-linear regression.

As a result of the enhanced level of eutrophication in the Black Sea, the organic loading to the sediments was expected to increase. Consequently, the benthic mineralization rates should have increased. Besides this temporal change, the northwestern Black Sea is also characterized by a spatial gradient in organic loading. Organic loading to the sediments is higher in the shallow coastal areas near river mouths compared to the offshore deep-sea. In **chapter 3** we investigate the influence of sedimentation processes that are related to the largest river, the Danube, on sediment geochemistry, benthic mineralization rates and macrofauna community. Using multivariate methods, different areas are identified on the northwestern shelf. The location of these areas relative to the Danube river is associated with differences in composition and total amount of the sedimenting material.

In order to investigate the effect of differences in sedimentation and other boundary conditions on the early diagenetic processes in the sediment, we have developed a numerical model that is presented in **chapter 4**. This model is based on the model of Soetaert et al. (1996a) and describes the transport (advection, molecular diffusion, bioturbation and bio-irrigation) and reaction processes (degradation of organic matter, re-oxidation of reduced substances and precipitation) of 14 solid and solute state variables in the sediment. Because anaerobic mineralization processes are expected to be relatively important in sediments of the Black Sea due to the high carbon loading compared to ocean margins (Soetaert et al., 1996a), the model has been extended with an explicit description of the anaerobic mineralization processes

(manganese reduction, iron reduction, sulfate reduction and methanogenesis) and accompanying secondary reactions (re-oxidation reactions, formation of iron monosulfide ( $FeS$ ) and pyrite ( $FeS_2$ )).

In **chapter 5**, the cycling of iron and sulfur in the sediments of the northwestern Black Sea is analyzed by means of depth profiles of solid and solute sulfur and iron species and stable sulfur isotopes. The early diagenetic processes involving iron and sulfur are sensitive to the fluxes of organic matter and reactive iron to the sea floor and the oxygen conditions of the overlying water. In the northwestern Black Sea strong gradients exist in these environmental conditions due to the input by the river Danube (discharging large amounts of organic matter, nutrients and reactive iron into the Black Sea) and the presence of anoxic, hydrogen sulfide containing water in the deep-sea. These features make the northwestern part of the Black Sea an interesting site to study the cycles of sulfur and iron.

Solid phase iron sulfides such as  $FeS$  and pyrite are usually formed in sediments (diagenetic fraction) through the reaction of reactive iron and sulfide, where reactive iron is defined as the iron fraction that could potentially react with sulfide (Raiswell and Canfield, 1998). However, in euxinic basins like the Black Sea, where free sulfide is present in the anoxic water column, iron sulfides could also form in the pelagic water phase (syngenetic fraction) (Raiswell and Berner, 1985). These iron sulfides settle to the sea floor where they are permanently buried in the sediment. In **chapter 6**, we describe the consequences of this syngenetic pyrite formation for the cycling of reactive iron in the Black Sea. In contrast to normal oxygenated marine sediments, the abyssal part of the Black Sea is a permanent sink for reactive iron. The possibility that the continental shelf is a source of reactive iron, balancing the sink in the deep-sea, is investigated. Finally, a summary of the results is given in **chapter 7** and **chapter 8**.



---

## CHAPTER 2

# Benthic mineralization in marine environments

*Jeroen W.M. Wijsman, Jack J. Middelburg, Karline Soetaert and Peter M.J. Herman*

---

### Introduction

Benthic mineralization of organic matter is the driving force for the cycling of *C*, *N* and *P* in marine sediments. Although in shallow and intertidal systems benthic primary production may be important (Heip et al., 1995), sediments are normally heterotrophic and the benthic community depends on the energy gained from oxidation of supplied organic matter. The importance of benthic mineralization for benthic–pelagic coupling is illustrated by the depletion of dissolved oxygen and enrichment of nutrients in the overlying bottom water, which is a common feature of many estuarine and coastal systems during summer (May, 1973; Kemp et al., 1992; Soetaert et al., 2000).

It is generally accepted that the rate of benthic degradation is primarily determined by the flux of organic matter to the sediment. The fraction of the yearly primary production arriving at the sea floor depends on the residence time of the organic matter in the water column, which is, among others, related to water depth (e.g. Hargrave, 1973). At higher residence times, a larger part of the organic matter will be degraded in the water column before it reaches the sediment. Therefore the sediment community oxygen consumption (SCOC), which is a measure for the total depth-integrated benthic carbon degradation (e.g. Pamatmat, 1971), will decrease with increasing water depth. For shallow estuaries and coastal waters, Heip et al. (1995) related the ratio between the carbon flux to the sediment and the primary production in the water column ( $C_{\text{flux}}/C_{\text{prod}}$ ) to water depth (Figure 2.1), based on sediment respiration data compiled by Kemp et al. (1992) with addition of data from Dollar et al. (1991) and Soetaert and Herman (1995). Since this relationship is based on data from shallow waters (<60 m) it cannot be applied uncritically in deeper environments. Conversely, various empirical relations have been suggested to describe the carbon flux to the sediment ( $C_{\text{flux}}$ ) as a function of water depth for continental slopes and deep-sea environments (e.g. Suess, 1980; Betzer et al., 1984; Berger et al., 1987; Martin et al., 1987; Najjar et al., 1999; Christensen, 2000). Also these relationships should not be used outside their calibration area and are therefore not applicable in

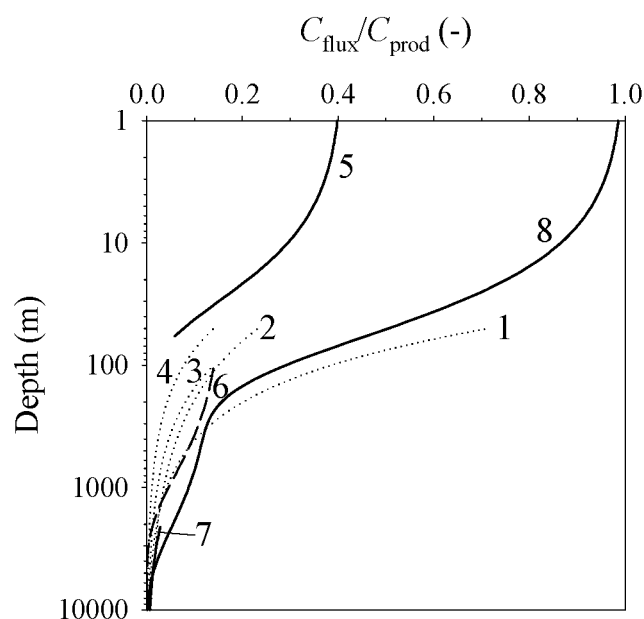


**Figure 2.1.** Empirical relations of the carbon fluxes relative to primary production as a function of water depth according to 1: Suess (1980); 2: Betzer et al. (1984); 3: Berger et al. (1987); 4: Martin et al. (1987); 5: Heip et al. (1995); 6: Najjar et al. (1999); 7: Christensen (2000); 8: This study. Solid lines indicate relations that were derived from SCOC recordings, broken lines are from water column models and dotted lines are based on sediment trap data. For relations 2, 3, 4, 6 and 7 we assumed a constant total and new production of 101 and 14 g C m<sup>-2</sup> yr<sup>-1</sup>, respectively, as derived from relation 8

shallow estuaries and coastal seas. Inclusion of data from estuaries and shallow waters will improve global estimates of carbon mineralization and oxygen consumption, since shallow systems have disproportionate importance in global processes. Based on empirical relationships, Middelburg et al. (1997) calculated that shelf sediments (0 – 200 m), occupying 7 % of the total area, are responsible for 52 % of the global organic matter mineralization in marine sediments. Slope sediments (200 – 2000 m; 9 % of the surface) take another 30% of the total, leaving only 18 % for the deep sediments with 84 % of the total surface.

In this paper we present a model for the carbon flux to the sediment that is globally applicable for marine systems ranging from shallow estuaries and coastal seas to the deep ocean. The relationship was derived by curve fitting of a conceptual model using a comprehensive database of SCOC recordings derived from literature.

## Material and methods

### *Methods to measure benthic respiration*

Henrichs (1992; 1993) gives a compilation of various methods that are used to measure the rates of total benthic mineralization and the individual pathways. Generally, the total rate of benthic mineralization is measured by the production of CO<sub>2</sub> (e.g. Anderson et al., 1986; Mackin and Swider, 1989; Middelburg et al., 1996a) or by the consumption of O<sub>2</sub> (Pamatmat, 1971; Revsbech et al., 1980b). In this study,

data on benthic mineralization rates are based on oxygen consumption rates. Oxygen is used in the sediment for aerobic mineralization of organic matter, nitrification and re-oxidation of reduced components that are produced by anaerobic mineralization processes (e.g.  $Mn^{2+}$ ,  $Fe^{2+}$ ,  $H_2S$  and  $CH_4$ ). Complete re-oxidation of reduced components formed through the oxidation of  $n$  mole of organic carbon requires  $n$  mole of oxygen, whatever anaerobic pathway is followed (Soetaert et al., 1996a). With correction for nitrification, burial of reduced substances (Bernier and Raiswell, 1983) and the flux of reduced components to the water column, SCOC is a quantitative measure for the total (aerobic and anaerobic), depth-integrated rate of carbon mineralization in the sediment (Pamatmat, 1971; Heip et al., 1995). In general it is assumed that each mole of  $O_2$  entering the sediment corresponds to 0.7 – 1.0 mole of carbon respired, depending on the composition of the carbon source (Hargrave, 1973). SCOC can be measured directly by *in situ* and shipboard flux chamber or whole-core incubations (Pamatmat, 1971; Hall et al., 1989; Booij et al., 1994; Berelson et al., 1996; Friedl et al., 1998; Wijsman et al., 1999) and indirectly through modeling micro-profiles of oxygen in the sediment (Bouldin, 1967; Revsbech et al., 1980a; Revsbech et al., 1980b; Helder, 1989; Reimers et al., 1992; Berg et al., 1998).

### ***Direct methods***

Flux chambers enclose an area of sediment with overlying bottom water for a period of hours or days, depending on the rate of benthic mineralization. The oxygen flux is then calculated from the concentration change of the bottom water in the chamber over time. In general the overlying water is continuously stirred during the measurement in order to restore the thickness of the diffusive boundary layer in the flux chamber at its *in situ* value and to prevent stratification. However, circular water flow in the incubators may induce pressure gradients at the sediment surface, which could enhance the oxygen fluxes (Booij et al., 1994). Also the use of stainless steel flux chambers can artificially increase the oxygen flux measurements due to electric potential gradients along the wall of the chamber (Cramer, 1989).

### ***Indirect methods***

Oxygen fluxes can also be calculated from depth profiles of oxygen in the sediment. Since oxygen is often consumed in the upper mm to cm range, depending on respiration rate, depth profiles are generally measured using micro-electrodes (Revsbech et al., 1980a) or micro-opt(r)odes (Glud et al., 1999). Various models have been used to calculate fluxes from micro-profiles of oxygen in the sediment (Bouldin, 1967; Revsbech et al., 1980b; Helder, 1989; Mackin and Swider, 1989; Bakker and Helder, 1993; Tahey et al., 1994; Epping and Helder, 1997; Berg et al., 1998). The flux can simply be calculated from the slope at the sediment water interface  $(dC/dx)_{x=0}$ , applying Ficks first law (e.g. Epping and Helder, 1997) or by fitting mathematical models through the data over the whole oxygenated zone. In general, these models are based on a diffusion–reaction type of model (Bouldin, 1967; Bernier, 1980b)

$$\frac{\partial C}{\partial t} = D_s^T \cdot \left( \frac{\partial^2 C}{\partial x^2} \right) - R, \quad (2.1)$$

where  $C$  is the oxygen concentration ( $\mu\text{M}$ ),  $D_s^T$  is the sediment diffusion coefficient at ambient temperature ( $\text{m}^2 \text{d}^{-1}$ ) corrected for tortuosity (Ullman and Aller, 1982; Boudreau, 1996b),  $t$  is time (d),  $x$  is depth in the sediment (m) and  $R$  is the consumption rate of oxygen in the sediment ( $\mu\text{M d}^{-1}$ ). At  $x=0$ , the oxygen concentration equals the oxygen concentration of the overlying bottom water. In general steady-state is assumed and the consumption rate  $R$  is assumed to be constant with depth in the sediment and independent of the ambient oxygen concentration (Model II sensu Bouldin, 1967), but also variable consumption rates with sediment depth are proposed (e.g. Epping and Helder, 1997; Berg et al., 1998). In some models (e.g. Berg et al., 1998) oxygen production by means of benthic primary production can even be included. Other models take into account the diffusion of oxygen through the diffusive boundary layer (Hall et al., 1989). After fitting  $R$ , oxygen fluxes are usually calculated by integration of the oxygen consumption rates ( $R$ ) over sediment depth (Revsbech et al., 1980b). Like flux chambers, micro-electrodes can be applied *in situ* using a lander (e.g. Archer and Devol, 1992) or in the laboratory.

### ***Description of the database***

In order to study the global range of benthic oxygen fluxes, we have compiled a comprehensive database of SCOC data from the literature (Table 2.1). Where possible we included additional parameters such as water depth, temperature, oxygen concentration of the bottom water and biomass of the macrofauna community. We have grouped the various methods that were used to measure oxygen fluxes in four different categories. (A) Deck incubations, where sediment cores were incubated aboard or in the laboratory. (B) *In situ* flux chambers, operated either by scuba divers or lander devices. (C) Oxygen fluxes calculated from oxygen profiles measured aboard or in the laboratory using micro-electrodes or by determining the oxygen concentration in the pore water after extraction (e.g. Murray and Kuivila, 1990). (D) *In situ* oxygen profiles, where the flux was calculated from depth profiles measured *in situ* with micro-electrodes operated by landers. We are well aware that this database is incomplete, but it covers a wide range of marine environments, including estuaries, continental shelf and slope areas, deep-sea basins and abyssal planes. Henrichs (1993) and Middelburg et al. (1997) already stated that it is very likely that there is a “hot spot bias” in literature. This is because methodological and logistic restrictions have focused attention to areas of high deposition and high mineralization rates.

## **Results**

### ***SCOC versus water depth***

Oxygen fluxes into the sediment are highly variable (Figure 2.2), ranging from  $0.02 \text{ mmol O}_2 \text{ m}^{-2} \text{ d}^{-1}$  in the deep-sea environments (Smith, 1978) to more than  $200 \text{ mmol O}_2 \text{ m}^{-2} \text{ d}^{-1}$  in shallow coastal areas like the Boston harbor (Giblin et al., 1997). This corresponds to benthic mineralization rates ranging from  $0.074$  to  $745 \text{ g C m}^{-2} \text{ yr}^{-1}$ , assuming a respiration coefficient of  $0.85$  (Hargrave, 1973). The average flux recorded in shelf sediments ( $<200 \text{ m}$ ) is  $22.6$  (S.E. =  $1.53$ )  $\text{mmol O}_2 \text{ m}^{-2} \text{ d}^{-1}$  while the average fluxes in continental slope ( $200 - 2000 \text{ m}$ ) and deep-sea ( $> 2000 \text{ m}$ )

**Table 2.1.** Ranges of recordings for various parameters reported for different marine environments. Numbers of observations are indicated between brackets. Methods for SCOC-measurement are: (A) deck incubations, (B) *in situ* flux chambers, (C) oxygen profiles measured in the lab and (D) oxygen profiles measured *in situ*

Area	Depth (m)	Temp (°C)	$O_2$ bw ( $\mu$ M)	Biomass (g AFDW $m^{-2}$ )	SCOC (mmol $O_2$ $m^{-2}$ $d^{-1}$ )	Method	References <sup>*</sup>
<b>Estuaries</b>							
Boston Harbor	7–15 (35)	1–18 (33)	-	-	7.2–221 (34)	A	1
Chesapeake Bay	5–12 (35)	3.4–27 (34)	7–410 (34)	-	0.6–26.2 (35)	A	2
Fourleague Bay	1.5 (1)	-	-	-	36.8 (1)	B	3
Norsminde Fjord	0.5–0.5 (13)	2–20 (13)	-	3.3–26.8 (9) <sup>†</sup>	27–179 (13)	A	4
<b>Continental shelf and slope areas</b>							
Adriatic Sea	18–251 (28)	8.4–21 (28)	160–282 (28)	1.9–44 (22) <sup>†</sup>	2.5–47.5 (49)	A,B,D	5,6,7
Barents Sea	170–2577 (18)	-1.9–2.8 (18)	287–348 (18)	1.7–4.6 (2) <sup>§</sup>	0.6–11.2 (32)	A,C	8,9
Bering Sea	19–54 (64)	1.5–1.5 (64)	-	3.3–148 (30) <sup>†</sup>	0.7–45.6 (61)	A	10,11
Black Sea	11–155 (46)	5.2–23 (39)	0–327 (45)	0.02–32 (19)	0–86.3 (45)	A,B	12,13,14
California Margin	585–4067 (15)	1.5–5.2 (15)	11–144 (15)	-	0.3–2.3 (22)	B,D	15
California Shelf	95–3375 (11)	-	16–113 (9)	-	0.6–11 (11)	B	16
Goban Spur	220–3661 (21)	2.5–11 (14)	-	0.1–2.5 (19) <sup>†</sup>	0.3–5.1 (16)	A,B	17
Gulf of Lyons	60–2725 (8)	-	193–249 (8)	0.01–3.4 (8)	0.8–8.8 (16)	A,C	18
Gulf of Mexico	14–106 (8)	27–30 (2)	181–238 (2)	-	5.3–155 (8)	B	19,20
Polar Sea	145–490 (24)	-1.6–1.2 (24)	-	0.03–5.5 (19) <sup>†</sup>	0.7–6.7 (23)	A,B	21
Skagerrak	35–677 (27)	5.4–12 (26)	226–285 (25)	-	2.1–17.9 (27)	C	22
Washington shelf	42–630 (18)	-	38–127 (18)	-	1.9–18.3 (25)	B,D	23,24
<b>Basins</b>							
California Basins	896–3707 (6)	-	5–131 (5)	-	0.5–1 (4)	B	16
Santa Catalina Basin	1250–1300 (7)	3.5 (6)	18–25 (7)	0.09–2.6 (3) <sup>§</sup>	0.7–3.4 (8)	B,D	25,23
Savu Basin	2570–3215 (5)	-	90–165 (5)	-	0.8–1.4 (5)	C	26
<b>Deep-sea</b>							
Central Pacific	3300–4910 (12)	-	146–182 (10)	-	0.1–0.8 (11)	B	27,28
Northeast Pacific	3570–5900 (25)	1.6–1.7 (20)	134–172 (25)	0.001–0.3 (19) <sup>§</sup>	0.1–3.4 (24)	B,C	25,29
Northwestern Atlantic	40–5380 (20)	2–3.7 (20)	229–311 (20)	0.01–11.1 (14) <sup>§</sup>	0.02–31.6 (19)	B,D	30,31
Porcupine Sea Bight	2000–4800 (6)	-	-	-	0.7–3.2 (6)	A,B	32
South Atlantic Ocean	399–4986 (13)	-	64–237 (13)	-	0.5–15.5 (39)	A,B,C,D	33
Western Indian Ocean	50–5285 (45)	1.4–27 (40)	8–254 (38)	0.2–7.9 (17) <sup>§</sup>	0–36 (52)	A,B	34

<sup>\*</sup> References: (1) (Giblin et al., 1997); (2) (Cowan and Boynton, 1996); (3) (Teague et al., 1988); (4) (Therkildsen and Lomstein, 1993); (5) (Tahey et al., 1996); (6) (Epping and Helder, 1997); (7) (Moodley et al., 1998); (8) (Hulth et al., 1994); (9) (Piepenburg et al., 1995); (10) (Grebmeier et al., 1988); (11) (Grebmeier and McRoy, 1989); (12) (Wijsman et al., 1999); (13) (Friedl et al., 1998); (14) (Chapter 5 of this thesis); (15) (Reimers et al., 1992); (16) (Berelson et al., 1996); (17) (Heip et al., 2000); (18) (Tahey et al., 1994); (19) (Warren and Kamykowski, 1984); (20) (Gardner et al., 1993); (21) (Rowe et al., 1997); (22) (Bakker and Helder, 1993); (23) (Archer and Devol, 1992); (24) (Devol and Christensen, 1993); (25) (Smith, 1987); (26) (Helder, 1989); (27) (Berelson et al., 1990); (28) (Hammond et al., 1996); (29) (Murray and Kuivila, 1990); (30) (Smith, 1978); (31) (Hales et al., 1994); (32) (Lampitt et al., 1995); (33) (Glud et al., 1994); (34) (Duineveld et al., 1997a)

<sup>†</sup> Calculated from carbon biomass, assuming that 1 g C equals 2.5 g AFDW (Lasker, 1966)

<sup>§</sup> Calculated from wet weight biomass, assuming that 1 g wet weight equals 0.132 g AFDW (Rumohr et al., 1987)

environments are 3.6 (S.E. = 0.25) and 1.5 (S.E. = 0.12) mmol  $O_2$   $m^{-2}$   $d^{-1}$ , respectively. The extremely low oxygen fluxes (<0.2 mmol  $O_2$   $m^{-2}$   $d^{-1}$ ) at depths >2000 m were measured in deep-sea sediments in the N.W. Atlantic Ocean, near Bermuda (Smith, 1978) and the N.E. Pacific (Smith, 1987). On a global scale, the SCOC is decreasing with water depth. Model I type of linear regression on the log-log-transformed data resulted in the power relation (Table 2.2):

$$SCOC = 93.10 \cdot Z^{-0.57} \cdot 1.44 = 134.1 \cdot Z^{-0.57} \quad (2.2)$$

( $n = 528$ ;  $R^2 = 0.68$ ;  $p < 0.01$ ), where SCOC is the sediment community oxygen consumption (mmol  $O_2$   $m^{-2}$   $d^{-1}$ ) and  $Z$  is water depth (m). The correction factor [ $1.44 = \exp(2.65 \cdot s^2)$ ] is required to counteract the systematic bias due to skewness (Middelburg et al., 1997). Although the overall trend seems to be well described by this power model, the residuals are not evenly distributed over the whole depth range.

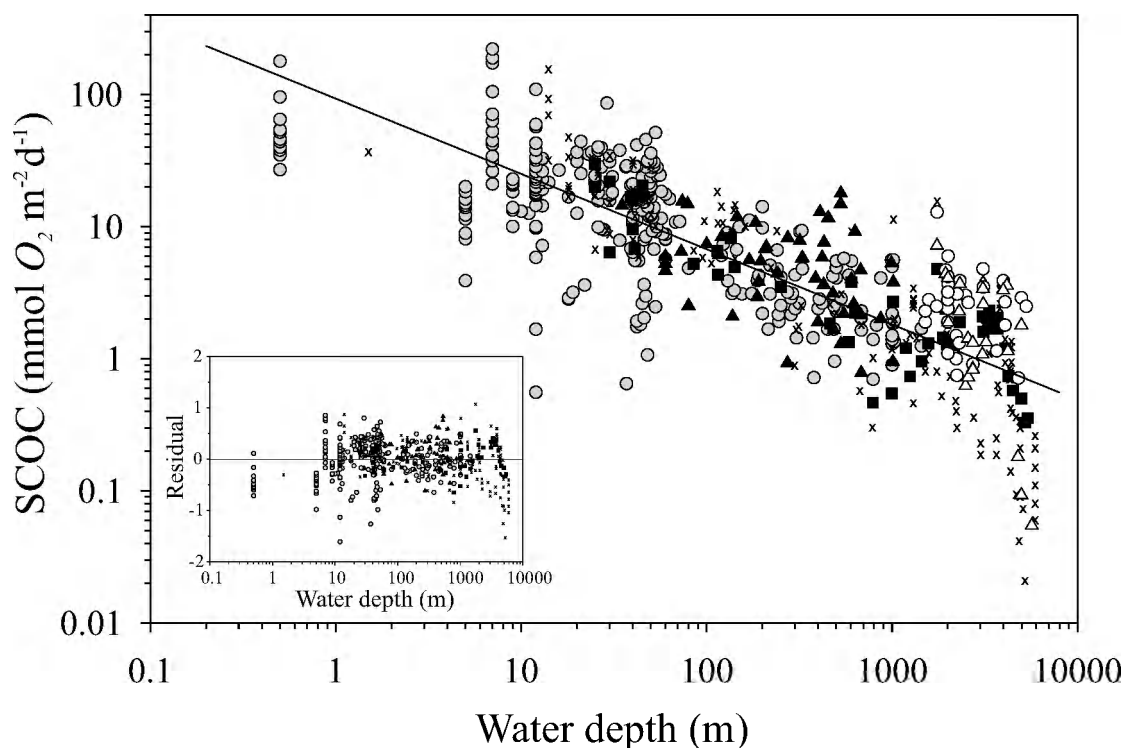


**Figure 2.2.** SCOC measured by deck incubation (dots), *in situ* flux chambers (crosses) and calculated from depth profiles measured in the laboratory (triangles) and *in situ* (squares) as a function of water depth. Deck incubations and laboratory profile measurements from water depths of more than 1500 m are indicated by open dots and triangles, respectively. Solid line indicates the linear regression model:  $\log(\text{SCOC}) = 1.97 - 0.57 \cdot \log(Z)$ . The graph in the inset represents the model residuals as a function of water depth. References are listed in table 2.1

**Table 2.2.** Summary type I linear regressions of  $\log(\text{SCOC})$  and  $\log(Z)$  for the total dataset and for each method.  $s^2$  is the of the unexplained variance,  $R^2$  the coefficient of determination and  $n$  the number of observations. Different letters indicate significant different slopes ( $p < 0.01$ )

$\log(\text{SCOC}) = a + b \log(Z)$					
Regression	$a$	$b$	$s^2$	$R^2$	$n$
Total	1.97	-0.57 <sup>a</sup>	0.138	0.68	528
Deck-incubations	1.80	-0.47 <sup>b</sup>	0.129	0.50	283
<i>In situ</i> landers	2.39	-0.74 <sup>c</sup>	0.155	0.74	148
Electrodes	1.59	-0.37 <sup>a,b,c</sup>	0.099	0.18	50
<i>In situ</i> electrodes	1.99	-0.56 <sup>a,b,c</sup>	0.068	0.76	47

Especially fluxes of less than  $0.2 \text{ mmol } O_2 \text{ m}^{-2} \text{ d}^{-1}$  in the deep-sea sediments ( $>2000 \text{ m}$ ) of the N.W. Atlantic Ocean, near Bermuda (Smith, 1978) and the Pacific Ocean (Smith, 1987; Murray and Kuivila, 1990; Hammond et al., 1996) are distinctly overestimated by the model. Moreover, extrapolation of the model to intertidal systems ( $Z = 0$ ) will result theoretically in infinitely high mineralization rates.

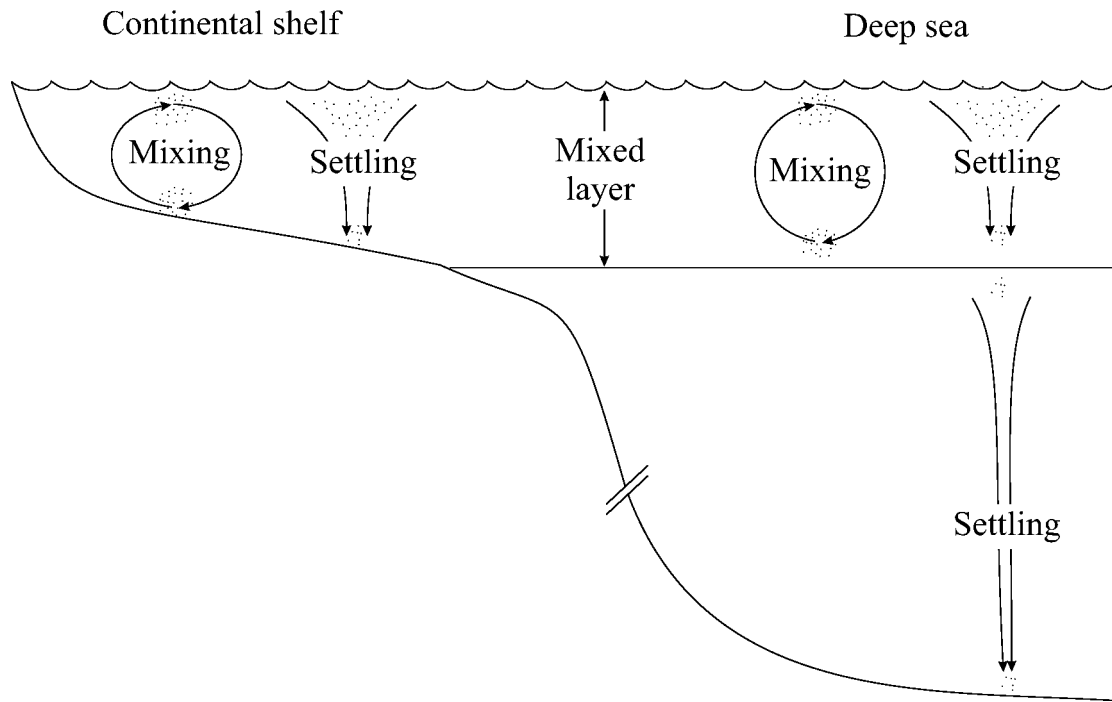


**Figure 2.3.** Schematic representation of the vertical transport regimes of organic matter to the sea floor in shallow continental shelf systems (turbulent mixing and settling) and deep-sea environments (settling)

The slope of the regression through the data measured by deck incubations is significantly different (ANCOVA,  $p < 0.01$ ) from that of the regression based on *in situ* lander experiments (Table 2.2) and both slopes are significantly different from the slope of the overall regression line (ANCOVA,  $p < 0.01$ ). Since deck incubations are usually applied in relatively shallower waters (average depth 154 m,  $\sigma = 270$  m) compared to *in situ* flux chamber measurements (average depth 1813 m,  $\sigma = 1912$  m), this also indicates that the data are non-linear over the whole depth range.

We have developed a conceptual model that better describes this non-linearity in the log-log-transformed data (Figure 2.3).

$$SCOC = \underbrace{(1-f) \cdot P \cdot e^{-a \cdot Z}}_{\text{turbulent mixing}} + \underbrace{f \cdot P \cdot e^{-b \cdot Z}}_{\text{settling}}, \quad (2.3)$$

where  $SCOC$  is the sediment community oxygen consumption ( $\text{mmol } O_2 \text{ m}^{-2} \text{ d}^{-1}$ ),  $P$  is the primary production which is potentially available for benthic respiration ( $\text{mmol } O_2 \text{ m}^{-2} \text{ d}^{-1}$ ),  $f$  is a partitioning parameter (–),  $a$  and  $b$  are attenuation coefficients ( $\text{m}^{-1}$ ) and  $Z$  is the depth of the water column (m).

This model assumes two dominant vertical transport regimes for organic matter to reach the sediment. (1) An upper regime in which particles are transported mainly by turbulent mixing processes which includes deposition–resuspension cycles. (2) A lower regime dominated by a settling flux, which may be composed of fecal pellets and marine snow, that reach the sea floor due to gravitational sinking. The turbulent regime is most important in shallow waters, where the water column is completely mixed at least during part of the year, and decreases rapidly with water depth. In the deep-sea, where the water column is never completely mixed surface to

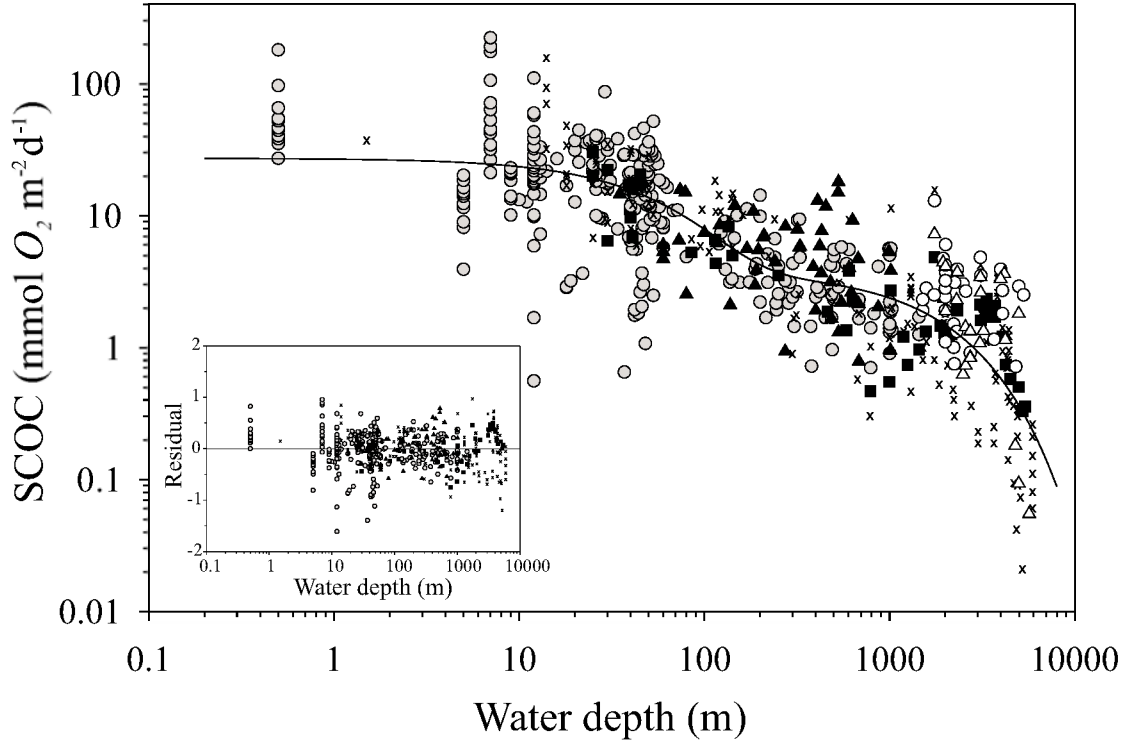


**Figure 2.4.** SCOC measured by deck incubation (dots), *in situ* flux chambers (crosses) and calculated from depth profiles measured in the laboratory (triangles) and *in situ* (squares) as a function of water depth. Deck incubations and laboratory profile measurements from water depths of more than 1500 m are indicated by open dots and triangles, respectively. Solid line indicates the regression model:  $SCOC = (1-0.14) \cdot 27 \cdot e^{-0.017 \cdot Z} + 0.14 \cdot 27 \cdot e^{-0.00047 \cdot Z}$ . The graph in the inset represents the model residuals as a function of water depth. References are listed in table 2.1

bottom, this turbulent regime is negligible, and the bulk of the organic matter reaches the deep-sea sediments by passive sinking processes. Least squares non-linear regression of equation 2.3 on the log-transformed SCOC data using a quasi-Newton iteration algorithm yielded the following parameterization (Figure 2.4):

$$SCOC = (1 - 0.14) \cdot 27 \cdot e^{-0.017 \cdot Z} + 0.14 \cdot 27 \cdot e^{-0.00047 \cdot Z} \quad (2.4)$$

( $n = 528$ ;  $R^2 = 0.71$ ;  $s^2 = 0.12$ ). The four parameters in this model were highly robust, and their optimal values independent of the initial values (as tested by extensive trials with varying initial conditions). We compared this non-linear model to the more simple power model (Equation 2.2) by means of a one-tailed  $F$ -test (Sokal and Rohlf, 1995; Soetaert et al., 1996c). The  $F_{(2,523)}$ -value for this test (31.5) is higher than the critical value ( $\alpha=0.01$ ), which implies that this more complex non-linear model provided a significantly better explanation for the observed data than the power model, even taking into account that it contains two additional parameters.



## Discussion

### *Methodological consequences*

#### ***In situ* versus shipboard**

Various authors have compared benthic oxygen fluxes measured by *in situ* flux chambers with shipboard measurements (Glud et al., 1994; Tahey et al., 1996; Duineveld et al., 1997a; Duineveld et al., 1997b). In principle, *in situ* methods have the advantage of provoking fewer disturbances due to sub-sampling and of keeping the benthic community at their environmental conditions of temperature and pressure. Shipboard incubations are generally easier to deploy and less expensive. However additional sub-sampling, temperature shock, pressure difference and the possibility of contamination of the bottom water with air-borne oxygen may introduce errors. Tahey et al. (1996) related SCOC measurements from *in situ* landers to shipboard incubations up to 45 meters depth and concluded that there was a reasonably good agreement between both methods. Miller-Way et al. (1994) concluded that there was no clear difference in SCOC rates between measurements from shipboard and *in situ* incubations at a fine-grained site at 20 m depth. In figure 2.5 we present a compilation of the data where both *in situ* flux chambers and deck incubations were applied simultaneously for water depths ranging from 25 to 4000 meter. At depths > 1500 m, deck incubations are a factor 2 higher than *in situ* measurements. Glud et al. (1994) attributed this discrepancy to the effect of decompression and temperature rise in the recovered cores. The pressure change could result in an expulsion of the pore water and destruction and lysis of the benthic organisms. The released labile organic compounds could increase the mineralization rates. At shallower depths, where the effect of pressure and temperature differences are less pronounced, shipboard and *in situ* measurements are in the same range. In this paper, the data from deck incubations and laboratory determined oxygen profiles from stations with depth > 1500 m were excluded from analysis.

#### **Electrodes versus incubations**

A major methodological difference between flux chambers and flux calculations from micro-profiles is the scale of observation. Flux chambers integrate the oxygen flux at a scale of  $10^{-2}$  to  $1 \text{ m}^2$  while micro-electrodes measure oxygen fluxes at a scale of less than  $10^{-8} \text{ m}^2$ . This is partly corrected for by taking multiple measurements distributed over a larger area with micro-electrodes. Fluxes are then either calculated from an averaged profile or by averaging the fluxes calculated from the individual profiles. Burrows and ventilation tubes constructed by benthic macrofauna can significantly increase the area of the sediment water interface (Aller, 1988). The effect of this bio-irrigation activity is usually not resolved by micro-electrodes. Therefore oxygen flux calculations derived from micro-profiles, often referred to as diffusive fluxes, are generally lower than the total sediment community oxygen consumption, measured by flux chambers (Tahey et al., 1994). The difference between both methods can be attributed to irrigation activity of benthic fauna (Archer and Devol, 1992; Tahey et al., 1994) or advective pore water transport (Lohse et al., 1996; Ziebis et al., 1996). In general the models that are used to calculate oxygen fluxes assume molecular diffusion for oxygen. However due to turbulent flow

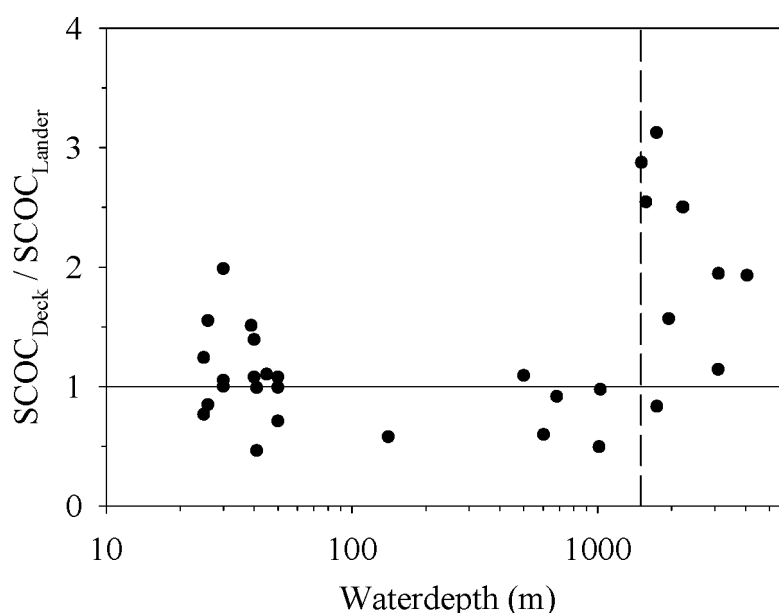


**Figure 2.5.** Ratio between SCOC measured by deck-incubations and *in situ* lander measurements plotted versus water depth. Solid line indicates the ratio of 1. Broken line represents a water depth of 1500 m. Data are from Glud et al. (1994), Tahey et al. (1996), Duineveld et al. (1997a; 1997b), Friedl et al. (1998) and Wijsman et al. (1999)

patterns, for example, due to wave actions and surface topography, the effective diffusive coefficient might be enhanced. This is especially the case for coarse-grained, coastal sediments (Lohse et al., 1996; Huettel et al., 1998).

### ***Other factors influencing respiration rates***

Although water depth is a major factor determining the rate of benthic mineralization, there is still a large scatter in the data of SCOC versus water depth (Figures 2.2 and 2.4). As discussed in previous sections of this paper, part of this scatter can be attributed to methodological reasons, but also spatial and temporal heterogeneity within and between the various marine environments can have its effect on the SCOC recordings.

An important source of this variation is the rate of primary production in the water column. Average primary productions of coastal margin areas (< 200 m), continental slopes (200 to 2000 m) and open oceans (> 2000 m) have been estimated at 230, 150 and 94 g C m<sup>-2</sup> yr<sup>-1</sup>, respectively (Wollast, 1998). This decrease in primary production with depth of the water column is implicitly modeled through the attenuation coefficients *a* and *b* (Equation 2.3). Additionally primary production, and therefore also SCOC rates show strong seasonal fluctuations and are highly influenced by local nutrient input due to upwellings and river discharges. For example, sediments located in areas influenced by river discharges have usually higher SCOC rates than comparable sediments in areas that are not influenced by nutrient and organic matter input through rivers (e.g. Wijsman et al., 1999). Spatial variation in benthic mineralization rates in deep-sea environments is less pronounced. Due to the large water depth, the sediments receive their organic matter from a relatively large area of

production in the water column, which averages the spatial variability in primary production (Lampitt and Antia, 1997).

Although strong seasonal fluctuations in benthic mineralization rates exist in deep-sea sediments due to pulse fluxes of organic matter after a phytoplankton bloom, this is difficult to measure in terms of SCOC due to the short period of response (Soetaert et al., 1996b) and spatial heterogeneity. Short-term variations in SCOC recordings could also be caused by other environmental conditions such as redox state and topography of the sediment, oxygen concentration and temperature of the bottom water and the composition of the benthic community. The effect of redox conditions on the rate of carbon degradation in marine sediments is not clear. Some authors indicate that oxygen has no or only a limited impact on the rate of organic matter degradation (e.g. Westrich and Berner, 1984; Canfield, 1989a) while others conclude that aerobic decomposition of organic matter is faster (e.g. Kristensen et al., 1995; Hulthe et al., 1998) or slower (e.g. Sun et al., 1993) than anaerobic degradation. Dauwe et al. (2000) show that aerobic mineralization is faster only at low degradation rates (coarse grained sediments and sediments with large amounts of refractory organic matter), probably because the biomass production of anaerobic bacteria becomes limiting. According to Aller (1994), the rate of degradation is promoted by alternating oxic and anoxic conditions of the organic material, for example, due to the bioturbation activity of macrofauna.

In figures 2.6 A to D the SCOC is plotted as a function of water depth and additional environmental parameters such as oxygen concentration and temperature of the near-bottom water and biomass of the macrofauna. Besides the negative correlation with  $\log(\text{Water depth})$  ( $r = -0.89$ ;  $p < 0.05$ ),  $\log(\text{SCOC})$  is positively correlated with  $\log(\text{Biomass})$  ( $r = 0.84$ ;  $p < 0.05$ ) and temperature of the near-bottom water ( $r = 0.69$ ;  $p < 0.05$ ). There is no significant correlation ( $\alpha = 0.05$ ) between  $\log(\text{SCOC})$  and the oxygen concentration in the near-bottom water. It should be noted however that these variables are not independent from each other, but correlated through the master variable water depth. For example, the temperature in deep-sea waters will generally not be warmer than 5 °C, while the temperature in shallow shelf sediments can range between -2 to 30 °C, depending on latitude and season. It is also well known that the biomass of macrofauna community is related to water depth (Rowe, 1983; Flach and Heip, 1996). This is because the flux of labile organic matter in the deep-sea decreases with water depth and becomes a limiting factor for the macrofauna biomass (Rowe, 1983). The higher carbon fluxes that are characteristic for the shallower shelf systems could potentially support a higher macrofauna biomass, and other environmental factors usually become limiting. Type I linear regression on the log-transformed data of macrofauna biomass versus water depth resulted in the relation

$$B_{\text{model}} = 17.25 \cdot e^{-0.0013 \cdot Z} \cdot 2.67 = 46.06 \cdot e^{-0.0013 \cdot Z} \quad (2.5)$$

( $n = 212$ ;  $R^2 = 0.68$ ;  $s^2 = 0.37$ ), where  $B_{\text{model}}$  is the estimated macrofauna biomass (g AFDW m<sup>-2</sup>),  $Z$  is water depth (m) and 2.67 is a correction factor that is required to correct for the systematic bias due to skewness (Middelburg et al., 1997).

We have attempted to analyze the combined effect of water depth, macrofauna biomass and oxygen concentration and temperature of the near bottom water on the

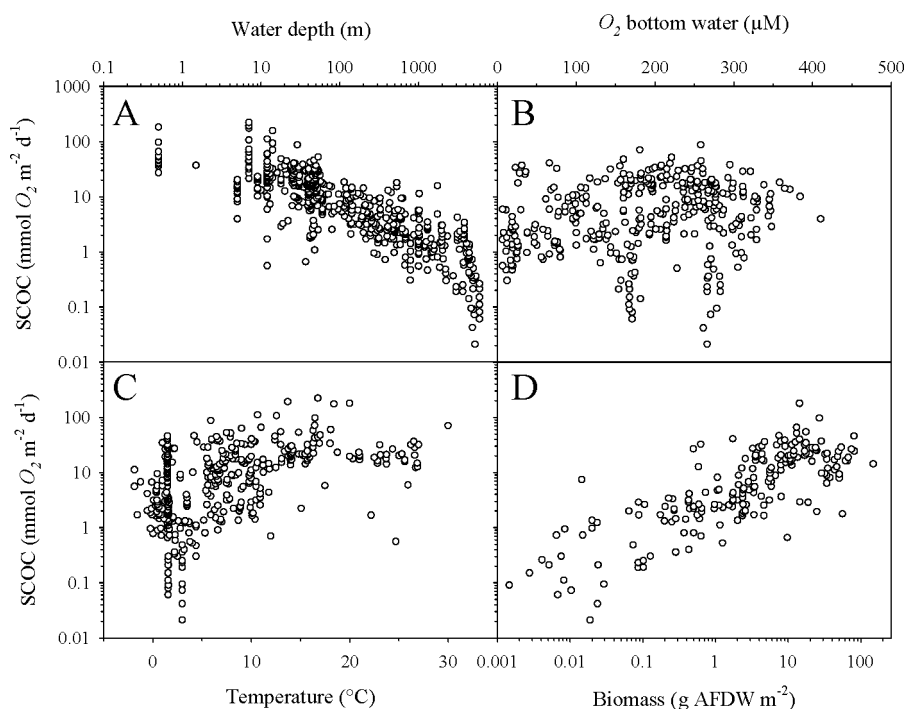


**Figure 2.6.** Scatter plots of SCOC versus (A) water depth, (B) oxygen concentration in the near-bottom water, (C) temperature of the bottom water and (D) biomass of the macrofauna. References are listed in table 2.1

benthic respiration rate by means of a multiple regression analysis. Stepwise multiple linear regression with backward elimination of  $\log(\text{SCOC})$  as dependent variable and  $\log(Z)$ ,  $\log(B)$ ,  $T$  and  $O_2(bw)$  as independent variables resulted in the relation:

$$\log(\text{SCOC}) = 2.34 - 0.59 \cdot \log(Z) - 0.0018 \cdot O_2(bw) + 0.186 \cdot \log(B) \quad (2.6)$$

( $n = 118$ ;  $R^2 = 0.83$ ), where SCOC is the sediment community oxygen consumption ( $\text{mmol } O_2 \text{ m}^{-2} \text{ d}^{-1}$ ),  $Z$  is the depth of the water column (m);  $O_2(bw)$  is the oxygen concentration of the bottom water ( $\mu\text{M}$ ) and  $B$  is the biomass of the macrofauna ( $\text{g AFDW m}^{-2}$ ). Inclusion of temperature did not improve the model significantly.  $t$ -values of the regression coefficients in this model are 12.1 for the intercept and -8.2, -4.5 and 3.2 for  $\log(Z)$ ,  $O_2(bw)$  and  $\log(B)$ , respectively. From this analysis we conclude that water depth is the major factor determining the total rate of benthic mineralization, although other environmental factors could influence the observed rate of benthic respiration.

### ***Relation with water depth***

Even though benthic mineralization accounts for only a moderate to small fraction (<5 % – 50 %) of the total system mineralization, the rates per unit volume are 1 to 2 orders of magnitude higher than in the water column since the particulate organic matter is concentrated in the sediments (Jørgensen, 1983). The combination of these high reaction rates and the low mixing rates in the sediments compared to the water column results in very strong gradients of various components in the sediments

such as oxygen, nitrate and ammonium (Soetaert et al., 2000). The presence of these strong gradients results in a complex collection of reaction pathways (e.g. Jørgensen, 1983) that controls the fluxes across the sediment-water interface. The rate of organic matter degradation in sediments is therefore a major regulating factor for benthic-pelagic coupling, and various models are developed to describe these rates. Biogeochemical models for carbon degradation are generally based on the one- $G$  model of Berner (1964)

$$\frac{dG_m}{dt} = -kG_m, \quad (2.7)$$

where  $G_m$  is the concentration of metabolizable organic matter,  $k$  is the first order rate constant and  $t$  is time. This model assumes that the rate of organic matter decomposition is proportional to the concentration of the degradable carbon fraction. Other factors such as microbial biomass and concentration of oxidants are not limiting (Berner, 1980b; Middelburg et al., 1993). Modifications of this model have been proposed like the multi- $G$  model (Jørgensen, 1978; Berner, 1980a; Westrich and Berner, 1984), which assumes that organic matter is composed of two or more discrete fractions with different degradability and continuum models that assume a gradual decrease in  $k$  with age of the organic matter (Middelburg, 1989; Boudreau and Ruddick, 1991). These models imply that in the end, all the labile organic matter will be degraded and that therefore the long-term, depth-integrated rate of benthic mineralization is determined by the flux of degradable organic matter to the sediment.

The fraction of the primary production that arrives at the sea floor depends on the residence time of the organic matter in the water column, which is a function of water depth and net sinking speed of the organic matter. For non-turbulent waters, this net sinking speed is related to the particle size (Stokes law). Organic matter in the water column is often categorized in three size fractions (e.g. Najjar et al., 1999), dissolved organic matter (DOM) including colloidal as well as purely dissolved material ( $< 1 \mu\text{m}$ ), suspended particulate organic matter (sPOM;  $1$  to  $50 \mu\text{m}$ ) and large particulate organic matter (POM;  $> 50 \mu\text{m}$ ). The large particulate organic matter is typically composed of fecal pellets from zooplankton. In our model, the total flux of organic matter is divided in two components reflecting different settling regimes. Turbulent mixing processes dominate in shallow coastal areas, where the water column is completely mixed, at least during part of the season. Macrofauna can actively enhance the turbulent flux of organic matter to the sediment. Filter feeding organisms among the benthic fauna could efficiently capture the suspended particles from the water column and incorporate the organic matter into the benthic food web. Heip et al. (1995) have argued that, in well-mixed estuaries, the average biomass of suspension feeders is largely determined by the exchange of water masses. But also surface deposit feeders could take advantage of the freshly deposited organic material by capturing it before it will be resuspended in the water column due to turbulent processes. The importance of this turbulent mixing transport decreases with water depth and becomes absent in deep-sea environments where turbulent mixing processes are restricted to the upper 100 to 200 meter of the water column and only during a short period of time. Here, the settling flux becomes the dominant transport process of organic matter to the sea floor and is often referred to as the export production or new production (Dugdale and Goering, 1967; Eppley and Peterson, 1979). In shallow coastal environments, the settling flux might represent the mass deposition of diatoms after a spring bloom or the settling of organic matter in the form

of fecal pellets. The attenuation coefficient of the settling transport regime ( $0.00047 \text{ m}^{-1}$ ) and the turbulent transport regime ( $0.017 \text{ m}^{-1}$ ) can be decomposed as  $k/v$ , where  $k$  is the first order rate constant of the organic matter degradation ( $\text{d}^{-1}$ ) and  $v$  is the net settling velocity of the organic matter in the water column ( $\text{m d}^{-1}$ ). Assuming a settling velocity of  $100 \text{ m d}^{-1}$ , the  $k$  of the sinking organic matter is estimated at  $0.047 \text{ d}^{-1}$  ( $= 17 \text{ yr}^{-1}$ ), which is slightly lower than the  $k$  of  $27.5 \text{ yr}^{-1}$ , which was derived by Boudreau and Ruddick (1991) for fast decaying marine particulate organic matter. Assuming a  $k$  of  $27.5 \text{ yr}^{-1}$  (Boudreau and Ruddick, 1991), the net settling velocity due to turbulent mixing is  $4.4 \text{ m d}^{-1}$ , whereas that due to settling is  $160 \text{ m d}^{-1}$ .

According to the model, the primary production that is potentially available for the benthos in equivalents of oxygen is  $27 \text{ mmol } O_2 \text{ m}^{-2} \text{ d}^{-1}$ . With a respiration coefficient of 0.85 (Hargrave, 1973), this corresponds to  $101 \text{ g C m}^{-2} \text{ yr}^{-1}$ . This corresponds to the global estimates of Wollast (1998) for primary production rates in shelf, slope and open ocean areas ( $230$ ,  $150$  and  $94 \text{ g C m}^{-2} \text{ yr}^{-1}$ , respectively). Our estimate is necessarily lower than those derived by Wollast (1998) because of water column respiration by algae and heterotrophs. The new production, as estimated by the settling fraction of the organic matter, is  $14.1 \text{ g C m}^{-2} \text{ yr}^{-1}$ . The  $f$ -ratio, calculated as the ratio of “new” production to primary production is 0.14 (Eppeley and Peterson, 1979), which is in concordance with  $f$ -ratios for open oceans (Eppeley and Peterson, 1979; Wollast, 1998).

Other empirical relations have been developed to describe the vertical carbon flux ( $C_{\text{flux}}$ ) as a function of water depth (Figure 2.1). The relations of Suess (1980), Betzer et al., (1984), Berger et al. (1987) and Martin et al. (1987) were based on best fits of data from sediment traps moored at a depth of more than 50 to 100 m. Sediment traps typically sample the larger, rapidly sinking particles (fecal pellets, aggregates, calcareous and siliceous hard parts of larger pelagic organisms) in the water column and DOM and suspended particle fluxes are usually not included. Moreover, the efficiency of particle trapping is variable for it depends on trap design, water currents and resolution. This may have caused some uncertainty in reported trap-based relations. Alternatively, the sea floor itself can be regarded as the ultimate sediment trap by translating measured oxygen fluxes across the sediment water interface into net carbon fluxes to the sea floor (Jahnke et al., 1990; Herman et al., 2000). The seafloor not only captures the larger fraction of the POM, but also the suspended POM and even DOM. Moreover, seafloor fluxes display less temporal variability than water column fluxes, primarily because early diagenetic processes and carbon utilization by the benthic community dampen short-term episodic depositional events (Jahnke, 1996; Soetaert et al., 2000). Similar to our relationship, those of Heip et al. (1995) and Christensen (2000) are also based on SCOC measurements from shallow estuaries and coastal waters ( $< 60 \text{ m}$ ) and deep-sea sediments ( $> 2000 \text{ m}$ ), respectively.

Finally, carbon deposition rates have been estimated by modeling nutrient profiles in the water column (e.g. Najjar et al., 1999). In these models carbon fluxes are estimated as the difference between production and degradation in the water column, which could introduce relative large uncertainties due to uncertainty about eddy mixing in the ocean interior (Jahnke, 1996). Also lateral transport processes are generally not incorporated into these flux estimates.

## Conclusions

It appears that carbon fluxes, calculated from sediment uptake rates are higher than those based on sediment traps at depth more than a few hundred meters (compare curves 7 and 8 vs. curves 1 – 4 in figure 2.1), consistent with Jahnke et al. (1988) Reimers et al. (1992) and Herman et al. (2000). This might indicate that sediment traps underestimate the delivery of carbon to sediments as argued before based on hydrodynamic considerations (Gust et al., 1992) and radionuclide data (Buesseler et al., 1994).

Our global relation seems to overestimate the carbon flux relative to production in shallow environments (compare curve 5 vs. curve 8 in figure 2.1). This apparent discrepancy is probably due to spatially variable primary production. The Heip et al. (1995) relationship is based on a subset of our data and restricted to temperate, shallow coastal environments, characterized by a higher primary production. Wollast (1998) reported a global average production of  $230 \text{ g C m}^{-2} \text{ yr}^{-1}$  for coastal environments whereas we have derived a global average production of  $101 \text{ g C m}^{-2} \text{ yr}^{-1}$ . Hence the  $C_{\text{flux}}/C_{\text{prod}}$  ratios based on our relation (curve 8 in figure 2.1) might be overestimated in shallow waters due to an underestimation of production. This clearly shows the limitation of our one-dimensional approach. Derivation of empirical relations taking into account spatial variable production might resolve the discrepancy at the expense of more parameters and conceptual elegance.





---

## CHAPTER 3

# Spatial distribution in sediment characteristics and benthic activity on the northwestern Black Sea shelf

*Jeroen W. M. Wijsman, Peter M. J. Herman, Marian-Traian Gomoiu*  
Published in *Marine Ecology Progress Series* **181**, p. 25–39 (1999)

---

### Introduction

The Black Sea is the largest (537 000 km<sup>3</sup>) permanently stratified marine basin of the world (Sorokin, 1983). A strong pycnocline at 150 to 200 m depth forms a barrier for intermixing between anoxic, hydrogen sulfide containing deep-water and oxic, productive surface water (Murray et al., 1989; Kempe et al., 1990; Lyons et al., 1993). The area shallower than 200 m, 27 % of the total area, is mainly located in the northwest. The northwestern continental shelf, here defined as the area shallower than 200 m, north of Varna and west of Sevastopol, covers an area of 70 000 km<sup>2</sup> (Figure 3.1). Since the bottom water in the abyssal part of the Black Sea is anoxic, most benthic fauna is restricted to the continental shelf area. Also, many pelagic species depend on the continental shelf for foraging and spawning (Tolmazin, 1985a; Niermann et al., 1994).

The ecosystem of the continental shelf is influenced by the major rivers, the Danube, the Dniester and the Dnieper, which together discharge more than 250 km<sup>3</sup> fresh water yr<sup>-1</sup> in the 3000 km<sup>3</sup> continental shelf (Tolmazin, 1985b; Sapozhnikov, 1992; Fabry et al., 1993). The River Danube accounts for 75 % of the total river input into the northwestern continental shelf of the Black Sea and is a major source of pollutants, nutrients and organic matter (Popa, 1993). Each year, the Danube discharges 45 to 50 × 10<sup>6</sup> t of suspended solids into the Black Sea (Popa, 1993). Due to intensification of agricultural and industrial activities in the catchment areas, the input of nutrients and waste products has increased since the 1960s (Kononov, 1995). Construction of dams in the River Danube has changed the nutrient composition of the Danube discharges (Humborg et al., 1997). As a result, the silicate to nitrogen ratio on the continental shelf has decreased, resulting in a shift in phytoplankton community from a diatom dominated phytoplankton community to a community dominated by non-siliceous species, such as coccolithophores and flagellates (Cociasu et al., 1996; Humborg et al., 1997; Mihnea, 1997).

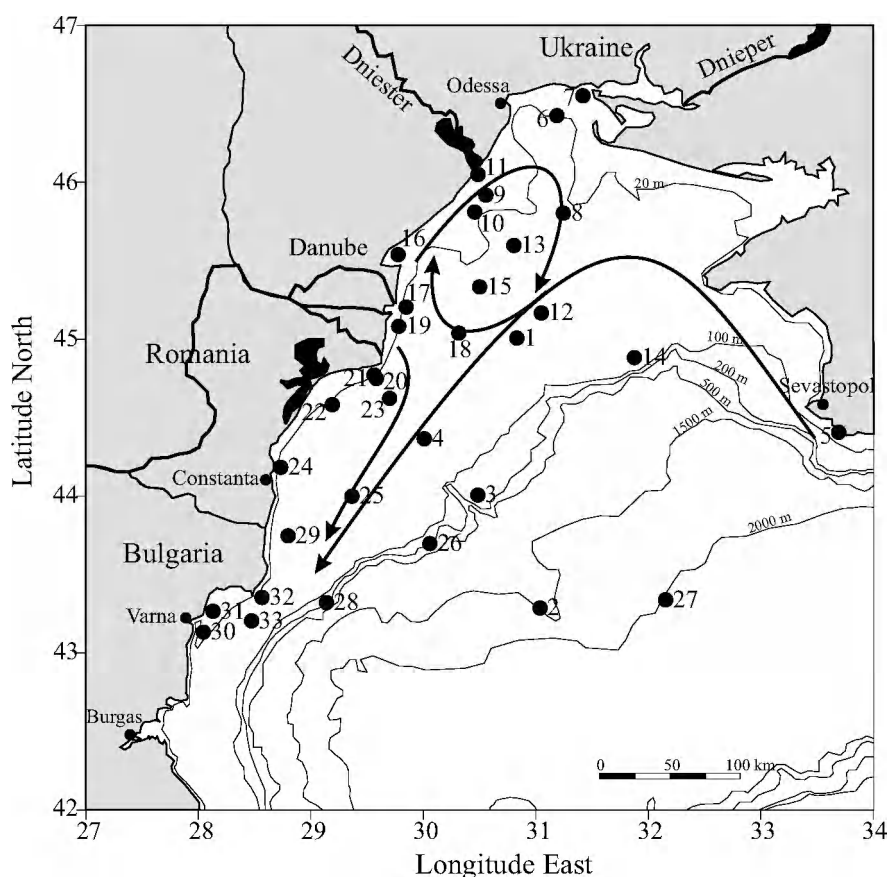


**Figure 3.1.** Map of the study area in the northwestern part of the Black Sea with sampling stations. The arrows indicate the general circulation pattern based on the results of a high-resolution hydrodynamic model (M.L. Grégoire & J.M. Beckers pers. comm.)

During the 1970s and 1980s, the ecosystem of the Black Sea changed significantly at various levels (Gomoiu, 1992; Mee, 1992; Zaitsev, 1993; Bologa et al., 1995; Leppäkoski and Mihnea, 1996). Many species disappeared or decreased in biomass, e.g. the macroalgae *Phyllophora* spp., the mussel *Mytilus galloprovincialis* (Zaitsev, 1993) and fish species such as sturgeon and turbot (Gomoiu, 1985a). Other species increased explosively in biomass, e.g. *Mya arenaria* (bivalve) (Gomoiu, 1985b), the flagellate *Noctiluca scintillans* (Porumb, 1992), the jellyfish *Aurelia aurita* (Gomoiu, 1980) and the comb jelly *Mnemiopsis leidyi* (Mutlu et al., 1994).

It is assumed that these modifications of the ecosystem were essentially caused by changes in nutrient discharges through major rivers, particularly the Danube (Gomoiu, 1992; Mee, 1992; Cociasu et al., 1996; Humborg et al., 1997). The majority of the Danube output is transported to the northeast, where it forms an anticyclonic gyre (Oguz and Malanotte-Rizzoli, 1996; Grégoire et al., 1997; Grégoire et al., 1999). From there the water is transported southward over the continental shelf (M.L. Grégoire & J.M. Beckers pers. comm. 1998). During the transportation, the composition of the watermass changes due to physical and biological processes. Sedimentation is a function of water column characteristics such as turbidity, current velocity and primary production. Sedimentation processes are reflected in the physico-chemical characteristics of the sediment such as grain-size distribution, organic carbon content, *C/N* ratio and iron concentration. Fluxes from the water

column to the sediment also influence early diagenetic processes (Henrichs, 1992) and biomass of the macrobenthos (Rowe et al., 1991). Changes in the benthic community during a process of eutrophication (Pearson and Rosenberg, 1978; Weston, 1990; Heip et al., 1995) show the sensitivity of the benthos to sedimentation, but since most interactions are complex and non-linear, the results are not always predictable. We hypothesize that if rivers can have such an impact on the ecosystem, the effect of the largest river, the Danube, must be visible in the spatial distribution of the biotic and abiotic sediment characteristics on the shelf.

In the framework of the EC project EROS–2000, the relationship between increased input of nutrients through the rivers and changes that occurred in the ecosystem of the Black Sea has been analyzed. The present paper focuses on the benthic part of the system. Structural sediment characteristics such as grain size and porosity that are indicative for the sedimentation regime and solid-phase constituents that are related to mineralization processes have been determined. The oxygen flux to the sediment has been measured as an estimation of the rate of benthic mineralization (Pamatmat, 1971; Heip et al., 1995), and the contribution of macrobenthos in total sediment respiration has been calculated. Spatial variations in biogeochemical characteristics were compared with the distribution of macrobenthos in order to identify common patterns. These distribution patterns have been related to the geographic location of the plume of the Danube.

## Material and Methods

### *Sampling sites*

From 5 to 27 August 1995, 33 stations were sampled on the northwest continental shelf on the 48<sup>th</sup> cruise of the RV ‘Professor Vodyanitsky’ (Table 3.1). The weather was calm and relatively constant during this period. From CTD profiles, a seasonal temperature stratification of the upper water layers could be detected at all stations. Sediment was sampled with a Reineck box corer (60 × 30 × 30 cm) at all stations, except stations 21 and 27 where only water samples were taken.

### *Sediment parameters*

Sediment cores from stations 1–6, 11, 12, 14, 16–20, 22–26 and 28–31 were sub-sampled from the box corer with Plexiglas tubes (5.8 cm i.d., 50 cm length) and closed with silicon stoppers. The cores were sliced at several depth intervals: 0–0.5; 0.5–1; 1–1.5; 1.5–2; 2–3; 3–4; 4–5; 5–7; 7–9; 9–11; 14–16 and 19–21 cm. The sediment was stored frozen in 50 ml polycarbonate vials. Within 2 months after sampling, the samples were dried by lyophilization. Water content was calculated from weight loss, and porosity was calculated from water content, assuming a sediment density of 2.55 g cm<sup>-3</sup>. The shell fraction was separated from the sediment by sieving over a 0.6 mm sieve. The CaCO<sub>3</sub> content of the remaining sediment was determined through volumetric gas analysis after acidification of 0.4 g dry sediment with 10 ml hydrochloric acid (8 N) (Scheibler method). Total carbonate concentration was defined as the sum of the dispersed CaCO<sub>3</sub> content of the sediment and the shell remains of bivalves. It was assumed that the bivalve shell residues were mainly

**Table 3.1.** Location, sampling date and water depth of the sampling stations

Station	Geographical position		Sampling date (1995)	Water depth (m)
	Latitude	Longitude		
1	45° 00' 23"	30° 49' 55"	6 Aug	57
2	43° 17' 13"	31° 02' 19"	8 Aug	1536
3	44° 00' 23"	30° 29' 06"	9 Aug	134
4	44° 21' 55"	30° 00' 32"	10 Aug	69
5	44° 24' 24"	33° 41' 34"	12 Aug	58
6	46° 25' 28"	31° 11' 15"	13 Aug	20
7	46° 33' 02"	31° 25' 07"	13 Aug	12
8	45° 48' 08"	31° 14' 41"	13 Aug	31
9	45° 55' 04"	30° 33' 24"	14 Aug	17
10	45° 48' 35"	30° 27' 24"	14 Aug	25
11	46° 02' 58"	30° 29' 11"	14 Aug	12
12	45° 10' 01"	31° 02' 60"	15 Aug	53
13	45° 35' 47"	30° 48' 17"	15 Aug	38
14	44° 52' 58"	31° 52' 35"	16 Aug	63
15	45° 19' 57"	30° 29' 59"	17 Aug	37
16	45° 32' 18"	29° 46' 34"	17 Aug	16
17	45° 12' 14"	29° 50' 50"	18 Aug	26
18	45° 02' 19"	30° 18' 56"	18 Aug	45
19	45° 04' 53"	29° 46' 53"	19 Aug	21
20	44° 44' 57"	29° 34' 56"	19 Aug	25
21	44° 46' 17"	29° 33' 40"	20 Aug	8
22	44° 34' 56"	29° 11' 23"	20 Aug	27
23	44° 37' 20"	29° 42' 03"	20 Aug	49
24	44° 10' 59"	28° 43' 54"	21 Aug	27
25	43° 59' 57"	29° 21' 54"	22 Aug	56
26	43° 41' 50"	30° 03' 30"	22 Aug	141
27	43° 20' 21"	32° 09' 15"	23 Aug	1997
28	43° 19' 14"	29° 08' 21"	24 Aug	123
29	43° 44' 49"	28° 47' 51"	24 Aug	51
30	43° 07' 59"	28° 02' 39"	25 Aug	20
31	43° 15' 57"	28° 07' 47"	25 Aug	24
32	43° 21' 16"	28° 33' 58"	25 Aug	50
33	43° 12' 18"	28° 28' 24"	26 Aug	64

composed of carbonate. Total *Fe* and total *Mn* were determined with a Perkin Elmer atomic absorption spectrometer, and total *P* was determined by using spectrophotometry after microwave extraction with hydrochloric acid (12 N) and nitric acid (14 N) (Nieuwenhuize et al., 1991). Total iron content was expressed on a carbonate free basis  $\{[g\ Fe/(g\ \text{dry sediment} - g\ CaCO_3 - g\ \text{shells})] \times 100\ \%\}$ . By correcting for carbonate content of the sediment, the iron content is made independent of dilution by  $CaCO_3$ . Organic carbon and total nitrogen were determined with a Carlo Erba NA 1500 elemental analyzer, after *in situ* hydrochloric acid (8 N) acidification to remove inorganic carbon (Nieuwenhuize et al., 1994). Grain-size distributions were determined using laser diffraction with a Malvern particle sizer (300 mm focal length) after removal of the organic matter and carbonates with peroxide (10 N) and hydrochloric acid (1 N).

### ***Sediment community oxygen consumption (SCOC)***

SCOC was measured at stations 1, 3–6, 11, 12, 14, 16–20, 22–26 and 28–30. Two Plexiglas core tubes (10.3 cm i.d., 30 cm length) were used to measure SCOC. Directly after retrieving the box corer, the cores were gently pushed 15 cm into the sediment and closed with a lid. In general, 10 to 20 cm of bottom water was still present on top of the sediment during sub-sampling. Only at stations 6, 22 and 29 did the box corer not contain enough bottom water. At these stations, bottom water, sampled by the GO–FLO rosette bottles, was added gently on top of the sediment with a siphon. Within 30 min after retrieval, the cores were sealed with Plexiglas lids with O-rings, containing a YSI 5739 oxygen electrode and a Teflon coated magnetic stirrer. The cores were incubated in the dark at *in situ* temperature in a thermostated bath for 4 to 8 h. A magnetic stirrer mixed the bottom water continuously without visual disturbance of the sediment. Oxygen concentration and temperature of the overlying water were measured every 20 s and stored on a datalogger. The electrodes were calibrated with filtered seawater at various oxygen concentrations using Winkler titration (Parsons et al., 1984). Oxygen flux was determined using linear regression from the moment that *in situ* temperature was reached (after 1 to 1.5 h). Enclosed incubations change the solute concentrations in the overlying water (Devol and Christensen, 1993; Duineveld et al., 1997a). Therefore, long time incubations change the concentration gradients and may, thus, influence the fluxes. To avoid this artifact only the initial, linear part of the curve was used to calculate the flux. A correction was applied for oxygen consumption by the probe and the bottom water through incubating non-filtered bottom water without sediment. On average this correction was  $1.4 \text{ mmol } O_2 \text{ m}^{-2} \text{ d}^{-1}$  (15 cm water column). All stations were sampled in duplicate from the same box corer, except stations 1, 12, 16, 20 and 24 where only single cores could be incubated. After incubation, the cores from the incubators were sectioned into 2 cm slices and preserved in formaldehyde for macrobenthos analysis.

### ***Macrobenthos***

Macrobenthos was sampled at 30 stations on the continental shelf. At these stations, 8.6 cm i.d. cores were taken from the box corer down to 10–12 cm depth. On board, the samples were stained with Congo Red and preserved in buffered formaldehyde (4 %). In the laboratory, the samples were washed through 1.0, 0.25 and 0.125 mm mesh sieves. Macrobenthic animals were identified and wet weight, including shells, was determined. Biomass was converted to g ash-free dry weight (AFDW)  $\text{m}^{-2}$  using conversion factors of Rumohr et al. (1987). For this study, only species larger than 1 mm were enumerated. Heterogeneity (Peet, 1974) was calculated as Hill's diversity numbers (Hill, 1973) of order 0, 1, 2 and  $\infty$ .  $N_0 = S$ ;  $N_1 = \exp[-\sum p_i \ln(p_i)]$ ;  $N_2 = 1/\sum(p_i^2)$ ;  $N_\infty = 1/p_1$ , where  $p_i$  ( $i = 1, 2, \dots, S$ ) = relative abundance of the  $i$ th most dominant species (Heip et al., 1988; Soetaert et al., 1991).

### ***Statistical analysis of data***

The relationship between the sediment characteristics was investigated using Principal Components Analysis (PCA) (Jongman et al., 1987). The ordination was performed with the Systat-package on the correlation matrix of the variables using the varimax rotation. The data presented in table 3.2, with addition of the sediment

**Table 3.2.** Sediment characteristics averaged over top 21 cm

Station	Porosity (cm <sup>3</sup> cm <sup>-3</sup> )	Med. grain (μm)	Silt < 63 μm (%)	CaCO <sub>3</sub> (%) <sup>a</sup>	Shells (%) <sup>b</sup>	Org. C (%) <sup>a</sup>	Total N (%) <sup>a</sup>	C/N ratio (mol mol <sup>-1</sup> )	Total Fe (%) <sup>c</sup>	Total Mn (%) <sup>a</sup>	Total P (%) <sup>a</sup>
1	0.79	15.67	99.38	42.97	44.73	2.71	0.31	10.25	3.45	0.71	0.8
2	0.89	18.59	99.97	59.7	0	4.69	0.36	15.36	4.02	0.38	0.65
3	0.75	10.23	93.4	34.64	11.47	1.38	0.13	12.25	3.42	0.38	0.57
4	0.79	9.35	99.81	40.89	40.14	2.64	0.28	11	4.6	0.91	0.87
5	0.64	9.5	95.28	15.88	1.81	1.01	0.11	10.77	3.79	0.37	0.71
6	0.87	19.81	99.88	10.75	1.67	3.36	0.41	9.59	3.39	0.6	0.74
11	0.67	19.84	86.21	9.78	1.93	0.89	0.09	11.29	1.93	0.47	0.54
12	0.71	21.37	96.04	50.32	68.65	3.03	0.33	10.69	2.8	0.84	0.74
14	0.79	9.5	99.98	24.49	37.58	2.84	0.32	10.31	4.13	0.9	0.72
16	0.81	11.32	99.98	11.91	0.19	2	0.23	9.94	3.7	0.58	0.78
17	0.82	9.67	99.93	9.46	0.7	2.01	0.24	9.73	3.8	0.57	0.85
18	0.7	6.64	94.11	27.19	47.71	1.82	0.24	8.79	2.94	0.4	0.53
19	0.74	12.22	99.04	9.88	0	1.88	0.19	11.25	3.94	0.77	1.2
20	0.74	11.78	98.88	11.08	0	1.4	0.17	9.88	3.61	0.7	0.94
22	0.76	11.22	99.87	9.29	1.24	1.58	0.18	10.45	3.94	0.63	0.75
23	0.63	7.8	79.79	17.3	25.4	0.94	0.12	9.25	2.25	0.25	0.37
24	0.54	34.89	62.14	10.96	33.42	0.51	0.05	11.35	2.01	0.31	0.42
25	0.63	58.09	51.54	13.26	38.61	1.26	0.14	10.51	1.34	0.21	0.27
26	0.62	70.89	45.97	28.97	29.05	0.82	0.09	10.86	1.38	0.22	0.52
28	0.77	9.95	99.99	41.87	44.44	3.21	0.33	11.37	3.82	1.75	0.59
29	0.67	10.62	92.01	31.28	22.93	0.87	0.11	9.39	2.96	0.34	0.37
30	0.54	57.99	54.44	10.2	0.94	0.33	0.04	8.8	1.89	0.32	0.61
31	0.83	10.01	99.86	9.95	0.01	2.51	0.31	9.45	4.08	0.69	0.91

<sup>a</sup>Shell-free dry weight basis<sup>b</sup>dry weight basis<sup>c</sup>carbonate-free dry weight basis

community oxygen consumption (SCOC), were used for the PCA. A complete set of data was available for 21 stations.

Correspondence Analysis (CA) was applied on the species abundance matrix using the software package CANOCO (Ter Braak, 1988; 1990). Station 28 was excluded from the analysis since only 2 species were found at this station: the cnidarian *Pachygerianthus imperator* and the polychaete *Heteromastus filiformis*. The hydrozoan *Obelia longissima* and the polychaete *Perinereis cultrifera* were given zero weight since they were only found in high densities at stations 13 and 15 and not at other stations. All data were log-transformed and sample scores were scaled as weighed mean species scores. The axes of the CA were related to site-specific environmental variables as summarized through the first 3 axes of the PCA, water depth and  $O_2$  flux into the sediment by means of indirect gradient analysis (Jongman et al., 1987). For stations 7, 8, 9, 10, 13, 15, 32 and 33, no solid-phase data were available and at station 31, no oxygen flux was measured.

All contour plots were computer generated using kriging gridding algorithm. The contour maps were restricted between the 0 and 200 m isobaths, west of 32° longitude, south of station 6 and north of station 30. If data for stations 2 and 5 were present, the value was visualized in a small rectangle.

## Results

### *Abiotic sediment characteristics*

Table 3.2 summarizes the results of the sediment analysis. Since we were interested in spatial distribution rather than depth profiles, each variable was integrated over the first 21 cm in the sediment, the zone in which most early diagenetic processes take place. The same analysis over the depth ranges 0–1 and 0–5 cm gave comparable results. Median grain sizes on the continental shelf varied between 6.6  $\mu\text{m}$  at station 18 and 70.9  $\mu\text{m}$  at station 26. The average grain size was 19.9  $\mu\text{m}$ . Very fine-grained sediments, with a silt fraction ( $<64 \mu\text{m}$ ) of more than 90 %, were observed seaward of the Danube Delta and in the northern part of the continental shelf (Figure 3.2A). The sediment became coarser grained south of the Danube Delta (Stations 24, 25 and 26) with median grain sizes of 35, 58 and 71  $\mu\text{m}$ , respectively, probably as a result of higher current velocities in this area. Generally, the total carbonate content of the sediment increased with water depth (Figure 3.2B), with lowest concentrations in front of the river mouths. Highest concentrations were found at the bivalve dominated, central part of the continental shelf, with carbonate concentrations up to 84 % of the sediment dry weight. In general, the concentration of iron (Figure 3.2C) was negatively related to the median grain size. Especially at the coarse-grained stations 24, 25 and 26 the measured iron concentrations were low. Iron concentration in front of the Danube Delta was higher than in front of the rivers Dnieper and Dniester. The  $C/N$  ratio is low in the Danube prodelta and in the southern part of the continental shelf (Stations 29, 30 and 31; Figure 3.2D). The station in front of the River Dniester had a higher  $C/N$  ratio than the stations in front of the rivers Danube and Dnieper. In general, the  $C/N$  ratio increased with water depth with the highest  $C/N$  ratio at station 2 located in the abyssal part of the Black Sea.

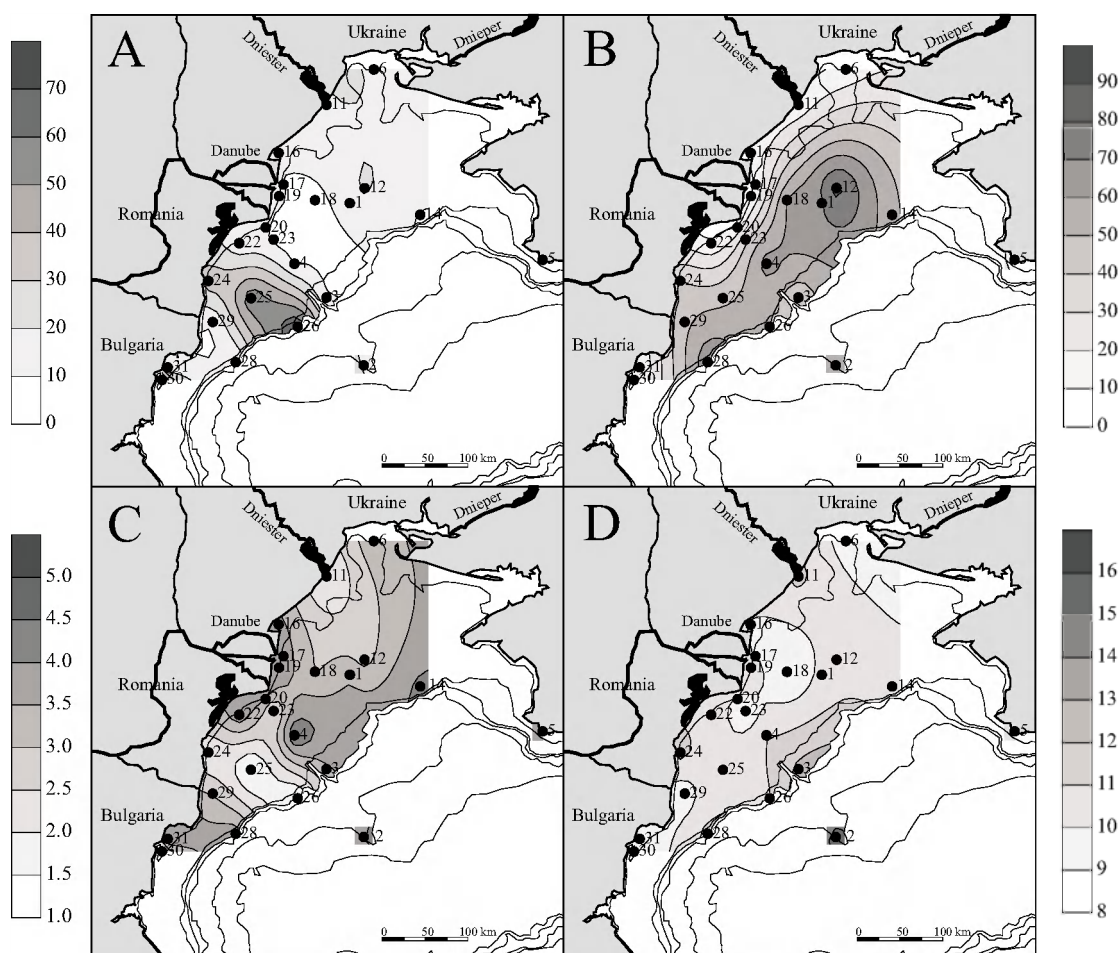


**Figure 3.2.** Spatial distribution of (A) median grain size ( $\mu\text{m}$ ), (B) total carbonate content (%), (C) iron content on a carbonate-free basis (%; see ‘Material and Methods’) and (D) molar  $C/N$  ratio (–) on the continental shelf. Only the stations for which specific data were available are indicated

The first 3 principal components explained 43.5, 22.5 and 13.3 %, respectively, of the total variance in the data (Figure 3.3). The first principal component ( $\lambda_1 = 5.22$ ) was mainly related to sediment texture. Median grain size was, as expected, inversely related with porosity and silt fraction. Coarse-grained sediments were generally poor in total iron, manganese and phosphorus. This is probably related to the decreasing number of potential binding sites with increasing grain size. The second principal component ( $\lambda_2 = 2.70$ ) was associated with carbonate parameters (shells and  $\text{CaCO}_3$ ) and the third principal component ( $\lambda_3 = 1.59$ ) was positively related to the oxygen flux to the sediment and negatively related to the  $C/N$  ratio. This confirms the notion that low  $C/N$  ratios indicate more labile organic matter and may therefore lead to higher rates of mineralization and higher oxygen fluxes.

The first principal component clearly separated the stations located on the southern part of the continental shelf (Stations 23, 24, 25, 26, 29 and 30) from the other stations. These coarse-grained sediments were relatively low in organic carbon and total nitrogen. Low carbonate contents were observed at the fine-grained sediments in front of the Danube Delta (Stations 16, 17, 19, 20 and 22). Highest



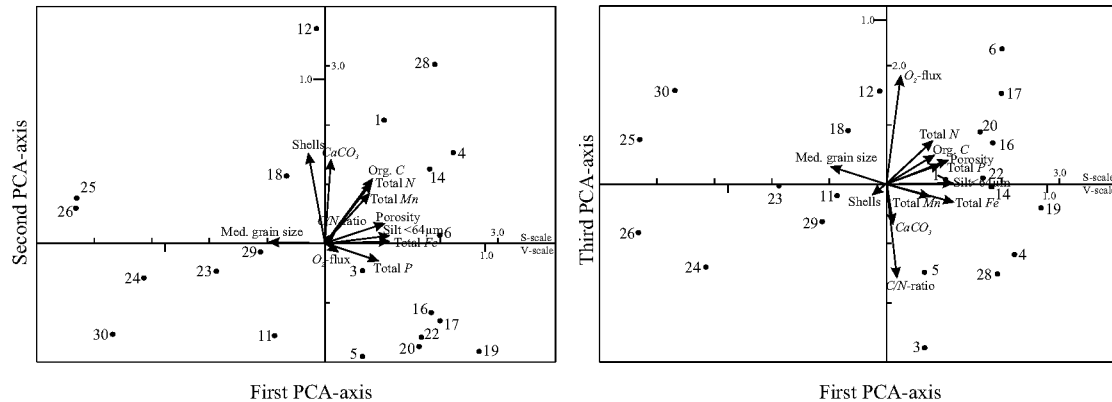


**Figure 3.3.** Euclidean distance bi-plots of the sampling stations (•) and the abiotic sediment characteristics (→) along the first 3 principal components. Note the different scale for sampling sites (S-scale) and variables (V-scale)

carbonate contents were observed at bivalve-dominated stations on the central continental shelf (Stations 1, 4, 12, 14 and 18) and at station 28, located at the oxic-anoxic interface. The stations in front of the rivers Dniester and Dnieper (Stations 11 and 6, respectively) showed no clear similarity with the stations in front of the Danube Delta. They were slightly coarser grained and station 6 had a higher organic carbon concentration (3.4 %) than the stations in front of the Danube Delta. Station 11, in front of the Dniester River, had a low concentration of total iron compared to the stations in front of the Danube Delta. The 3 stations located near the oxic-anoxic interface (Stations 3, 26 and 28) showed no similarity in their biogeochemical characteristics.

### ***Sediment community oxygen consumption***

The average SCOC was  $21.4$  ( $\sigma = 13.4$ )  $\text{mmol } O_2 \text{ m}^{-2} \text{ d}^{-1}$ . The difference between duplicate measurements averaged 24 % of the mean. The spatial distribution on the continental shelf is shown in figure 3.4. Highest rates were measured at the coastal stations and at station 12 on the continental shelf. Despite the absence of data in the relatively large area between stations 6, 11 and 12, the algorithm interpolates between those stations. The average flux at the stations in the vicinity of the 3 major rivers (Stations 6, 11, 16, 17, 19, 20, and 22) was  $32.1$  ( $\sigma = 5.6$ )  $\text{mmol } O_2 \text{ m}^{-2} \text{ d}^{-1}$ , which was significantly higher ( $t$ -test,  $p < 0.01$ ) than the average flux at the other stations ( $16.1$  [ $\sigma = 13.0$ ]  $\text{mmol } O_2 \text{ m}^{-2} \text{ d}^{-1}$ ). The high flux at station 30 may have been caused by the influence of the harbor of Varna. The highest oxygen flux was recorded at station 12 ( $51.6 \text{ mmol } O_2 \text{ m}^{-2} \text{ d}^{-1}$ ). This station was dominated by the bivalves *Modiolus phaseolinus* and *Mytilus galloprovincialis* with a total biomass of  $13 \text{ g AFDW m}^{-2}$ . Lowest fluxes were measured at stations with low oxygen concentrations in the near bottom water, located at the oxic-anoxic interface (Stations 3, 26 and 28). Macrobenthos biomass was extremely low at these stations (0 to  $0.01 \text{ g AFDW m}^{-2}$ ).

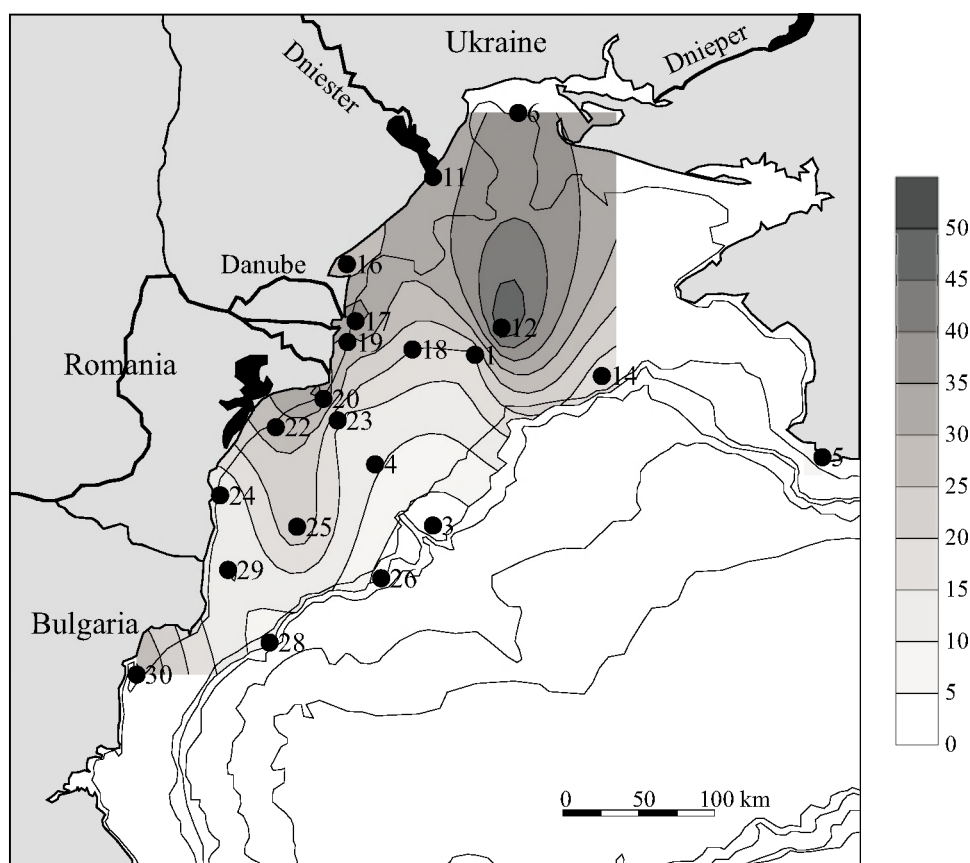


**Figure 3.4.** Spatial distribution of sediment community oxygen consumption (SCOC) ( $\text{mmol O}_2 \text{ m}^{-2} \text{ d}^{-1}$ ) on the continental shelf measured using deck incubation. (•) stations where SCOC was measured

### Macrobenthos

A total of 73 macrobenthos species ( $>1 \text{ mm}$ ) were identified. Dominant species were defined as species that account for more than 10 % of the total AFDW at, at least, 1 station on the continental shelf. A total of 18 dominant species were distinguished (Figure 3.5). The polychaetes *Polydora ciliata* and *Melinna palmata* were most widely spread and found at 16 of the 30 stations on the continental shelf. The total macrobenthos biomass ranged from  $0 \text{ g AFDW m}^{-2}$  at stations 3 and 26 to  $31.9 \text{ g AFDW m}^{-2}$  at station 29, which was dominated by the bivalve *Mytilus galloprovincialis*. On average, the macrobenthos biomass was  $11.8 (\sigma = 9.8) \text{ g AFDW m}^{-2}$ . The average, total density was  $2520 (\sigma = 3320) \text{ ind. m}^{-2}$ . Highest densities were found at station 19 in front of the Danube Delta with  $18\,000 \text{ ind. m}^{-2}$ . At the stations on the continental margin, the macrobenthos density was low (Station 28) or zero (Stations 3 and 26). At station 28, only the polychaete *Heteromastus filiformis* ( $79 \text{ ind. m}^{-2}$ ) and the cnidarian *Pachyercianthus imperator* ( $158 \text{ ind. m}^{-2}$ ) were found. Species heterogeneity expressed as  $N_1$  was highest at station 5 ( $N_1 = 16.6$ ). Lowest diversity was recorded at stations 8 and 28 ( $N_1 = 1.24$  and  $1.89$  respectively).  $N_1$  correlated strongly with  $N_2$  ( $r = 0.97$ ) but less with  $N_0$  ( $r = 0.81$ ) and  $N_\infty$  ( $r = 0.84$ ).

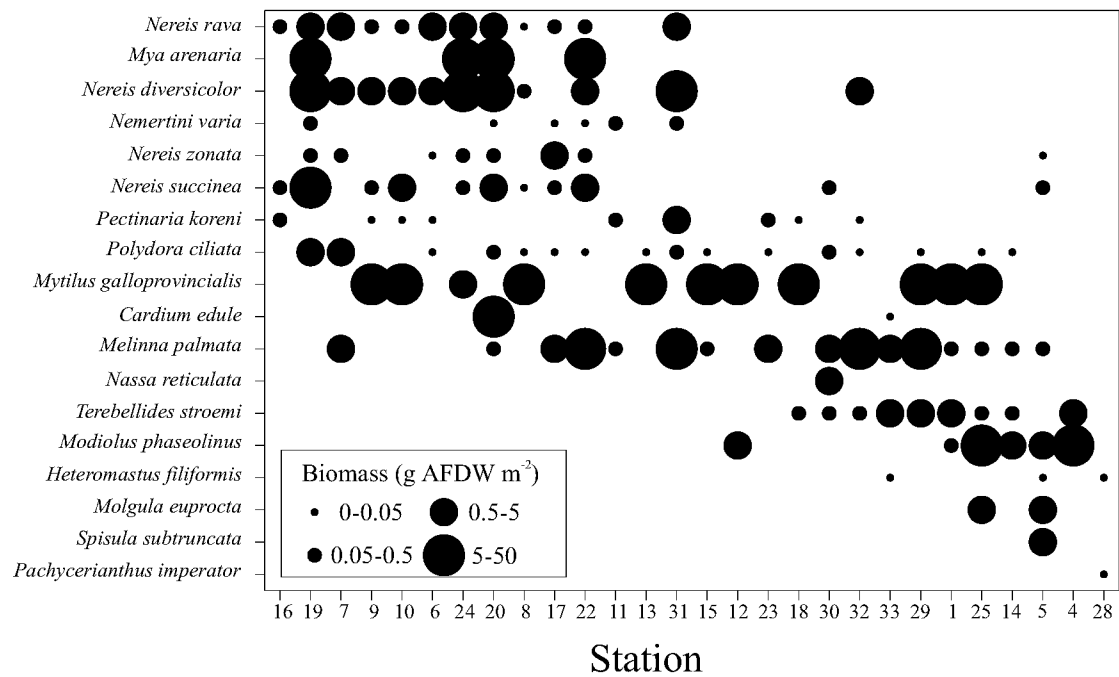


**Figure 3.5.** Distribution of the dominant macrobenthic species on the continental shelf. The biomass (g ash-free dry weight [AFDW]  $\text{m}^{-2}$ ) is classified into 4 size groups as indicated by the size of the marker. Dominant species were defined as species that account for more than 10 % of the total macrobenthos biomass (g AFDW  $\text{m}^{-2}$ ) at, at least, 1 station. Both stations and species were ordered according to their location on the first CA-axis

The first 3 axes of the correspondence analysis explained 31.5 % of the total variation in the species data (Figure 3.6). The first axis ( $\lambda_1 = 0.60$ ) was mainly related to water depth. The shallow coastal stations were dominated by the Nereidae species (*Nereis diversicolor*, *N. rava*, *N. succinea* and *N. zonata*) while the bivalve *Modiolus phaseolinus* and the polychaete *Terebellides stroemi* dominated the deeper stations. The second axis ( $\lambda_2 = 0.44$ ) was indicative for station 30 (characterized by the gastropod *Nassa reticulata*) and station 5 (characterized by the bivalve *Spisula subtruncata*). The higher value of station 31 on the second axis compared to the other shallow water stations might be related to a different macrobenthos composition due to its southern geographical position. The third axis ( $\lambda_3 = 0.39$ ) separated the stations on the northern part of the continental shelf (Stations 8, 9, 10, 13 and 15) from the stations in front of the river mouths. This division was mainly based on the absence of the bivalve *Mytilus galloprovincialis* at the stations in front of the major rivers that were characterized by fine-grained sediments (indicated by a high value of PCA-1). Although no abiotic data for the stations from cluster I (Stations 8, 9, 10, 13 and 15) were available, the relation with PCA-1 suggests that the sediments at these stations were relatively fine grained. The low carbonate content at the stations in front of the major rivers is reflected in the low value of the second principal component (PCA-2), which was mainly related to the third CA-axis.

Dissolved and particulate

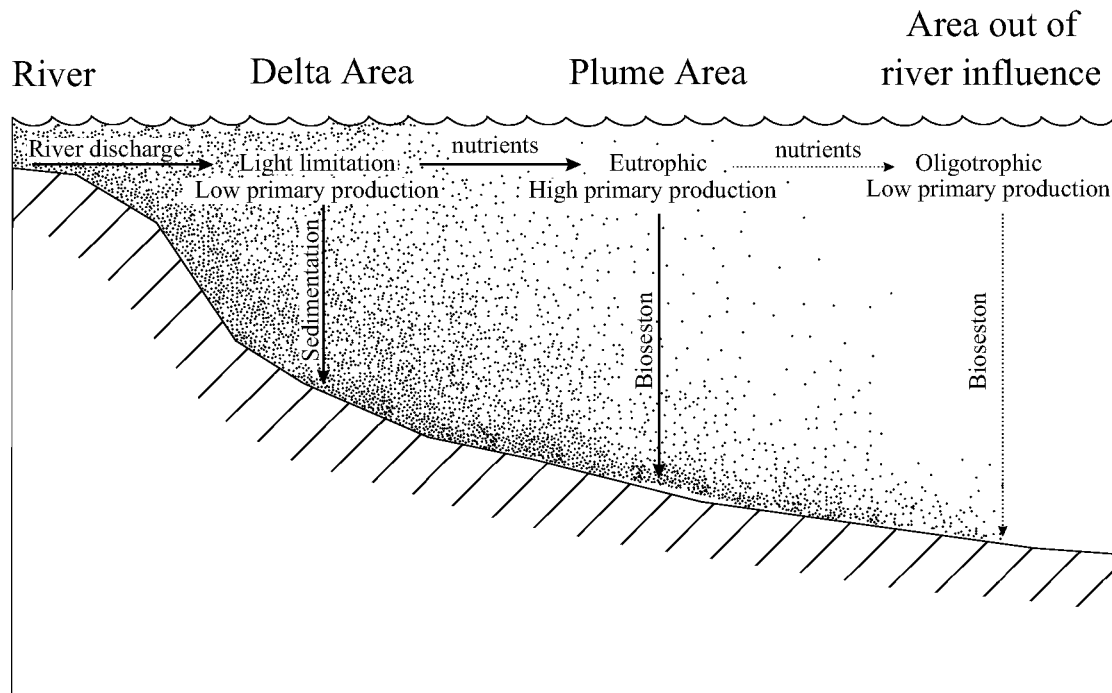


**Figure 3.7.** Generalized model for influence of the discharge of a large river on the sedimentation processes at the shelf. Arrows indicate nutrient transport and sedimentation. Adapted from Rhoads et al. (1985)

In this paper we have attempted to identify the different sedimentological regions on the continental shelf in relation to the River Danube, which is by far the most important river on the continental shelf in terms of freshwater, suspended solids and nutrient discharge into the Black Sea (Popa, 1993). Referring to the general current pattern on the continental shelf, we can indicate the 3 different areas. The stations located just in front of the River Danube (Stations 16, 17, 19, 20 and 22) are directly influenced by the Danube discharges and can be identified as the ‘Delta’ stations. The water is turbid in this area (Krustalev et al., 1990) with relatively high rates of sedimentation. From  $^{137}\text{Cs}$  data at a station just in front of the Danube Delta (Curtis and Broadway, 1992) the sedimentation has been estimated at  $0.7 \text{ cm yr}^{-1}$ . From here, the majority of the Danube water is transported north to the anticyclonic gyre (M.L. Grégoire & J.M. Beckers pers. comm., based on results of a high-resolution hydrodynamic model). Though the exact location of this gyre is dependent on wind patterns, it is very robust and generally located northwest of the mouth of the Danube (Stations 1, 8, 12, 13, 15 and 18). During the transportation, which takes about 2 wk, the concentration of suspended solids in the water column decreases (Krustalev et al., 1990), resulting in a higher light-penetration depth. It can be expected that this will lead to a higher primary production in this area, and, therefore, this area can be characterized as the ‘eutrophic’ area. From the gyre, the water is transported southward over the continental shelf along the Romanian shore towards Bulgaria. The decreased nutrient concentrations in the water column will reduce the primary production and, therefore, this area can be characterized as the ‘oligotrophic’ area.

The PCA showed that sediments in the Danube Delta area were very fine grained with median grain sizes ranging from  $9.7$  to  $12.2 \mu\text{m}$ . Since high amounts of

organic matter are generally transported by rivers (Ittekkot and Laane, 1991), the carbon flux to the sediment is expected to be high in this area. This is also reflected in the relatively high SCOC recorded in this area. The source of the organic matter transported by the Danube can be either allochthonous (terrestrial) or the generally more labile autochthonous material such as river phytoplankton (Mook and Tan, 1991). The  $C/N$  ratio of fresh terrestrial organic matter is typically higher than organic matter derived from phytoplankton (respectively  $>12$  and 6 to 9) (Thornton and McManus, 1994). During the process of aging, the  $C/N$  ratio of terrestrial-based detritus will decrease while the  $C/N$  ratio of algal-based detritus will increase (Rice and Tenore, 1981; Jørgensen, 1983). The  $C/N$  ratio can be used as a measure for the 'quality' of the organic matter to the benthos (Burdige, 1991), but one should be aware of this source effect (Cowie and Hedges, 1994). The relatively low  $C/N$  ratios in the Danube Delta area were an indication that the organic matter was mainly algal-based detritus. Probably the terrestrially derived material, transported by the river, was trapped in the inner-delta. The slight decrease in  $C/N$  ratio towards stations 16, 17, 18 and 23 indicated that the deposited organic matter became more labile at these stations.

Going to the anticyclonic gyre in the northern part of the continental shelf (i.e. the 'eutrophic' area), the sedimentation rate decreases. However, the oxygen fluxes recorded in this area remained relatively high. At station 12, which was dominated by the filter-feeding bivalve *Mytilus galloprovincialis*, the highest SCOC was measured ( $52 \text{ mmol } O_2 \text{ m}^{-2} \text{ d}^{-1}$ ). This is an indication of a high flux of labile organic carbon to the sediment in this area. All the stations in this area were high in carbonate content and dominated by *M. galloprovincialis*.

In the southern part of the continental shelf (i.e. the 'oligotrophic' area) the influence of the River Danube is reduced. The sediment became coarser grained and oxygen flux to the sediment decreased, indicating a low flux of labile detritus to the sediment.

The effect of the River Danube was also reflected in the macrobenthos distribution. The low carbonate concentrations recorded in the delta area already suggested that this region was less dominated by bivalves compared to the offshore area. The polychaetes *Nereis diversicolor*, *N. rava* and *N. succinea* and the bivalve *Mya arenaria*, characteristic for the delta area, are adapted to the high rates of sedimentation and corresponding factors such as sediment stability, food supply and larval supply (Snelgrove and Butman, 1994). The macrobenthos community of the northern part of the continental shelf, where the anticyclonic gyre is located, was characterized by a high biomass of *Mytilus galloprovincialis*. This confirms the suggestion of a relatively high deposition rate of labile organic matter in this 'eutrophic' area.

### ***Sedimentation and trophic structure***

Abiotic environmental characteristics (hydrology and sediment composition) and population dynamics (competition, mortality/predation and reproduction) are the major factors determining the macrobenthos composition in the sediment (Gaston and Nasci, 1988; Rosenberg, 1995). In this study we were mainly interested in the effects of sedimentation on the macrobenthos community composition. Since feeding type of the macrobenthos community is an adaptation to the sedimentological environment, it can be expected that differences in sedimentation will be reflected in the distribution of the different trophic groups on the shelf.

Macrobenthos was classified into 6 different feeding groups according to Fauchald & Jumars (1979). The biomass of interface feeders and deep deposit feeders was, in general, less than 3 % of the total macrobenthos population, except for station 7, where interface feeders accounted for 21 % of the total biomass. Therefore, interface feeders and deep deposit feeders were grouped together with surface deposit feeders. In figure 3.8 the relative contribution of the different trophic groups to the total macrobenthos biomass is given. Stations 3, 26 and 28 were neglected in these figures.

Deposit feeders forage on organic matter in the sediment or deposited at the sediment-water interface. The standing stock of bacteria in the sediments is usually too low to supply the total carbon demand of the deposit feeders (Kemp, 1987). Therefore, they need an additional (non-living) carbon source. Since deposit feeders subsist on a remarkably poor food source, they depend on high accumulation rates of

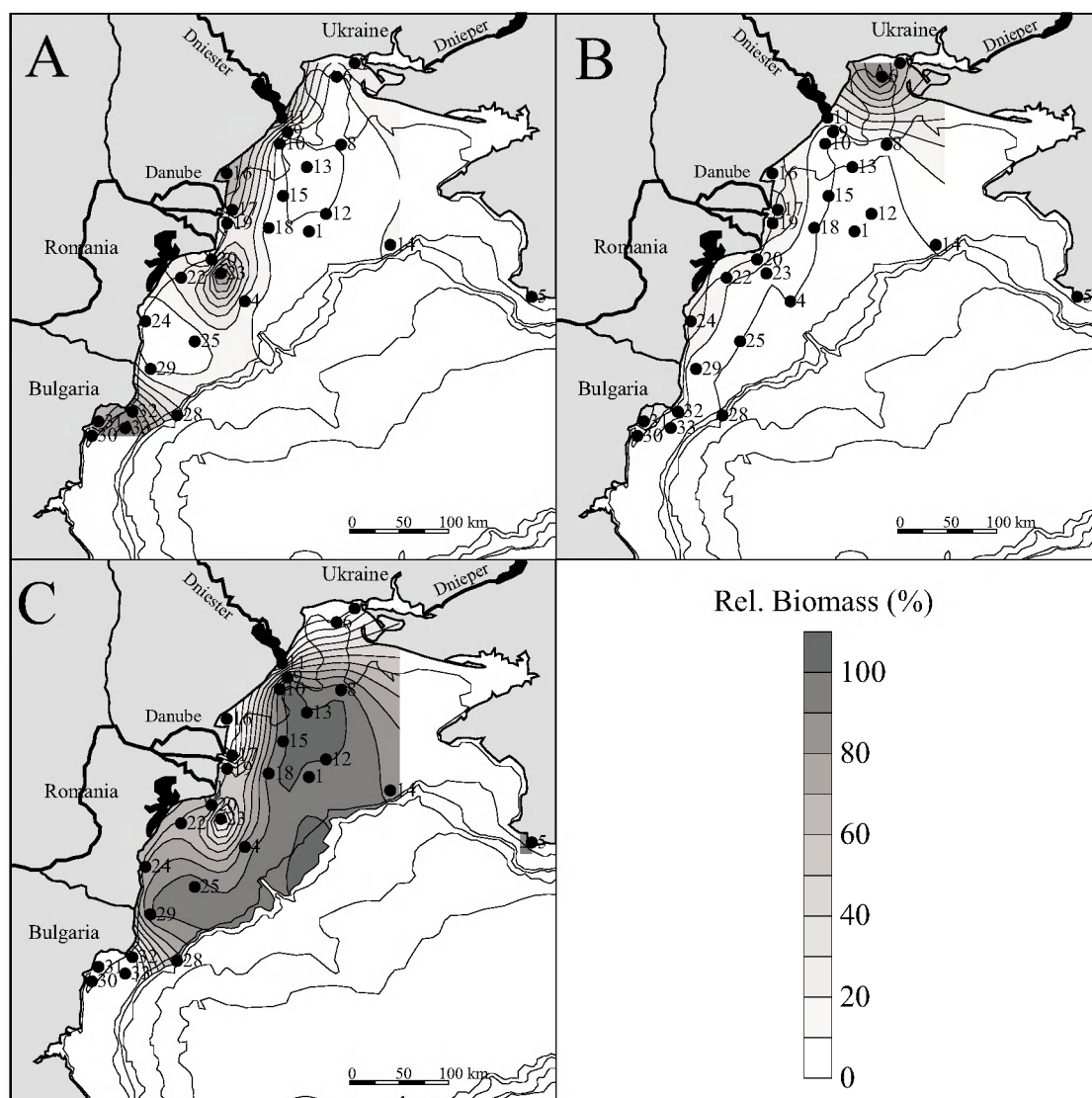


**Figure 3.8.** Relative contribution (%) to the total macrobenthos biomass in the continental shelf of (A) the sum of interface, surface and deep deposit feeders, (B) omnivores/predators and (C) suspension feeders

organic carbon (Pearson and Rosenberg, 1978; Lopez and Levinton, 1987; Weston, 1990). Deposit feeders dominated the macrobenthos biomass in the stations located in front of the river mouths (Stations 11, 16, 17 and 19) and in front of the Bulgarian coast (Stations 30 to 33), where the surface deposit feeder *Melinna palmata* was dominant. Station 23, where the total biomass was low ( $2.3 \text{ g AFDW m}^{-2}$ ), was also dominated by *M. palmata*.

Omnivores and predators are more directed towards their food item, and will, in general, not consume the sediment as a whole as deposit feeders do. This is less energy consuming, but, since they are more selective, the proper food type is, in general, less abundant. Predators and omnivores were, like deposit feeders, abundant at the near-shore stations. This suggests that the carbon flux in this area is high enough to support a substantial density of higher trophic levels. Stations 6 and 7, located in front of the Dnieper river were dominated by *Nereis diversicolor*. This polychaete accounted for 83 and 47 %, respectively, of the total macrobenthos biomass at these stations.

Suspension feeders retrieve their food directly from the water column. When the food source in the near bottom water is continuously renewed, suspension feeders can locally increase the flux of organic matter to the sediment (Heip et al., 1995). Suspension feeders are often negatively related to the percentage of mud in the sediment (Eleftheriou and Basford, 1989; Aller and Stupakoff, 1996). Depending on morphology, the filtering apparatus may be vulnerable to clogging at high concentrations of suspended solids in the near bottom water. The lack of suspension feeders in front of the river mouths may be caused by high concentrations of suspended solids in this area. Both in the northern part (Stations 1, 8, 9, 10, 13, 14, 15 and 18) and in the southern part of the continental shelf (Stations 4, 22, 24, 25 and 29), suspension feeders replace the deposit feeders. At low carbon fluxes it is expected that suspension feeders dominate since they have first access to the sedimenting organic matter (Pearson and Rosenberg, 1978; Weston, 1990). This might be the case in the southern part of the continental shelf and at the oxic-anoxic interface, but the high SCOC recorded at stations 1, 12, 18 and 25, however, do not support this idea for the northern part of the continental shelf. The sediments in this sediment starvation zone consisted of 39 to 69 % of shell remains. Apparently deposit feeders in this area have no access to the organic matter between the shell remains.

### ***Macrobenthos oxygen consumption***

Only part of the oxygen flux into the sediment is consumed through respiration of macrobenthos. The rest is used by micro- and meiobenthos, microorganisms and chemical re-oxidation of reduced substances. In estuaries the macrobenthos can account for up to 90 % of the total SCOC (Heip et al., 1995). Typical values for the part of the SCOC consumed by the macrobenthos reported by various authors are 23 % in the northwestern Barents Sea (Piepenburg et al., 1995), 38 % in the northwestern Adriatic Sea (Moodley et al., 1998) and 16 to 50 % in the Goban Spur area with the lowest values in the lower slope and the abyss (Heip et al., 2000).

We used data on individual body mass to assess the oxygen demand of the macrobenthos. Species-dependent allometric relations ( $R = aW^b$ ) are often used to calculate individual respiration rate ( $R$ ) from the body mass ( $W$ ) (Banse, 1982; Bayne and Newell, 1983). It is impossible to retrieve from literature these relations for all Black Sea species. Even if we were able to find these relations for all species,



application of the relations in calculating the total respiration rate of the macrobenthos would not be straightforward. For a well known species, such as the blue mussel (*Mytilus edulis*) for example, the reported estimations of the parameters  $a$  and  $b$  range from 0.164 to 0.698 and 0.595 to 0.930 respectively, depending on factors such as temperature, feeding, activity, oxygen tension and salinity (Bayne et al., 1976). In this study we used the relation of Mahaut et al. (1995) based on a compilation of shallow water organisms, ranging from bacteria and nematodes to fish.

$$R = 0.0174 \cdot W^{-0.156}, \quad (3.1)$$

where  $R$  = weight-specific respiration rate ( $\text{d}^{-1}$ ) and  $W$  = individual weight (mg C). Carbon biomass was estimated assuming that 50 % of the AFDW was organic carbon. Respiration rates were converted to oxygen consumption ( $\text{mmol } O_2 \text{ m}^{-2} \text{ d}^{-1}$ ) assuming a respiratory coefficient of 0.85 (Hargrave, 1973) and corrected for temperature assuming a  $Q_{10}$  value of 2 (Wells, 1980; Piepenburg et al., 1995).

It is obvious that a number of uncertainties are involved in the calculation of macrobenthos respiration. Beside errors in sampling and determination of the macrobenthos, there are many assumptions made for the calculation of the respiration rates of the macrobenthos. Conversion factors to AFDW are based on species from the Baltic Sea (Rumohr et al., 1987). The relation of Mahaut et al. (1995) is a compilation of data from a wide range of different species in different marine shallow water environments.

On average, 21 % of the total oxygen flux to the sediment at the continental shelf of the Black Sea was consumed by macrobenthos (Figure 3.9). From the SCOC, it was concluded that the carbon supply to the sediment in front of the major rivers and in the northern part of the continental shelf was high. High mineralization rates result in anoxic conditions in the sediments, which is unfavorable for many macrobenthos species. Therefore, macrobenthos was not important in terms of oxygen consumption in the northern part of the shelf (Stations 6, 11, 12, 16 and 17) and microorganisms, micro- and meiobenthos became more important. At stations 19, 20 and 22, where high mineralization rates were also recorded, the contribution of macrobenthos to the total SCOC was higher. This was mainly due to the high biomass of *Mya arenaria*, a bivalve buried deep in the anoxic sediment, that can transport oxygenated water from the water column with its siphons. The lack of burrow-building organisms at the shell-rich stations in the northern part of the continental shelf prevented oxygen to be transported into the deeper sediment layers. The contribution of macrobenthos to the total SCOC was low in these bivalve-dominated sediments. Since micro- and meiobenthos is also dependent on oxygenated sediments, it can be expected that a large part of the oxygen consumption was due to the (microorganism mediated) re-oxidation of reduced substances in the sediments (Chapter 4 of this thesis).

South of the Danube Delta the contribution of the macrobenthos to the total oxygen consumption increased. At stations 24 and 29 most of the SCOC was used by the macrobenthos (75 and 89 %, respectively). Station 24 was characterized by a high biomass ( $14 \text{ g AFDW m}^{-2}$ ) of large individuals of *Nereis diversicolor*, which accounted for 53 % of the total oxygen consumption of the macrobenthos. Station 29 had a high biomass ( $26 \text{ g AFDW m}^{-2}$ ) of *Mytilus galloprovincialis*, accounting for 73 % of the oxygen consumption of the macrobenthos.

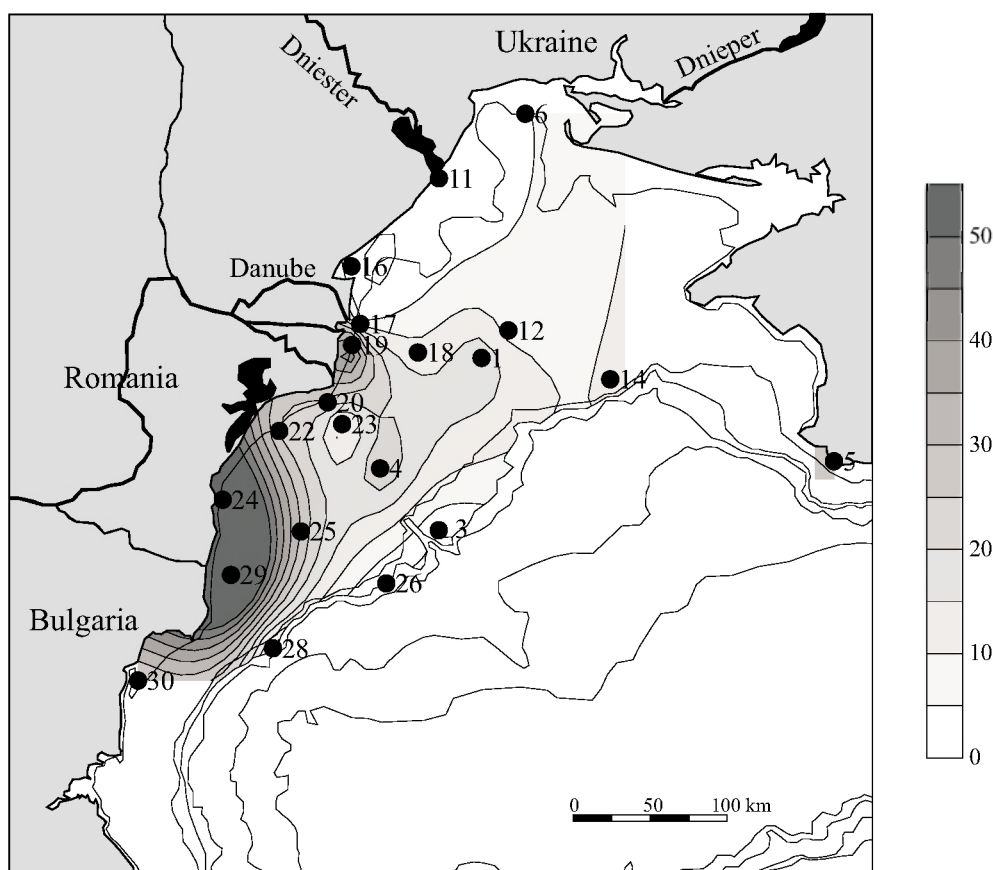


**Figure 3.9.** Spatial distribution of the fraction of the total SCOC (%) consumed by the macrobenthos on the continental shelf

The importance of the macrobenthos in the total oxygen consumption decreased towards the oxic-anoxic interface. The stations at the oxic-anoxic interface (Stations 26 and 28) had little or no macrobenthos. Frequently occurring upwellings of anoxic water from the deep-sea makes this area a harsh environment for macrobenthos (Kempe et al., 1990). Microorganisms, and micro- and meiobenthos probably consume most of the oxygen in this area.

For the Goban Spur area (200 to 4500 m), Soetaert et al. (1997) and Heip et al. (2000) found that the relative importance of smaller organisms, such as bacteria and protozoa, on the total oxygen consumption increased with decreasing carbon flux. This is probably caused by the low turnover rate of these organisms in the sediment. The relative importance of the macrobenthos in the total carbon respiration also decreased with water depth in this area. The absolute amount of organic carbon supply to the sediment in the deep-sea area may not be sufficient for the larger macrobenthos species to occur. In the Goban Spur area, ( $\text{SCOC} = 0.3 \text{ to } 5.4 \text{ mmol } O_2 \text{ m}^{-2} \text{ d}^{-1}$ ) (Duineveld et al., 1997b), the carbon flux is limiting the benthic community. In the shallow continental shelf of the Black Sea, where the SCOC ranged from 2 to 52  $\text{mmol } O_2 \text{ m}^{-2} \text{ d}^{-1}$ , the benthic community is likely to be more inhibited by the oxygen conditions in the sediment resulting from the high carbon input.

## Conclusions

The influence of the Danube could be traced back in the biotic and abiotic sediment composition of the continental shelf of the Black Sea. Fine-grained, carbonate-poor sediments and a high SCOC characterized the delta area. Only a minor part of the oxygen consumption could be attributed to the macrobenthos community, which was dominated by deposit feeders, and predators such as *Nereis* spp. In the northern part of the continental shelf, where the anticyclonic gyre was located, the rate of sedimentation was lower. However, high oxygen fluxes into the sediment were recorded, indicating a high flux of labile organic matter to the sediment. The macrobenthos community in this area, dominated by suspension feeders such as *Mytilus galloprovincialis*, was responsible for only a small fraction of the total SCOC. The southern part of the continental shelf can be characterized as the 'oligotrophic' area. Low oxygen fluxes into the sediment were recorded in these coarse-grained sediments. The scarce organic matter arriving at the sediments in this area is efficiently used by the mostly suspension feeding macrobenthos, accounting for a major part of the SCOC.



---

## CHAPTER 4

# A model for early diagenetic processes in sediments of the continental shelf of the Black Sea

*J.W.M. Wijsman, P.M.J. Herman, J.J. Middelburg and K. Soetaert*  
Accepted for publication in *Estuarine, Coastal and Shelf Science*

---

### Introduction

The river Danube is a major source of organic matter and nutrients for the Black Sea (Popa, 1993), increasing the primary production on the shelf. The enhanced rates of benthic mineralization following the deposition of the plankton material, in combination with a pronounced stratification of the water column in the summer period, may result in anoxic or hypoxic bottom waters. As a result, mass mortality among the benthic community is frequently observed in the coastal zone of the Black Sea continental shelf (Tolmazin, 1985b). Seasonal depletion of oxygen contents in the near bottom waters have been reported for various coastal systems (Harper et al., 1981; Faganeli et al., 1985). In general oxygen depletion events are limited to the summer periods when the water column is stratified. Movement of the chemocline by (wind-induced) upwellings or internal waves can be an additional source for anoxic bottom water on the continental shelf of the Black Sea (Kempe et al., 1990).

The low oxygen concentration of the bottom water and the high rates of organic matter sedimentation increase the importance of the anaerobic degradation processes in the sediment. Hydrogen sulfide, which may be toxic for many benthic organisms, is produced by sulfate reduction in the sediment when the more favorable electron acceptors such as oxygen, nitrate, manganese oxides and iron oxides are exhausted (Froelich et al., 1979). The hydrogen sulfide may react with iron to form iron sulfides such as  $FeS$  and  $FeS_2$ . As such, iron may buffer the release of free sulfide. Larger rivers are a major source of reactive iron for continental shelf systems (Aller et al., 1986; Canfield, 1989b). Although iron and sulfur cycling has been studied in sediments of the Black Sea (Calvert and Karlin, 1991; Lyons and Berner, 1992; Lyons et al., 1993; Lyons, 1997), there are no data on the northwestern shelf sediments, that receive significant quantities of reactive iron from the Danube.

Diagenetic models can be used as a tool to study diagenetic processes in the sediments. Recent development in diagenetic modeling resulted in a complex description of multiple reaction pathways with a high degree of interaction between

the acting species, *pH* dependence and non-linear reaction kinetics (Boudreau, 1991; Rabouille and Gaillard, 1991a; Boudreau and Canfield, 1993; Cai et al., 1995; Van Cappellen and Wang, 1995; Boudreau, 1996a, Dhakar and Burdige, 1996; Soetaert et al., 1996a; Soetaert et al., 1996b; Van Cappellen and Wang, 1996; Wang and Van Cappellen, 1996). The development of these complex models was facilitated by the availability of more powerful computer hardware and advanced numerical methods (Steeff and MacQuarrie, 1996). Especially the models of Boudreau (1996a), Van Cappellen & Wang (1995; 1996) and Wang & Van Cappellen (1996) provided an extensive description of the iron and sulfur chemistry in sediments. Their models include the description of alkalinity conservation in the pore water, which determines the *pH*.

In this paper we present a model for early diagenetic processes in the sediments of the Black Sea. The *pH* in this model is introduced as a forcing function and is not determined by the concentrations of all the other species. The obtained reduction of the number of state variables makes the model easier to interpret and minimizes computing time, so that extensive sensitivity analysis could be performed. The model is capable to generate steady state profiles as well as to run dynamic simulations. The present model is an extension of the model of Soetaert et al. (1996a), which was constructed for a range of marine systems. Since they were mainly interested in organic carbon, oxygen and nitrogen they lumped the anoxic mineralization processes, including manganese reduction, iron reduction, sulfate reduction and methanogenesis together. The reduced substances ( $Mn^{2+}$ ,  $Fe^{2+}$ ,  $H_2S$  and  $CH_4$ ) were represented as one pool of oxygen demand units (Soetaert et al., 1996a; Soetaert et al., 1996b). Since we were especially interested in the interaction between the sulfur and iron cycling in the sediment, we extended the model with an explicit description of the anaerobic mineralization (manganese reduction, iron reduction, sulfate reduction and methanogenesis) and re-oxidation processes. The model will be applied to a station on the northwestern shelf of the Black Sea and its performance will be discussed.

## Material and methods

The output of the model will be compared to data from station 9 of the 49<sup>th</sup> cruise of the Prof. Vodyanitsky in May 1997. This station at a water depth of 57 m was located 44°34' North and 29°46' East just in front of the Danube delta (Figure 4.1). The temperature of the bottom water at the time of sampling was 5.8°C. This station has been selected because a rather complete set of data was available and depth profiles of iron and sulfur components indicated that it comprised iron and sulfate reducing layers.

### *Shipboard procedures*

Sediment was recovered with a Reineck box-corer (60 × 30 × 30 cm) and was sub-sampled with Plexiglas core tubes (10.3 cm inner diameter, 50 cm length). The cores were sectioned in several depth intervals 0–0.5, 0.5–1, 1–2, 2–3, 3–4, 4–5, 5–7, 7–9, 9–11, 14–16, 19–21 and 24–26 cm under a nitrogen atmosphere ( $O_2$ -concentration < 0.05 %) in a glove box. The pore water was collected by squeezing the sediment over a 0.45 µm filter with a small (< 1 bar) overpressure of nitrogen gas.

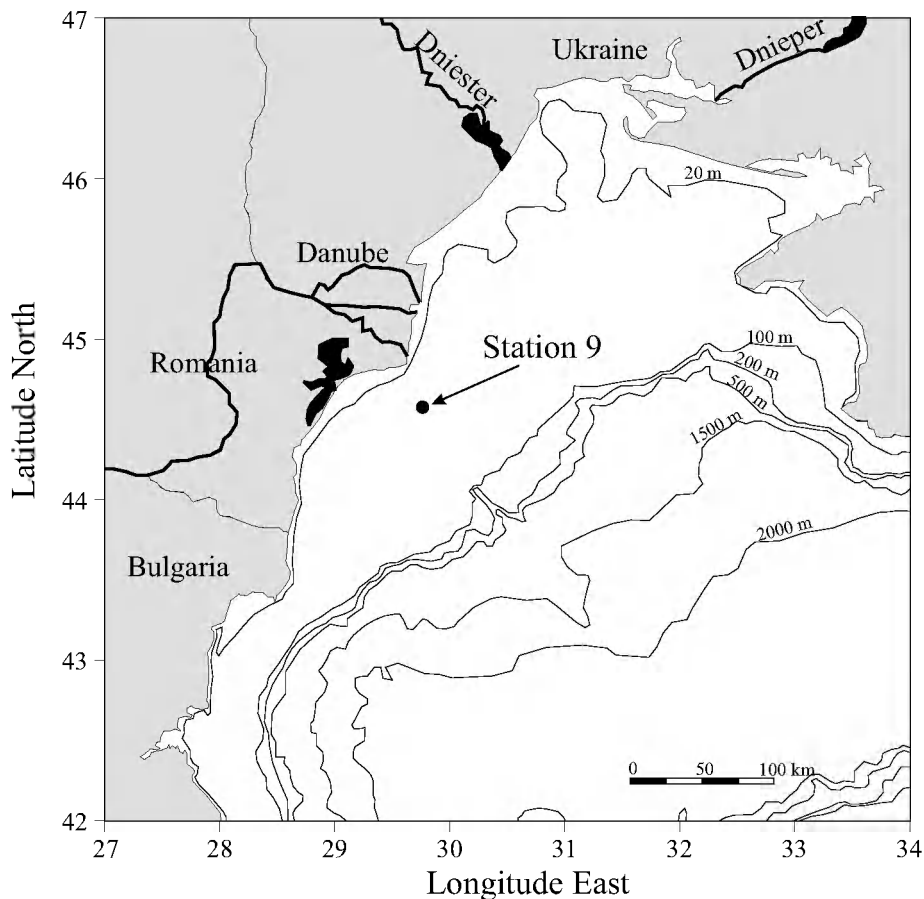


**Figure 4.1.** Location of station 9 on the northwestern continental shelf of the Black Sea

A sub-sample of 3 ml pore water was collected in 10 ml headspace vials, capped and acidified with 20%  $H_2SO_4$ . A second sub-sample of 1 ml was put into an eppendorf vial to which 50  $\mu$ l of  $Zn(Ac)_2$  (20%) was added. The rest of the pore water was stored in 20 ml PVC bottles and sealed in diffusion-free bags to prevent oxygen contamination of the samples. The remainder of the sediment after squeezing was collected in 20 ml glass vials and sealed in diffusion-free bags under nitrogen atmosphere. All samples were removed from the glove box and stored at 4°C (headspace vials) or frozen (PVC bottles, eppendorf vials and sediment samples).

Additional sediment was sub-sampled from the box-corer with Plexiglas core tubes (5.8 cm inner diameter, 50 cm length) for organic carbon content and porosity analysis. The cores were sectioned in several depth intervals 0–0.5, 0.5–1, 1–1.5, 1.5–2, 2–3, 3–4, 4–5, 5–7, 7–9, 9–11, 14–16, 19–21 and 24–26 cm. Care was taken that no pore water was lost. The sediment was put into 50 ml polycarbonate vials and stored frozen.

Depth profiles of oxygen in the sediment were obtained using Clark style micro-electrodes with guard cathode (Diamond General #737GC) at 0.2 mm resolution. The electrodes had a tip-diameter of 40–60  $\mu$ m and an output of 300 to 1000 pA at oxygen saturation. The overlying water was continuously refreshed with bottom water at *in situ* temperature to prevent depletion of oxygen during measurement. Depth profiles of *pH* in the sediment with a resolution of 2 mm were obtained with a *pH* micro-electrode.

### Laboratory procedures

Dissolved *Fe* and *Mn* were determined in the acidified headspace samples with a Perkin Elmer graphic furnace atomic absorption spectrophotometer equipped with Zeeman background correction.  $\text{NO}_3^-$ ,  $\text{NO}_2^-$ ,  $\text{NH}_4^+$  and  $\text{SO}_4^{2-}$  were measured using an auto-analyzer.  $\Sigma\text{H}_2\text{S}$  ( $\text{H}_2\text{S}$ ,  $\text{HS}^-$  and  $\text{S}^{2-}$ ) was determined by spectrophotometry (Cline, 1969).

The sediment from the glass vials was analyzed for iron sulfides (*FeS* and *FeS*<sub>2</sub>) and dithionite-extractable iron. Samples were transferred into a Coy anaerobic chamber (Coy Laboratory Products, Ann Arbor, Michigan) with an atmosphere of 5% hydrogen plus 95% nitrogen. Any traces of oxygen were consequently removed by reaction with hydrogen.

Acid Volatile Sulfide (AVS), the sum of free sulfide and *FeS*, was determined by cold acid distillation (Fossing and Jørgensen, 1989). About 0.5 g homogenized wet sediment was put into a 100 ml reaction vessel and acidified with 10 ml de-oxygenated 6.0 N *HCl*. The liberated  $\text{H}_2\text{S}$  was stripped from the slurry for 2 hours using  $\text{N}_2$  as carrier gas and trapped in 10 ml de-oxygenated  $\text{Zn}(\text{Ac})_2$  (2%). The concentration of *ZnS* in the traps was determined with the methylene-blue method (Cline, 1969).

Pyrite was determined by the chromium reduction method (Zhabina and Volkov, 1978; Canfield et al., 1986). The samples were dried (40°C) and extracted with acetone to remove AVS, organic polysulfides and elemental sulfur (Passier et al., 1996). About 10 mg acetone extracted sediment was put into a 100 ml reaction vessel and degassed for 20 minutes with  $\text{N}_2$ . Subsequently 16 ml 1 M  $\text{Cr}^{2+}$  in 0.5 N *HCl* and 8 ml de-oxygenated 12 N *HCl* were added to the sample. The sulfide generated was stripped from the solution for 2 hours and trapped in 10 ml  $\text{Zn}(\text{Ac})_2$  (2%). The *ZnS* in the traps was measured spectrophotometrically as described above.

Dithionite extractable iron content was determined in duplicate following Kostka & Luther (1994). Ten ml dithionite (sodium dithionite 50 g l<sup>-1</sup> in 0.2 M sodium citrate / 0.35 M acetic acid *pH*=4.8) was added to 0.5 – 1.0 g wet weight sediment in 20 ml glass vials. The vials were vortex mixed and shaken for 2 hours on a rotary shaker. After extraction, the samples were filtered and stored > 1 day to oxidize the dithionite (Canfield et al., 1993b). Total iron [*Fe*(II) + *Fe*(III)] in the sample was determined with reducing ferrozine. Dithionite is supposed to extract *Fe*(III) from poorly and well crystallized *Fe*-oxides (except magnetite) and *Fe*(II) from AVS and carbonates or adsorbed to sedimentary particles (Canfield, 1989b, Canfield et al., 1993b). The amount of *Fe*(OH)<sub>3</sub> in the sediment was estimated by the difference between the dithionite-extractable iron and the iron present in *FeS*.

Water content was calculated from weight loss. The porosity was calculated from the water content assuming a sediment density of 2.55 g cm<sup>-3</sup>. Organic carbon was determined with a Carlo Erba NA 1500 elemental analyzer, after *in situ* hydrochloric acid (25%) acidification to remove the inorganic carbon (Nieuwenhuize et al., 1994).

Chl-*a* was extracted from freeze-dried samples using methanol (95%) buffered with ammonium acetate and sonicated for 10 minutes. The extracts were analyzed for chloropigments by reverse-phase high performance liquid chromatography (RP-HPLC).



## Concept of the model

### *Generalized diagenetic equation*

Models for early diagenesis are usually based on the so-called General Diagenetic equation, an Advection–Diffusion–Reaction type of equation (Berner, 1980b; Boudreau, 1997):

$$\frac{\partial \xi C_i}{\partial t} = -\frac{\partial}{\partial x} \left[ -\xi D \frac{\partial C_i}{\partial x} + \omega \xi C_i \right] + \sum \xi REAC_i, \quad (4.1)$$

where  $x$  is sediment depth (cm),  $t$  is time (d) and  $\xi C_i$  is the concentration of species  $i$  (in units of  $\text{mol cm}^{-3}$  bulk sediment). For solute species  $\xi$  stands for porosity and for solid components  $\xi$  stands for (1-porosity).  $D$  is the total dispersion–diffusion coefficient ( $\text{cm}^2 \text{d}^{-1}$ ),  $\omega$  is the advection rate ( $\text{cm d}^{-1}$ ) and  $\sum \xi REAC_i$  is the sum of all production/consumption of species  $i$  in biogeochemical reactions ( $\text{mol cm}^{-3}$  bulk sediment  $\text{d}^{-1}$ ). The transport processes included are molecular diffusion and bio-irrigation for solute species, bioturbation for solid components and advection for both solids and solutes.

At the lower boundary concentrations of solid and dissolved components do not change with depth (zero gradient boundary). The upper boundary condition for dissolved components is the bottom water concentration and a deposition flux is imposed for the solid components. The model is able to calculate steady-state profiles as well as to run dynamically under time-variable forcing, using the steady-state concentration profiles as a starting condition.

### *Biogeochemical processes*

#### **State variables**

A set of 14 state variables was included in the model (Table 4.1). Concentrations of dissolved species are all expressed in units of  $\mu\text{mol L}^{-1}$  pore water and those for solid species in units of  $\mu\text{mol dm}^{-3}$  total solids. Since benthic primary production on the Black Sea continental shelf can be neglected, it can be assumed that all the oxygen originates from the water column. In the sediment oxygen is consumed by the degradation of organic matter and the re-oxidation of reduced substances. The flux of oxygen is consequently always directed into the sediment. Nitrate can either be consumed (denitrification) or produced (nitrification) in the sediment. Depending on the relative importance of these processes and the nitrate concentration of the bottom water, there may either be an influx or an outflux of nitrate into the sediment. Sulfate is a major constituent in the seawater and is used as an oxidant for degradation processes by sulfate reducers. The other dissolved species ( $\text{NH}_4^+$ ,  $\text{Mn}^{2+}$ ,  $\text{Fe}^{2+}$ ,  $\text{SH}_2\text{S}$  and  $\text{CH}_4$ ) are reduced components that are produced during degradation of organic matter. In general there is an outflux of these components from the sediment. A constant fraction of ammonium is adsorbed to the sediment (Berner, 1980b; Soetaert et al., 1996a). Adsorption of  $\text{Fe}^{2+}$  and  $\text{Mn}^{2+}$  to sediment particles (Van Cappellen and Wang, 1996) is not taken into account.

**Table 4.1.** Dissolved and solid species included in the model. Units of the dissolved species are  $\mu\text{mol L}^{-1}$  and units of solid species are  $\mu\text{mol dm}^{-3}$

Solute species	Solid Species
$O_2$	$(CH_2O)_x(NH_3)_y(H_3PO_4)_{fast}$
$NO_3^-$	$(CH_2O)_x(NH_3)_y(H_3PO_4)_{slow}$
$SO_4^{2-}$	$MnO_2$
$NH_4^+$	$Fe(OH)_3$
$Mn^{2+}$	$FeS$
$Fe^{2+}$	$FeS_2$
$\Sigma H_2S$	
$CH_4$	

The model does not resolve sulfide speciation ( $H_2S$ ,  $HS^-$  and  $S^{2-}$ ). However, this is not necessary because the  $pH$  is imposed (see below) and the concentrations of these sulfide components can be calculated from the total sulfide ( $\Sigma H_2S$ ) concentration. In marine sediments the  $pH$  is always lower than 12 and the contribution of the sulfide ion ( $S^{2-}$ ) can therefore be neglected (Goldhaber and Kaplan, 1975). The  $H_2S$  concentration at a specific  $pH$  value is then calculated from the total sulfide concentration  $\Sigma H_2S$ :

$$[H_2S] = \left( 1 - \frac{K'_1}{10^{-pH}} \right)^{-1} \cdot [\Sigma H_2S], \quad (4.2)$$

where the dissociation constant ( $K'_1$ ) is depending on temperature and salinity (Millero, 1986). The remainder of the total sulfide is bisulfide ( $HS^- = \Sigma H_2S - H_2S$ ).

Six solid components are distinguished in the model, including fast and slow decaying organic carbon, represented as  $(CH_2O)_x(NH_3)_y(H_3PO_4)_{fast}$  and  $(CH_2O)_x(NH_3)_y(H_3PO_4)_{slow}$  respectively. The coefficients  $x$  and  $y$  denote molar  $C:P$  and  $N:P$  ratios respectively. This organic matter is deposited from the water column and degraded in the sediment. Two metal oxides, manganese oxide ( $MnO_2$ ) and iron (hydr)oxides ( $Fe(OH)_3$ ) reach the sediment by sedimentation and are formed by oxidation. A fraction of the  $Fe(OH)_3$  reaching the sediment is assumed not to be reducible on the timescale relevant for early diagenesis. Iron monosulfide ( $FeS$ ) and pyrite ( $FeS_2$ ) are formed by interaction of sulfide and ferrous iron.

An important difference with the models of Boudreau (1996a) and Van Cappellen and Wang (1996) is that the alkalinity conservation equation is not included and it is therefore not possible to model the  $pH$ -profiles. The  $pH$  profile was therefore imposed via a fourth-order polynome for a depth less than 8 cm (Figure 4.2). The  $pH$  was assumed not to change at depths  $> 8$  cm. Imposing rather than modeling sediment  $pH$  not only simplifies the model and significantly reduces computing time, but also reduces uncertainty in modeling  $pH$  dependent processes. Minimization of computing time is a requirement for coupling with water column biogeochemical models. Our understanding of the factors controlling sedimentary  $pH$  values is rather incomplete so that models are not yet able to accurately produce  $pH$  profiles (Boudreau, 1996a; Van Cappellen and Wang, 1996; Meysman, pers. Comm. 1999).

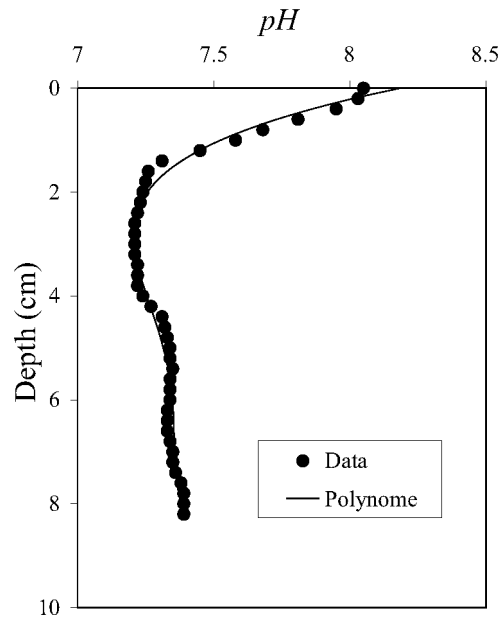


**Figure 4.2.** *pH* versus depth. A fourth-order polynome (solid line) was fitted through the measured data (dots). This polynome was used as a forcing function for the model

### Mineralization reactions

The degradation of organic matter is an oxidative process that requires an electron acceptor. The sequence in which the electron acceptors are utilized is determined by the inhibition of various oxidants on the different mineralization pathways (Van Cappellen et al., 1993). In marine sediments the organic matter is initially decomposed by aerobic respiration. When the oxygen in the interstitial water is depleted, the remainder of the organic matter will be degraded successively by denitrification, manganese reduction, iron reduction, sulfate reduction and finally methanogenesis till all metabolizable organic matter is depleted (Froelich et al., 1979).

A variety of enzymatic reactions involving a variety of organisms take part in the decomposition of sedimentary organic matter. During this decomposition various intermediate compounds are produced. Despite the complexity of the reactions, the main pathways of the degradation of organic matter can be described by standard set of overall reactions (Table 4.2).

### Kinetic formulations – mineralization reactions

Organic detritus is composed of many different substrates with different degradability. It is supposed that microbial communities sequentially consume the different organic fractions according to their decreasing reactivity. As a result the overall reactivity of the organic matter decreases with time (Berner, 1980a; Westrich and Berner, 1984). Different models are generally used to describe this decrease in degradability during decomposition (Middelburg, 1989; Boudreau and Ruddick, 1991). In this paper we applied a multi-G type of model (Berner, 1980a; Westrich and Berner, 1984).

The organic matter is divided into three fractions. The "refractory" organic matter is defined as the fraction that is not utilized by microorganisms in the timescale

**Table 4.2.** Mineralization reactions included in the model. In bold are the components that are modeled. Organic matter is represented by  $(CH_2O)_x(NH_3)_y(H_3PO_4)$  where  $x$  and  $y$  denote the molar  $C/P$ - and  $N/P$ -ratios of the organic matter respectively

<p>Aerobic respiration</p> $(CH_2O)_x(NH_3)_y(H_3PO_4) + xO_2 + yH^+ \rightarrow xCO_2 + yNH_4^+ + HPO_4^{2-} + 2H^+ + xH_2O$
<p>Denitrification</p> $(CH_2O)_x(NH_3)_y(H_3PO_4) + \frac{4}{5}xNO_3^- + (\frac{4}{5}x + y)H^+ \rightarrow xCO_2 + yNH_4^+ + \frac{2}{5}xN_2 + HPO_4^{2-} + \frac{7}{5}xH_2O$
<p>Dissimilatory manganese reduction</p> $(CH_2O)_x(NH_3)_y(H_3PO_4) + 2xMnO_2 + (4x + y)H^+ \rightarrow xCO_2 + 2xMn^{2+} + yNH_4^+ + HPO_4^{2-} + 2H^+ + 3xH_2O$
<p>Dissimilatory iron reduction</p> $(CH_2O)_x(NH_3)_y(H_3PO_4) + 4xFe(OH)_3 + (8x + y)H^+ \rightarrow xCO_2 + 4xFe^{2+} + yNH_4^+ + HPO_4^{2-} + 2H^+ + 11xH_2O$
<p>Sulfate reduction</p> $(CH_2O)_x(NH_3)_y(H_3PO_4) + \frac{1}{2}xSO_4^{2-} + (\frac{1}{2}x + y)H^+ \rightarrow xCO_2 + \frac{1}{2}x\Sigma H_2S + yNH_4^+ + HPO_4^{2-} + H^+ + xH_2O$
<p>Methanogenesis</p> $(CH_2O)_x(NH_3)_y(H_3PO_4) + yH^+ \rightarrow \frac{1}{2}xCO_2 + \frac{1}{2}xCH_4 + yNH_4^+ + HPO_4^{2-} + 2H^+$

of early diagenesis. The reactive organic matter is divided in a fast and a slow decaying fraction with different stoichiometry. A Redfield  $N/C$  ratio (0.1509) is assumed for the fast decaying fraction. The slow decaying organic matter is assumed to be poorer in nitrogen and a  $N/C$  ratio of 0.105 was derived by model calibration. The result is that the model simulates the increase in  $N/C$  ratio with depth in the sediment that is observed in coastal, marine and estuarine sediments (Jørgensen, 1983; Klump and Martens, 1987; Burdige, 1991). The first-order degradation constant at 20°C for the fast decaying organic matter is  $7.53 \times 10^{-2} \text{ d}^{-1}$  (Westrich and Berner, 1984; Boudreau and Ruddick, 1991). For the slow decaying part, a degradation constant of  $3.0 \times 10^{-3} \text{ d}^{-1}$  was derived by model calibration. The rate constants are corrected for temperature, assuming a  $Q_{10}$ -value of 2 (Wells, 1980; Piepenburg et al., 1995). The ratio between the fast and slow decaying organic matter sedimenting on the bottom is dependent on the water depth (Soetaert et al., 1996a), and is included in the model as an input parameter.

It has been well recognized that the rate of metabolic activity of each degradation pathway is not only depending on the reactivity of the organic matter, but also on the availability of the electron acceptor (Rabouille and Gaillard, 1991a; Dhakar and Burdige, 1996). The limitation of oxidants is modeled by a Monod-type hyperbolic limitation function (Boudreau and Westrich, 1984; Soetaert et al., 1996a)

$$Limit = \frac{[EA]}{[EA] + K_m}, \quad (4.3)$$

**Table 4.3.** Parameter values used in the model simulations. *M*: parameters derived by model calibration; *A*: independent parameters that have been assumed; *D*: independent parameters based on observations

Parameter	Value	Units	Description	
$Db_0$	$3.3 \times 10^{-2}$	$\text{cm}^2 \text{d}^{-1}$	Bioturbation coefficient in bioturbated layer ( $0-x_b$ cm)	<i>M</i>
$x_b$	1	cm	Thickness of constant bioturbation layer	<i>M</i>
$coeff_{db}$	1	cm	Coefficient for exponential bioturbation decrease	<i>M</i>
$\omega$	$3 \times 10^{-4}$	$\text{cm d}^{-1}$	Sedimentation rate	<i>M</i>
$PF_{det}$	0.29	-	Part of reactive organic matter that is fast decaying	<i>M</i>
$T$	5.8	$^{\circ}\text{C}$	Temperature of the bottom water	<i>D</i>
$O_2(\text{bw})$	295	$\mu\text{M}$	Oxygen concentration in the bottom water	<i>D</i>
$NO_3(\text{bw})$	5	$\mu\text{M}$	Nitrate concentration in the bottom water	<i>A</i>
$NH_3(\text{bw})$	0.58	$\mu\text{M}$	Ammonia concentration in the bottom water	<i>D</i>
$Mn(\text{bw})$	0	$\mu\text{M}$	Manganese concentration in the bottom water	<i>A</i>
$Fe(\text{bw})$	0	$\mu\text{M}$	Ferrous iron concentration in the bottom water	<i>A</i>
$SO_4(\text{bw})$	$1.604 \times 10^4$	$\mu\text{M}$	Sulfate concentration in the bottom water	<i>A</i>
$H_2S(\text{bw})$	0	$\mu\text{M}$	Hydrogen sulfide concentration in the bottom water	<i>A</i>
$CH_4(\text{bw})$	0	$\mu\text{M}$	Methane concentration in the bottom water	<i>A</i>
$MnO_2\text{-flux}$	0.01	$\mu\text{mol Mn cm}^{-2} \text{d}^{-1}$	Manganese-oxide flux to the sediment	<i>M</i>
$Fe(OH)_3\text{-flux}$	0.028	$\mu\text{mol Fe cm}^{-2} \text{d}^{-1}$	Iron-oxide flux to the sediment	<i>M</i>
$FeS\text{-flux}$	0	$\mu\text{mol FeS cm}^{-2} \text{d}^{-1}$	Iron-monosulfide flux to the sediment	<i>A</i>
$FeS_2\text{-flux}$	0	$\mu\text{mol FeS}_2 \text{cm}^{-2} \text{d}^{-1}$	Pyrite flux to the sediment	<i>A</i>
$R_{m1}$	$7.53 \times 10^{-2}$	$\text{d}^{-1}$	First order degradation constant fast decaying detritus at $20^{\circ}\text{C}$	(1)
$R_{m2}$	$3 \times 10^{-3}$	$\text{d}^{-1}$	First order degradation constant slow decaying detritus at $20^{\circ}\text{C}$	(1)
$Q_{10}$	2	-	$Q_{10}$ -factor organic matter degradation	<i>A</i>
$\Sigma R_{min}$	0.5	$\text{mmol C cm}^{-2} \text{yr}^{-1}$	Total depth-integrated carbon mineralization rate	<i>M</i>
$IrrEnh$	2.5	-	Irrigation enhancement factor	<i>M</i>
$NH_3\text{-ads}$	1.3	-	Adsorption coefficient of ammonia	(1)
$\gamma_{TOC1}$	0.1509	$\text{mol N (mol C)}^{-1}$	$N/C$ ratio of fast decaying detritus	(1)
$\gamma_{TOC2}$	0.105	$\text{mol N (mol C)}^{-1}$	$N/C$ ratio of slow decaying detritus	<i>M</i>
$K_{in}(O_2 \text{ denit})$	10	$\mu\text{M } O_2$	Half-saturation conc. $O_2$ inhibition for denitrification	(1)
$K_{in}(O_2)$	8	$\mu\text{M } O_2$	Half-saturation conc. $O_2$ inhibition for anoxic mineralization	(2)
$K_{in}(NO_3)$	10	$\mu\text{M } NO_3$	Half-saturation conc. $NO_3$ inhibition	(2)
$K_{in}(MnO_2)$	5000	$\mu\text{mol MnO}_2 \text{dm}^{-3}$	Half-saturation conc. $MnO_2$ inhibition	(2)
$K_{in}(Fe(OH)_3)$	$1.25 \times 10^4$	$\mu\text{mol Fe(OH)}_3 \text{dm}^{-3}$	Half-saturation conc. $Fe(OH)_3$ inhibition	(2)
$K_{in}(SO_4)$	1000	$\mu\text{M } SO_4$	Half-saturation conc. $SO_4$ inhibition	(2)
$K_s(O_2)$	3.1	$\mu\text{M } O_2$	Half-saturation conc. $O_2$ limitation for oxic mineralization	(1)
$K_s(\text{nit})$	1	$\mu\text{M } O_2$	Half-saturation conc. $O_2$ limitation for nitrification	(1)
$K_s(NO_3)$	30	$\mu\text{M } NO_3$	Half-saturation conc. $NO_3$ limitation for nitrification	(1)
$K_s(MnO_2)$	5000	$\mu\text{mol MnO}_2 \text{dm}^{-3}$	Half-saturation conc. $MnO_2$ limitation for manganese reduction	(2)
$K_s(Fe(OH)_3)$	$1.25 \times 10^4$	$\mu\text{mol Fe(OH)}_3 \text{dm}^{-3}$	Half-saturation conc. $Fe(OH)_3$ limitation for iron reduction	<i>M</i>
$K_s(SO_4)$	1620	$\mu\text{M } SO_4$	Half-saturation conc. $SO_4$ limitation for sulfate reduction	(3)
$K_{sFeS}$	$6.31 \times 10^3$	$\mu\text{M}$	Saturation constant $FeS$	(4)
$k_{nitr}$	20	$\text{d}^{-1}$	Rate constant nitrification	(1)
$k_{MnO_2}$	$1.37 \times 10^{-2}$	$\mu\text{M}^{-1} \text{d}^{-1}$	Rate constant $Mn^{2+}$ oxidation by $O_2$	(4)
$k_{FeO_2}$	$2.938 \times 10^{-1}$	$\mu\text{M}^{-3} \text{d}^{-1}$	Rate constant $Fe^{2+}$ oxidation by $O_2$	(5)
$k_{H_2SO_2}$	$4.39 \times 10^{-4}$	$\mu\text{M}^{-1} \text{d}^{-1}$	Rate constant $H_2S$ oxidation by $O_2$	(4)
$k_{CH_4O_2}$	27.4	$\mu\text{M}^{-1} \text{d}^{-1}$	Rate constant $CH_4$ oxidation by $O_2$	(4)
$k_{FeSO_2}$	$8.22 \times 10^{-4}$	$\mu\text{M}^{-1} \text{d}^{-1}$	Rate constant $FeS$ oxidation by $O_2$	(4)
$k_{pyrO_2}$	$4.38 \times 10^{-4}$	$\mu\text{M}^{-1} \text{d}^{-1}$	Rate constant $FeS_2$ oxidation by $O_2$	<i>M</i>
$k_{FeMn}$	$8.22 \times 10^{-3}$	$\mu\text{M}^{-1} \text{d}^{-1}$	Rate constant $Fe^{2+}$ oxidation by $MnO_2$	(4)
$k_{H_2SMn}$	$5.48 \times 10^{-5}$	$\mu\text{M}^{-1} \text{d}^{-1}$	Rate constant $H_2S$ oxidation by $MnO_2$	(4)
$k_{H_2SFe}$	$1 \times 10^{-7}$	$\mu\text{M}^{-1} \text{d}^{-1}$	Rate constant $H_2S$ oxidation by $Fe(OH)_2$	<i>M</i>
$k_{CH_4SO_4}$	$2.74 \times 10^{-5}$	$\mu\text{M}^{-1} \text{d}^{-1}$	Rate constant $CH_4$ oxidation by $SO_4^{2-}$	(4)
$k_{FeS,1}$	1	$\mu\text{M}^{-1} \text{d}^{-1}$	Rate constant $FeS$ formation	(4)
$k_{FeS,2}$	$2.74 \times 10^{-6}$	$\text{d}^{-1}$	Rate constant $FeS$ dissolution	(4)
$k_{pyrite}$	$8.90 \times 10^{-6}$	$\mu\text{M}^{-1} \text{d}^{-1}$	Rate constant pyrite formation	(6)

(1) (Soetaert et al., 1996a), (2) (Van Cappellen and Wang, 1995), (3) (Boudreau and Westrich, 1984), (4) (Van Cappellen and Wang, 1996), (5) (Millero et al., 1987), (6) (Rickard, 1997b)

where  $[EA]$  is the concentration of the limiting electron acceptor and  $K_m$  is the half-saturation concentration. The  $K_m$ -values used in the model are given in table 4.3. In addition, the presence of oxidants may inhibit the oxidation of carbon by energetically less powerful electron acceptors. This inhibition is described by a reciprocal hyperbolic function (Van Cappellen et al., 1993; Soetaert et al., 1996a)

$$Inhib = \left( 1 - \frac{[IN]}{[IN] + K_{in}} \right), \quad (4.4)$$

where  $[IN]$  is the concentration of the inhibiting oxidant and  $K_{in}$  is the inhibition constant. The inhibition constants used in the model have been derived from literature and are summarized in table 4.3. Mineralization proceeds up till all degradable carbon is removed. The degradation rates of the individual respiratory pathways are finally re-scaled to ensure that sum of the individual rates equals the total degradation rate (Soetaert et al., 1996a). As such the degradation rate of the organic matter is independent of the various oxidants and the organic carbon profile can be solved independently of the distribution of the other components in the sediment (Soetaert et al., 1996a). The result of the use of limitation and inhibition functions is that the model represents the spatial sequence of the successive degradation pathways as observed in marine sediment. The extent of vertical overlap between the various mineralization processes can be adjusted with the parameters  $K_m$  and  $K_{in}$ .

### Secondary reactions

The mineralization reactions of the organic matter produce a variety of reduced pore-water species such as  $NH_4$ ,  $Mn$ ,  $Fe$ ,  $H_2S$  and  $CH_4$ . These reduced substances diffuse upward in the sediment column, where they are re-oxidized in a more oxidized environment. When sulfide produced by sulfate reduction meets ferrous iron it can form iron monosulfide ( $FeS$ ), which can again react with sulfide to form pyrite ( $FeS_2$ ). The secondary reactions incorporated in the model are given in table 4.4. A description of the various reactions can be found in Boudreau (1996a) and Van Cappellen and Wang (1996) and references therein.

### Kinetic formulations – secondary reactions

The kinetics of most secondary redox reactions in the sediment is not fully understood. Microorganisms mediate most, if not all the reactions and Monod-type kinetics seems to be appropriate. Nitrification is described by Monod-type kinetics and it is assumed that the ammonium produced by aerobic mineralization is directly converted into nitrate (Soetaert et al., 1996a)

$$R_{nitr} = k_{nitr} \cdot [NH_3] \cdot \frac{[O_2]}{[O_2] + K_s(nit)} + N_{coupled}, \quad (4.5)$$

where  $R_{nitr}$  is the rate of nitrification ( $\mu M d^{-1}$ ),  $k_{nitr}$  is the rate constant for nitrification ( $d^{-1}$ ),  $K_s(nit)$  is the half saturation constant ( $\mu M$ ) and  $N_{coupled}$  is the rate of nitrification coupled to the oxic degradation of organic matter ( $\mu M d^{-1}$ ).

For most other re-oxidation reactions we followed Van Cappellen and Wang (1996), who used bi-molecular reaction rate laws to describe the reaction kinetics. Bi-molecular kinetics approaches Monod-kinetics when the concentrations of both electron acceptor and electron donor are low. In natural sediments the secondary redox reactions are often confined to areas of limiting concentrations (Berner, 1980b; Van Cappellen and Wang, 1996). Reaction rates have then first-order dependence on the electron acceptor and donor.

$$R = k \cdot [EA] \cdot [ED], \quad (4.6)$$

**Table 4.4.** Secondary reactions included in the model. In bold are the modeled components

Re-oxidation reactions with oxygen as oxidant $NH_4^+ + 2O_2 + 2HCO_3^- \rightarrow NO_3^- + 2CO_2 + 3H_2O$ $Mn^{2+} + \frac{1}{2}O_2 + 2HCO_3^- \rightarrow MnO_2 + 2CO_2 + H_2O$ $Fe^{2+} + \frac{1}{4}O_2 + 2HCO_3^- + \frac{1}{2}H_2O \rightarrow Fe(OH)_3 + 2CO_2$ $\Sigma H_2S + 2O_2 + 2HCO_3^- \rightarrow SO_4^{2-} + 2CO_2 + 2H_2O$ $FeS + 2O_2 \rightarrow Fe^{2+} + SO_4^{2-}$ $FeS_2 + \frac{7}{2}O_2 + H_2O \rightarrow Fe^{2+} + 2SO_4^{2-} + 2H^+$ $CH_4 + 2O_2 \rightarrow CO_2 + 2H_2O$
Re-oxidation with Mn-Fe oxides as oxidant $MnO_2 + 2Fe^{2+} + HCO_3^- + 2H_2O \rightarrow Mn^{2+} + 2Fe(OH)_3 + 2CO_2$ $MnO_2 + \Sigma H_2S + 2CO_2 \rightarrow Mn^{2+} + S^0 + 2HCO_3^-$ $2Fe(OH)_3 + \Sigma H_2S + 4CO_2 \rightarrow 2Fe^{2+} + S^0 + 4HCO_3^- + 2H_2O$
Re-oxidation reactions with sulfate as oxidant $CH_4 + SO_4^{2-} + CO_2 \rightarrow 2HCO_3^- + \Sigma H_2S$
Precipitation reactions $Fe^{2+} + HS^- + HCO_3^- \leftrightarrow FeS + CO_2 + H_2O$ $FeS + H_2S \rightarrow FeS_2 + H_2$

where  $R$  is the reaction rate ( $\mu M d^{-1}$ ),  $k$  is the reaction rate constant ( $\mu M^{-1} d^{-1}$ ) and  $[EA]$  and  $[ED]$  are the concentrations of the electron acceptor and electron donor respectively ( $\mu M$ ). The rate constants were derived from Van Cappellen and Wang (1996) who give a compilation of model-derived and literature data (Table 4.3). Unlike Van Cappellen and Wang (1996), the re-oxidation of ferrous iron with oxygen is dependent on  $pH$  and is described in this model by (Millero et al., 1987):

$$R = k_{FeO_2} \cdot [O_2] \cdot [Fe^{2+}] \cdot [OH^-]^2, \quad (4.7)$$

where  $k_{FeO_2}$  is the reaction rate constant ( $\mu M^{-3} d^{-1}$ ).

The precipitation of  $FeS$  from  $Fe^{2+}$  and  $(HS^-)$  is a reversible reaction. The variable  $\Omega_{FeS}$  gives the degree of saturation of the pore water with  $Fe^{2+}$  and  $HS^-$ :

$$\Omega_{FeS} = \frac{[Fe^{2+}] \cdot [HS^-]}{\{H^+\} \cdot Ks_{FeS}}, \quad (4.8)$$

where  $Ks_{FeS}$  is the apparent solubility product. When  $\Omega_{FeS} > 1$ , precipitation takes place at a rate of

$$\frac{dFeS}{dt} = k_{FeS,1} \cdot (\Omega - 1) \quad (4.9)$$

and when  $\Omega_{FeS} < 1$ , dissolution of  $FeS$  takes place at a rate of

$$\frac{dFeS}{dt} = -k_{FeS,2} \cdot [FeS] \cdot (1 - \Omega), \quad (4.10)$$

where  $k_{FeS,1}$  and  $k_{FeS,2}$  are forward and backward first-order rate constants respectively.

The formation of pyrite is described by bi-molecular rate kinetics (Rickard, 1997a, Rickard, 1997b).

$$\frac{dFeS_2}{dt} = k_{Pyrite} \cdot [FeS] \cdot [H_2S], \quad (4.11)$$

where  $k_{Pyrite}$  is the first order rate constant.

## Transport processes

### Molecular diffusion

Molecular diffusion is important for the dissolved pore water components. The free-solution diffusion coefficient ( $D^T$ ) (units of  $\text{cm}^2 \text{s}^{-1}$ ) for electrolytes at the ambient temperature  $t$  ( $^{\circ}\text{C}$ ) is calculated from the zero-degree coefficient  $D^0$ :

$$D^T = D^0 + \alpha t, \quad (4.12)$$

where  $\alpha$  is an ion-specific coefficient. The regression parameters  $D^0$  and  $\alpha$  for the electrolytes included in the model are given in table 4.5.

**Table 4.5.** Linear regression coefficients free-solution diffusion coefficient  $D^T$  ( $10^{-6} \text{ cm}^2 \text{s}^{-1}$ ) versus temperature  $t$  ( $^{\circ}\text{C}$ ). Adapted from Boudreau (1997) based on data from Li and Gregory (1974)

Cations	$D^0$ ( $10^{-6} \text{ cm}^2 \text{s}^{-1}$ )	$\alpha$ ( $10^{-6} \text{ cm}^2 \text{s}^{-1} ^{\circ}\text{C}^{-1}$ )	Anions	$D^0$ ( $10^{-6} \text{ cm}^2 \text{s}^{-1}$ )	$\alpha$ ( $10^{-6} \text{ cm}^2 \text{s}^{-1} ^{\circ}\text{C}^{-1}$ )
$NH_4^+$	9.50	0.413	$NO_3^-$	9.50	0.388
$Fe^{2+}$	3.31	0.150	$HS^-$	10.4	0.273
$Mn^{2+}$	3.43	0.144	$SO_4^{2-}$	4.88	0.232

For the non-electrolyte  $CH_4$ , the free solution diffusion coefficient is described by an empirical correlation developed by Wilke and Chang (1955) and corrected by Hayduk and Laudie (1974)

$$D^T = 4.72 \cdot 10^{-9} \cdot \frac{T}{\mu V_b^{0.6}}, \quad (4.13)$$

where  $D^T$  is the free-solution diffusion coefficient ( $\text{cm}^2 \text{s}^{-1}$ ),  $T$  is the absolute temperature ( $^{\circ}\text{K}$ ),  $\mu$  is the dynamic viscosity in units of poise ( $\text{g cm}^{-1} \text{s}^{-1}$ ) and  $V_b$  is  $37.7 \text{ cm}^3 \text{mol}^{-1}$  for  $CH_4$  (Hayduk and Laudie, 1974).

Finally for  $O_2$ , the following empirical relation is used to calculate  $D^T$  (Boudreau, 1997)



$$D^T = (0.2604 + 0.006383 \cdot (\frac{T}{\mu \cdot 0.01})) \cdot 10^{-5}, \quad (4.14)$$

where  $T$  is the absolute temperature (°K) and  $\mu$  is the dynamic viscosity in units of poise ( $\text{g cm}^{-1} \text{s}^{-1}$ ).

The diffusion coefficient of a dissolved substance in the sediment ( $D_s^T$ ) is lower than its free-solution diffusion coefficient in water ( $D^T$ ) because of the convoluted path molecules must follow to circumvent the sediment particles. According to Berner (1980b),  $D_s^T$  is related to  $D^T$  by:

$$D_s^T = \frac{D^T}{\theta^2}, \quad (4.15)$$

where  $\theta$  is the tortuosity of the sediment. The tortuosity is related to the sediment porosity (Boudreau, 1996b). In this model we used Archie's Law with the empirical coefficient  $m$  set to 3 (Ullman and Aller, 1982; Reimers et al., 1992). The effective diffusion coefficient of a dissolved substance in the sediment is then calculated as (Soetaert et al., 1996a)

$$D_s^T = D^T \cdot \phi^2 \quad (4.16)$$

### Advection

Advection is the process of material transport due to deposition of new material at the sediment surface (Berner, 1980b). As a result of this deposition the sediment will be compacted. In general compaction results in an increasing advection rate with sediment depth for solute substances and a decrease in advection rate with depth for solids (Rabouille and Gaillard, 1991a). We neglected the effect of compaction and assumed the rate of advection to be equal to the sedimentation rate for all components at all sediment depths.

Sediment compaction was not explicitly modeled, but the result of compaction, i.e. an exponential decrease of porosity with sediment depth was imposed (Berner, 1980b; Rabouille and Gaillard, 1991a; Rabouille and Gaillard, 1991b; Soetaert et al., 1996a):

$$\phi_x = \phi_\infty + (\phi_0 - \phi_\infty) \cdot e^{-\tau \cdot x}, \quad (4.17)$$

where  $\phi_0$  and  $\phi_\infty$  are the porosity at the sediment water interface and at infinitive depth respectively and  $\tau$  is the attenuation coefficient ( $\text{cm}^{-1}$ ). For station 9, the parameters  $\phi_0$  ( $= 0.95$ ),  $\phi_\infty$  ( $= 0.73$ ) and  $\tau$  ( $= 0.23 \text{ cm}^{-1}$ ) were derived by least squares curve fitting (Figure 4.3).

### Bioturbation

Bioturbation, the process of sediment displacement by the activity of benthic organisms, is modeled as a random diffusion-like process (Boudreau, 1986). It is assumed to be constant in the upper part of the sediment ( $0 \leq x \leq x_b$ ) and decreasing exponentially at depth  $> x_b$  (Figure 4.4):

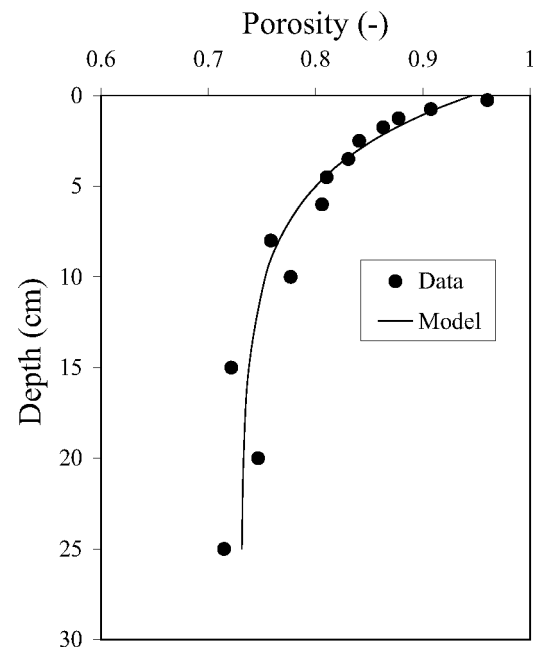


**Figure 4.3.** Sediment porosity versus depth. The solid line represents the exponential curve that was fitted through the data

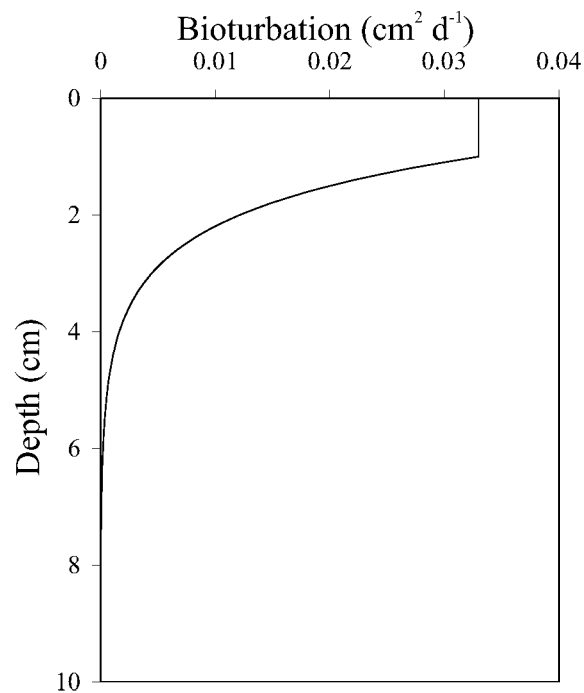


**Figure 4.4.** Imposed bioturbation profile

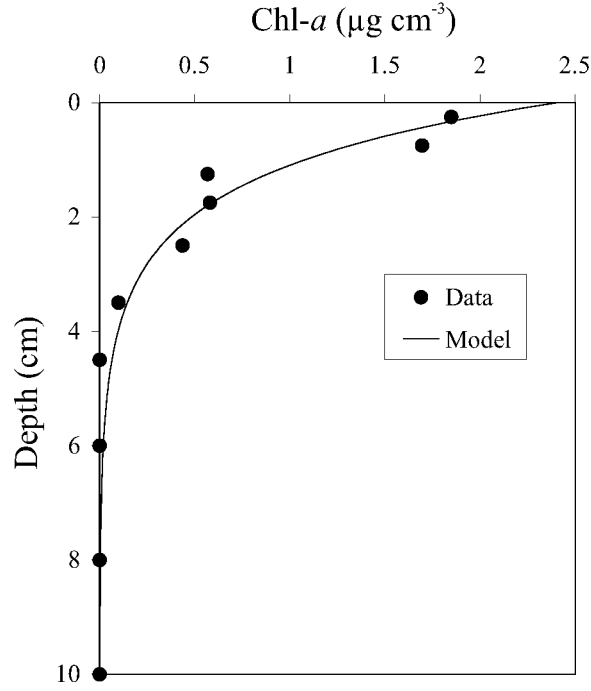


**Figure 4.5.** Chlorophyll *a* ( $\mu\text{g cm}^{-3}$  bulk sediment) versus depth. The solid line was derived by curve fitting of a simple advection–diffusion–reaction equation through the data

$$Db_x = \begin{cases} Db_0 & (x \leq x_b) \\ Db_0 \cdot e^{-\frac{x-x_b}{\text{coeff}Db}} & (x > x_b) \end{cases}, \quad (4.18)$$

where  $Db_x$  the rate of bioturbation at depth  $x$  ( $\text{cm}^2 \text{d}^{-1}$ ) and  $\text{coeff}Db$  is the coefficient for exponential bioturbation decrease (cm).

The rate of bioturbation has been derived by least squares curve-fitting of the depth profiles of chlorophyll *a* in the sediment (Figure 4.5). Assuming steady-state conditions, constant porosity, no compaction and first order degradation, the chlorophyll *a* kinetics can be described by (Sun et al., 1994; Soetaert et al., 1996c; Boon and Duineveld, 1998)

$$\frac{\partial C}{\partial t} = Db_0 \cdot \left( \frac{\partial^2 C}{\partial x^2} \right) - \omega \left( \frac{\partial C}{\partial x} \right) - k \cdot C, \quad (4.19)$$

where  $C$  is the chlorophyll *a* concentration (in units of  $\mu\text{g dm}^{-3}$  bulk sediment),  $\omega$  is the advection rate ( $\text{cm d}^{-1}$ ) and  $k$  is the first order degradation rate of chlorophyll *a* ( $\text{d}^{-1}$ ). Based on cesium data from Curtis & Broadway (1992) the advection rate ( $\omega$ ) on the continental shelf of the Black Sea has been estimated to be typically lower than  $2.7 \times 10^{-3} \text{ cm d}^{-1}$  (i.e.  $1 \text{ cm yr}^{-1}$ ). The first-order degradation constant ( $k$ ) for chlorophyll *a* is assumed to range between 0.02 and 0.04  $\text{d}^{-1}$  and depends on temperature (Sun et al., 1991). With no advection ( $\omega = 0$ ), the calculated bioturbation ranged between  $3.1 \times 10^{-2} - 6.2 \times 10^{-2} \text{ cm}^2 \text{d}^{-1}$ . An advection rate of  $2.7 \times 10^{-3} \text{ cm d}^{-1}$

resulted in a slight decrease of derived bioturbation coefficients ( $2.8 \times 10^{-2} - 5.9 \times 10^{-2} \text{ cm}^2 \text{ d}^{-1}$ ). It should be noticed that selective feeding by organisms might result in differences in bioturbation efficiencies with labile organic matter being mixed at a higher rate than more refractory organic matter and inorganic particles (Smith et al., 1993; Soetaert et al., 1998).

### Bio-irrigation

Bio-irrigation is the result of construction of tubes by benthic organisms and their ventilation, which causes enhanced exchange of interstitial water with the overlying water (Aller, 1988; Aller and Aller, 1992). As a result the apparent diffusion coefficient in the sediment is increased. In the model we applied a diffusion enhancement factor (*IrrEnh*) of 2.5 for station 9. The apparent sediment diffusion coefficient  $D_{sed}$  is calculated from the sediment diffusion coefficient  $D_S^T$  multiplied by *IrrEnh*. The irrigation enhancement factor is maximum in the layer of maximum bioturbation ( $0 \leq x \leq x_b$ ) and then decreases exponentially to  $D_S^T$  at infinite depth:

$$D_{sed} = \begin{cases} IrrEnh \cdot D_S^T & (x \leq x_b) \\ D_S^T \cdot \left( 1 + (IrrEnh - 1) \cdot e^{-\frac{(x-x_b)}{coeffDb}} \right) & (x > x_b) \end{cases} \quad (4.20)$$

## Numerical methodology

Since the differential equations in this model are non-linear and highly coupled, and because of the use of depth-variable profiles for porosity, bioturbation and *pH*, the system of differential equations can only be solved numerically. The sediment column is divided into  $n$  separate layers. The thickness of the first sediment layer ( $\Delta x_{sw}$ ) is 1 mm. (Soetaert et al., 1996a). The thickness of the subsequent layers ( $\Delta x_i$ ) increases exponentially with depth in the sediment:

$$\Delta x_i = \Delta x_{sw} \cdot \lambda^{i-1}, \quad (4.21)$$

where  $\lambda$  is the coefficient for the exponential increase in sediment thickness.

We applied the weighted finite differencing method of Fiadeiro and Veronis (1977) to describe the partial differential equations of the solid fractions numerically (Soetaert et al., 1996a). This scheme is appropriate when bioturbation is a function of depth, as is the case in this model. In the bioturbation area, diffusive-like processes will dominate the transport of the solid components and central differencing will be stable and second-order accurate (Boudreau, 1997). At greater sediment depth, advection gradually becomes the dominant transport process for the solid phase components. The central difference scheme is not stable anymore in this area and a switch to backward differences is required. The parameter  $\sigma$  describes this gradual switch from backward to central differencing:

$$\sigma = \frac{I}{\tanh(Pe_h)} - \frac{I}{Pe_h}, \quad (4.22)$$

where  $Pe_h$  is one-half of the cell Peclet number (Boudreau, 1996a):

$$Pe_h = \frac{\omega \cdot \Delta x}{2 \cdot Db_x} \quad (4.23)$$

When  $\sigma = 0$ , diffusive mixing dominates and a central differences scheme is used. When  $\sigma = 1$  advective transport processes dominate the transport and a backward differences scheme is used. For dissolved components, diffusive transport always dominates advective transport and is therefore described in a central differencing scheme. Both these numerical schemes can be used for unequally spaced grids and the mass budget is fully closed.

At steady state, the rates of change ( $dC/dt$ ) must equal zero for all 14 state variables in every compartment. The 14n coupled partial differential equations are solved iteratively with the Newton-Raphson method (Press et al., 1994) starting from imposed initial depth profiles for all variables. When the model failed to reach steady state after 20 iterations, the iteration procedure is restarted with a new set of initial profiles. Since other constituents do not influence the two carbon fractions they can be solved separately. After the carbon profiles are at steady state, the other components are solved with a reduced number of compartments, since their concentrations will not change in the deepest compartments where all the labile carbon has disappeared. This saves computing time. Dynamic simulations were performed using Euler integration with a time step of 10 seconds to avoid numerical instability (Press et al., 1994).

## Application of the model

### Steady state simulation

Our model is rather simplistic in some respects (e.g.  $pH$ -profile imposed, number of processes included, bi-molecular rate laws), yet already contains > 50 parameters (Table 4.3). Most parameters were set *a priori*, based on literature information, field measurements (indicated by D) or estimations (indicated by A). The remaining parameters (indicated by M) were obtained by fitting the model profiles to the observations. The performance of the model is demonstrated with a steady state run for station 9 (Figure 4.6). During the fitting procedure, the values were allowed to vary within predetermined ranges. The values of the parameters  $\Sigma R_{min}$ ,  $pFdet$ ,  $R_{m2}$ ,  $\omega$ ,  $Db_0$ ,  $x_b$  and  $coeff_{Db}$  were determined *a priori* on the observed TOC-profile. A depth-integrated rate of carbon mineralization ( $\Sigma R_{min}$ ) of  $0.33 - 0.39 \text{ mmol C cm}^{-2} \text{ yr}^{-1}$  was calculated from the Sediment Community Oxygen Consumption (SCOC) obtained by deck incubation as described by Wijsman et al. (1999). This value was slightly lower than the value obtained by the model ( $0.5 \text{ mmol C cm}^{-2} \text{ yr}^{-1}$ , Table 4.3). Parameters  $MnO_2$ -flux,  $Fe(OH)_3$ -flux,  $K_s(Fe(OH)_3)$  and  $k_{H2SMn}$  were subsequently derived from the observed  $FeS$ ,  $FeS_2$  and  $Mn^{2+}$  profiles. And finally the values of  $IrrEnh$  and  $\gamma_{TOC2}$  were derived from the  $NH_4^+$  and the  $Mn^{2+}$  profiles.

The model failed to describe the high values measured near the sediment surface, but gave a reasonable fit at depths > 2 cm. The model reasonably describes both the depth as well as the height of the subsurface peak of  $FeS$ . Also the pyrite concentration at depth is in the same range as the field observations. The model

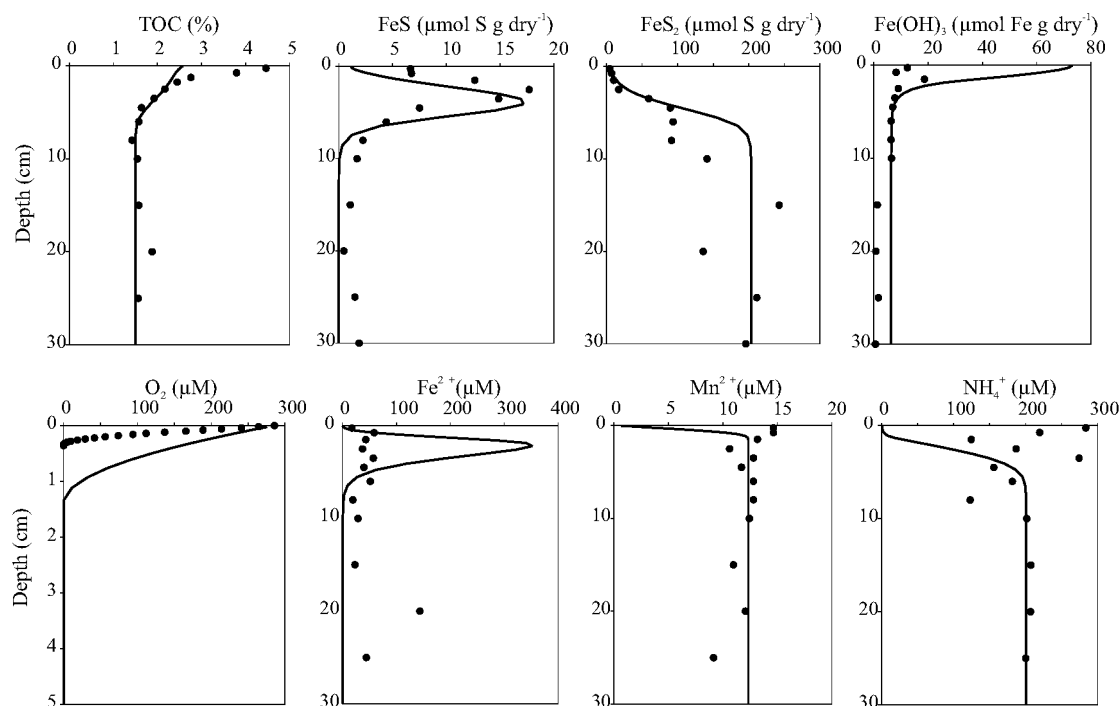


**Figure 4.6.** Depth distributions of the solid species: total organic carbon (TOC, %), iron monosulfide ( $FeS$ ,  $\mu\text{mol S g dry}^{-1}$ ), pyrite ( $FeS_2$ ,  $\mu\text{mol S g dry}^{-1}$ ) and iron oxides ( $Fe(OH)_3$ ,  $\mu\text{mol Fe g dry}^{-1}$ ) and the pore water components: oxygen ( $O_2$ ,  $\mu\text{M}$ ), ferrous iron ( $Fe^{2+}$ ,  $\mu\text{M}$ ), manganese ( $Mn^{2+}$ ,  $\mu\text{M}$ ) and ammonium ( $NH_4^+$ ,  $\mu\text{M}$ ). The dots indicate the measured data for station 9 and the solid lines indicate the model results of the steady state simulation. Note the different depth scale for oxygen

predicts that all  $FeS$  has disappeared at depths  $> 10$  cm. However small amounts of  $FeS$  are still present, indicating either that  $FeS$  is still being formed at these depths or that the conversion rate to pyrite is slower than predicted. The burial of pyrite can be taken as a measure for the total biologically reactive  $Fe(OH)_3$  flux to the sediment when corrected for the flux of  $Fe^{2+}$  out of the sediment. The  $Fe^{2+}$ -flux out of the sediment was low ( $7.48 \times 10^{-3} \mu\text{mol Fe cm}^{-2} \text{ d}^{-1}$ ) compared to the  $Fe(OH)_3$ -flux ( $2.8 \times 10^{-2} \mu\text{mol Fe cm}^{-2} \text{ d}^{-1}$ ) into the sediment. The concentration of  $Fe(OH)_3$  in the surface sediment layer is significantly overestimated by the model. The build-up of  $Fe(OH)_3$  is due to re-oxidation of  $Fe^{2+}$  with oxygen.  $Fe(OH)_3$ -concentrations at a depth  $> 15$  cm are lower than predicted because of non-steady state input of iron-oxides or iron reduction at depth due to variable reactivities of the iron-oxide. Oxygen penetration calculated by the steady state model is much too deep compared to the micro-electrode recordings, indicating a higher consumption rate of oxygen. The subsurface peak of  $Fe^{2+}$  predicted by the model is not observed. The predicted iron peak is due to a relative thin layer of iron reduction. Iron that diffuses upward will be re-oxidized with oxygen or  $MnO_2$  and that diffusing downward will react with  $H_2S$  to form  $FeS$ . There is no adsorption of iron to sediment particles (Van Cappellen and Wang, 1996) nor iron carbonate formation (Berner, 1980b; Aller et al., 1986) with the result that iron liberation is likely overestimated. Predicted concentrations of dissolved manganese are consistent with field observations. However, the decrease near the sediment water interface as calculated by the model was not observed. The ammonium concentration at depths  $> 10$  cm is well reproduced, but again deviations

occur near the sediment surface. Observed sulfide concentrations were always below the detection limit ( $< 1 \mu\text{M}$ ), yet the model predicts hydrogen sulfide up to  $560 \mu\text{M}$  at depth. This is probably caused by the exhaustion of  $\text{Fe}^{2+}$  to trap the hydrogen sulfide. Iron from the pools of  $\text{FeCO}_3$  or  $\text{Fe}^{2+}$  adsorbed to sediment particles may act as a buffer and maintain a considerable amount of  $\text{Fe}^{2+}$  at depth.

### ***Dynamic simulation***

For most constituents, the results of the steady state model deviate from the observed profiles near the sediment water interface. Especially the modeled profiles of TOC, iron oxides, oxygen and ammonium seem to fail near the sediment water interface. Although sampling of pore water in the upper sediment layers is difficult and subject to considerable error, non-steady state sedimentation could also change the concentrations in the top layer of the sediment. Our observations were done in May, i.e. after the spring bloom, and it might well be possible that the sediment is still recovering from a pulse deposition of fresh organic matter. A steady state model can not cope with such temporal variability. With a dynamic simulation, we tested whether a temporal change in the organic matter flux from the spring bloom just before we sampled the sediment could have caused some of the discrepancies. Starting from the steady state situation we forced a sinusoidal peak of degradable organic matter ( $\Sigma R_{\text{min}}$ ) to the sediment (Figure 4.7, upper panel). All other parameters and forcings were kept the same as during the steady state simulation. The period of the pulse was 15 days, and a maximum of  $17.4 \mu\text{mol C cm}^{-2} \text{ d}^{-1}$  was reached after 7.5 days. The total carbon flux to the sediment on a yearly basis increased about 25% due to this pulse flux.

The depth profiles of TOC, oxygen, iron and ammonium are plotted for  $t=0$  (steady state situation),  $t=15$  (directly after the pulse) and  $t=60$  days in figure 4.7, lower panels. Especially the profiles of TOC and oxygen after the pulse (i.e. at  $t=15$  days) are notably better than the profiles from the steady state run. Iron reacts very quickly on the pulse of organic matter, while the reaction of the ammonium profiles is more retarded. It will be clear that the pore water concentrations near the sediment water interface are vulnerable to non-steady state conditions. This puts severe restrictions on the use of steady state models to systems subject to seasonal deposition.

### ***Mineralization pathways as a function of carbon loading***

Organic matter, either derived from the water column by sedimentation or from the benthic primary production is the ultimate energy source for the early diagenetic processes in the sediment. In deep-sea stations where the organic matter flux to the sediment is generally low, oxic mineralization and denitrification are important pathways for the degradation of the organic matter in the sediment (Soetaert et al., 1996b). With an increase of the total rate of mineralization in the sediment, anoxic degradation pathways, including iron and sulfate reduction become more important (Canfield et al., 1993b).

To investigate the effect of the carbon loading on the relative importance of mineralization pathways, we performed 300 steady state simulations, with all parameters identical to that of the steady state simulation (Table 4.3). The total

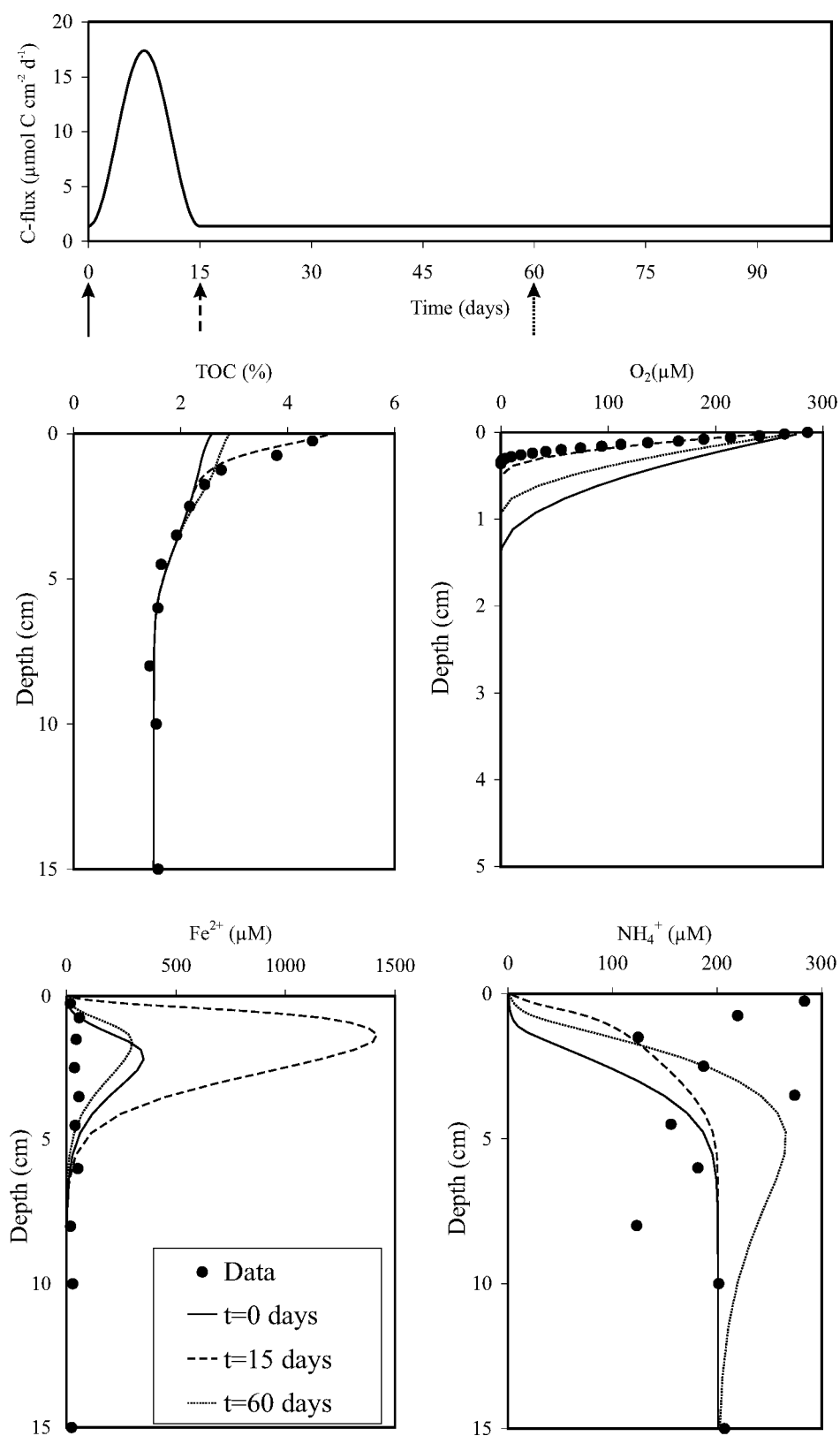


**Figure 4.7.** Results of a dynamic simulation with the model. The upper panel shows the sinusoidal pulse flux of organic matter to the sediment that was forced to the model. Maximum flux is at day 7.5 and the period is 15 days. The lower panels show the depth distributions in the sediment of total organic carbon (TOC, %) and the dissolved components oxygen ( $\text{O}_2$ ,  $\mu\text{M}$ ), ferrous iron ( $\text{Fe}^{2+}$ ,  $\mu\text{M}$ ) and ammonium ( $\text{NH}_4^+$ ,  $\mu\text{M}$ ). The lines represent the results of the dynamic simulation at  $t=0$  days (solid line),  $t=15$  days (dashed line) and  $t=60$  days (dotted line)



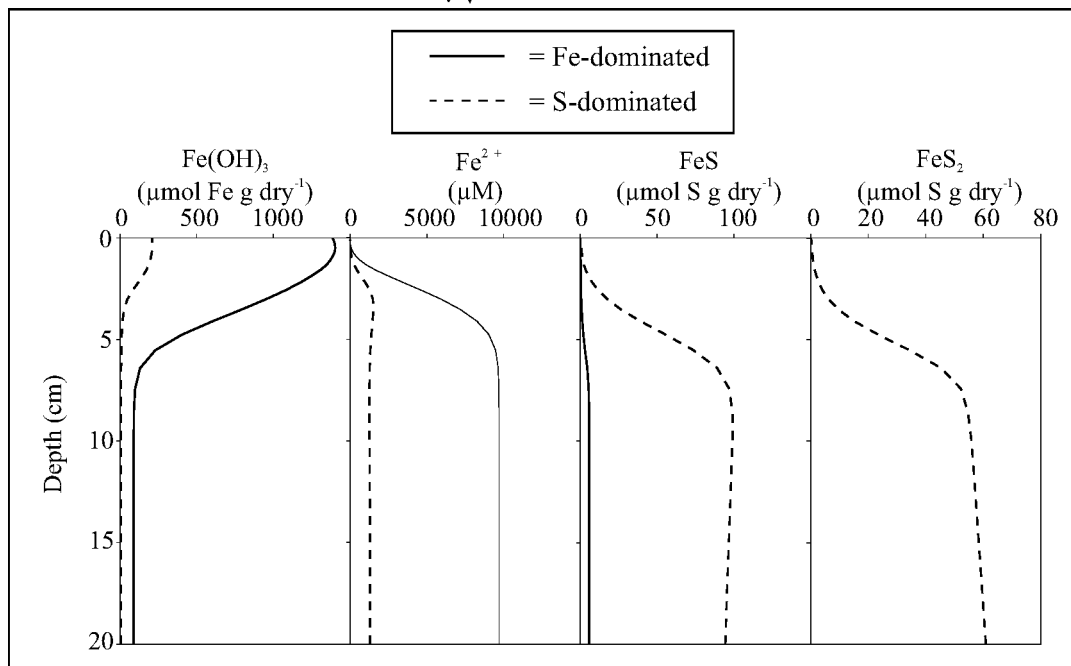
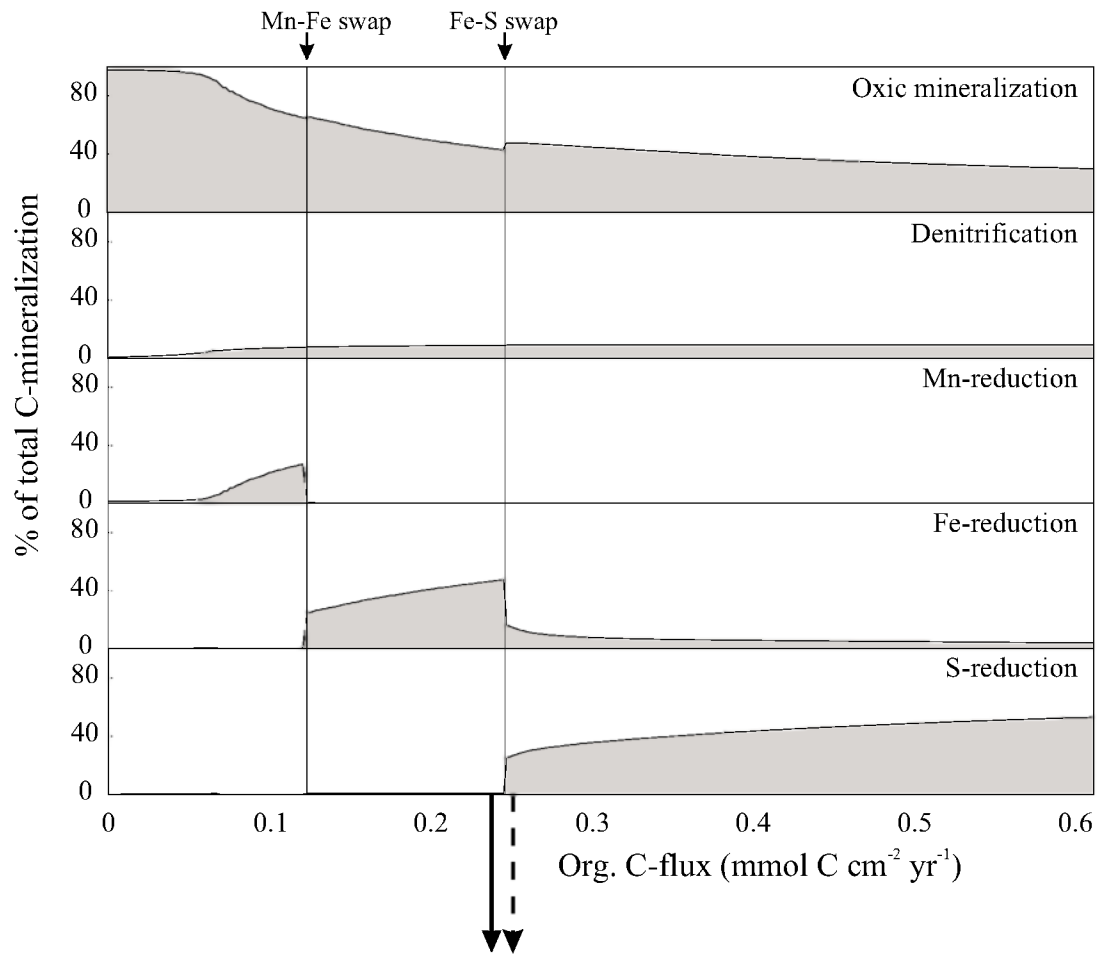


**Figure 4.8.** The upper panel represents the effect of the organic matter flux to the sediment on the relative importance (%) of the various mineralization pathways. The *Mn-Fe* and *Fe-S* swaps are indicated. The lower panel shows the depth distributions of iron oxides ( $Fe(OH)_3$ ,  $\mu\text{mol Fe g dry}^{-1}$ ), ferrous iron ( $Fe^{2+}$ ,  $\mu\text{M}$ ), iron monosulfide ( $FeS$ ,  $\mu\text{mol S g dry}^{-1}$ ) and pyrite ( $FeS_2$ ,  $\mu\text{mol S g dry}^{-1}$ ) for a *Fe*-dominated situation (Org. C flux =  $0.24 \text{ mmol C cm}^{-2} \text{ yr}^{-1}$ , solid line) and a *S*-dominated situation (Org. C flux =  $0.25 \text{ mmol C cm}^{-2} \text{ yr}^{-1}$ , dashed line)

degradable organic carbon flux to the sediment ( $\Sigma R_{min}$ ) was varied by means Latin hypercube sampling technique (Press et al., 1994) between 0 and 0.6 mmol C cm<sup>-2</sup> yr<sup>-1</sup>. The relative contribution of each degradation pathway as a function of total carbon mineralization is shown in figure 4.8, upper panel. Methanogenesis always accounted for less than 4% of the total carbon mineralization and is therefore not plotted. Oxidic mineralization is the dominant degradation pathway at low carbon fluxes. With increasing carbon loading, suboxic and anoxic degradation pathways become more important. Denitrification then accounts for 8 to 10% of the total carbon degradation, consistent with an extensive Monte Carlo sensitivity analysis by Middelburg et al. (1996b). Carbon degradation by manganese reduction is only of importance at mineralization rates between 0.05 and 0.12 mmol C cm<sup>-2</sup> yr<sup>-1</sup>. At a mineralization rate of 0.12 mmol C cm<sup>-2</sup> yr<sup>-1</sup> there is an abrupt change from manganese reduction to iron reduction (indicated by *Mn-Fe* swap). At this carbon loading, manganese oxides become exhausted in the sediments and iron reduction will occur. Ferrous iron produced by iron reduction diffuses upward and consumes manganese oxides, which are therefore not anymore available for organic matter degradation. This has in turn a positive feedback on the rate of iron reduction. Accordingly manganese reduction changes abruptly from reduction coupled to organic matter oxidation to reduction coupled to ferrous iron oxidation. A similar situation is observed at a degradation rate between 0.24 and 0.25 mmol C cm<sup>-2</sup> yr<sup>-1</sup> where an abrupt change occurs from iron reduction to sulfate reduction (indicated by *Fe-S* swap).

The effect of the *Fe-S* swap on the steady state profiles is illustrated in the lower panel of figure 4.8. The solid and broken lines are steady state profiles for a *Fe*-dominated situation (Org. C flux = 0.24 mmol C cm<sup>-2</sup> yr<sup>-1</sup>) and a *S*-dominated situation (Org. C flux = 0.25 mmol C cm<sup>-2</sup> yr<sup>-1</sup>), respectively. In the *Fe*-dominated situation, *Fe(OH)<sub>3</sub>* and the *Fe*<sup>2+</sup> reach extreme high concentrations, free sulfide is not observed since all the produced sulfide is directly converted into iron monosulfide and pyrite is not produced. In the *S*-dominated situation, concentrations of *Fe*<sup>2+</sup> and *Fe(OH)<sub>3</sub>* are much lower, free sulfide is observed in the pore water (up to 40 μM) and significant quantities of iron monosulfide and pyrite are produced.

The steady state budgets for iron and sulfur before and after the *Fe-S* swap are given in figure 4.9. Fluxes and depth-integrated reaction rates higher than 10 nmol cm<sup>-2</sup> d<sup>-1</sup> have been accentuated. Just before the swap (*Fe*-dominated situation), no free sulfide is observed in the pore water because the sulfide generated is efficiently trapped by abundant iron. At a slightly higher mineralization rate (*S*-dominated situation), the rate of iron monosulfide production is increased and a substantial part of reduced iron is trapped into *FeS* and *FeS<sub>2</sub>* and will therefore not be re-oxidized to *Fe(OH)<sub>3</sub>*. Consequently less iron is available for organic matter mineralization and more labile carbon becomes available for sulfate reducers, hence the rate of sulfate reduction is enhanced.

Ferrous iron, produced by the reduction of iron (oxy)hydroxides coupled to carbon oxidation can be re-oxidized in the less reducing layer with oxygen or manganese oxide. Iron atoms can thus cycle many times through their oxidized and reduced state before ultimate removal to depth in the sediment or escape to the water column (Canfield et al., 1993b). The cycling efficiency of iron, a measure for the average number of cycles in which *Fe* is involved is defined as:

$$E = \frac{R_{red}}{J + R_{red}}, \quad (4.24)$$

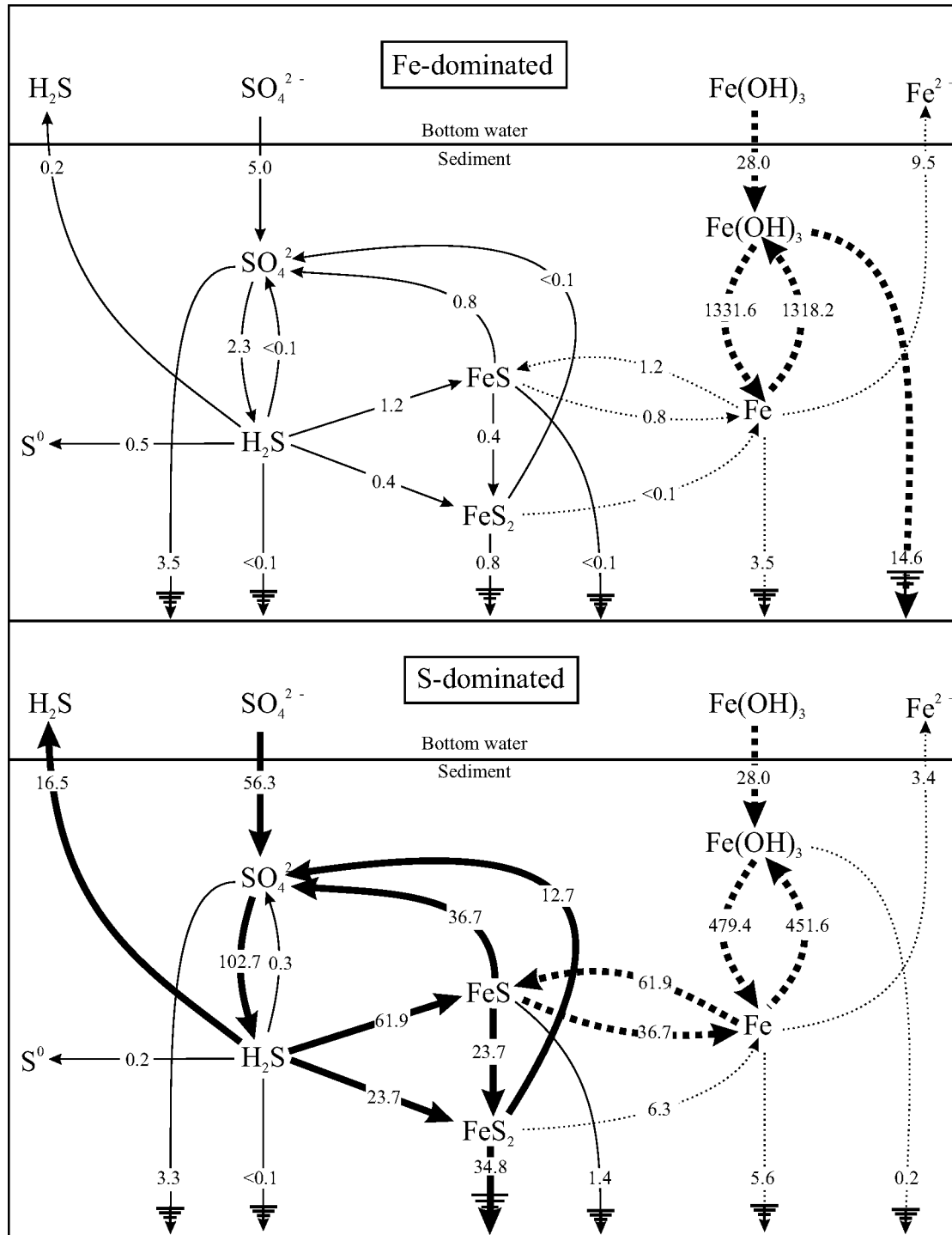


**Figure 4.9.** Schematic representation of the cycling of iron (dashed arrows) and sulfur (solid arrows). The depth-integrated reaction rates and fluxes are indicated in  $\text{nmol cm}^{-2} \text{d}^{-1}$ . Fluxes higher than  $10 \text{ nmol cm}^{-2} \text{d}^{-1}$  have been accentuated. The upper panel represents the situation for a carbon flux of  $0.24 \text{ (Fe-dominated)}$  and the lower panel for carbon flux of  $0.25 \text{ mmol C cm}^{-2} \text{yr}^{-1} \text{ (S-dominated)}$

where  $R_{\text{red}}$  is the depth integrated rate of iron reduction and  $J$  is the flux of  $\text{Fe}(\text{OH})_3$  to the sediment (Wang and Van Cappellen, 1996). The cycling efficiency may vary between 0 (no iron reduction) and 1 (no burial of  $\text{Fe}$ -atoms in the sediment and no

efflux of  $Fe^{2+}$  to the water column). A value between 0.5 and 1 indicates active redox recycling of iron in the sediment (Wang and Van Cappellen, 1996). The higher the cycling efficiency, the more important the recycling of  $Fe$ -atoms in the sediment. Just before the swap from a iron-dominated system to a sulfur-dominated system, the cycling efficiency of iron was 0.98, indicating that a  $Fe$ -atom is on average 54 times recycled. Just after the swap the cycling efficiency decreased to 0.94, which means that each  $Fe$ -atom is recycled only 16 times because they become fixed as iron sulfides.

## Conclusions

Organic matter mineralization in sediments from the northwestern continental shelf of the Black Sea induces metal oxide and sulfate reduction. These processes have resulted in the transformation of iron oxides into pyrite. A simple diagenetic model including only 14 state variables reproduces the main features observed in these sediments. It was not possible to conceal all observations: i.e. observed dissolved iron concentrations were significantly higher than modeled ones and modeled sulfide concentrations were higher than those observed. Moreover, steady-state predictions in the near surface layer of the sediment deviated from those observed for oxygen, ammonium, ferrous iron, manganese and total organic carbon. Dynamic simulations revealed that the upper few centimeters of the sediments were still recovering from the spring bloom. Exploration of the model over a range of carbon loadings resulted in the identification of two abrupt changes in mineralization pathways, namely from manganese-oxide based to iron- oxide based respiration and from iron-oxide based to sulfate based respiration. These sudden changes have also consequences for buffer capacity of these sediments towards sulfide and phosphorus release.

---

## CHAPTER 5

# Sulfur and iron speciation in surface sediments along the northwestern margin of the Black Sea

*Jeroen W. M. Wijsman, Jack J. Middelburg, Peter M. J. Herman, Michael E. Böttcher, Carlo H. R. Heip*

Submitted to *Marine Chemistry*

---

### Introduction

River deltas and continental shelf areas play an important role in the global cycles of sulfur and iron and are important sites for the formation and burial of authigenic iron sulfides (Berner, 1982; Jørgensen, 1982; Lin and Morse, 1991). This is due to high rates of organic matter fluxes to the sediments in combination with the input of reactive iron through rivers (e.g. Lin and Morse, 1991). With increasing load of reactive organic matter to the sediment, the relative importance of sulfate reduction usually increases (Canfield, 1989a; Thamdrup and Canfield, 1996 and chapter 4 of this thesis). Sulfate reduction is, therefore, the major mineralization pathway in sediments of productive coastal marine systems, accounting for 10 – 90 % of the total organic matter degradation (Jørgensen, 1977; Jørgensen, 1982; Henrichs and Reeburgh, 1987; Canfield et al., 1993a; Thamdrup and Canfield, 1996; Kostka et al. 1999).

Dissolved hydrogen sulfide that is produced during bacterial dissimilatory sulfate reduction may quickly react with sedimentary reactive iron compounds to form iron monosulfide,  $FeS$ , (Rickard, 1995), which can further react with dissolved sulfide, elemental sulfur or polysulfides (Berner, 1970; Luther, 1991; Rickard, 1997a) to form pyrite ( $FeS_2$ ). This immobilization of free sulfide within the sediment has major consequences for the cycling of iron and sulfur. Transport processes and turnover rates are significantly reduced by the formation of solid-phase iron sulfides. Moreover, the formation of iron sulfides and the subsequent burial in the sediment has been recognized as the dominant pathway for the permanent removal of sulfur and iron (Berner, 1982; Berner and Raiswell, 1983). Since hydrogen sulfide ( $H_2S \equiv H_2S_{(aq)} + HS^- + S^{2-}$ ) dissolved in the pore waters is toxic for many macrofaunal species (e.g. Bagarinao, 1992), the fixation of  $H_2S$  through the formation of metal sulfides is also an important detoxifying mechanism for the macrofauna community.

In the absence of sufficient sedimentary reactive iron,  $H_2S$  can diffuse into underlying sediments or the water column (Passier et al., 1999), can be chemically or microbially reoxidized to sulfur intermediates (elemental sulfur, thiosulfate, sulfite) or sulfate (Fossing and Jørgensen, 1990; Zhang and Millero, 1993) or react with organic matter (e.g. Sinninghe and De Leeuw, 1990). Additionally, bioturbating organisms can transport iron sulfide minerals from the reduced to the oxidized part of the sediments, where they are subsequently re-oxidized (Berner and Westrich, 1985; Aller, 1988; Aller and Rude, 1988). Thus benthic organisms might have a positive effect on the recycling of sulfur and iron within the sediments by their bioturbating and bio-irrigating activities. Oxygen has a direct effect on sulfur and iron cycling through re-oxidation, but also an indirect effect by its influence on the biomixing and bio-irrigating activity of the macrofauna that, in turn, depend on oxygen to respire.

It has been shown that a significant part of  $H_2S$ , which is produced in the sediments, is not permanently buried but reoxidized (Jørgensen, 1977). Besides diagenetic pyrite formation in the sediment, syngenetic precipitation in the anoxic water column has been shown to significantly contribute to sedimentary pyrite in the Black Sea (Fry et al., 1991; Muramoto et al., 1991; Raiswell and Canfield, 1998; Neretin et al., 2000).

The overall effect of early diagenetic reactions is not only reflected in the depth distributions of various dissolved and particulate sulfur and iron compounds within the sediment (e.g. Jørgensen, 1983), but also in the stable isotopic composition of metal sulfides, in particular pyrite (e.g. Goldhaber and Kaplan, 1974). The bacterial dissimilatory reduction of sulfate is associated with a significant discrimination of the stable sulfur isotopes  $^{34}S$  and  $^{32}S$ , leading to an enrichment of the lighter isotope in the  $H_2S$  produced (e.g. Chambers and Trudinger, 1979). Since no significant further isotope discrimination occurs upon iron sulfide formation (Price and Shieh, 1979; Böttcher et al., 1998b), the overall isotopic composition of the metabolic product  $H_2S$  should be preserved in the pyrite fraction. Therefore, the sulfur isotope ratios of sedimentary sulfur species in marine sediments have been found to be extremely useful in the characterization of biogeochemical processes in the coupled sulfur – carbon – iron cycles during early diagenesis (e.g. Goldhaber and Kaplan, 1974; Raiswell, 1997; Böttcher et al. 1998a; Passier et al., 1999; Böttcher et al., 2000). Most previous studies on the sulfur isotope geochemistry of Black Sea sediments were related to the water column or sediments deposited below the chemocline (Sweeney and Kaplan, 1980; Fry et al., 1991; Muramoto et al., 1991; Calvert et al., 1996; Lyons, 1997; Neretin et al., 1998; Neretin et al., 2000). Pyrite which is found in the water column and the surface sediments in the anoxic part is extremely depleted by up to -62 ‰ compared to coexisting sulfate (e.g. Fry et al., 1991; Lyons, 1997; Neretin et al., 1998). However, experiments with sulfate-reducing bacteria isolated from the Black Sea water column yielded an isotope fractionation of only about -30 ‰ (Fry et al., 1991). This discrepancy has been attributed to contributions from the oxidative part of the sulfur cycle (Canfield and Thamdrup, 1994) but is still a matter of debate (Fry et al., 1991; Neretin et al., 2000).

In the present study, we present data on the distribution of iron sulfur speciation and the sulfur isotopic composition of pyrite in surface sediments of the northwestern Black Sea along a transect from the coastal area, just in front of the river deltas, down to the anoxic deep-sea. It was the aim to provide additional information on the influence of depositional environments on the formation of and sulfur isotope partitioning into early diagenetic pyrite.

## Study area

The Black Sea is the world's largest anoxic basin with a permanent reservoir of hydrogen sulfide in the water column at depths  $> 100$  m (Sweeney and Kaplan, 1980; Sorokin, 1983; Codispoti et al., 1991). It has been an object of intensive study concerning the cycling of iron and sulfur (e.g. Berner and Raiswell, 1983; Berner, 1984; Calvert and Karlin, 1991; Middelburg et al., 1991; Lyons and Berner, 1992; Lyons, 1997; Wilkin et al., 1997 and chapter 6 of this thesis). The Black Sea is often seen as the modern equivalent of ancient euxinic basins with pyrite formation and sulfide oxidation processes existing in the upper part of the sulfidic water column of the deep-sea (Goldhaber and Kaplan, 1974; Calvert and Karlin, 1991; Jørgensen et al., 1991; Luther et al., 1991). Consequently, most previous studies concerning the iron and sulfur cycling in the Black Sea focused on the deep-sea.

Three major rivers (Danube, Dniester and Dnieper), accounting for 76 % of the total river input into the whole Black Sea (Tolmazin, 1985b; Mee, 1992; Fabry et al., 1993) discharge their water on the northwestern shelf which represents only 17 % of the total Black Sea area (Tolmazin, 1985b; Wijsman et al., 1999). The effect of these rivers on one side and the anoxic deep-sea on the other side introduce strong gradients across the northwestern shelf that could potentially affect the cycling of iron and sulfur within these sediments. The rivers discharge large amounts of nutrients and organic matter to the shelf. Consequently the benthic mineralization rates in the area just in front of the river mouths are much higher compared to the offshore areas (Wijsman et al., 1999). Large rivers such as the Danube are also a major source of reactive iron to continental shelf sediments (Martin and Windom, 1991; Guieu et al., 1998). In the Black Sea, this reactive iron is re-allocated from the shelf to the deep-sea sediments due to the pyrite formation in the water column of the deep-sea (Chapter 6 of this thesis). The oxygen concentration of the near-bottom water on the northwestern shelf is also variable. Due to upwelling/downwelling, internal waves and seasonal and long-term changes in mean circulation (Shaffer, 1986; Dimitrov et al., 1987; Lyons et al., 1993), the oxic/anoxic interface migrates over the shelf edge. As a consequence the bottom water oxygen concentration in the area near the oxic/anoxic interface fluctuates between fully oxic and anoxic. Moreover, oxygen depletions could occur in the shallow coastal waters as a result of high degradation rates in the sediment after a phytoplankton bloom in combination with a temperature stratification of the water column (Zaitsev, 1993).

## Material and Methods

### *Sampling locations*

Sediment was collected from nine stations in the northwestern part of the Black Sea in May 1997 (Figure 5.1; Table 5.1). Stations 2, 9, 10, 24 and 22, respectively, were positioned on a transect ranging from high organic loading in the shallow coastal waters to low organic loading in the permanently anoxic deep-sea. The coastal station 13 was located in front of the mouth of the river Dniester. Station 16 was situated in the northern part of the central shelf and is supposed to be directly influenced by (the discharge of) the Danube river (Wijsman et al., 1999), while station

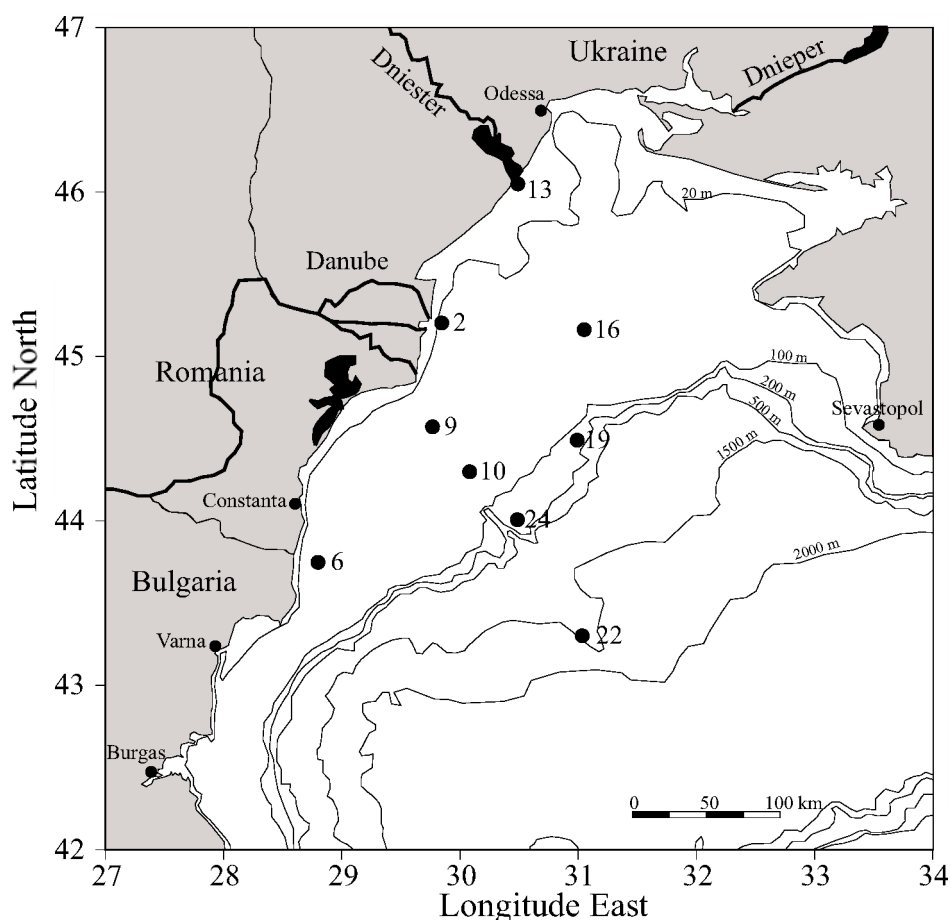


**Figure 5.1.** Locations of the sampling stations in the northwestern part of the Black Sea

**Table 5.1.** Characteristics of sampling stations in the northwestern part of the Black Sea

Stn	Area	Location		Depth (m)	Oxygen ( $\mu\text{M}$ )	Temp ( $^{\circ}\text{C}$ )	Org. C (%) <sup>*</sup>	Total S ( $\mu\text{mol g}^{-1}$ ) <sup>*</sup>	Total Fe ( $\mu\text{mol g}^{-1}$ ) <sup>*</sup>	SCOC ( $\text{mmol O}_2 \text{ m}^{-2} \text{ d}^{-1}$ )
		Latitude	Longitude							
13	Delta	46°03'N	30°29'E	13	350	8.4	0.64	72	202	26.3
2	Delta	45°12'N	29°51'E	26	207	6.5	2.15	244	807	37.9
6	Central shelf	43°45'N	28°48'E	52	285	6.8	0.84	70	205	13.5
16	Central shelf	45°10'N	31°03'E	54	314 <sup>†</sup>	5.5 <sup>†</sup>	2.78	46	123	10
9	Central shelf	44°34'N	29°46'E	57	243	6.6	1.71	194	504	11.6
10	Central shelf	44°18'N	30°05'E	72	284	6.6	2.93	115	200	11
19	Shelf edge	44°29'N	31°00'E	120	126 <sup>†</sup>	7.7	2.53	200	486	6.1
24	Shelf edge	44°00'N	30°29'E	137	190 <sup>†</sup>	7.5	1.56	164	368	3.7
22	Deep-sea	43°18'N	31°02'E	1494	0	9	4.64	488	298	n.d. <sup>§</sup>

<sup>\*</sup> Upper 16 cm of the sediment

<sup>†</sup> Measured in the bottom water from the box-corer

<sup>§</sup> Not determined

6 in the southern part of the central shelf is less influenced by the Danube river. Stations 19 and 24 were positioned at the shelf-edge, near the interface between oxic and anoxic bottom water. Station 22 was located in the anoxic deep-sea at a depth of 1494 m. Sediment was sampled at all stations using a Reineck box-corer (60 × 30 × 30 cm).



### ***Pore water collection and analysis***

Sediment cores were sub-sampled from the box-corer using Plexiglas core tubes (10.3 cm i.d., 50 cm length) and closed with rubber stoppers. The cores were transferred into a  $N_2$  gas filled glove box ( $O_2$  concentration < 500 ppm) through an air lock at the bottom of the box and sectioned in various intervals (0–0.5, 0.5–1, 1–2, 2–3, 3–4, 4–5, 5–7, 7–9, 9–11, 14–16, 19–21, 24–26 and 29–31 cm). Pore water was obtained by squeezing over a 0.45  $\mu$ m filter using manually operated Teflon squeezers at a maximum pressure of 1 bar  $N_2$  gas inside the glove box. A sub-sample of 1 ml pore water was collected and preserved in anoxic  $Zn(Ac)_2$  (50  $\mu$ l; 1M) for  $H_2S$  determination (Cline, 1969) and stored frozen until analysis. Another sub-sample of 3 ml was acidified with  $H_2SO_4$  (100  $\mu$ l; 7 N) and analyzed within one month for total dissolved iron concentration using a graphite furnace atomic absorption spectrometer with Zeeman background correction. Some complexed  $Fe(III)$  may contribute to the measured concentration of total dissolved iron.  $SO_4^{2-}$  concentration was measured spectrophotometrically in the remainder of the pore water using an autoanalyzer.

### ***Solid phase analysis***

The solid residues that remained after squeezing were put into diffusion-free bags and stored frozen for solid phase iron and sulfur analysis. All further processing of these solid residue samples were performed in a Coy anaerobic chamber (Coy Laboratory Products, Ann Arbor, Michigan) to prevent oxidation. The anaerobic chamber was filled with a mixture of  $H_2$  gas (5 %) and  $N_2$  gas (95 %). Any traces of oxygen were consequently removed by reaction with  $H_2$  gas on a palladium catalyst. The oxygen concentration in the chamber was always less than 0.5 ppm.

Acid volatile sulfides (AVS), which include iron monosulfides ( $FeS$ ) and dissolved hydrogen sulfide, were extracted from 0.5 g homogenized wet sediment samples by means of cold acid distillation (Fossing and Jørgensen, 1989) for 2 hours in deoxygenated  $HCl$  (10 ml, 6 N). The liberated sulfide was stripped from the solution with  $N_2$  gas and trapped in 10 ml deoxygenated  $Zn(Ac)_2$  (0.1 M). At the end of the distillation, the  $ZnS$  concentration in the traps was measured using the methylene blue method (Cline, 1969).

For pyrite determination 2–3 g wet sediment was dried 3 days in a hood at 40°C to oxidize the AVS to elemental sulfur (Henneke et al., 1991; Passier et al., 1999) and ground by pestle and mortar. The elemental sulfur produced by AVS oxidation, together with the elemental sulfur originally present in the sediment were removed by double extraction with acetone (Passier et al., 1996). Pyrite was determined using the  $Cr(II)$  reduction method (Zhabina and Volkov, 1978; Canfield et al., 1986; Fossing and Jørgensen, 1989). About 10 mg of the dry, acetone-extracted sediment was digested in 16 ml of 1 M  $Cr^{2+}$  in 0.5 N  $HCl$  and 8 ml 12 N anoxic  $HCl$ . Hydrogen sulfide that evolved was quantified as for AVS. Additionally for pyrite sulfur isotope analysis ( $\delta^{34}S_{pyrite}$ ), about 0.2 g acetone extracted sediment was exposed to a cold chromium reduction. The evolved hydrogen sulfide was trapped in  $Zn(Ac)_2$  and subsequently converted to  $Ag_2S$  by addition of a slight excess of  $AgNO_3$ . The  $Ag_2S$  was collected on 0.45  $\mu$ m filters, carefully washed and dried. The sulfur isotopic compositions was measured by means of combustion isotope–ratio–monitoring mass spectrometry (C-irmMS) using a Carlo Erba elemental analyzer connected to a Finnigan MAT 252 gas isotope mass spectrometer via a Finnigan Conflo II split

interface (Böttcher et al., 1998b).  $^{34}\text{S}/^{32}\text{S}$  ratios are expressed in the  $\delta$ -notation relative to the Vienna Canyon Diablo Troilite (V-CDT) standard.

Sub-samples of 1 g wet sediment were extracted for elemental sulfur ( $\text{S}^0$ ) determination. First, the samples were rinsed with anoxic sodium chloride (0.5 M) to remove the residual pore water sulfate. Then elemental sulfur was extracted twice with deoxygenated methanol. The methanol mixture was analyzed for elemental sulfur by means of reverse-phase HPLC (Henneke et al., 1997). Total sulfur content of the sediment was determined on dried and homogenized samples with a Carlo Erba NA 1500 elemental analyzer using vanadium pentoxide as catalyst to ensure complete oxidation.

Dithionite extractable iron (FeD) was determined by adding 0.5 to 1 g wet sediment to 10 ml dithionite (sodium dithionite  $50 \text{ g l}^{-1}$  in 0.2 M sodium citrate / 0.35 M acetic acid;  $\text{pH} = 4.8$ ) in 20 ml glass vials (Kostka and Luther, 1994). Samples were vortex mixed and placed on a rotary shaker for two hours. After extraction, the samples were filtered over a  $0.45 \mu\text{m}$  filter and stored for 1 day to oxidize the dithionite and sulfite (Canfield et al., 1993b). The extracted iron was determined by the injection of 50  $\mu\text{l}$  solution into 5 ml reducing HEPES (12 g HEPES plus 20 ml hydroxylamine ( $10 \text{ g} / 100 \text{ ml}$ ) per l,  $\text{pH} = 7.0$ ). After 30 minutes 300  $\mu\text{l}$  Ferrozine ( $5 \text{ g l}^{-1}$ ) was added and iron was determined spectrophotometrically after a minimum of 3 hours for complete color development (Stookey, 1970; Canfield et al., 1993b). Dithionite was expected to extract both poorly and well-crystallized iron oxides (except magnetite), AVS, iron-containing carbonates and iron adsorbed onto sediment particles (Canfield, 1988, Canfield et al., 1993b). Additionally there may be a small contribution of iron from silicate minerals. Porosity of the solid residue was calculated from water contents (weight loss on drying  $105^\circ\text{C}$ ) assuming a sediment dry density of  $2.55 \text{ g cm}^{-3}$ .

### ***Sediment community oxygen consumption (SCOC)***

Oxygen fluxes across the sediment water interface were measured by shipboard core incubations. Two Plexiglas core tubes (10.3 cm i.d.; 30 cm length) were sub-sampled from the box-corer and sealed with a lid containing a YSI 5739 oxygen electrode and a Teflon coated magnetic stirrer. The cores were incubated in the dark in a thermo stated bath at *in situ* temperature for 4 to 8 hrs. SCOC was calculated by linear regression of the oxygen concentration of the overlying water versus incubation time. A more detailed description of the flux chamber measurements is given by Wijsman et al. (1999).

## **Results**

### ***Sulfur and iron species inventory***

Depth-integrated data for the various sulfur fractions (AVS, pyrite, sulfate and others) and dithionite extractable iron (FeD) are presented in figure 5.2. The stations are ordered with respect to a decreasing SCOC (Table 5.1), which is an indicator for the depth-integrated rate of carbon mineralization in sediments (Heip et al., 1995). For each station, the data are integrated over the upper 16 cm of the sediment column,

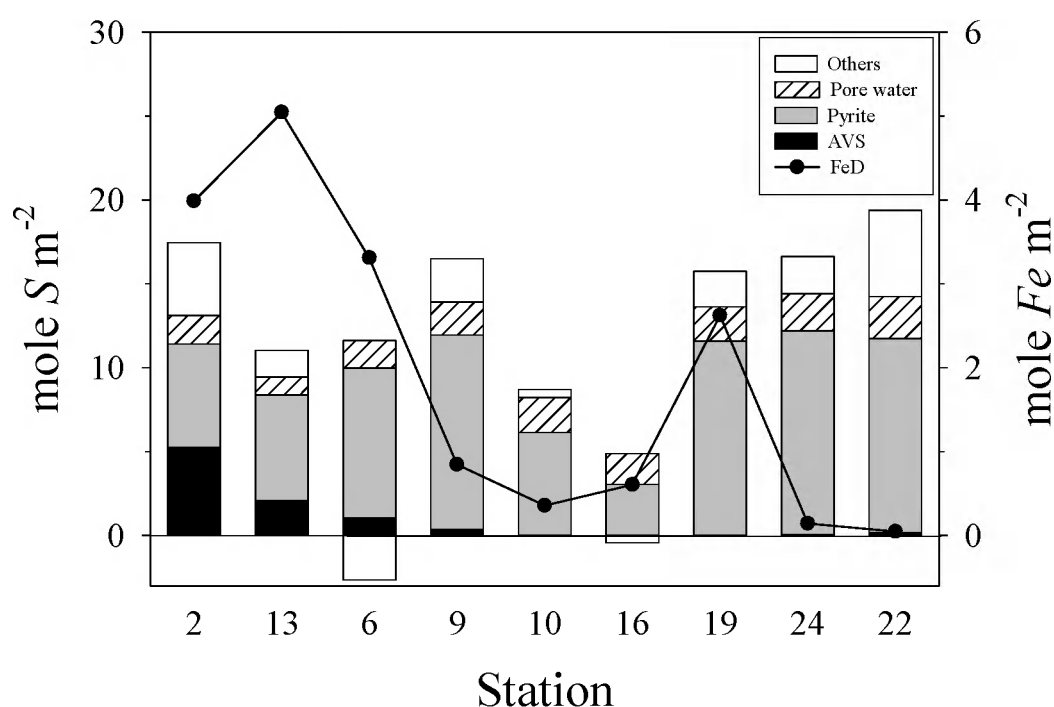


**Figure 5.2.** Distribution of various sulfur species (stacked bars) and dithionite extractable iron (line graph) integrated over the upper 16 cm of the sediment. Others represent total sulfur minus AVS, pyrite and pore water sulfur ( $SO_4^{2-}$  and  $H_2S$ ), and include elemental sulfur. Stations are ordered with a decreasing organic matter loading as implied by the sediment community oxygen consumption

which is the maximum depth for which data are available for all stations. Pyrite sulfur was the major sulfur phase at all stations accounting on average for 67 % of the total sulfur pool. Highest contents were found at the central shelf station 9 (11.6 mole  $S\ m^{-2}$ ), the stations 19 and 24 near the oxic anoxic interface (11.6 and 12.1 mole  $S\ m^{-2}$ , respectively) and at the deep-sea station 22 (11.5 mole  $S\ m^{-2}$ ). AVS contents were highest in the active stations (2 and 13) in front of the rivers Danube and Dniester (5.3 and 2.1 mole  $S\ m^{-2}$ , respectively) and decreased offshore. This is in agreement with previous observations of high AVS concentrations in sediments with high deposition rates (Middelburg, 1991; Kostka and Luther, 1994; Gagnon et al., 1995; Lyons, 1997). Pore water  $SO_4^{2-}$  ranged from 1.1 mole  $S\ m^{-2}$  at station 13 to 2.5 mole  $S\ m^{-2}$  at station 22, which is partly due to differences in porosity. The low  $SO_4^{2-}$  concentrations at the coastal stations 2 and 13 are caused by the low salinity in this area and sulfate reduction within the sediment. The sulfur fraction indicated by 'Others' is calculated by difference from the total sulfur content and pyrite, AVS and  $SO_4^{2-}$ . Due to analytical uncertainty and propagation of errors this resulted in negative concentrations at stations 6 and 16 (-0.26 and -0.04 mole  $S\ m^{-2}$ , respectively). The fraction of elemental sulfur was always less than 1.5 % of the total sulfur content and was assigned to 'Others'. Dithionite extractable iron (FeD) includes oxidized forms of iron that are available for iron reduction and iron in the form of AVS. FeD was highest in the coastal stations (2, 13 and 6) and decreased offshore. Remarkably high

FeD concentrations were found at stations 19, which was located near the oxic/anoxic interface.

### *Down core distribution of sulfur and iron species*

The pore water profiles of the active river delta sediments (Stations 2 and 13) showed a clear decrease in  $SO_4^{2-}$  from 15 mM near the sediment-water interface to 10 and 2 mM at 25 cm depth, respectively (Figure 5.3). At both stations, the decline was strongest at depths more than 10 cm. This decrease in  $SO_4^{2-}$  concentration with depth in the sediment suggests relatively high rates of sulfate reduction at these stations (Klump and Martens, 1989). In spite of these high sulfate reduction rates no free sulfide was observed in the pore water. This is probably caused by the presence of excess reactive iron in these sediments that is able to react with free sulfide to form iron sulfides (Chapter 6 of this thesis). The concentrations of AVS in these delta sediments were relatively high (up to 153 and 54  $\mu\text{mole } S \text{ g}^{-1}$  for stations 2 and 13, respectively). The AVS remained high at greater depth in the sediment and were not converted into pyrite. Due to oxidation, the AVS concentrations near the sediment-water interface were very low at both stations. Relatively high amounts of pyrite were observed near the sediment-water interface of both stations. At these coastal stations with a relatively high biomass of deposit feeders (Wijsman et al., 1999) pyrite can be transported from the deeper sediment layers to the sediment-water interface. Since pyrite is less vulnerable to oxidation than AVS, it will not be completely oxidized. A remarkable feature in the pyrite profiles at stations 2 and 13 was the abrupt decrease at

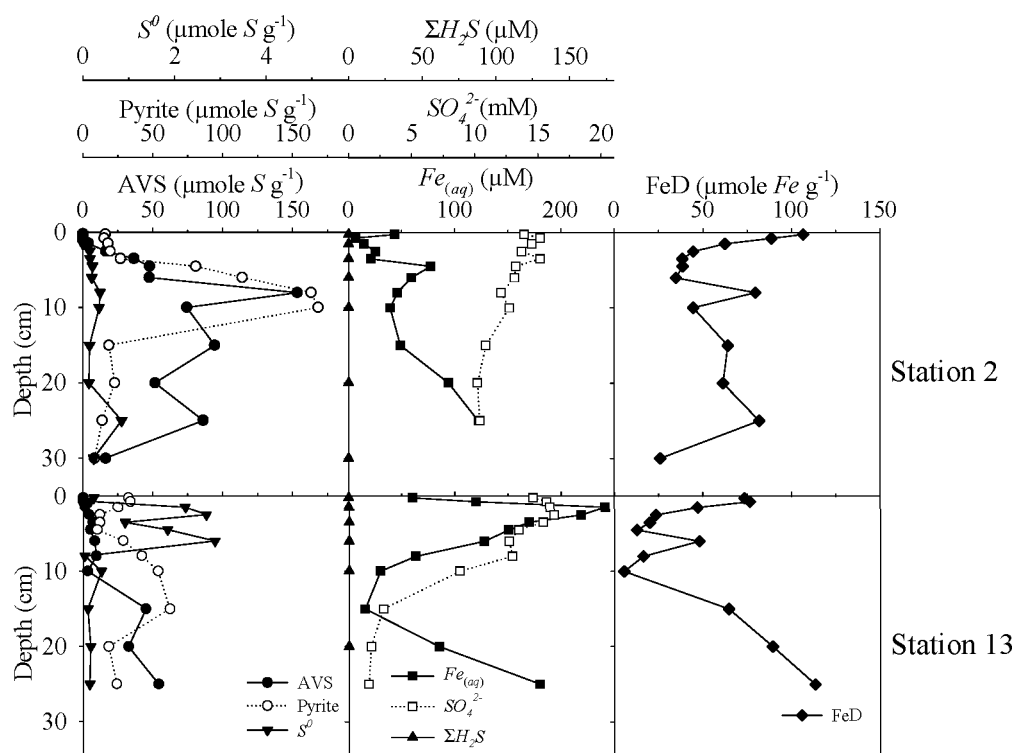


**Figure 5.3.** Concentration versus depth profiles of AVS, pyrite,  $S^0$ , dissolved iron ( $Fe_{(aq)}$ ),  $SO_4^{2-}$ ,  $\Sigma H_2S$  and dithionite extractable iron (FeD) for stations 2 and 13 located in front of river deltas

depths of 15 and 20 cm, respectively. Since it is not likely that pyrite is oxidized at these depths, we suggest this decrease reflects a non-steady state deposition. Moreover, the dissolved iron and FeD profiles show that reactive iron oxides were still present at these sediment depths.

The straight profiles of sulfate that were observed at the central shelf stations (Figure 5.4) indicate that the net sulfate reduction (i.e. sulfate reduction - sulfide oxidation) was low compared to the delta stations. Also sulfide was below the detection limit ( $< 1 \mu\text{M}$ ). The profiles of  $S^0$ , AVS and pyrite display classical patterns for coastal sediments. The AVS profiles are characterized by a subsurface peak at a depth of 2 to 5 cm, which is the depth where  $\text{FeS}$  is formed through the reaction of sulfide with reactive iron. In the more oxidized conditions near the sediment-water interface AVS is consumed by oxidation which is reflected by a peak in  $S^0$ . At greater depth in the sediments,  $\text{FeS}$  reacts further to pyrite. As a result the pyrite concentration increased asymptotically from a depth of about 2 to 5 cm. The strong decrease of dithionite extractable iron in the upper part of the sediment suggests a high activity of iron reduction at this depth. However, this is not reflected in a clear peak in dissolved iron. Dissolved iron produced by iron reduction was likely removed by secondary reactions such as iron sulfide formation and iron oxidation.

The profiles of dithionite extractable iron were very different between the two stations located near the oxic/anoxic interface (Figure 5.5). Station 19 (120 m) showed a distinct peak in FeD at the sediment-water interface of more than  $300 \mu\text{mole Fe g}^{-1}$ , while this peak was absent at the slightly deeper station 24 (137 m). Apparently dissolved iron that is produced by iron reduction was efficiently oxidized at or near the sediment-water interface of station 19, while at station 24 iron was probably lost from the sediments by diffusion into the water column. The uniform distribution of sulfate concentration with sediment depth and the absence of free sulfide in the pore water suggest that the net effect of sulfate reduction was relatively limited in this area. This is confirmed by the low respiration rates at these stations (Table 5.1). The pyrite profiles corresponded to the profiles observed at the central shelf stations, with an asymptotic increase from  $< 15 \mu\text{mole S g}^{-1}$  in the upper 5 cm to a maximum value of 200 to  $300 \mu\text{mole S g}^{-1}$  at depths of more than 10 cm. AVS concentrations at these stations were very low ( $< 3 \mu\text{mole S g}^{-1}$ ) and increased with depth in the sediment. The peak in elemental sulfur near the sediment-water interface reflected oxidation of reduced sulfur.

At the deep-sea station 22  $\text{H}_2\text{S}$  was observed in the pore water (Figure 5.6). The decreased concentration near the sediment-water interface is probably an artifact due to oxidation during sampling. The majority of this  $\text{H}_2\text{S}$  was probably not produced locally by sedimentary sulfate reduction since there was no sulfate gradient. The sulfide likely originates from the sulfidic water column. In the euxinic Black Sea, pyrite is formed in the upper part of the water column through the reaction of reactive iron with sulfide (Goldhaber and Kaplan, 1974; Leventhal, 1983; Calvert and Karlin, 1991). As a result all reactive iron is converted to AVS and pyrite before reaching the sediments. Consequently the dithionite-extractable iron at station 22 was entirely composed of iron sulfides. Although the majority of the iron sulfides reach the sediment in the form of pyrite, there is also a small fraction of  $\text{FeS}$  reaching the sediment or formed in the sediments. During burial in the sediment this  $\text{FeS}$  is converted to pyrite.

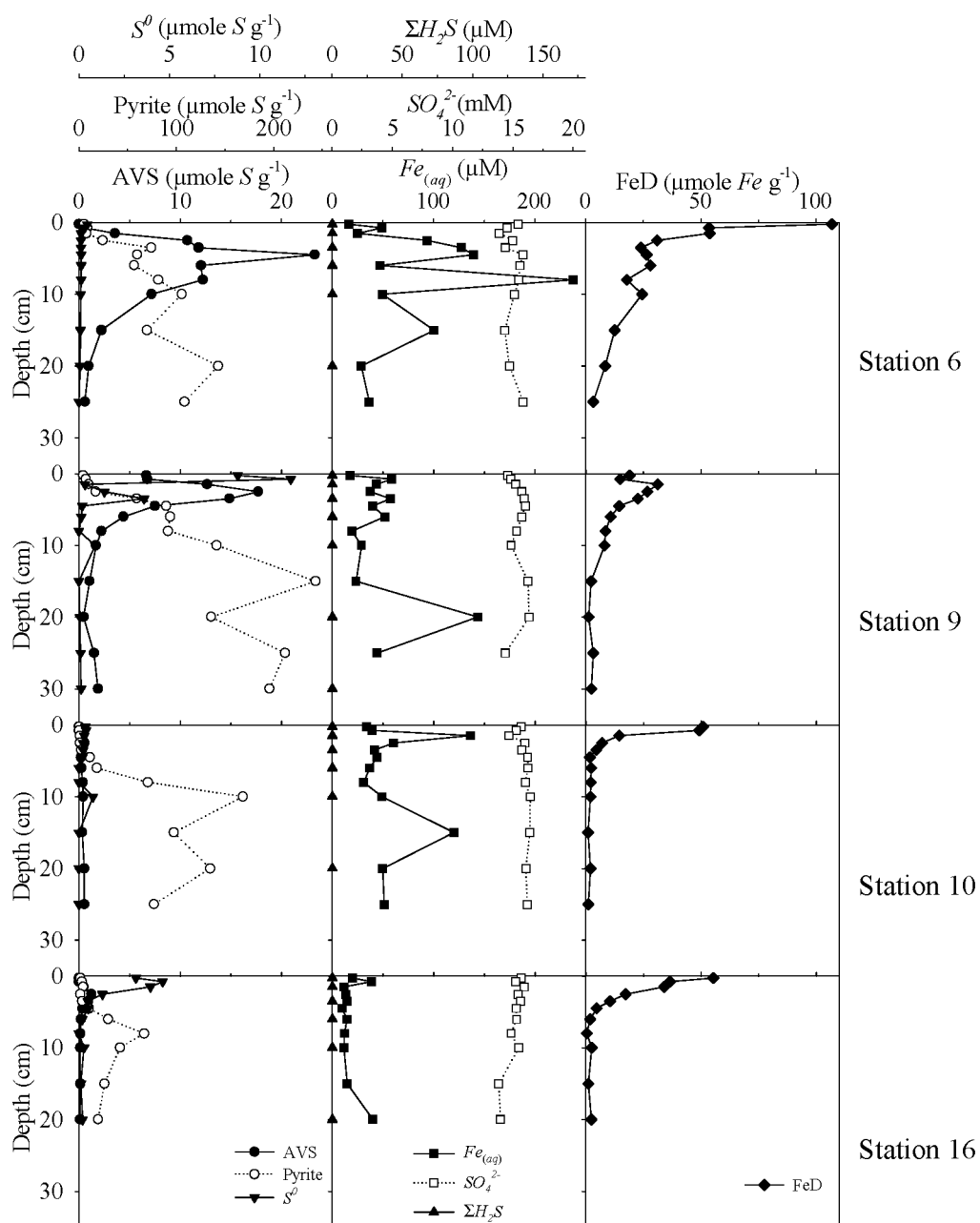


**Figure 5.4.** Concentration versus depth profiles of AVS, pyrite,  $S^0$ , dissolved iron ( $Fe_{(aq)}$ ),  $SO_4^{2-}$ ,  $\Sigma H_2S$  and dithionite extractable iron (FeD) for stations 6, 9, 10 and 16 located in central part of the continental shelf

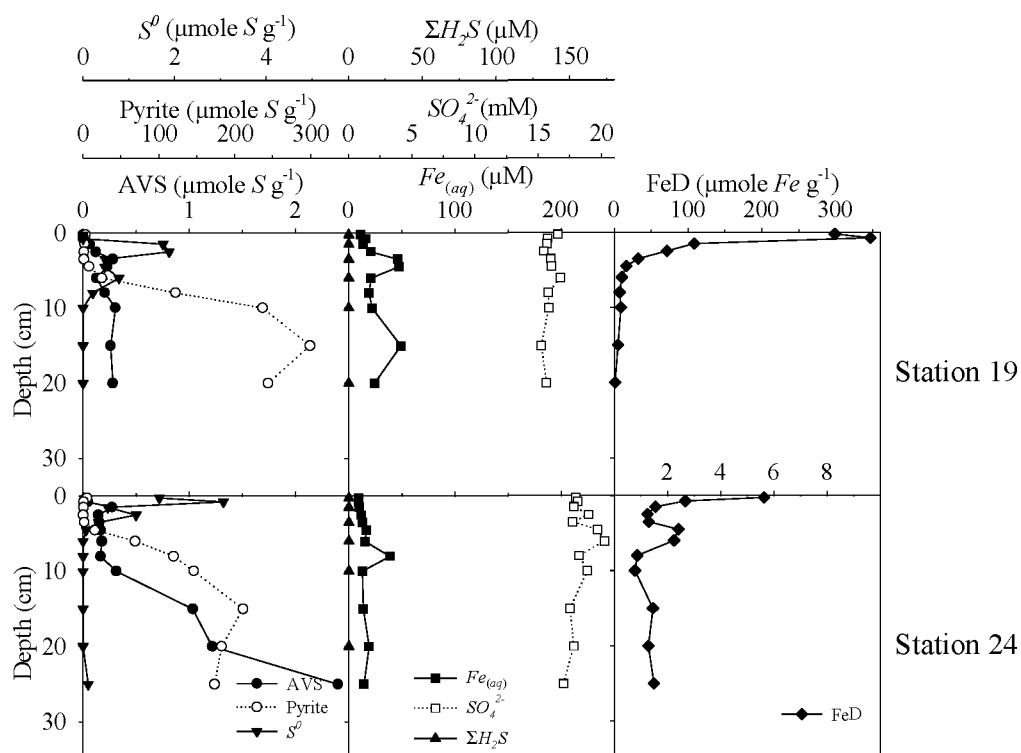


**Figure 5.5.** Concentration versus depth profiles of AVS, pyrite,  $S^0$ , dissolved iron ( $Fe_{(aq)}$ ),  $SO_4^{2-}$ ,  $\Sigma H_2S$  and dithionite extractable iron (FeD) for stations 19 and 24 located in at the shelf-edge, near the interface between oxic and anoxic bottom water. Mind the different scales for FeD

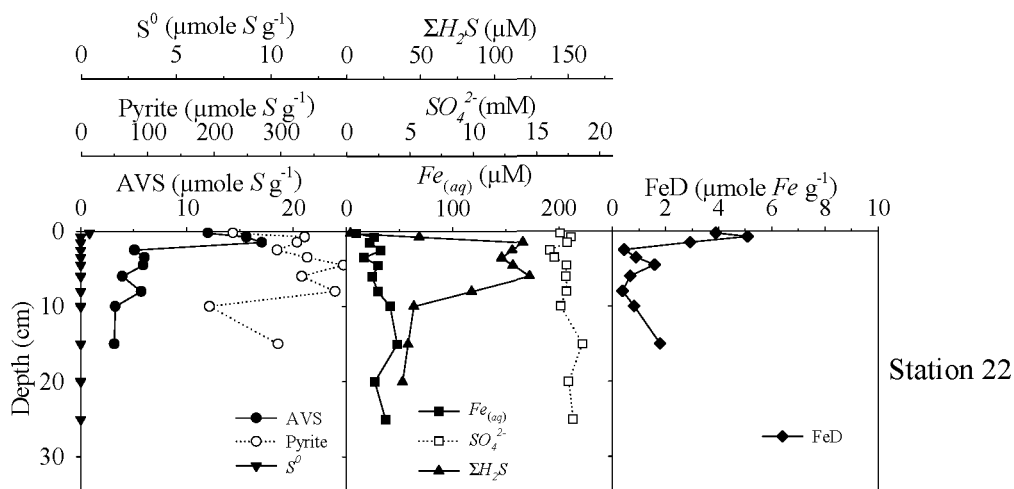


**Figure 5.6.** Concentration versus depth profiles of AVS, pyrite,  $S^0$ , dissolved iron ( $Fe_{(aq)}$ ),  $SO_4^{2-}$ ,  $\Sigma H_2S$  and dithionite extractable iron (FeD) for the deep-sea station 22

### ***Sulfur isotopic composition of sedimentary pyrite***

Since only minor isotope fractionation seems to occur during the reaction of  $H_2S$  with iron compounds to form pyrite (Price and Shieh, 1979), the isotopic composition of pyrite at a certain depth in the sediment can be used as a proxy for the  $\delta^{34}S$  of  $H_2S$ . Heaviest  $\delta^{34}S$  values (-13.7 ‰;  $\sigma = 4.6$  ‰) were observed at station 2 in front of the Danube delta (Figure 5.7). Assuming an isotopic composition for dissolved sulfate of about +19 ‰ (Sweeney and Kaplan, 1980) for the near bottom water at the continental shelf, this corresponds to an apparent isotopic fractionation of about -32 ‰. At the central shelf stations (9 and 10) the  $\delta^{34}S$  values of pyrite were much lower (-46.3 ‰ to -38.5 ‰), resulting in apparent isotope fractionation between -57 ‰ and -65 ‰. At station 9, pyrite became slightly enriched in  $^{34}S$  towards the sediment water interface. The isotope values in the upper 10 cm of station 24, located near the interface between oxic and anoxic bottom waters, correspond to those observed in the central shelf stations. At greater depth pyrite became rapidly heavier up to -5.8 ‰ at 25 cm depth. The  $\delta^{34}S$  values at the deep-sea station 22 ranged from -37.0 to -38.9 ‰. This is similar to previous data reported for Unit 1 sediments in the Black Sea (Table 5.2) and corresponds to  $\delta^{34}S$  values between of -35 to -40 ‰ that are reported for  $H_2S$  near the chemocline (Fry et al., 1991; Lyons, 1997) or in the deeper part or the anoxic water column (Neretin et al., 1998), as well as pore water  $H_2S$  from deep-sea sediments (Neretin et al., 2000). The isotopic composition of pyrite corresponds to an apparent isotopic enrichment factor of about -57 ‰.

## **Discussion**

### ***Down core distribution of iron and sulfur species***

The presence of large rivers discharging high amounts of suspended solids and nutrients (Popa, 1993) cause clear gradients in sedimentation, organic loading and iron input into the sediments of the northwestern continental shelf. This is also reflected in the depth distribution of the various sulfur and iron fractions in the sediments. The delta area, with sedimentation rates of about 1 cm yr<sup>-1</sup> (Wijsman et al., 1999) is characterized by relatively high rates of benthic mineralization (Table 5.1). As a result of high sulfate reduction rates, the sulfate concentration decreases with depth in the sediment at both delta stations (2 and 13). The break in sulfate profiles that is observed at a depth of 10 cm at both stations could mark the maximum depth of bio-irrigation in these sediments (Goldhaber et al., 1977). However, we suggest that this break is caused by enhanced rates of sulfate reduction at depths greater than 10 cm. This is supported by the relatively high concentrations of AVS at these depths, which are apparently not (yet) converted to pyrite. According to Boesen and Postma (1988) and Middelburg (1991) preservation of  $FeS$  in modern sediments could be attributed to a lack of elemental sulfur, polysulfides or hydrogen sulfide that are necessary to transform  $FeS$  to  $FeS_2$ . However, this does not seem to be the case at these stations, where elemental sulfur is observed over the whole measured depth range. Besides the presence of elemental sulfur, polysulfides or hydrogen sulfide, the transformation of  $FeS$  to pyrite requires time (Middelburg, 1991). According to Berner (1970) the process occurs on a timescale of years. Apparently pyrite formation in these active sediment layers is not completed yet, which is also reflected in the



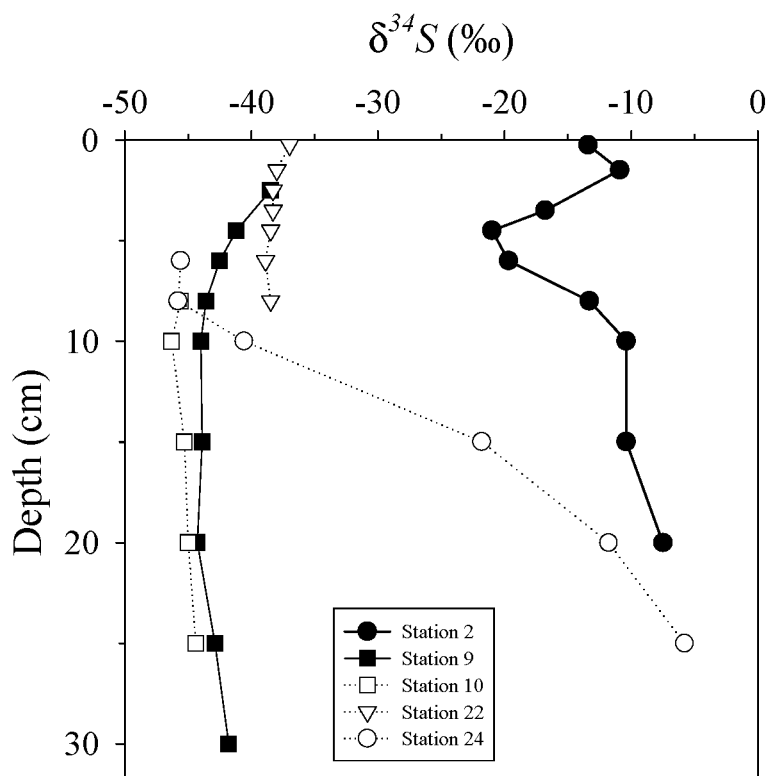


**Figure 5.7.** Distribution of  $\delta^{34}S$  values of pyrite versus sediment depth at stations 2, 9, 10, 22 and 24

abrupt decrease in the pyrite concentrations at 15 cm (Station 2) and 20 cm (Station 13). We suggest that there is an active layer present at a depth of 10 to 20 cm at both delta stations with high rates of sulfate reduction and high concentrations of reactive iron oxides. These sediments have recently been covered with less active sediment with higher pyrite concentration.

In comparison to the Delta stations, the central shelf stations are characterized by lower carbon loading to the sediment, as is reflected in the SCOC (Table 5.1). The depth profiles of the various sulfur and iron fractions show classical patterns that could largely be described by the use of a steady state diagenetic model (Chapter 4 of this thesis). There are exponential decreases in FeD with depth in the upper part of the sediment, subsurface peaks in AVS at depths of 2 to 5 cm, asymptotic increases in pyrite and peaks in  $S^0$  at sediment water interfaces due to oxidation. These sulfur and iron profiles were consistent among the stations, but the total amount varies between the stations. The maximal concentrations of AVS at stations 6 and 9 that are located closer to the coast are higher ( $23.3 \mu\text{mole } S \text{ g}^{-1}$  and  $17.7 \mu\text{mole } S \text{ g}^{-1}$ , respectively) than the more offshore stations 10 and 16 ( $0.6 \mu\text{mole } S \text{ g}^{-1}$  and  $1.2 \mu\text{mole } S \text{ g}^{-1}$ , respectively). This difference could partly be explained by differences in carbon loading, but also factors such as the availability of reactive iron and mixing processes by bioturbating and bio-irrigating benthic organisms in the sediment could cause this.

**Table 5.2.** Compilation of  $\delta^{34}\text{S}$  data (‰) for sulfur species from the water column, sediment traps and surface sediments of the Black Sea

Station	Water depth (m)	Depth	$\delta^{34}\text{S}$ (‰)				Ref.
			Sulfate	$\Sigma\text{H}_2\text{S}$	$\text{S}^0$ (+polysulfide)	$\text{S}_2\text{O}_3^{2-}$ (+ $\text{SO}_3^{2-}$ )	
Water column							
St.6	396	>324 m		-39.5 to -40.3			(1)
St.7	1176	>472 m		-38.7 to -39.9	-39.7		(1)
1136	2000	0-200 m	+18.5 ( $\sigma$ =0.3)				(2)
		>200 m	+19.4 ( $\sigma$ =0.7)	-39.6 ( $\sigma$ =0.7)			(2)
St.8	2045	>475 m		-39.4 to -40.1	-31.3 to -39.3	-38.5	(1)
1135	2050	0-200 m	+18.4 ( $\sigma$ =0.2)				(2)
		>200 m	+19.6 ( $\sigma$ =0.5)	-40.1 ( $\sigma$ =0.6)			(2)
BS2-1	2128	0-300 m		-40 to -38			(3)
		>300 m		-40.5 *			(3)
BS2-2	2130	0-300 m		-41 to -37			(3)
		>300 m		-40.5 *			(3)
BS2-3	2220	0-300 m		-41 to -35			(3)
		>300 m	+19.5 †	-40.5 *			(3)
			Sulfate	$\Sigma\text{H}_2\text{S}$	Pyrite	TIRS §	
Sediment traps							
BSC2	~2100	1065 m			-37.6 ( $\sigma$ =1.6) #		(4)
BSK2S	~2100	477 m			-32.7 #		(4)
Sediments							
Station 2	26	0-21 cm			-13.7 ( $\sigma$ =4.6)		(5)
Station 9	57	2-31 cm			-42.5 ( $\sigma$ =1.8)		(5)
Station 10	72	7-26 cm			-45.3 ( $\sigma$ =0.7)		(5)
Station 24	137	5-26 cm			-28.6 ( $\sigma$ =17.8)		(5)
15	198	Slope			-27.6 ( $\sigma$ =1.1)		(6)
Shelf	<200 m	Surface**	+19.6 ( $\sigma$ =1.0)		-30.7 ( $\sigma$ =14.5)		(7)
Deep-Sea	>200 m	Surface**	+20.4 ( $\sigma$ =0.5)		-33.4 ( $\sigma$ =3.3)		(7)
St.6	396	2-4 cm		-38.7			(1)
St.7	1176	2-10 cm		-36.1			(1)
Station 22	1494	0-9 cm			-38.2 ( $\sigma$ =0.6)		(5)
1136	2000	Surface††				-27.0	(2)
St.8	2045	10-18 cm		-40.4			(1)
1135	2050	Surface††				-27.4	(2)
9	2094	Unit 1			-37.3 ( $\sigma$ =0.7) #		(6)
1474K	2117	Unit 1			-33.5 ( $\sigma$ =1.2)	-29.4 ( $\sigma$ =0.1)	(8)
14	2218	Unit 1			-37.0 ( $\sigma$ =1.1) #		(6)
BS4-14GC	2218	Unit 1			-33.6 ( $\sigma$ =0.5)	-27.3 ( $\sigma$ =0.6)	(8)

Data are derived from: (1) (Neretin et al., 2000), (2) (Sweeney and Kaplan, 1980), (3) (Fry et al., 1991), (4) (Muramoto et al., 1991), (5) This study, (6) (Lyons, 1997), (7) (Vaynshteyn et al., 1986) and (8) (Calvert et al., 1996)

\* Average value for deep-water (> 300 m) at all 3 stations

† Water sample taken at 500 m depth

§ TIRS: Total reduced inorganic sulfur

# Chromium reducible sulfur fraction (including AVS)

\*\* Surface sediments (0-10 cm). Data averaged for all stations

†† Surface sediments, depth not specified

Wijsman et al. (1999) show that the macrofauna community in the offshore shelf stations are dominated by suspension feeders. Their irrigation activity could result in more oxidized conditions of the sediments.

The organic loading to the sediments at the stations located near the shelf-edge is low compared to the other shelf stations. This is reflected in low concentrations of AVS. The sulfur and iron cycling in these sediments is to a large extent influenced by changes in the oxygen concentration in the near-bottom water, which is highly variable in this region. The shallowest station 19 is dominated by iron reduction. The extremely high concentrations of FeD in the upper part of the sediment column suggest intensive recycling of iron by oxidation reactions. This is clearly not the case at station 24 where FeD concentrations in the upper sediments are two orders of

magnitude lower. Although the concentration of AVS is low at station 24 ( $<2.5 \mu\text{mole S g}^{-1}$ ), it increases with depth in the sediment. This might be related to a recent shift from anoxic to oxic conditions of the near-bottom water. During anoxia, AVS could also exist near the sediment water interface. During the oxic conditions this AVS becomes readily oxidized.

The processes in the water column largely determine the cycling of iron and sulfur in the sediments of the deep-sea station 22. The flux of labile organic matter to these sediments is very low and consequently the rate of sulfate reduction in these sediments is also very low. According to the depth profile of AVS, some of the  $\text{FeS}$  that is deposited on the sediment is converted to pyrite in the upper centimeters. In normal, non-euxinic sediments, pyrite is formed near the redox boundary through the reaction of  $\text{FeS}$  with intermediate sulfur species such as elemental sulfur and polysulfides (Berner, 1970; Rickard, 1975). In the euxinic sediments of station 22, it is not likely that intermediate sulfur species are present and pyrite could only be formed through the reaction of  $\text{FeS}$  with  $\text{H}_2\text{S}$  (Rickard, 1997a).

### ***Sulfur isotopic composition of sedimentary pyrite***

In the surface sediments at station 2 in front of the river Danube relatively heavy  $\delta^{34}\text{S}$  values ( $-13.7 \text{ ‰}$ ;  $\sigma = 4.6 \text{ ‰}$ ) were observed which differ significantly from the compositions at the stations 9, 10, 22, and 24 (Figure 5.7). However, the apparent isotope fractionation is well within the range observed in experiments with pure sulfate-reducing bacteria (Chambers and Trudinger, 1979). Experimental studies have shown that sulfur isotope fractionation decreases with increasing cellular sulfate reduction rate (e.g. Kaplan and Rittenberg, 1964; Chambers and Trudinger, 1979). Therefore, the data at station 2 suggest that the cellular rates of microbial sulfate reduction were probably high when compared to the other stations. Additionally, the sediment at station 2 was (partially) closed for bottom water sulfate, as indicated by a decrease in pore water sulfate with depth (Figure 5.3). The pore water profile of the other station in front of a river delta (station 13) shows also a distinct decrease with sediment depth, suggesting that sulfate reduction out competes sulfide oxidation and sulfate resupply by diffusion. In a (partially) closed system, the diffusive transport processes are not sufficient to prevent a depletion of the sulfate pool with depth, resulting in an increase of the  $\delta^{34}\text{S}$  value for the remaining sedimentary sulfate pool and consequently of the produced sulfide (Hartmann and Nielsen, 1969). As a result, the apparent isotope fractionation with respect to seawater will decrease. Also the openness of the sediments with respect to sulfide could affect the isotopic composition of the sediment (Jørgensen, 1979). If all sulfide produced by sulfate reduction is trapped as pyrite immediately and buried permanently in the sediments, the system is closed with respect to sulfide. Conversely, if most of the produced sulfide is reoxidized via intermediates to sulfate in the upper sediment layers, the sediment experiences open system diagenesis (Jørgensen, 1979). In general, large apparent isotopic fractionations are often associated with open systems, while small differences in isotopic composition between seawater sulfate and pyrite are an indication for a (partially) closed diagenesis system of sulfur. The isotopic composition of dissolved species may additionally be influenced by preferential diffusion of  $^{32}\text{SO}_4^{2-}$  into the sediment (Goldhaber and Kaplan, 1974; Jørgensen, 1979; Chanton and Martens, 1987). Although the diffusion coefficients for  $^{32}\text{SO}_4^{2-}$  and  $^{34}\text{SO}_4^{2-}$  are almost the same (Trudinger, pers. communication in Jørgensen, 1979; Piel and Böttcher, unpublished experimental data), the concentration gradient of  $^{32}\text{SO}_4^{2-}$

could be higher due to the preferential microbial consumption of  $^{32}\text{SO}_4^{2-}$  in the sediments. The same could apply for the diffusion of dissolved sulfide into the water column when dissolved sulfide accumulates at the sediment water interface (Chanton and Martens, 1987; Chanton et al., 1987).

Several factors could cause the (partial) closed diagenesis system for sulfur at the coastal stations. Since the rivers discharge large amounts of suspended solids, the sedimentation rates are supposed to be high in this area. These high deposition rates could restrict the exchange of sulfate with the water column. Also high sulfate reduction rates in the sediments of these coastal stations could reduce the openness of the system for sulfate. The relatively high SCOC rates recorded at stations 2 and 13 (37.9 and 26.3 mmole  $\text{O}_2 \text{ m}^{-2} \text{ d}^{-1}$ , respectively) suggest a high sulfate reduction activity in these sediments. Finally, the availability of large amounts of reactive iron in these sediments (Chapter 6 of this thesis, Figure 6.2) could partially be responsible for the relatively low apparent isotopic fractionation. The reactive iron will trap most of the produced sulfide in the form of iron sulfides preventing re-oxidation of sulfide after diffusion to the oxidized upper sediment layers. Bioturbating organisms may additionally have influenced the depth variation in the isotopic composition of pyrite.

In the central part of the continental shelf (Stations 9 and 10) the  $\delta^{34}\text{S}$  values are very light (-38.5 ‰ to -46.3 ‰). These results are comparable to data from Vaynshteyn et al. (1986), who report a value of -45 ‰ in the upper 10 cm of a station located in the southern part of the northwestern continental shelf. Assuming that the  $\delta^{34}\text{S}$  value of the sulfate in the near bottom water of the continental shelf is equal to sulfate in the upper 200 meter of the deep-sea (i.e. +19 ‰, Sweeney and Kaplan, 1980), this corresponds to an apparent maximum isotope fractionation of -65 ‰ at the central shelf stations. In an open system, (bio-enhanced) transport processes are faster than the microbial rate of sulfate reduction (Jørgensen, 1979; Chanton et al., 1987). As a result, the sulfate concentration in the sediment will not decrease and its isotopic composition will not change due to sulfate reduction. In such an open system, the apparent and instantaneous isotope fractionations coincide. The light isotopic values at stations 9 and 10 and the more or less constant concentrations of sulfate with depth, therefore, indicate that the sediments were open with respect to sulfate. The abundance of bio-irrigating benthic fauna in this area (Wijsman et al., 1999) might have enhanced the openness of these sediments for sulfate due to enhanced sulfate supply and enhanced re-oxidation. The magnitude of isotopic fractionation at stations 9 and 10, however, is extremely high when compared to the results of experimental studies. Laboratory experiments with pure-cultures of sulfate-reducing bacteria yielded isotope enrichment factors up to a maximum of -46 ‰ (Kaplan and Rittenberg, 1964). This indicates that isotope discrimination was not only controlled by microbial sulfate reduction alone and additional processes may have contributed to the observed overall isotope effect. Reoxidation of  $\text{H}_2\text{S}$  leads to the formation of sulfur species with intermediate oxidation states, as elemental sulfur and thiosulfate (Zhang and Millero, 1993). Whereas only minor isotope fractionation seems to occur during oxidation of  $\text{H}_2\text{S}$  (Fry et al., 1986), the microbial disproportionation of the sulfur intermediate has experimentally been shown to produce isotopically light  $\text{H}_2\text{S}$  (Canfield and Thamdrup, 1994; Cypionka et al., 1998), therefore, increasing the overall isotope discrimination between sulfate and  $\text{H}_2\text{S}$ . In sediments that are open to the supply of oxidants, repetitive cycles of sulfate reduction, oxidation and disproportionation have been suggested to result in progressively lighter isotopic sulfur values (Canfield and Thamdrup, 1994).

A significant variability with a steep down core increase in the  $\delta^{34}S$  values was observed in the depth profile of station 24 (Figure 5.7). This trend is in agreement with data of Vaynshteyn et al. (1986) for shelf sediments near the oxic/anoxic interface. At present, there is no indication for a limited supply of dissolved sulfate and a related “reservoir effect” (Jørgensen, 1979) on the isotopic composition of pyrite because the sulfate concentrations remained nearly constant with depth (Figure 5.5). We, therefore, suggest that the observed increase in  $\delta^{34}S$  values has to be attributed to a non-steady state process where the system was essentially closed in a previous period. Possibly a high carbon input or a high sedimentation rate in the past had restricted the diffusion of sulfate into the sediments. However, there is no indication for an abrupt decrease in sedimentation rate and/or carbon flux to the sediment in this area in a previous period. Also a switch between oxic and anoxic conditions of the near bottom water could affect the openness of the system for sulfate. At low oxygen and anoxic conditions re-oxidation of reduced sulfide, hence sulfate resupply in the sediment is low, enhancing the closed behavior of the system and limiting the substrate for the activity of disproportionating bacteria. Moreover, anoxic conditions could reduce the bio-irrigation activity of the benthic fauna, decreasing the openness of the system for sulfate (Jørgensen, 1979; Chanton and Martens, 1987). It is possible that as a result of the long-term fluctuations of the oxic/anoxic interface (Lyons et al., 1993) the bottom water at this station has recently changed from anoxic to oxic, which caused more depleted  $\delta^{34}S$  values in the upper part of the sediment column. As discussed in the previous section, the AVS profile at station 24 also indicates a recent change from anoxic to oxic conditions of the near bottom water at this station.

Isotope results for pyrite in sediments from the deep-sea station 22 are light (-37.0 to -38.9 ‰) and compare well with the results of previous studies on deep-sea surface sediments of the Black Sea (Table 5.2). They are similar to the isotopic composition of  $H_2S$  near the chemocline or close to the sediment-water interface (Table 5.2; Sweeney and Kaplan, 1980; Fry et al., 1991; Neretin et al., 1998; Neretin et al., 2000) and pore waters of deep-sea surface sediments (Neretin et al., 2000). It has previously been argued that the isotopic composition of deep-sea sediments is indicative for pyrite formation in the water column. From the compiled data for deep-water column and pore water  $H_2S$  in table 5.2, however, it is obvious that part of the pyrite may also form in the surface sediments of the deep-sea, in agreement with balance calculations by Neretin et al. (2000). Data on suspended particle composition in the anoxic water column (Cutter and Kluckhohn, 1999) indicate that significant concentrations of  $FeS$  and greigite are present in the near bottom water of the deep-sea. These components could act as an iron source for pyrite formation at these depths. The extremely light  $\delta^{34}S$  values of  $H_2S$  in the anoxic water column have been attributed to internal recycling of sulfur (Canfield and Thamdrup, 1994). Elemental sulfur that is extensively formed by oxidation of hydrogen sulfide near the chemocline (Jørgensen et al., 1991; Luther et al., 1991), settles through the water column where it might be subjected to bacterial disproportionation, resulting in more negative values of the reduced sulfur pool (Canfield and Thamdrup, 1994). Unfortunately, there are only very limited isotope data available for sulfur intermediates from the anoxic water column (Neretin et al., 1998; Neretin et al., 2000) and no measurements have been done on samples from the chemocline, yet. Sulfur intermediates as elemental sulfur and thiosulfate seem to follow closely the isotopic composition of  $H_2S$  (Table 5.2), indicating isotope exchange reactions to occur. The trend in  $S^0$  may additionally be explained by microbial reduction with depth (Kaplan and Rittenberg, 1964; Böttcher

and Surkov, unpublished experimental data). A comparison of the concentrations of  $H_2S$  and coexisting  $S^0$  (Neretin et al., 2000), indicating that in the deeper part of the anoxic water column hydrogen sulfide should control the isotopic composition of elemental sulfur by isotope exchange reactions via polysulfides and not vice versa. The present study demonstrates that pyrite which is extremely enriched in  $^{32}S$  can be found in the Black Sea surface sediments which are positioned both above and below the chemocline, in spite of different biogeochemical and microbial controlling factors.

The upper slope sediments are a major source for the turbidite mud layers that are observed in the abyssal plane of the Black Sea (Lyons, 1997). During earthquake-related events,  $FeS$ -rich upper slope sediments can be transported to the deep-sea where the  $FeS$  may react with the  $H_2S$  present in the near bottom water to pyrite. According to the model of Lyons (1997)  $\delta^{34}S$  values of turbidite sediments are therefore determined by both the concentration and isotopic composition of the  $FeS$  and pyrite in the upper slope sediments and the  $\delta^{34}S$ -value of  $H_2S$  in the deep anoxic water (Fry et al., 1991; Neretin et al., 1998). In the model of Lyons (1997), the upper slope muds were assumed to be relatively constant in contents and  $\delta^{34}S$  values of AVS ( $152 \mu\text{mol } S \text{ g}^{-1}$ ;  $-25.0 \text{ ‰}$ ) and pyrite ( $90 \mu\text{mol } S \text{ g}^{-1}$ ;  $-27.6 \text{ ‰}$ ).

In contrast, the present study demonstrates that shelf and upper slope sediments in the Black Sea are highly variable in AVS and pyrite contents and sulfur isotopic compositions. Differences in carbon load and oxygen conditions in the overlying bottom water on the shelf are the major causes for these variations. Even the upper slope sediments vary not only in AVS and pyrite concentrations but also in  $\delta^{34}S$ -composition. This is mainly caused by variations in redox conditions of the bottom water overlying these upper slope sediments. Since it is most likely that the turbidite mud layers originate from those upper slope sediments, their isotopic composition is expected to be variable and largely determined by the oxygen conditions in the area where the turbidite originate from and cannot be assumed to be constant.

---

## CHAPTER 6

# Reactive iron in Black Sea Sediments: implications for iron cycling

*Jeroen W. M. Wijsman, Jack J. Middelburg and Carlo H. R. Heip*  
Accepted for publication in *Marine Geology*

---

### Introduction

The Black Sea is the world's largest permanently anoxic body of water and has been proposed as the modern equivalent of ancient euxinic basins (e.g., Berner and Raiswell, 1983; Berner, 1984; Calvert and Karlin, 1991; Lewis and Landing, 1991; Middelburg et al., 1991; Lyons and Berner, 1992; Lyons, 1997; Wilkin et al., 1997). Pyrite formation in euxinic basins is not limited to the sediment, but also takes place in the upper reaches of the anoxic water column, where dissolved sulfide is in contact with reactive iron phases (Goldhaber and Kaplan, 1974; Leventhal, 1983; Calvert and Karlin, 1991; Muramoto et al., 1991; Lyons, 1997; Wilkin et al., 1997). The production of pyrite in the water column and its settling to the sea floor leads to a decoupling of carbon and sulfur burial (Leventhal, 1983; Raiswell and Berner, 1985; Calvert and Karlin, 1991; Lyons and Berner, 1992), higher degrees of pyritization (Berner, 1970; Canfield et al., 1996) and higher reactive iron contents for euxinic sediments of the Black Sea compared to "normal" oxic marine sediments (Canfield et al., 1996; Raiswell and Canfield, 1998).

In marine deposits underlying oxic water, pyrite is formed in the sediments during early diagenesis (Goldhaber and Kaplan, 1974; Berner, 1984). In these sediments, sulfur concentrations are linearly related to the organic carbon content (Goldhaber and Kaplan, 1974; Berner, 1984) because (1) pyrite production is usually limited by the availability of biologically metabolizable organic matter (Berner, 1984) and (2) sulfide retention and carbon preservation are often coupled (Berner and Westrich, 1985). In euxinic basins, where iron sulfides form in the water column, pyrite production is to a certain degree decoupled from the amount of locally deposited sedimentary organic matter. In these systems, the availability of reactive iron is a more important factor limiting the production of pyrite (Raiswell and Berner, 1985; Boesen and Postma, 1988; Middelburg, 1991). This is often reflected in a lack of relation between concentrations of sulfur and organic carbon in these sediments (Berner and Raiswell, 1983; Leventhal, 1983; Calvert and Karlin, 1991; Lyons and Berner, 1992). Another indicator of iron-limitation for pyrite formation is the degree of pyritization (DOP) in the sediment. DOP indicates the extent to which "reactive"

iron is present in the form of pyrite (Berner, 1970). The relatively high DOP values of deep-water sediments in the Black Sea and the absence of a relation between DOP and organic carbon content support the idea of iron limitation for pyrite formation (Raiswell and Berner, 1985; Calvert and Karlin, 1991; Lyons and Berner, 1992).

Formation of pyrite in the upper reaches of the anoxic water column is also reflected in the reactive iron enrichment relative to the total iron content of euxinic sediments (Canfield et al., 1996; Raiswell and Canfield, 1998). The term “reactive iron” refers to the iron fraction that is reactive towards dissolved sulfide at early diagenetic time scales, or is present in the form of pyrite (Berner, 1970; Goldhaber and Kaplan, 1974; Raiswell and Canfield, 1998). Despite the generally high rates of sulfate reduction in coastal sediments, the abundance of reactive iron can prevent free sulfide from accumulating in the pore water (Canfield, 1989b; Raiswell and Canfield, 1998). However, in addition to the amount of reactive iron, the time scale of reactivity is critical. Half-time reaction rates of various sedimentary iron minerals with sulfide are known and vary over orders of magnitude (Canfield et al., 1992), and it is not possible to measure the concentration of most of these specific iron minerals in the sediment using standard techniques. However, they can be delineated through extraction into general “classes” of reactivity. A number of chemical extraction techniques have been used to subdivide the iron pool that is active on the time scale of early diagenesis (Lovley and Phillips, 1987; Canfield, 1989b; Kostka and Luther, 1994; Raiswell et al., 1994). Based on such extraction procedures, Raiswell and Canfield (1998) found that the euxinic sediments in the Black Sea are enriched in highly reactive iron compared to “normal” marine sediments deposited under an oxygenated water column. They also provided evidence for a small enrichment in highly reactive iron relative to total iron in euxinic Cariaco Basin sediments, but other euxinic systems such as the Orca Basin and Kau Bay were not enriched. Since Raiswell and Canfield (1998) had no data for the oxic continental shelf sediments, they could not show if this enrichment in highly reactive iron relative to total iron is restricted to the deep-sea or is characteristic of the Black Sea as a whole.

Previous studies in the Black Sea have focused on the upper part of the anoxic water column (e.g. Lewis and Landing, 1991), the euxinic sediments of the deep-sea (e.g. Canfield et al., 1996; Lyons, 1997) or the sediments at the shelf edge, near the interface between oxic and anoxic bottom water (e.g. Shaffer, 1986; Lyons et al., 1993). In this study, special emphasis was paid to the oxic northwestern continental shelf area. This allows direct evaluation of reactive iron enrichment of Black Sea euxinic sediments relative to shelf settings. Moreover, assuming that the iron source to the Black Sea as a whole is not enriched in reactive iron relative to other marine systems, any enrichment of deep-water sediments should be balanced quantitatively by depletion in reactive iron of shelf sediments.

## Sample collection and analysis

Nine stations of the 49<sup>th</sup> cruise of the R. V. Prof. Vodyanitsky spawning a range of sedimentological settings in the northwestern Black Sea were selected for this study (Figure 6.1; Table 6.1). Stations 2 and 13 were situated just in front of the Danube and Dniester deltas, respectively. Stations 6, 9, 10 and 16 were located on the shallow central shelf. Two stations (19 and 24) were positioned near the oxic/anoxic interface on the shelf edge, and Station 22 was located in the euxinic deep basin with



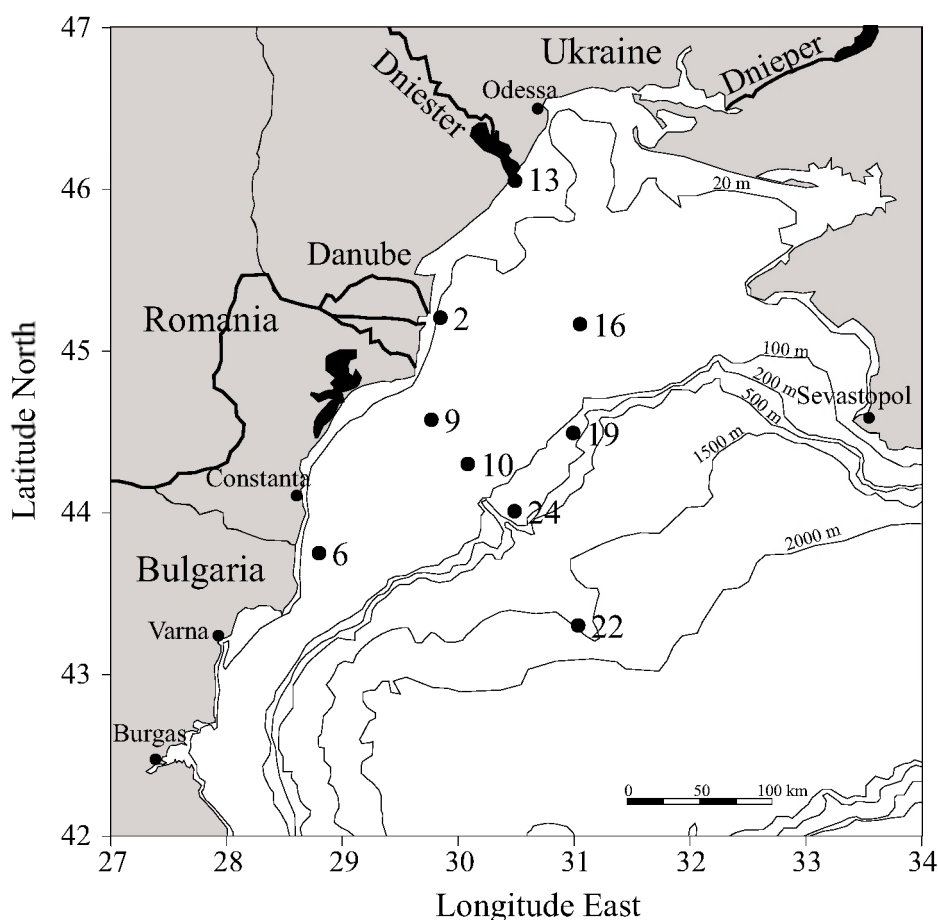


**Figure 6.1.** Map of the northwestern Black Sea showing sampling locations

**Table 6.1.** Sampling characteristics of the stations in the northwestern part of the Black Sea. Stations are grouped into 5 areas according to their geographical position. Oxygen concentration of the bottom water was measured by CTD, except data indicated by \* that were measured in the overlying water from the box corer

Station	Location		Area	Depth (m)	Oxygen ( $\mu\text{M}$ )	Oxygen uptake ( $\text{mmol O}_2 \text{ m}^{-2} \text{ d}^{-1}$ ) <sup>†</sup>
	Latitude	Longitude				
2	45°12'N	29°51'E	Danube Delta	26	207	37.9
6	43°45'N	28°48'E	Central shelf	52	285	14.0
9	44°34'N	29°46'E	Central shelf	57	243	11.6
10	44°18'N	30°05'E	Central shelf	72	284	11.0
13	46°03'N	30°29'E	Dniester Delta	13	350	26.3
16	45°10'N	31°03'E	Central shelf	54	314*	10.0
19	44°29'N	31°00'E	Shelf edge	120	126*	6.1
22	43°18'N	31°02'E	Deep-sea	1494	0*	N.D. <sup>§</sup>
24	44°00'N	30°29'E	Shelf edge	137	190*	3.1

<sup>†</sup> Measured by deck incubations (For a description of the method, see Wijsman et al., 1999)

<sup>§</sup> N.D. = not determined

Unit I micro laminated sediments. Sediment was sampled using a Reineck box-corer ( $60 \times 30 \times 30$  cm), and subcores were sliced with a resolution of 0.5 to 5 cm aboard

ship inside a  $N_2$ -filled glove box. Sediments were stored frozen in diffusion-free bags under  $N_2$ -atmosphere until analysis.

The sediment was subjected to several chemical leaching experiments to determine various iron fractions: *HCl* extractable iron (FeH; cold 1 N hydrochloric acid, 24 hrs)(Canfield, 1988; Canfield, 1989b), dithionite extractable iron (FeD; sodium dithionite 50 g l<sup>-1</sup> in 0.2 M sodium citrate / 0.35 M acetic acid, *pH* = 4.8, 2 hrs)(Canfield, 1988; Kostka and Luther, 1994) and total iron (FeT; microwave extraction with hydrochloric acid (12 N) and nitric acid (14 N)). This method for total iron extraction has been shown to be consistent with traditional total iron extractions involving HF (Nieuwenhuize et al., 1991). Iron from the *HCl* (FeH) and dithionite (FeD) extractions was determined spectrophotometrically using reducing ferrozine (Stookey, 1970; Phillips and Lovley, 1987). The *HCl* extractions were measured directly, but the dithionite extractions were stored > 1 day before adding reducing ferrozine in order to oxidize the dithionite, as recommended by Canfield et al. (1993b). Total iron was measured on a Perkin Elmer atomic absorption spectrometer (FeT). Dithionite extracts iron from poorly and well crystallized iron oxides (except magnetite) as well as iron from acid-volatile sulfides (AVS) and carbonates and adsorbed onto sediment particles (Canfield 1989b, 1993b). *HCl* extracts the same iron fractions as dithionite with addition of poorly reactive iron silicates. Acid-volatile sulfides (AVS) were determined by means of a cold acid distillation with hydrochloric acid (6 N, 2 hrs)(Fossing and Jørgensen, 1989). Pyrite content was measured by the chromium reduction method (1 M  $Cr^{2+}$  in 4 N *HCl*, 2 hrs)(Zhabina and Volkov, 1978; Canfield et al., 1986) after acetone extraction to remove elemental sulfur (Passier et al., 1996). The liberated  $H_2S$  from the AVS and pyrite extractions was stripped with  $N_2$  gas and trapped in de-oxygenated  $Zn(Ac)_2$  (for a more detailed description of the methods, see chapter 4 of this thesis). *Fe* in pyrite (FeP) and AVS (FeAVS) was calculated from the sulfur concentrations and mineral stoichiometry, assuming "*FeS*" for AVS.

## Results and discussion

### *Reactive iron*

Raiswell and Canfield (1998) partitioned the total sediment iron pool into three operationally defined iron fractions with respect to their reactivity towards dissolved sulfide. Highly reactive iron (Fe<sub>HR</sub>) is the sum of the dithionite extractable iron (FeD) and the iron that is present in the form of pyrite (FeP). Poorly reactive iron (Fe<sub>PR</sub>) is defined as the difference between the *HCl* extractable iron (FeH) and the dithionite extractable iron (FeD) and consists mainly of iron silicates that are not very reactive towards sulfide (half life time > 10<sup>5</sup> yr) on early diagenetic time scales (Canfield et al., 1992). The unreactive iron (Fe<sub>U</sub>) is defined as the total iron pool (FeT) minus the *HCl* extractable iron (FeH) and the iron present in the form of pyrite (FeP).

Figure 6.2 shows the partitioning of total iron over the various fractions as a function of depth in the sediments of stations 2, 13, 16, 19 and 22. The shelf stations (2, 13, 16 and 19) were characterized by a surface peak of highly reactive iron, other than *FeS* and pyrite. These iron enrichments, probably composed of iron oxides, are

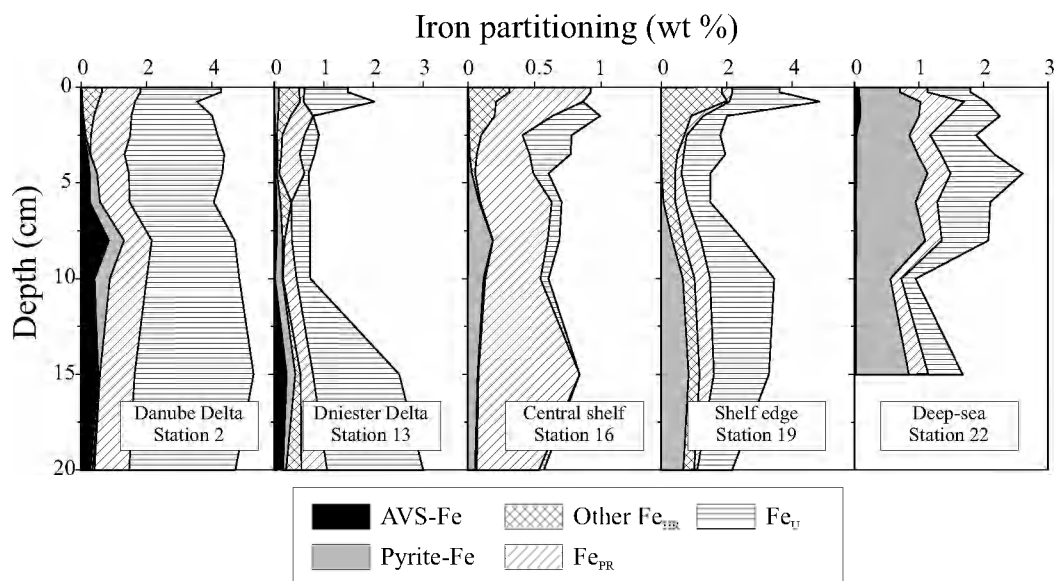


**Figure 6.2.** Depth profiles of highly reactive iron present in acid volatile sulfides (AVS), pyrite and other highly reactive (oxidized) iron species, poorly reactive iron and unreactive iron at representative stations in the Black Sea. All data are in units of weight percentage iron of the total dry sediment. For station 22 no data were available for depths greater than 15 cm

either derived from sedimentation or from re-oxidation in the upper part of the sediment. The contribution of pyrite to the highly reactive fraction increased with depth at the expense of highly reactive iron oxides. The stations near the Danube and Dniester rivers (Stations 2 and 13, respectively) were characterized by relatively high concentrations of AVS in the sediment, as is usually observed in rapidly accumulating sediments (Middelburg, 1991; Kostka and Luther, 1994; Gagnon et al., 1995; Lyons, 1997; Hurtgen et al., 1999). At the deep-sea station (22), pyrite was the dominant form of highly reactive iron, and oxidized forms were absent.

Figure 6.3 shows the relationships between the highly reactive, poorly reactive and unreactive iron fractions and total iron for Black Sea samples together with the global trends derived by Raiswell and Canfield (1998). The latter are based on a comprehensive global data set of aerobic and dysaerobic continental margin and deep-sea sediments. The highest concentration of highly reactive iron ( $> 1.5$  wt %) was found in the upper cm of station 19 located at the shelf edge. This enrichment, relative to total iron, is probably due to intensive recycling (remobilization) of iron by redox reactions near the sediment-water interface (Chapter 4 of this thesis). The fraction of highly reactive iron in iron-rich sediments of the Danube delta ( $\text{Fe}_{\text{HR}}/\text{Fe}_{\text{T}} = 0.12 \pm 0.012$  SE) is significantly lower (Students  $t$ -test,  $p < 0.01$ ) compared to the Dniester delta sediments ( $\text{Fe}_{\text{HR}}/\text{Fe}_{\text{T}} = 0.27 \pm 0.035$  SE) (Table 6.2). Sediments from the euxinic deep-water station 22 were enriched in highly reactive iron but not as pronounced as the non-turbidite Black Sea sediments of Raiswell and Canfield (1998). Nevertheless, the  $\text{Fe}_{\text{HR}}/\text{Fe}_{\text{T}}$  ratio at station 22 ranged from 0.38 to 0.58 (average  $0.47 \pm 0.018$  SE), which is significantly higher (Students  $t$ -test,  $p < 0.01$ ) than the data of Raiswell and Canfield (1998) for aerobic and dysaerobic marine environments. The highly reactive iron fraction at this deep-sea station was almost entirely composed of pyrite

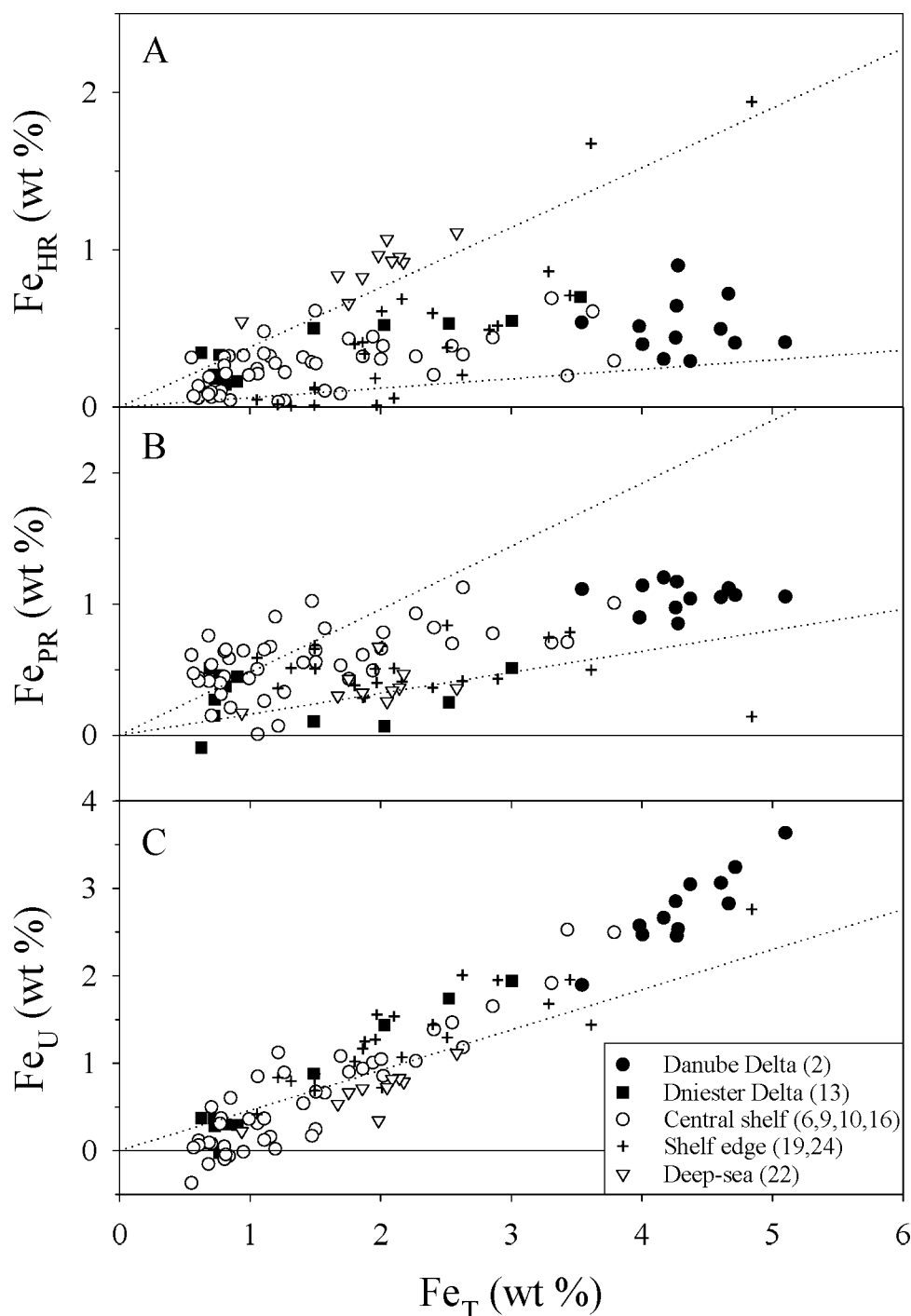


**Figure 6.3.** Variations in the content of (A) highly reactive iron ( $Fe_{HR} = FeD + FeP$ ), (B) poorly reactive iron ( $Fe_{PR} = FeH - FeD$ ) and (C) unreactive iron ( $Fe_U = FeT - FeH - FeP$ ) with total iron in the sediments of the Black Sea. For each station within the various regions, the individual data for all sediment depths are presented. Dotted lines in (A) and (B) represent the upper and lower ranges, and the line in (C) represents the regression based on the comprehensive global data set of Raiswell and Canfield (1998) encompassing aerobic and dysaerobic continental shelf and deep-sea sediments. Station number are indicated between brackets

**Table 6.2.** Summary of ratios of highly reactive iron content to total iron content ( $\text{Fe}_{\text{HR}}/\text{Fe}_{\text{T}}$ ), measured in this study and as compiled by Raiswell and Canfield (1998)

Station	Average	S.E.	n
This study			
<b>Delta area</b>			
2	0.12	0.012	12
13	0.27	0.035	12
Total	0.19	0.024	24
<b>Central shelf</b>			
6	0.29	0.022	12
9	0.13	0.016	11
10	0.15	0.033	12
16	0.20	0.042	11
Total	0.20	0.017	46
<b>Shelf-edge</b>			
19	0.23	0.039	11
24	0.10	0.027	12
Total	0.16	0.027	23
Total shelf	0.19	0.012	93
<b>Deep-sea</b>			
22	0.47	0.018	10
<b>Overall Black Sea</b>	<b>0.21</b>	<b>0.014</b>	<b>103</b>
Raiswell and Canfield (1998)			
Continental margin	0.28	0.009	46
Deep Sea	0.25	0.013	56
Dysaerobic	0.28	0.020	26
All data	0.27	0.008	128

(97 – 100 %; Figure 6.2), which formed in the upper part of the anoxic water column (Muramoto et al., 1991; Lyons, 1997). The  $\text{Fe}_{\text{HR}}/\text{Fe}_{\text{T}}$  ratio in the non-turbiditic Black Sea sediments of Raiswell and Canfield (1998) ranged from 0.5 to 1. These higher ratios might be attributed to an overestimation of the  $\text{Fe}_{\text{D}}$ . Based on a cross-calibration with a small number of samples ( $n=5$ ), Raiswell and Canfield (1998) estimated that 38 % of the *HCl* extractable iron is extractable by dithionite. However, in our deep-sea samples dithionite extractable iron contributed only 2.5 % to the *HCl* extractable iron pool.

About 35 % ( $\pm 2.3$  % SE) of the total iron content in all our northwestern Black Sea sediments, was composed of poorly reactive iron. The shelf stations were enriched with poorly reactive iron compared to the continental margin sediments studied by Raiswell and Canfield (1998). Finally the unreactive iron content shows a linear relation with the total iron:  $\text{Fe}_{\text{U}} = 0.72 \cdot \text{Fe}_{\text{T}} - 0.40$  ( $n = 99$ ;  $R^2 = 0.91$ ). The negative intercept indicates that at total iron concentrations lower than 0.56 wt % ( $= -\text{intercept} / \text{slope} = 0.4 / 0.72$ ), the iron pool is entirely composed of reactive iron ( $\text{Fe}_{\text{HR}} + \text{Fe}_{\text{PR}}$ ).

### ***Degree of pyritization (DOP)***

The DOP has successfully been used as a marker for ancient euxinic sediments (Raiswell et al., 1988). It measures the extent to which reactive iron has been converted to pyrite and is usually calculated as

$$DOP = \frac{FeP}{FeP + Fe^*}, \quad (6.1)$$

where FeP is the iron present in the form of pyrite and Fe\* is the reactive iron that has not yet reacted with sulfide. The reactive iron fraction (Fe\*) in the sediments is usually determined using a boiling *HCl* extraction (12 N, 1 min) (Berner, 1970) or a cold *HCl* extraction (1 N, 24 h). The cold *HCl* extraction is suggested to yield DOP values for Black Sea sediments comparable to those of the traditional boiling *HCl* method (Leventhal and Taylor, 1990), but this does not necessarily hold for all type of sediments. Typical values of DOP based on *HCl* extraction (DOP<sub>HCl</sub>) are less than 0.42 for sediments deposited during oxygenated conditions, 0.42 to 0.8 for low oxygen environments and 0.55 to 0.93 for euxinic depositional conditions (Raiswell et al., 1988). In this study, the DOP<sub>HCl</sub> values for the deep-sea station 22 ranged from 0.57 in the upper part to 0.80 at depths  $\geq \sim 10$  cm in the sediment (Figure 6.4), consistent with observations by Lyons and Berner (1992), Canfield et al. (1996), Calvert and Karlin (1991), and Lyons (1997). The slight increase with depth might result from the diagenetic component of pyrite formation (Lyons, 1997). The oxic shelf stations have lower DOP<sub>HCl</sub> values ( $< 0.4$ ). However, at stations 19 and 24, located in the zone of alternating oxic and anoxic bottom water conditions (Lyons et al., 1993), the DOP<sub>HCl</sub> increased to  $> 0.5$  at depths of more than 10 and 6 cm, respectively.

Due to the high sedimentation rates at the shallow water stations, their surficial sediments are relatively young compared to surficial sediments in the deep-sea. The processes of carbon degradation and pyrite formation at these shallow stations are not yet completed, and part of the reactive iron might still be converted to pyrite during burial, see station 15 in Lyons (1997) and Hurtgen et al. (1999) for related observations. The degree of sulphidization (DOS; Boesen and Postma, 1988; Middelburg, 1991), calculated as

$$DOS = \frac{FeP + FeAVS}{FeP + FeH} \quad (6.2)$$

yielded similar values as the DOP<sub>HCl</sub> for stations 19, 22 and 24, which are poor in FeAVS. However, at the AVS-rich delta stations 2 and 13, DOS values were higher than the DOP<sub>HCl</sub> values and ranged from 0.03 to 0.75. The abrupt decrease in DOP values at a depth of 10 cm probably results from a non-steady state deposition.

Suits and Wilkin (1998) introduced DOP<sub>Dith</sub> in which dithionite extractable iron (FeD) is used as a measure of reactive iron because it extracts only a small fraction of the poorly reactive iron silicates (Raiswell et al., 1994). At all stations, DOP<sub>Dith</sub> approached unity at depths greater than 10 cm, except for the stations located in front of the river estuaries (Stations 2 and 13). Therefore, DOP<sub>Dith</sub> values of subsurface sediments have limited power to resolve ancient bottom-water oxygen conditions.

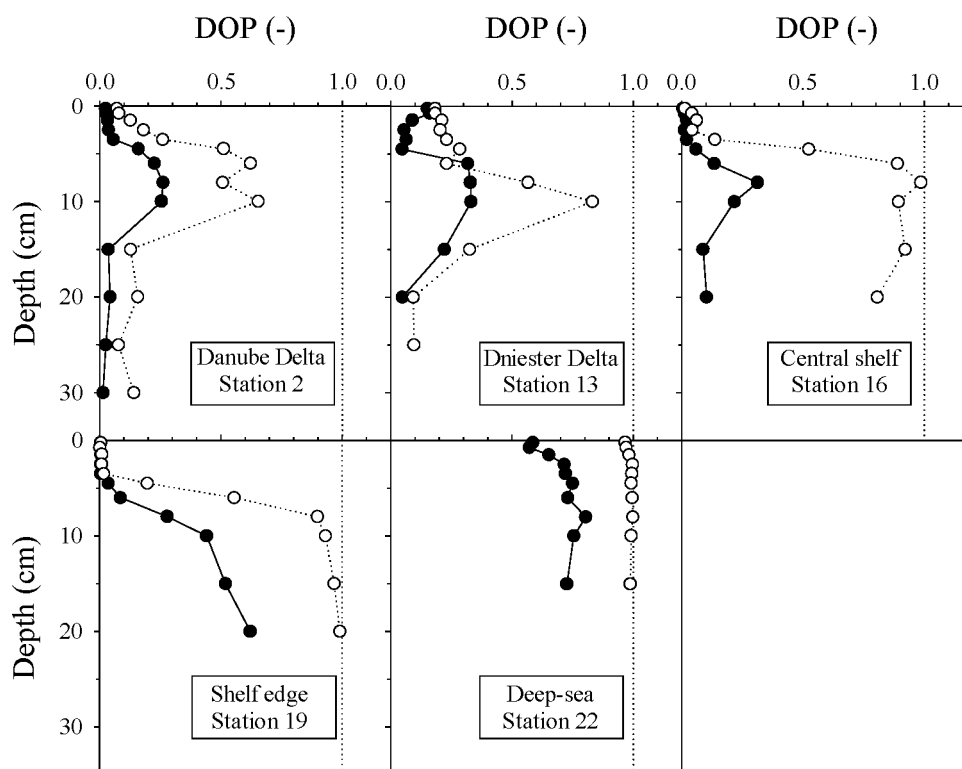


**Figure 6.4.** Depth profiles of  $\text{DOP}_{\text{HCl}}$  (filled circles) and  $\text{DOP}_{\text{Dith}}$  (open circles) in the sediment at representative stations in the Black Sea. Dotted reference lines indicate  $\text{DOP} = 1$ , i.e. the situation where all the reactive iron has been converted into pyrite

### *The source of reactive iron*

In contrast to the deep-sea sediments of the Black Sea, the shelf sediments were significantly depleted (Students  $t$ -test,  $p < 0.01$ ) in highly reactive iron ( $\text{Fe}_{\text{HR}}/\text{FeT}$  ratio =  $0.19 \pm 0.012$  SE) compared to normal oxic and suboxic marine sediments in general (Raiswell and Canfield, 1998)(Table 6.2). This might be due to a re-allocation of highly reactive iron from the continental shelf to the deep-water euxinic sediments. A possible mechanism for this re-allocation is that dissolved iron, produced by iron reduction, is lost from the shelf sediments and subsequently transported to the chemocline in the euxinic part of the Black Sea. Lewis and Landing (1991) found elevated concentrations in dissolved iron in the upper part of the anoxic water column where pyrite formation occurs (Muramoto et al., 1991). The pyrite formed in the water column is lost from the system through sedimentation and burial in the sediment. Assuming that the micro laminated station 22 is representative for the whole euxinic part of the Black Sea, this sediment type is enriched in highly reactive iron by 0.24 and 0.81 wt% as compared to the upper and lower boundary, respectively, of the range characterizing normal aerobic and dysaerobic continental margin and deep-sea sediments (Raiswell and Canfield, 1998). This may represent an overestimate because turbiditic sediments cover only part of the basin and have lower reactive iron contents (Lyons, 1997). Based on a sediment accumulation rate of  $0.02 \text{ cm yr}^{-1}$  in the deep-sea area (Buesseler and Benitez, 1994) and an average porosity of

0.86 in the upper 15 cm, this results in a supplementary highly reactive iron flux of 0.82 to 2.75 nmol  $Fe\text{ cm}^{-2}\text{ d}^{-1}$ . Since the euxinic part covers 73 % of the total area of the Black Sea (Sorokin, 1983), a net flux of 2.2 to 7.4 nmol  $Fe\text{ cm}^{-2}\text{ d}^{-1}$  is required from the continental shelf sediments to account for the enrichment in highly reactive iron in the deep-sea.

Oxygen present in the bottom water and in the upper few mm of the sediment column can possibly act as a trap for dissolved iron in the sediment. The reactive iron will then be recycled within the sediment through iron reduction at depth and iron oxidation and precipitation in the surface layer. We have investigated the influence of bottom water oxygen concentration on the internal cycling of iron and the dissolved iron flux out of the sediment by means of a numerical model for early diagenetic processes in Black Sea sediments (Chapter 4 of this thesis). This model explicitly resolves the major processes involved in sedimentary iron cycling. The parameter settings from chapter 4 of this thesis were used, with a total depth integrated rate of mineralization ( $\Sigma R_{min}$ ) of 1370 nmol  $C\text{ cm}^{-2}\text{ d}^{-1}$  and a reactive iron flux to the sediment ( $J_{Fe(OH)3}$ ) of 28 nmol  $\text{cm}^{-2}\text{ d}^{-1}$ . The oxygen concentration in the bottom water was varied in the calculations between 0 and 300  $\mu\text{M}$ . Figure 6.5 shows the dissolved iron flux over the sediment-water interface and the cycling efficiency of iron ( $E$ ) as a function of bottom-water oxygen concentrations. The cycling efficiency of iron is defined as

$$E = \frac{R_{red}}{J_{Fe(OH)3} + R_{red}}, \quad (6.3)$$

where  $R_{red}$  is the rate of iron reduction, and  $J_{Fe(OH)3}$  is the flux of iron oxides to the sediment (Chapter 4 of this thesis). At all bottom water oxygen levels, sulfate reduction is the dominant pathway for organic matter degradation. Under anoxic bottom water conditions, the iron cycling efficiency is low (0.5), indicating that on average each mole of reactive iron arriving on the sediment is used once for iron reduction. The cycling efficiency of iron increases with increasing oxygen concentration in the bottom water, to a maximum value of 0.9 at an oxygen concentration of 300  $\mu\text{M}$ . At this oxygen concentration, each iron molecule is reduced 9 times before it is lost by burial or escapes into the water column. The calculated dissolved iron efflux reaches a maximum of 23 nmol  $\text{cm}^{-2}\text{ d}^{-1}$  at a bottom-water oxygen concentration of about 50  $\mu\text{M}$ . At lower oxygen concentrations more iron is permanently buried in the sediment in the form of iron sulfides. At higher oxygen concentrations the dissolved iron flux decreases to a minimum value of 7 nmol  $\text{cm}^{-2}\text{ d}^{-1}$  because of a more efficient trapping in the surface layer. However, the trapping of iron in the surface layer is never complete, not even under fully oxygenated conditions. Friedl et al. (1998) and Friedrich et al. (2000) measured iron fluxes at 11 sites in the northwestern continental shelf using an *in situ* benthic flux chamber. Neglecting one extreme high value of 1633 nmol  $Fe\text{ cm}^{-2}\text{ d}^{-1}$  at the shelf edge (Friedl et al., 1998, station BS26), iron fluxes ranged from 0.5 to 184 (average 46) nmol  $Fe\text{ cm}^{-2}\text{ d}^{-1}$ .

The gross dissolved iron fluxes out of the sediment as calculated by the diagenetic model (7–22 nmol  $\text{cm}^{-2}\text{ d}^{-1}$ ; Figure 6.5) and as measured *in situ* (average 46 nmol  $\text{cm}^{-2}\text{ d}^{-1}$ ) were higher than the net transfer of reactive iron from shelf sediments to the deep-sea, predicted from reactive iron enrichment (2.4 to 7 nmol  $\text{cm}^{-2}\text{ d}^{-1}$ ). Clearly, the majority of the sedimentary iron efflux does not reach the deep-sea and is



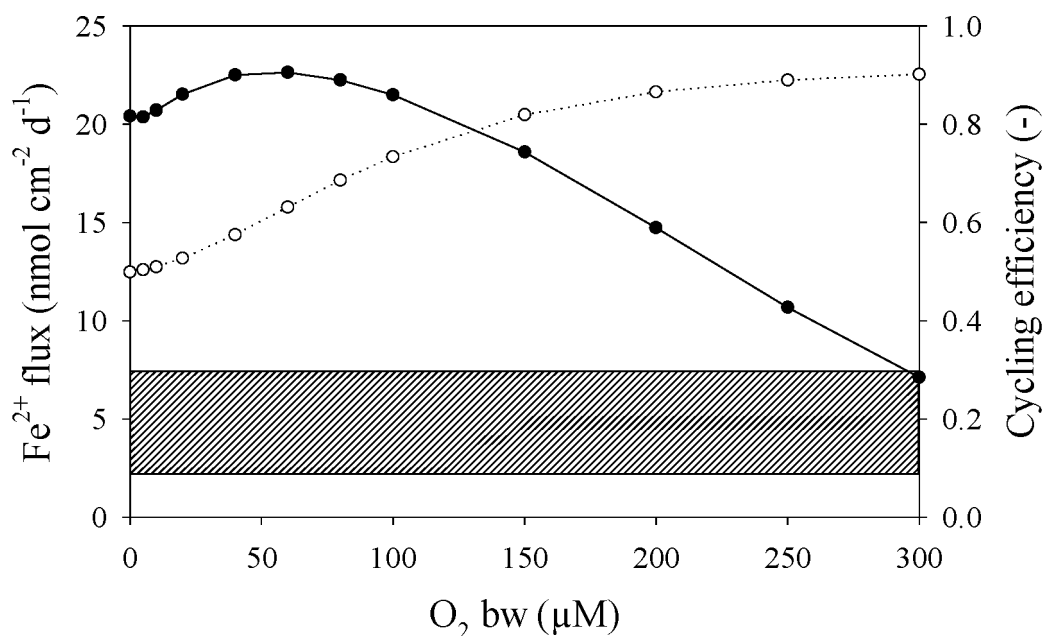


**Figure 6.5.** Diagenetic model derived fluxes of dissolved iron into the water column (filled circles) and cycling efficiencies of iron in the sediment (open circles) as a function of the bottom water oxygen concentration. Hatched area indicates the range of net iron fluxes ( $2.22 - 7.44 \text{ nmol Fe cm}^{-2} \text{ d}^{-1}$ ) that is required to sustain enrichment of highly reactive iron in the deep-sea

redeposited on the continental shelf. Most of the reduced iron diffusing out of sediments is rapidly oxidized and reprecipitated, but part of it may be transported laterally after incorporation in algae, bacteria or colloids (Schoeman et al., 1998). The northwestern shelf of the Black Sea is similar to other temperate continental shelf systems in terms of sediment characteristics and organic matter fluxes (Wijsman et al., 1999). The iron mobilization mechanism observed in the Black Sea likely operates in other shelf ecosystems as well e.g., the North Sea and Californian shelf (Slomp et al., 1997; Johnson et al., 1999). Such an iron mobilization mechanism might be important to sustain high shelf productivity (Martin, 1990). The net effect of this iron mobilization mechanism becomes apparent only if (1) there is a process driving (or facilitating) lateral transport and (2) there is a sink of reactive iron. Both criteria are met in the Black Sea. The sulfidic water column and underlying sediments act as an efficient scavenger of any reactive iron being delivered, and there is significant transfer from the shelf to the interior of the Black Sea related to formation of the cold intermediate waters at the shelf (Tolmazin, 1985b; Stanev, 1990; Oguz and Malanotte-Rizzoli, 1996). A similar mechanism may explain the transfer of dissolved iron from the shelf to the ocean interior in the low oxygen zones along the ocean margin. Landing and Bruland (1987) and Saager et al. (1989) clearly documented the importance of shelf mobilization and lateral transport in iron supply to the ocean interior. The mechanism underlying transfer of reactive iron (shelf-mobilization, lateral transport, and sulfide trapping) is generic, i.e. not specific to the Black Sea, and may be the key to understand ancient euxinic systems.

## Conclusions

It has been suggested by Canfield et al. (1996) and Raiswell and Canfield (1998) that the formation of iron sulfides in the upper part of the anoxic water column of the Black Sea results in enrichment in highly reactive iron of the deep-sea sediments. New data from the abyssal part of the Black Sea show that these sediments are indeed enriched in highly reactive iron. The flux of iron sulfides from the water column to the sea bottom is also reflected in the relatively high DOP values (0.57 to 0.80) in the deep-sea sediments. Additional data from the oxic continental shelf show that these sediments are depleted in highly reactive iron compared to other oxic and suboxic marine environments as summarized by Raiswell and Canfield (1998)(see Table 6.2). This depletion in reactive iron indicates that reactive iron is lost from these sediments. The total flux of dissolved iron from the sediments of the continental shelf into the water column is more than sufficient to balance for the burial of excess highly reactive iron in the deep-sea sediments. The reported iron-transfer mechanism is generic and likely operates in most environments, but it is highly efficient in the Black Sea due efficient mechanisms for lateral transport and iron scavenging by sulfides.

---

## CHAPTER 7

### Summary

---

Transport between the sea floor and the overlying water is essential for benthic pelagic coupling in marine systems (Graf, 1992). Not only organic matter, but also other solid phase components such as iron- and manganese-oxides that are crucial for many early diagenetic processes reach the sea floor through deposition. Additionally, dissolved nutrients and gasses are exchanged between the sediment and water column through diffusive-type of transport. This thesis deals with the response of early diagenetic processes in Black Sea sediments to changes in sedimentation and nutrient composition of the water overlying the sea floor.

Sediment respiration, which is directly linked to the flux of degradable organic matter to the sea floor, is the key factor for many early diagenetic processes in the sediment. In **chapter 2** we have developed a conceptual model for sediment respiration versus water depth that takes into account different transport modes of organic matter to the sediment operating in shallow and deep-water columns. In shallow water, turbulent mixing dominates, while in deep water, rapid sinking is the major deposition pathway. Fitting of this model to a comprehensive dataset of sediment community oxygen consumption (SCOC) measurements from a variety of marine systems (ranging from shallow estuaries and coastal seas to deep-sea sediments up to 6,000 m depth) from all over the world resulted in relation 2.4. SCOC in this model is a measure for the flux of degradable organic matter to the seafloor. According to this model, 86 % of the organic matter production in the water column at  $Z=0$  is subject to turbulent mixing, deposition-resuspension cycles and has a low net settling velocity. The remaining 14 % reaches the sediment by rapid particle settling. This settling transport is by far the major transport mechanism of organic carbon to deep-sea sediments and can be regarded as the “new” production, resulting in an  $f$ -ratio of 0.14, which corresponds to previous reported  $f$ -ratios for deep-sea environments (Eppley and Peterson, 1979; Wollast, 1998).

Although on a global scale water depth seems to be the dominant factor determining sediment respiration rates, other factors such as primary production in the water column and the quality of the sedimenting material account for much of the variation in benthic respiration rates at a local scale. In the northwestern continental shelf of the Black Sea, for example, sedimentation processes are largely influenced by the river Danube. In **chapter 3**, we have distinguished three areas on the northwestern shelf based on the spatial distribution of abiotic sediment characteristics and the macrobenthos community: (1) The area just in front of the Danube Delta where large amounts of nutrients and suspended solids are discharged. High sedimentation rates of relatively fine-grained sediments and high benthic mineralization rates characterized

this area. The macrobenthos community was dominated by deposit feeders. (2) The northern part of the continental shelf, where an anticyclonic gyre is located. The majority of the Danube discharge is transported to this region. This area is characterized by low sedimentation rates. However, the deposited material contained a larger fraction of labile organic matter than the delta area, resulting in high benthic mineralization rates. Suspension feeders dominated the macrobenthos community. (3) The southern part of the continental shelf was characterized by low sedimentation rates and low rates of benthic mineralization. In this area suspension feeders dominated the macrobenthos community. SCOC rates ranged between 2 and 52 mmol  $O_2$  m<sup>-2</sup> d<sup>-1</sup> (average 21 mmol  $O_2$  m<sup>-2</sup> d<sup>-1</sup>) decreasing with water depth. Macrobenthos accounted on average for 20 % of the total benthic oxygen consumption. In the northern part of the continental shelf and in the coastal stations, microorganisms, and micro- and meiobenthos dominated benthic community respiration, while macrobenthos became relatively more important in terms of oxygen consumption in the southern part of the continental shelf.

In order to study the response of early diagenetic processes in the northwestern Black Sea sediments to changes in the boundary conditions, a numerical model has been developed, which is presented in **chapter 4**. Low oxygen concentrations in the bottom water and high carbon deposition rates, which are characteristic features of the northwestern Black Sea, resulted in a dominance of anoxic mineralization processes including manganese, iron and sulfate reduction. The model includes six solid phase (two carbon fractions with different reactivity, iron- and manganese oxides, iron monosulfide and pyrite) and eight solute variables (oxygen, nitrate, ammonium, manganese, iron, sulfate, hydrogen sulfide and methane). The cycling of iron and sulfur is explicitly incorporated in the model because these elements play an important role in the mineralization of organic matter on the continental shelf. The model is capable to perform both steady state and dynamic simulations and because of its simplicity and calculation speed it can easily be coupled to biogeochemical models for water-column processes. The output of the model is composed of depth profiles of the state variables and their biogeochemical reaction rates and fluxes of the solute substances across the sediment-water interface. The model has been applied to solid-phase and pore-water data from station 9 (May 1997) near the Danube Delta. A steady state simulation reasonably reproduced the main features, but not the distribution of iron and the concentrations of oxygen and total organic carbon in the first two cm. A dynamic simulation revealed that a pulse flux of organic matter, resulting from the spring bloom, could be responsible for the deviation from steady state in the near surface distribution of total organic carbon and oxygen.

With the use of the model, the effect of variable carbon loading on organic matter degradation pathways has been investigated. There is a gradual increase in the relative importance of anoxic mineralization pathways as carbon loadings increase, but the transitions from manganese-based respiration to iron-based respiration and from iron-based respiration to sulfate reduction are rather abrupt. The first jump is due to the positive feedback between manganese reduction coupled to ferrous iron oxidation and iron oxide reduction. The second swap is due to the formation of iron sulfides. This will consume part of the reduced iron, which is consequently not available for re-oxidation to iron oxide and iron-reducing bacteria then become iron oxide limited. The cycling efficiency of iron changes abruptly and a larger part of the iron will be fixed as iron sulfides.

The model confirmed that anaerobic mineralization processes such as iron- and sulfate reduction were relatively important in the sediments of the northwestern

Black Sea. At station 9 (May 1997), for example, sulfate reduction alone accounted for almost 50 % of the total benthic carbon mineralization. The dissolved sulfide that is formed during this sulfate reduction quickly reacts with the reactive iron that is present in the sediments to form iron sulfides such as  $FeS$  and pyrite. Through this mechanism, reactive iron acts as a buffer to prevent free sulfide accumulation in the sediment. As a result of the formation of iron sulfides, the cycling patterns of iron and sulfur are intensively coupled. In **chapter 5**, the cycling of sulfur and iron was analyzed in the sediments of the northwestern Black Sea by means of depth profiles of various sulfur (pyrite; acid volatile sulfides (AVS);  $S^0$ ;  $H_2S$ , sulfate) and iron (dissolved and dithionite-extractable iron, pyrite and AVS) species and the sulfur isotope ratios of sedimentary pyrite. Sulfur and iron cycling in surface sediments of the northwestern part of the Black Sea is largely influenced by (1) organic matter supply to the sediment, (2) availability of reactive iron compounds and (3) oxygen concentrations in the near-bottom waters. Biologically active sediments just in front of the river deltas were characterized by high AVS contents and a fast depletion of pore water sulfate with depth, most likely due to high sulfate reduction rates (SRR). The  $\delta^{34}S$  values of pyrite in these sediments were relatively high (-8 ‰ to -21 ‰ vs. V-CDT). On the central shelf, where benthic mineralization rates are lower, re-oxidation processes may become more important resulting in pyrite extremely depleted in  $^{34}S$  (-39 ‰ to -46 ‰ vs. V-CDT). A high variability in  $\delta^{34}S$  values of pyrite in sediments from the shelf-edge (-6 ‰ to -46 ‰ vs. V-CDT) reflects characteristic fluctuations in the oxygen concentrations of near-bottom waters. During oxic conditions, re-oxidation processes became important, resulting in low AVS concentrations and light  $\delta^{34}S$  values. Anoxic conditions of the bottom waters overlying shelf-edge sediments are reflected in enhanced AVS contents and higher sulfur isotope values. The sulfur and iron contents, and the pyrite isotopic composition (-37 ‰ to -39 ‰ vs. V-CDT) of sediments in the permanently anoxic deep-sea (1494 m water depth) reflect the formation of pyrite in the upper part of the sulfidic water column and the anoxic surface sediment. It is demonstrated that pyrite, extremely enriched in  $^{32}S$ , can be found in the Black Sea surface sediments which are positioned both above and below the chemocline, in spite of different biogeochemical and microbial controlling factors.

A remarkable feature of the euxinic Black Sea is that iron sulfides are formed in the anoxic water column and sink to the deep-sea floor where they are buried in the sediment (e.g. Goldhaber and Kaplan, 1974). Consequently, the deep-sea is a sink for sulfur and reactive iron from the system. The flux of iron sulfides from the water column is reflected in enhanced concentrations of highly reactive iron and a high degree of pyritization (0.57 – 0.80) for the deep-water sediments of the Black Sea (**Chapter 6**). The iron enrichment of deep-water sediments is balanced by a loss of highly reactive iron from the oxic continental shelf. Calculations from a numerical diagenetic model and reported *in situ* flux measurements indicate that the dissolved iron flux out of the shelf sediments is more than sufficient to balance for the excess sink of reactive iron in deep-sea sediments. This iron mobilization mechanism likely operates in most shelf areas, but its net effect becomes only apparent when reactive iron is trapped in sulfidic water bodies as iron sulfides or when iron is incompletely oxidized in low oxygen zones of the ocean.

Due to a lack of historical data on sediment respiration, we were not able to relate benthic mineralization rates on the northwestern Black Sea shelf to eutrophication effects. However, gradients in organic loading induced by the Danube discharges allowed us to investigate effects of this predicted increase in organic

loading due to eutrophication. SCOC measurements were in the same range as other (eutrophicated) continental shelf systems and did not reveal an extremely eutrophicated situation in the Black Sea in summer 1995 and spring 1997. This does not mean that the Black Sea has not suffered from enhanced levels of eutrophication in a previous period (between 1960 and 1990). It could be that the level of eutrophication has decreased during the last couple of years. Recently, some positive signs of ecosystem recovery in the Black Sea were observed. Due to the economic collapse of the Eastern and Central-European countries in the early nineties, phosphorus and nitrogen loads have decreased (Cociasu and Popa, 2000). Consequently, a diminution of algal blooms and total phytoplankton abundance was observed on the shelf (Bodeanu et al., 2000). Some planktonic and benthic species that were considered to be extinct or very rare have become very common again in the Black Sea. Moreover, the abundance of undesirable jellyfish has leveled out and the number of anchovy eggs and larvae has increased (Final report EROS-21 project, January 1999).

The recent history has shown that the ecosystem of the Black Sea continental shelf is very vulnerable to human perturbations. This is mainly caused by the large number of people that live in the catchment areas of the rivers discharging in the shallow continental shelf. In 1992, about 81 million people lived in the drainage basin of the Danube compared to 41 million for the drainage basin of the Rhine (Mee, 1992). Much of the pollutants and nutrients that are produced by this population reach the waters of the continental shelf where they can enhance the primary production. High benthic mineralization rates that result from mass deposition of organic material at the sea floor after a phytoplankton bloom could easily result in anoxic conditions of the near-bottom water. Especially during summer, when mixing processes in the water column are restricted due to temperature stratification.

---

## CHAPTER 8

### Samenvatting

---

Sinds de jaren zestig hebben er dramatische veranderingen plaatsgevonden in het ecosysteem van de Zwarte Zee. Vele flora- en faunasoorten zijn sterk in aantal achteruit gegaan of zelfs geheel verdwenen, terwijl andere soorten, die voorheen niet of slechts in kleine aantallen voorkwamen, zich sterk hebben ontwikkeld. Er zijn aanwijzingen dat deze veranderingen primair zijn te wijten aan de toename van economische en agrarische activiteit in de stroomgebieden van de aanvoerende rivieren naar de Zwarte Zee. Door het intensieve gebruik van kunstmest en lozing van rioolwater in de rivieren is de toevoer van nutriënten (voedingsstoffen) naar de Zwarte Zee de laatste decennia sterk toegenomen. Dit heeft geleid tot eutrofiëring in het relatief ondiepe continentaal plat in het noordwesten waar drie belangrijke rivieren uitmonden, de Donau, de Dnjestr en de Dnjepr.

Binnen twee Europese onderzoekprojecten (EROS-2000 en EROS-21) zijn de effecten van eutrofiëring op de veranderingen in het ecosysteem van de noordwestelijke Zwarte Zee onderzocht. Als onderdeel van deze projecten behandelt dit promotieonderzoek de gevolgen van eutrofiëring voor de vroege diagenese. Onder vroege diagenese verstaan we de verzameling van biologische-, chemische- en fysische processen, die plaatsvinden in de bovenste decimeters van de zeebodem. De afbraak van organisch materiaal, voornamelijk afkomstig van afgestorven organismen uit de waterkolom, is een sleutelfactor voor deze processen. De in de zeebodem aanwezige fauna en allerlei micro-organismen breken het organisch materiaal af tot kooldioxide, en verbruiken hierbij de in het water aanwezige zuurstof als oxidator. Echter, sommige micro-organismen zijn in staat om het organisch materiaal onder zuurstofloze omstandigheden af te breken. Zij gebruiken hiertoe alternatieve oxidanten als nitraat, ijzeroxides en sulfaat. De eindproducten van deze reacties zijn op hun beurt weer betrokken bij een complex van chemische reacties. De mate waarin deze processen in de zeebodem plaatsvinden is grotendeels afhankelijk van de hoeveelheid en de kwaliteit van het organisch materiaal dat op de zeebodem wordt afgezet. Verhoogde algenproductie in het water als gevolg van eutrofiëring leidt in het algemeen tot een verhoogde organische belasting en dientengevolge tot intensivering van de afbraakprocessen en een verhoogd zuurstofverbruik van de levensgemeenschap in de zeebodem.

De toevoer van organisch materiaal naar de zeebodem is niet alleen afhankelijk van de productie door algen (primaire productie), maar ook van de omzettingen en de verblijftijd ervan in het water. Bij een langere verblijftijd zal er relatief meer zijn afgebroken wanneer het organisch materiaal de zeebodem bereikt. De verblijftijd is afhankelijk van de waterdiepte en de netto zinksnelheid. In

**hoofdstuk 2** wordt een model gegeven voor de hoeveelheid organisch materiaal dat de zeebodem bereikt in relatie tot de waterdiepte. Volgens dit model wordt 86 % van het organisch materiaal naar de zeebodem getransporteerd door middel van turbulente menging in het water. De verhouding tussen de afbraakconstante ( $k$ ) en de netto zinksnelheid ( $v$ ) van deze fractie organisch materiaal is  $0.017 \text{ m}^{-1}$ . De overige 14 % bereikt de zeebodem door bezinking en heeft een  $k/v$  ratio van  $0.00047 \text{ m}^{-1}$ . Turbulente menging is het belangrijkste transportmechanisme in ondiepe kustzeeën en estuaria terwijl in de diepzee bezinking overheerst.

Naast de tijdelijke veranderingen in organische belasting van de bodem van de Zwarte Zee ten gevolge van eutrofiëring, zijn er ook ruimtelijke verschillen waar te nemen, vooral op het noordwestelijk gelegen continentaal plat. Deze worden voornamelijk veroorzaakt door kwantitatieve en kwalitatieve verschillen in sedimenterend materiaal als gevolg van de aanvoer van nutriënten en gesuspendeerd materiaal via de grootste rivier, de Donau. In **hoofdstuk 3** worden, aan de hand van de bodemfaunasamenstelling en abiotische sedimenteigenschappen, drie verschillende gebieden in het noordwestelijke continentaal plat van de Zwarte Zee onderscheiden: (1) Het delta gebied vlak voor de monding van de Donau, waar het troebele water rijk aan nutriënten is. De bodem van dit gebied wordt gekenmerkt door hoge depositiesnelheden van relatief fijn materiaal, hoge afbraaksnelheden en een macrofauna (bodemfauna  $> 1 \text{ mm}$ ) gemeenschap die wordt gedomineerd door sediment-etende organismen. (2) Een gebied in het noordelijk gedeelte van het continentaal plat. Het merendeel van het nutriëntenrijke water van de Donau wordt in eerste instantie naar dit gebied getransporteerd. Omdat het meeste gesuspendeerde materiaal intussen is bezonken is het water hier aanzienlijk helderder. De depositie in dit gebied is dan ook veel lager en bestaat veel meer uit vers algenmateriaal. De afbraaksnelheden van organisch materiaal in de bodem zijn daarom nog steeds hoog en de macrofauna gemeenschap wordt gedomineerd door organismen die hun voedsel uit het water filtreren. (3) Het zuidelijke deel van het continentaal plat wordt gekenmerkt door lage depositie- en afbraaksnelheden. De bodemfauna bestaat vooral uit filtrerende organismen. Door de individuele zuurstofconsumptie van de aanwezige macrofauna organismen te berekenen aan de hand van hun lichaamsgewicht is een schatting gemaakt van de zuurstofconsumptie van de macrofauna gemeenschap. Gemiddeld is de macrofauna gemeenschap verantwoordelijk voor 20 % van het totale zuurstof verbruik van de zeebodem. In het noordelijke gedeelte van het continentaal plat en de ondiepe kustgebieden was het aandeel van de macrofauna in de totale zuurstof consumptie lager dan in het zuidelijke gebied van het continentaal plat.

Om meer inzicht te krijgen in de invloed van organische belasting van de zeebodem op de individuele processen van de vroege diagenese werd een simulatie model ontwikkeld. Dit model, dat in **hoofdstuk 4** wordt gepresenteerd, beschrijft het transport en de reacties van zes vaste fase (twee fracties organisch materiaal met verschillende reactiviteit, ijzer- en mangaanoxiden, ijzermonosulfide en pyriet) en acht opgeloste componenten (zuurstof, nitraat, ammonium, mangaan, ijzer, sulfaat, sulfide en methaan) in de zeebodem. Speciale aandacht is hierbij besteed aan de beschrijving van de verschillende fracties van zwavel en ijzer. Dit was nodig omdat processen als sulfaatreductie en ijzerreductie in de bodem van de Zwarte Zee belangrijk zijn door de relatief hoge organische belasting en de aanvoer van ijzer via de grote rivieren. De uitvoer van het model bestaat uit diepteprofielen van de verschillende componenten en uitwisselingssnelheden van de opgeloste fracties tussen de zeebodem en het bovenstaande water. Het model is getest met behulp van gegevens die verzameld zijn op station 9 (mei 1997), dat gelegen is op het centrale



deel van het continentaal plat in de buurt van de monding van de Donau. Hoewel de gesimuleerde diepteprofielen van de meeste componenten redelijk overeenkwamen met de gemeten profielen, was het met een stationaire simulatie (i.e. onveranderlijk in de tijd), niet mogelijk om de profielen van zuurstof, organisch koolstof en ijzer in de bovenste centimeters goed te simuleren. Uit een dynamische simulatie met het model bleek dat de waargenomen profielen van organisch koolstof en zuurstof mogelijk zijn beïnvloed door een plotselinge toename in de aanvoer van organisch materiaal naar de zeebodem, waarschijnlijk als gevolg van de algenbloei in het voorjaar. Door het model 300 stationaire simulaties te laten uitvoeren waarbij alleen de aanvoer van organisch materiaal naar de zeebodem is gevarieerd, hebben we het effect van deze organische belasting op het relatieve belang van de verschillende afbraak processen (aërobe respiratie, denitrificatie, mangaanreductie, ijzerreductie, sulfaatreductie en methanogenese) bestudeerd. Het relatieve belang van de anaërobe afbraakprocessen nam toe met een toenemende organische belasting.

De modelberekeningen bevestigden dat anaërobe processen als ijzer- en sulfaatreductie in de bodem van de noordwestelijke Zwarte Zee van belang zijn voor de afbraak van het organisch materiaal. Op station 9 (mei 1997) bijvoorbeeld, kwam bijna 50 % van de totale afbraak voor rekening van sulfaatreducerende bacteriën. Het sulfide, dat wordt gevormd door sulfaatreductie en veelal schadelijk is voor de aanwezige bodemfauna, kan snel reageren met reactief ijzer en ijzersulfide mineralen vormen als ijzermonosulfide en pyriet. Dit mechanisme zorgt ervoor dat, indien er voldoende buffer van reactief ijzer in de zeebodem aanwezig is, al het geproduceerde sulfide direct wordt vastgelegd. De kringlopen van ijzer en zwavel zijn, door de vorming van ijzersulfide mineralen, sterk aan elkaar gekoppeld. In **hoofdstuk 5** worden deze kringlopen in de bodem van de Zwarte Zee bestudeerd aan de hand van diepte profielen van diverse zwavel (sulfaat, vrije sulfide, pyriet, AVS [ $\approx$  ijzermonosulfide + vrije sulfide] en elementair zwavel [ $S^0$ ]) en ijzer (opgelost ijzer, dithioniet-extraheerbaar ijzer, pyriet en AVS) fracties. Tevens zijn er diepteprofielen geanalyseerd van de stabiele isotoopsamenstelling van zwavel in pyriet ( $\delta^{34}S$ ). In de noordwestelijke Zwarte Zee worden de kringlopen van ijzer en zwavel voornamelijk beïnvloed door (1) de organische belasting van de zeebodem, (2) de beschikbaarheid van reactief ijzer en (3) de zuurstofcondities van het bovenstaande water.

Normaal worden ijzersulfiden uitsluitend gevormd in de zeebodem. In de Zwarte Zee echter vindt ijzersulfide vorming voornamelijk plaats in het bovenstaande zuurstofloze water, waar vrij sulfide in contact komt met reactief ijzer. De ijzersulfide mineralen zinken naar de zeebodem om daar vervolgens permanent begraven te worden. Er verdwijnt dus continu reactief ijzer uit het systeem naar de zeebodem in het zuurstofloze, diepe gedeelte van de Zwarte Zee. In **hoofdstuk 6** is gekeken naar de consequenties van ijzersulfide vorming in de waterkolom van de Zwarte Zee voor de kringloop van reactief ijzer. De zuurstofloze bodem van de diepzee is verrijkt met reactief ijzer in vergelijking met normale zuurstofrijke mariene systemen. De sedimenten van het continentaal plat daarentegen zijn verarmd in reactief ijzer. In dit hoofdstuk suggereren we dat er opgelost reactief ijzer uit de bodem van het continentaal plat weglekt naar het bovenstaande water. Dit ijzer wordt met de stromingen getransporteerd naar de diepzee waar het kan reageren met sulfide om vervolgens in de vorm van ijzersulfiden permanent naar de bodem te verdwijnen. Om weg te kunnen lekken uit de bodem van het continentaal plat mag het opgeloste reactieve ijzer niet reageren met zuurstof omdat het dan immobiel wordt. Tevens vereist dit mechanisme dat er voldoende ijzer weglekt vanuit de bodem van het continentaal plat om het verlies naar de diepzee te compenseren. Uit berekeningen

met het diagenetisch model is gebleken dat er, ongeacht de zuurstofconcentratie van het bovenstaande water, meer dan genoeg ijzer uit de zeebodem weglekt om te compenseren voor het verlies aan reactief ijzer in de diepzee.

Vanwege een gebrek aan historische data voor de noordwestelijke Zwarte Zee was het niet mogelijk om de procesveranderingen ten gevolge van de eutrofiëring in de zeebodem te onderzoeken. Door de grote verschillen in organische belasting van de zeebodem in dit gebied, veroorzaakt door de dominante invloed van de rivieren, was het wel mogelijk om de invloed van organische belasting op de vroege diagenese te onderzoeken. De totale afbraaksnelheden van het organisch materiaal in de bodem van het continentaal plat van de Zwarte Zee in de zomer van 1995 en het voorjaar van 1997 waren vergelijkbaar met andere (veelal ook eutrofe) systemen en gaven geen aanwijzing voor extreem hoge organische belasting in deze perioden. Het is echter goed mogelijk dat in het verleden (tussen 1960 en 1990) de afbraaksnelheden in de zeebodem veel hoger zijn geweest. Er zijn recentelijk meer aanwijzingen voor verbetering van het ecosysteem van de Zwarte Zee gevonden. Door de economische achteruitgang van de Oostbloklanden in het begin van de negentiger jaren is de toevoer van stikstofverbindingen en fosfaten naar de Zwarte Zee sterk verminderd. Als gevolg hiervan is ook de algenproductie op het continentaal plat aanzienlijk verminderd. Sommige organismen die zeldzaam waren geworden in de Zwarte Zee hebben zich weer hersteld. De ongewenste ribkwallen (*Mnemiopsis leidyi*) zijn flink in aantal afgenomen en de stand van de ansjovis is weer toegenomen.

Het verleden heeft aangetoond dat het ecosysteem van de Zwarte Zee zeer gevoelig is voor menselijke invloeden. Dit wordt voornamelijk veroorzaakt door de grote bevolking in de stroomgebieden van de aanvoerende rivieren naar het relatief ondiepe continentaal plat van de Zwarte Zee. In het stroomgebied van de Donau alleen al woonden er in 1992 81 miljoen mensen terwijl er bijvoorbeeld in het stroomgebied van de Rijn slechts 41 miljoen mensen woonden. Veel van het afvalwater dat door deze bevolking wordt geproduceerd bereikt uiteindelijk het continentaal plat van de Zwarte Zee, waar de meegevoerde voedingsstoffen de algenproductie kunnen beïnvloeden. De afbraak van het organische algenmateriaal in de zeebodem kan resulteren in zuurstofloosheid van het bovenstaande water. Dit is vooral het geval in de vroege zomer, wanneer er door opwarming een gelaagdheid in de waterkolom optreedt die de menging belemmert.

# References

- Aller, J.Y. and Aller, R.C. (1986) General characteristics of benthic faunas on Amazon inner continental shelf with comparison to the shelf off Changjiang River, East China Sea. *Continental Shelf Research* **6**: 291-310.
- Aller, J.Y. and Stupakoff, I. (1996) The distribution and seasonal characteristics of benthic communities on the Amazon shelf as indicators of physical processes. *Continental Shelf Research* **16**: 717-751.
- Aller, R.C. (1988) Benthic fauna and biogeochemical processes in marine sediments: The role of burrow structures. In: Blackburn, T.H. (Ed.), *Nitrogen Cycling in Coastal Marine Environments*. Chichester, John Wiley & Sons. pp. 301-338.
- Aller, R.C. (1994) The sedimentary mn cycle in long-island sound - its role as intermediate oxidant and the influence of bioturbation, O<sub>2</sub>, and C<sub>org</sub> flux on diagenetic reaction balances. *Journal of Marine Research* **52**: 259-295.
- Aller, R.C. and Aller, J.Y. (1992) Meiofauna and solute transport in marine muds. *Limnology and Oceanography* **37**: 1018-1033.
- Aller, R.C., Mackin, J.E. and Cox, R.T. (1986) Diagenesis of Fe and S in Amazon inner shelf muds: Apparent dominance of Fe reduction and implications for the genesis of ironstones. *Continental Shelf Research* **6**: 263-289.
- Aller, R.C. and Rude, P.D. (1988) Complete oxidation of solid phase sulfides by manganese and bacteria in anoxic marine sediments. *Geochimica et Cosmochimica Acta* **52**: 751-765.
- Anderson, L.G., Hall, P.O.J., Iverfeldt, Å., Rutgers-van-der-Loeff, M.M., Sundby, B. and Westerlund, S.F.G. (1986) Benthic respiration measured by total carbonate production. *Limnology and Oceanography* **31**: 319-329.
- Archer, D. and Devol, A. (1992) Benthic oxygen fluxes on the Washington shelf and slope: A comparison of in situ microelectrode and chamber flux measurements. *Limnology and Oceanography* **37**: 614-629.
- Bagarinao, T. (1992) Sulfide as an environmental factor and toxicant: tolerance and adaptations in aquatic organisms. *Aquatic Toxicology* **24**: 21-62.
- Bakker, J.F. and Helder, W. (1993) Skagerrak (northeastern North Sea) oxygen microprofiles and porewater chemistry in sediments. *Marine Geology* **111**: 299-321.
- Banse, K. (1982) Mass-scaled rates of respiration and intrinsic growth in very small invertebrates. *Marine Ecology Progress Series* **9**: 281-297.
- Bayne, B.L. and Newell, R.C. (1983) Physiological energetics of marine molluscs. In: Saleudin, A.S.M. (Ed.), *The mollusca*. New York, Academic Press. pp. 407-515.
- Bayne, B.L., Thompson, R.J. and Widdows, J. (1976) Physiology: I. In: Bayne, B.L. (Ed.), *Marine mussels their ecology and physiology*. Cambridge, Cambridge University Press. pp. 121-159.
- Berelson, W.M., Hammond, D.E., O'Neill, D., Xu, X.M., Chin, C. and Zuckin, J. (1990) Benthic fluxes and pore water studies from sediments of the central equatorial North Pacific: Nutrient diagenesis. *Geochimica et Cosmochimica Acta* **54**: 3001-3012.
- Berelson, W.T., McManus, J., Coale, K.H., Johnson, K.S., Kilgore, T., Burdige, D.J. and Pilskaln, C.H. (1996) Biogenic matter diagenesis on the sea floor: A comparison between two continental margin transects. *Journal of Marine Research* **54**: 731-762.
- Berg, P., Risgaard-Petersen, N. and Rysgaard, S. (1998) Interpretation of measured concentration profiles in sediment pore water. *Limnology and Oceanography* **43**: 1500-1510.

- Berger, W.H., Fisher, K., Lai, C. and Wu, G. (1987) *Ocean Productivity and Organic Carbon Flux: Part I. Overview and Maps of Primary Production and Export Production*. La Jolla, Calif., Scripps Institute of Oceanography, 67 p.
- Berner, R.A. (1964) An idealized model of dissolved sulfate distribution in recent sediments. *Geochimica et Cosmochimica Acta* **28**: 1497-1503.
- Berner, R.A. (1970) Sedimentary pyrite formation. *American Journal of Science* **268**: 1-23.
- Berner, R.A. (1980a) A rate model for organic matter decomposition during bacterial sulfate reduction in marine sediments. In: *Biogéochimie de la Matière Organique à l'interface Eau-Sédiment Marin* pp. 35-44.
- Berner, R.A. (1980b) *Early Diagenesis - A Theoretical Approach*. Princeton, Princeton University Press, 241 p.
- Berner, R.A. (1982) Burial of organic carbon and pyrite sulfur in the modern ocean: Its geochemical and environmental significance. *American Journal of Science* **282**: 451-473.
- Berner, R.A. (1984) Sedimentary pyrite formation: An update. *Geochimica et Cosmochimica Acta* **48**: 605-615.
- Berner, R.A. and Raiswell, R. (1983) Burial of organic carbon and pyrite sulfur in sediments over Phanerozoic time: A new theory. *Geochimica et Cosmochimica Acta* **47**: 855-862.
- Berner, R.A. and Westrich, J.T. (1985) Bioturbation and the early diagenesis of carbon and sulfur. *American Journal of Science* **285**: 193-206.
- Betzer, P.R., Showers, W.J., Laws, E.A., Winn, C.D., DiTullio, G.R. and Kroopnick, P.M. (1984) Primary productivity and particulate fluxes on a transect of the equator at 153 °W in the Pacific Ocean. *Deep-Sea Research I* **31**: 1-11.
- Bodeanu, N., Moncheva, S., Ruta, M. and Popa, L. (2000) On the response of phytoplankton to eutrophication - evolution of microalgal blooms in Romanian and Bulgarian coastal Black Sea area. *Estuarine, Coastal and Shelf Science* (In Press).
- Boesen, C. and Postma, D. (1988) Pyrite formation in anoxic environments of the Baltic. *American Journal of Science* **288**: 575-603.
- Bologa, A.S., Bodeanu, N., Petran, A., Tiganus, V. and Zaitsev, Y.P. (1995) Major modifications of the Black Sea benthic and planktonic biota in the last three decades. *Bulletin de l'Institut Oceanographique, Monaco* **15**: 85-110.
- Booij, K., Sundby, B. and Helder, W. (1994) Measuring the flux of oxygen to a muddy sediment with a cylindrical microcosm. *Netherlands Journal of Sea Research* **32**: 1-11.
- Boon, A.R. and Duineveld, G.C.A. (1998) Chlorophyll *a* as a marker for bioturbation and carbon flux in southern and central North Sea sediments. *Marine Ecology Progress Series* **162**: 33-43.
- Boudreau, B.P. (1986) Mathematics of tracer mixing in sediments: I. Spatially-dependent, diffusive mixing. *American Journal of Science* **286**: 161-198.
- Boudreau, B.P. (1991) Modelling the sulfide-oxygen reaction and associated *pH* gradients in porewaters. *Geochimica et Cosmochimica Acta* **55**: 145-159.
- Boudreau, B.P. (1996a) A method-of-lines code for carbon and nutrient diagenesis in aquatic sediments. *Computers & Geosciences* **22**: 479-496.
- Boudreau, B.P. (1996b) The diffusive tortuosity of fine-grained unlithified sediments. *Geochimica et Cosmochimica Acta* **60**: 3139-3142.
- Boudreau, B.P. (1997) *Diagenetic Models and Their Implementation - Modelling transport and Reactions in Aquatic Sediments*. Heidelberg, Springer-Verlag, 414 p.
- Boudreau, B.P. and Canfield, D.E. (1993) A comparison of closed- and open-system models for porewater *pH* and calcite-saturation state. *Geochimica et Cosmochimica Acta* **57**: 317-334.
- Boudreau, B.P. and Ruddick, B.R. (1991) On a reactive continuum representation of organic matter diagenesis. *American Journal of Science* **291**: 507-538.

- Boudreau, B.P. and Westrich, J.T. (1984) The dependence of bacterial sulfate reduction on sulfate concentration in marine sediments. *Geochimica et Cosmochimica Acta* **48**: 2503-2516.
- Bouldin, D.R. (1967) Models for describing the diffusion of oxygen and other mobile constituents across the Mud-water interface. *Journal of Ecology* **56**: 77-87.
- Böttcher, M.E., Oelschläger, B., Höpner, T., Brumsack, H.J. and Rullkötter, J. (1998a) Sulfate reduction related to the early diagenetic degradation of organic matter and "black spot" formation in tidal sandflats of the German Wadden Sea (southern North Sea): stable isotope ( $^{13}\text{C}$ ,  $^{34}\text{S}$ ,  $^{18}\text{O}$ ) and other geochemical results. *Organic Geochemistry* **29**: 1517-1530.
- Böttcher, M.E., Schale, H., Schnetger, B., Wallmann, K. and Brumsack, H.J. (2000) Stable sulfur isotopes indicate net sulfate reduction in near-surface sediments of the deep Arabian Sea. *Deep-Sea Research* (In Press).
- Böttcher, M.E., Smock, A. and Cypionka, H. (1998b) Sulfur isotope fractionation during experimental precipitation of iron(II) and manganese(II) sulfide at room temperature. *Chemical Geology* **146**: 127-134.
- Buesseler, K.O. and Benitez, C.R. (1994) Determination of mass accumulation rates and sediment radionuclide inventories in the deep Black Sea. *Deep-Sea Research* **41**: 1605-1615.
- Buesseler, K.O., Michaels, A.F., Siegel, D.A. and Knap, A.H. (1994) A three dimensional time-dependent approach to calibrating sediment trap fluxes. *Global Biogeochemical Cycles* **8**: 179-193.
- Burdige, D.J. (1991) The kinetics of organic matter mineralization in anoxic marine sediments. *Journal of Marine Research* **49**: 727-761.
- Cai, W.J., Reimers, C.E. and Shaw, T.J. (1995) Microelectrode studies of organic carbon degradation and calcite dissolution at a California Continental rise site. *Geochimica et Cosmochimica Acta* **59**: 497-511.
- Calvert, S.E. and Karlin, R.E. (1991) Relationships between sulphur, organic carbon, and iron in the modern sediments of the Black Sea. *Geochimica et Cosmochimica Acta* **55**: 2483-2490.
- Calvert, S.E., Thode, H.G., Yeung, D. and Karlin, R.E. (1996) A stable isotope study of pyrite formation in the late Pleistocene and Holocene sediments of the Black Sea. *Geochimica et Cosmochimica Acta* **60**: 1261-1270.
- Canfield, D.E. (1988) *Sulfate reduction and the diagenesis of iron in anoxic marine sediments*, [Ph.D. thesis]: Yale University, 248 p.
- Canfield, D.E. (1989a) Sulfate reduction and oxic respiration in marine sediments: Implications for organic carbon preservation in euxinic environments. *Deep-Sea Research* **36**: 121-138.
- Canfield, D.E. (1989b) Reactive iron in marine sediments. *Geochimica et Cosmochimica Acta* **53**: 619-632.
- Canfield, D.E., Jørgensen, B.B., Fossing, H., Glud, R.N., Gundersen, J., Ramsing, N.B., Thamdrup, B., Hansen, J.W., Nielsen, L.P. and Hall, P.O.J. (1993a) Pathways of organic carbon oxidation in three continental margin sediments. *Marine Geology* **113**: 27-40.
- Canfield, D.E., Lyons, T.W. and Raiswell, R. (1996) A model for iron deposition to euxinic Black Sea sediments. *American Journal of Science* **296**: 818-834.
- Canfield, D.E., Raiswell, R. and Bottrell, S. (1992) The reactivity of sedimentary iron minerals towards sulfide. *American Journal of Science* **292**: 659-683.
- Canfield, D.E., Raiswell, R., Westrich, J.T., Reaves, C.M. and Berner, R.A. (1986) The use of chromium reduction in the analysis of reduced inorganic sulfur in sediments and shales. *Chemical Geology* **54**: 149-155.
- Canfield, D.E. and Thamdrup, B. (1994) The production of  $^{34}\text{S}$ -depleted sulfide during bacterial disproportionation to elemental sulfur. *Science* **266**: 1973-1975.
- Canfield, D.E., Thamdrup, B. and Fleischer, S. (1998) Isotope fractionation and sulfur metabolism by pure and enrichment cultures of elemental sulfur-disproportionating bacteria. *Limnology and Oceanography* **43**: 253-264.

- Canfield, D.E., Thamdrup, B. and Hansen, J.W. (1993b) The anaerobic degradation of organic matter in Danish coastal sediments: Iron reduction, manganese reduction, and sulfate reduction. *Geochimica et Cosmochimica Acta* **57**: 3867-3883.
- Chambers, L.A. and Trudinger, P.A. (1979) Microbial fractionation of stable sulfur isotopes: a review and critique. *Geomicrobiology Journal* **1**: 249-293.
- Chanton, J.P. and Martens, C.S. (1987) Biogeochemical cycling in an organic-rich coastal marine basin. 8. A sulfur isotopic budget balanced by differential diffusion across the sediment-water interface. *Geochimica et Cosmochimica Acta* **51**: 1201-1208.
- Chanton, J.P., Martens, C.S. and Goldhaber, M.B. (1987) Biogeochemical cycling in an organic-rich coastal marine basin. 7. Sulfur mass balance, oxygen uptake and sulfide retention. *Geochimica et Cosmochimica Acta* **51**: 1187-1199.
- Christensen, J.P. (2000) A relationship between deep-sea benthic oxygen demand and oceanic primary productivity. *Oceanologica Acta* **23**: 65-82.
- Cline, J.D. (1969) Spectrophotometric determination of hydrogen sulfide in natural waters. *Limnology and Oceanography* **14**: 454-458.
- Cociasu, A.M., Dorogan, L., Humborg, C. and Popa, L. (1996) Long-term ecological changes in Romanian coastal waters of the Black Sea. *Marine Pollution Bulletin* **32**: 32-38.
- Cociasu, A.M. and Popa, L. (2000) Long-term evolution of the nutrient concentration on the North-Western shelf of the Black Sea. *Estuarine, Coastal and Shelf Science* (In Press).
- Codispoti, L.A., Friederich, G.E., Murray, J.W. and Sakamoto, C.M. (1991) Chemical variability in the Black Sea - implications of continuous vertical profiles that penetrated the oxic anoxic interface. *Deep-Sea Research* **38**: S691-S710.
- Cowan, J.L.W. and Boynton, W.R. (1996) Sediment-water oxygen and nutrient exchanges along the longitudinal axis of Chesapeake Bay: seasonal patterns, controlling factors and ecological significance. *Estuaries* **19**: 562-580.
- Cowie, G.L. and Hedges, J.I. (1994) Biochemical indicators of diagenetic alteration in natural organic matter mixtures. *Nature* **369**: 304-307.
- Cramer, A. (1989) A common artifact in estimates of benthic community respiration caused by the use of stainless steel. *Netherlands Journal of Sea Research* **23**: 1-6.
- Curtis, W.R. and Broadway, J.A. (1992) Preliminary caesium data from a cooperative US/USSR monitoring survey for Chernobyl radioactivity in the Black Sea. *Chemistry and Ecology* **7**: 161-172.
- Cutter, G.A. and Kluckhohn, R.S. (1999) The cycling of particulate carbon, nitrogen, sulfur and sulfur species (iron monosulfide, greigite, pyrite, and organic sulfur) in the water columns of Framvaren Fjord and the Black Sea. *Marine Chemistry* **67**: 149-160.
- Cypionka, H., Smock, A.M. and Böttcher, M.E. (1998) A combined pathway of sulfur compound disproportionation in *Desulfovibrio desulfuricans*. *FEMS Microbiology Letters* **166**: 181-186.
- Dauwe, B., Middelburg, J.J. and Herman, P.M.J. (2000) Organic matter mineralization in coastal sediments: oxic versus anoxic degradability. *Marine Ecology Progress Series* (In Press).
- Deuser, W.G. (1974) Evolution of anoxic conditions in Black Sea during Holocene. In: Degens, E.T., et al. (Eds.), *The Black Sea - Geology, Chemistry and Biology*. Tulsa, Oklahoma, The American Association of Petroleum Geologists. pp. 133-136.
- Devol, A.H. and Christensen, J.P. (1993) Benthic fluxes and nitrogen cycling in sediments of the continental margin of the eastern North Pacific. *Journal of Marine Research* **51**: 345-372.
- Dhakar, S.P. and Burdige, D.J. (1996) A coupled, non-linear, steady state model for early diagenetic processes in pelagic sediments. *American Journal of Science* **296**: 296-330.
- Dimitrov, P.S., Stoyanov, A.S., Demirov, E.K. and Solakov, D.P. (1987) On the phenomenon of upwelling in the western part of the Black Sea and its connection with the bloom of plankton. *Bulgarian Academy of Sciences* **40**: 127-130.

- Dollar, S.J., Smith, S.V., Vink, S.M., Obrebski, S. and Hollibaugh, J.T. (1991) Annual cycle of benthic nutrient fluxes in Tomales Bay, California, and contribution of the benthos to total ecosystem metabolism. *Marine Ecology Progress Series* **79**: 115-125.
- Dugdale, R.C. and Goering, J.J. (1967) Uptake of new and regenerated forms of nitrogen in primary productivity. *Limnology and Oceanography* **12**: 196-206.
- Duineveld, G.C.A., De Wilde, P.A.W.J., Berghuis, E.M., Kok, A., Tahey, T.M. and Kromkamp, J. (1997a) Benthic respiration and standing stock on two contrasting continental margins in the western Indian Ocean: The Yemen-Somali upwelling region and the margin off Kenya. *Deep-Sea Research* **44**: 1293-1317.
- Duineveld, G.C.A., Lavaleye, M.S.S., Berghuis, E.M., De Wilde, P.A.W.J., Van Der Weele, J., Kok, A., Batten, S.D. and De Leeuw, J.W. (1997b) Patterns of benthic fauna and benthic respiration on the Celtic continental margin in relation to the distribution of phytodetritus. *Internationale Revue der gesamten Hydrobiologie* **82**: 395-424.
- Eleftheriou, A. and Basford, D.J. (1989) The macrobenthic infauna of the offshore northern North Sea. *Journal of the Marine Biological Association of the United Kingdom* **69**: 123-143.
- Epping, E.H.G. and Helder, W. (1997) Oxygen budgets calculated from *in situ* oxygen microprofiles for Northern Adriatic sediments. *Continental Shelf Research* **17**: 1737-1764.
- Eppley, R.W. and Peterson, B.J. (1979) Particulate organic matter flux and planktonic new production in the deep ocean. *Nature* **282**: 677-680.
- Fabry, V., Froehlich, K. and Osvath, I. (1993) Environmental pollution of the Black Sea: a search for answers. *International Atomic Agency Bulletin* **35**: 20-24.
- Faganeli, J., Avcin, A., Fanuko, N., Malej, A., Turk, V., Tusnik, P., Vrizer, B. and Vukovic, A. (1985) Bottom layer anoxia in the central part of the Gulf of Trieste in the late summer of 1983. *Marine Pollution Bulletin* **16**: 75-78.
- Fauchald, K. and Jumars, P.A. (1979) The diet of worms: a study of polychaete feeding guilds. *Oceanography and Marine Biology: an Annual Review* **17**: 193-284.
- Fiadeiro, M.E. and Veronis, G. (1977) On weighted-mean schemes for the finite-difference approximation to the advection-diffusion equation. *Tellus* **29**: 512-522.
- Flach, E. and Heip, C.H.R. (1996) Vertical distribution of macrozoobenthos within the sediment on the continental slope of the Goban Spur area (NE Atlantic). *Marine Ecology Progress Series* **141**: 55-66.
- Fossing, H. and Jørgensen, B.B. (1989) Measurement of bacterial sulfate reduction in sediments: Evaluation of a single-step chromium reduction method. *Biogeochemistry* **8**: 205-222.
- Fossing, H. and Jørgensen, B.B. (1990) Oxidation and reduction of radiolabeled inorganic sulfur compounds in an estuarine sediment, Kysing Fjord, Denmark. *Geochimica et Cosmochimica Acta* **54**: 2742.
- Friedl, G., Dinkel, C. and Wehrli, B. (1998) Benthic fluxes of nutrients in the northwestern Black Sea. *Marine Chemistry* **62**: 77-88.
- Friedrich, J., Dinkel, C., Friedl, G., Pimenov, N.V., Wijsman, J.W.M., Gomoiu, M.T., Cociasu, A.M., Popa, A. and Wehrli, B. (2000) Benthic nutrient cycling and diagenetic pathways in the northwestern Black Sea. *Estuarine, Coastal and Shelf Science* (In Press).
- Froelich, P.N., Klinkhammer, G.P., Bender, M.L., Luedtke, N.A., Heath, G.R., Cullen, D., Dauphin, P., Hammond, D., Hartman, B. and Maynard, V. (1979) Early oxidation of organic matter in pelagic sediments of the eastern equatorial Atlantic: Suboxic diagenesis. *Geochimica et Cosmochimica Acta* **43**: 1075-1090.
- Fry, B., Cox, J., Gest, H. and Hayes, J.M. (1986) Discrimination between  $^{34}\text{S}$  and  $^{32}\text{S}$  during bacterial metabolism of inorganic sulfur compounds. *Journal of Bacteriology* **165**: 328-330.
- Fry, B., Jannasch, H.W., Molyneaux, S.J., Wirsén, C.O., Muramoto, J.A. and King, S. (1991) Stable isotope studies of the carbon, nitrogen and sulfur cycles in the Black Sea and the Cariaco Trench. *Deep-Sea Research* **38**: S1003-S1019.

- Gagnon, C., Mucci, A. and Pelletier, É. (1995) Anomalous accumulation of acid-volatile sulphides (AVS) in a coastal marine sediment, Saguenay Fjord, Canada. *Geochimica et Cosmochimica Acta* **59**: 2663-2675.
- Gardner, W.S., Briones, E.E., Kaegi, E.C. and Rowe, G.T. (1993) Ammonium excretion by benthic invertebrates and sediment-water nitrogen flux in the gulf of Mexico near the Mississippi River outflow. *Estuaries* **16**: 799-808.
- Gaston, G.R. and Nasci, J.C. (1988) Trophic structure of macrobenthic communities in the Calcasieu Estuary, Louisiana. *Estuaries* **11**: 201-211.
- Giblin, A.E., Hopkinson, C.S. and Tucker, J. (1997) Benthic metabolism and nutrient cycling in Boston Harbor, Massachusetts. *Estuaries* **20**: 346-364.
- Glenn, C.R. and Arthur, M.A. (1985) Sedimentary and geochemical indicators of productivity and oxygen contents in modern and ancient basins: The holocene Black Sea as the "type" anoxic basin. *Chemical Geology* **48**: 325-354.
- Glud, R.N., Gundersen, J.K., Jørgensen, B.B., Revsbech, N.P. and Schulz, H.D. (1994) Diffusive and total oxygen uptake of deep-sea sediments in the eastern South Atlantic Ocean: *In situ* and laboratory measurements. *Deep-Sea Research* **41**: 1767-1788.
- Glud, R.N., Klimant, I., Holst, G., Kohls, O., Meyer, V., Kühl, M. and Gundersen, J.K. (1999) Adaptation, tests and *in situ* measurements with O<sub>2</sub> microopt(r)odes on benthic landers. *Deep-Sea Research I* **46**: 171-183.
- Goldhaber, M.B., Aller, R.C., Cochran, J.K., Rosenfeld, J.K., Martens, C.S. and Berner, R.A. (1977) Sulfate reduction, diffusion, and bioturbation in Long Island Sound sediments: report of the FOAM group. *American Journal of Science* **277**: 193-237.
- Goldhaber, M.B. and Kaplan, I.R. (1974) The sulfur cycle. In: Goldberg, E.D. (Ed.), *Marine Chemistry*. New York, John Wiley. pp. 569-655.
- Goldhaber, M.B. and Kaplan, I.R. (1975) Apparent dissociation constants of hydrogen sulfide in chloride solutions. *Marine Chemistry* **3**: 83-104.
- Gomoiu, M.T. (1980) Ecological observations on the jellyfish *Aurelia aurata* (L.) populations from the Black Sea. *Cercetari Marine* **13**: 91-102.
- Gomoiu, M.T. (1985a) Problems concerning marine eutrophication. *Cercetari Marine* **18**: 59-95.
- Gomoiu, M.T. (1985b) On the productive potential of the benthos from the Romanian continental shelf of the Black Sea. *Cercetari Marine* **18**: 191-200.
- Gomoiu, M.T. (1992) Marine eutrophication syndrome in the north-western part of the Black Sea. In: Vollenweider, R.A. (Ed.), *Science of the total environment*. Amsterdam, Elsevier Sci. pp. 683-692.
- Graf, G. (1992) Benthic-pelagic coupling: A benthic view. *Oceanography and Marine Biology: an Annual Review* **30**: 149-190.
- Grebmeier, J.M. and McRoy, C.P. (1989) Pelagic-benthic coupling on the shelf of the northern Bering and Chukchi Seas. III. Benthic food supply and carbon cycling. *Marine Ecology Progress Series* **53**: 79-91.
- Grebmeier, J.M., McRoy, C.P. and Feder, H.M. (1988) Pelagic-benthic coupling on the shelf of the northern Bering and Chukchi Seas. I. Food supply source and benthic biomass. *Marine Ecology Progress Series* **48**: 57-67.
- Grégoire, M., Beckers, J.M., Nihoul, J.C.J. and Stanev, E. (1997) Coupled hydrodynamic ecosystem model of the Black Sea at basin scale. In: Özsoy, E., et al. (Eds.), *Sensitivity to change: Black Sea, Baltic Sea and North Sea*. Dordrecht, Kluwer Academic Publishers. pp. 487-499.
- Grégoire, M., Beckers, J.M., Nihoul, J.C.J. and Stanev, E. (1999) Reconnaissance of the main Black Sea's ecohydrodynamics by means of a 3D interdisciplinary model. *Journal of Marine Research* **16**: 85-105.



- Guieu, C., Martin, J.M., Tankéré, S.P.C., Mousty, F., Trincherini, P., Bazot, M. and Dai, M.H. (1998) On trace metal geochemistry in the Danube River and the Western Black Sea. *Estuarine, Coastal and Shelf Science* **47**: 471-485.
- Gust, G., Byrne, R.H., Bernstein, R.E., Betzer, P.R. and Bowles, W. (1992) Particle fluxes and moving fluids: experience from synchronous trap collections in the Sargasso Sea. *Deep-Sea Research I* **39**: 1071-1083.
- Hales, B., Emerson, S.R. and Archer, D. (1994) Respiration and dissolution in the sediments of western North Atlantic: estimates from models of *in situ* microelectrode measurements of porewater oxygen and pH. *Deep-Sea Research* **41**: 695-715.
- Hall, P.O.J., Anderson, L.G., Rutgers-van-der-Loeff, M.M., Sundby, B. and Westerlund, S.F.G. (1989) Oxygen uptake kinetics in the benthic boundary layer. *Limnology and Oceanography* **34**: 734-746.
- Hammond, D.E., McManus, J., Berelson, W.M., Kilgore, T.E. and Pope, R.H. (1996) Early diagenesis of organic material in equatorial Pacific sediments: stoichiometry and kinetics. *Deep-Sea Research II* **43**: 1365-1412.
- Hargrave, B.T. (1973) Coupling carbon flow through some pelagic and benthic communities. *Journal of the Fisheries Research Board of Canada* **30**: 1317-1326.
- Harper, D.E., McKinney, L.D., Salzer, R.R. and Case, R.J. (1981) The occurrence of hypoxic bottom water off the upper Texas coast and its effects on the benthic biota. *Contributions in Marine Science* **24**: 53-79.
- Hartmann, M. and Nielsen, H. (1969)  $\delta^{34}\text{S}$ -Werte in rezenten Meeressedimenten und ihre Deutung am Beispiel einiger Sedimentprofile aus der westlichen Ostsee. *Geologischen Rundschau* **58**: 621-655.
- Hayduk, W. and Laudie, H. (1974) Prediction of diffusion coefficients for nonelectrolytes in dilute aqueous solutions. *American Institute of Chemical Engineers Journal* **20**: 611-615.
- Heip, C.H.R., Duineveld, G.C.A., Flach, E., Graf, G., Helder, W., Herman, P.M.J., Lavaleye, M.S.S., Middelburg, J.J., Pfannkuche, O., Soetaert, K., Soltwedel, T., De Stigter, H.S., Thomsen, L., Vanaverbeke, J. and De Wilde, P.A.W.J. (2000) The role of benthic biota in sedimentary metabolism and sediment-water exchange processes in the Goban Spur area (N.E. Atlantic). *Deep-Sea Research* (In Press).
- Heip, C.H.R., Goossen, N.K., Herman, P.M.J., Kromkamp, J., Middelburg, J.J. and Soetaert, K. (1995) Production and consumption of biological particles in temperate tidal estuaries. *Oceanography and Marine Biology: an Annual Review* **33**: 1-149.
- Heip, C.H.R., Warwick, R.M., Carr, M.R., Herman, P.M.J., Huys, R., Smol, N. and Van Holsbeke, K. (1988) Analysis of community attributes of the benthic meiofauna of Frierfjord/Langesundfjord. *Marine Ecology Progress Series* **46**: 171-180.
- Helder, W. (1989) Early diagenesis and sediment-water exchange in the Savu Basin (eastern Indonesia). *Netherlands Journal of Sea Research* **24**: 555-572.
- Henneke, E., Luther, G.W. and De Lange, G.J. (1991) Determination of inorganic sulfur speciation with polarographic techniques: Some preliminary results for recent hypersaline anoxic sediments. *Marine Geology* **100**: 115-123.
- Henneke, E., Luther, G.W., De Lange, G.J. and Hoefs, J. (1997) Sulphur speciation in anoxic hypersaline sediments from the eastern Mediterranean Sea. *Geochimica et Cosmochimica Acta* **61**: 307-321.
- Henrichs, S.M. (1992) Early diagenesis of organic matter in marine sediments: progress and perplexity. *Marine Chemistry* **39**: 119-149.
- Henrichs, S.M. (1993) Early diagenesis of organic matter: the dynamics (rates) of cycling of organic compounds. In: Engel, M.H. (Ed.), *Organic geochemistry: Principles and applications*. New York, Plenum Press. pp. 101-117.

- Henrichs, S.M. and Reeburgh, W.S. (1987) Anaerobic mineralization of marine sediment organic matter: rates and the role of anaerobic processes in the oceanic carbon economy. *Geomicrobiology Journal* **5**: 191-238.
- Herman, P.M.J., Soetaert, K., Middelburg, J.J., Heip, C.H.R., Lohse, L., Epping, E.H.G., Helder, W., Antia, A.N. and Peinert, R. (2000) The seafloor as the ultimate sediment trap - using sediment properties to constrain benthic-pelagic exchange processes at the Goban Spur. *Deep-Sea Research II* (In Press).
- Hill, M.O. (1973) Diversity and evenness: a unifying notation and its consequences. *Ecology* **54**: 427-432.
- Huettel, M., Ziebis, W., Forster, S. and Luther, G.W. (1998) Advective transport affecting metal and nutrient distributions and interfacial fluxes in permeable sediments. *Geochimica et Cosmochimica Acta* **62**: 613-631.
- Hulth, S., Blackburn, T.H. and Hall, P.O.J. (1994) Arctic sediments (Svalbard): Consumption and microdistribution of oxygen. *Marine Chemistry* **46**: 293-316.
- Hulthe, G., Hulth, S. and Hall, P.O.J. (1998) Effect of oxygen on degradation rate of refractory and labile organic matter in continental margin sediments. *Geochimica et Cosmochimica Acta* **62**: 1319-1328.
- Humborg, C., Ittekkot, V.A., Cociasu, A.M. and Von Bodungen, B. (1997) Effect of Danube River dam on Black Sea biogeochemistry and ecosystem structure. *Nature* **386**: 385-388.
- Hurtgen, M.T., Lyons, T.W., Ingall, E.D. and Cruse, A.M. (1999) Anomalous enrichments of iron monosulfide in euxinic marine sediments and the role of H<sub>2</sub>S in iron sulfide transformations: examples from Effingham Inlet, Orca Basin, and the Black Sea. *American Journal of Science* **299**: 556-588.
- Ittekkot, V.A. and Laane, R.W.P.M. (1991) Fate of riverine particulate organic matter. In: Degens, E.T., et al. (Eds.), *Biogeochemistry of major world rivers*. Chichester, John Wiley & Sons. pp. 233-243.
- Jahnke, R.A. (1996) The global ocean flux of particulate organic carbon: areal distribution and magnitude. *Global Biogeochemical Cycles* **10**: 71-88.
- Jahnke, R.A., Reimers, C.E. and Craven, D.B. (1990) Intensification of recycling of organic matter at the sea floor near ocean margins. *Nature* **348**: 50-54.
- Johnson, K.S., Chavez, F.P. and Friederich, G.E. (1999) Continental-shelf sediment as a primary source of iron for coastal phytoplankton. *Nature* **398**: 697-700.
- Jongman, R.H.G., Ter Braak, C.J.F. and Van Tongeren, O.F.R. (1987) *Data analysis in community and landscape ecology*. Wageningen, Pudoc, 299 p.
- Jørgensen, B.B. (1977) The sulfur cycle of a coastal marine sediment (Limfjorden, Denmark). *Limnology and Oceanography* **22**: 814-832.
- Jørgensen, B.B. (1978) A comparison of methods for the quantification of bacterial sulfate reduction in coastal marine sediments. *Geomicrobiology Journal* **1**: 29-47.
- Jørgensen, B.B. (1979) A theoretical model of stable sulfur isotope distribution in marine sediments. *Geochimica et Cosmochimica Acta* **43**: 363-374.
- Jørgensen, B.B. (1982) Mineralization of organic matter in the sea bed - the role of sulfate reduction. *Nature* **296**: 643-645.
- Jørgensen, B.B. (1983) Processes at the sediment-water interface. In: Bolin, B. (Ed.), *The Major Biogeochemical Cycles and their Interactions*. New York, John Wiley. pp. 477-509.
- Jørgensen, B.B., Fossing, H., Wirsén, C.O. and Jannasch, H.W. (1991) Sulfide oxidation in the anoxic Black Sea chemocline. *Deep-Sea Research* **38**: S1083-S1103.
- Kaplan, I.R. and Rittenberg, R.C. (1964) Microbiological fractionation of sulphur isotopes. *Journal of General Microbiology* **34**: 195-212.
- Kemp, P.F. (1987) Potential impact on bacteria of grazing by a macrofaunal deposit-feeder, and the fate of bacterial production. *Marine Ecology Progress Series* **36**: 151-161.

- Kemp, W.M., Sampou, P.A., Garber, J., Tuttle, J. and Boynton, W.R. (1992) Seasonal depletion of oxygen from bottom waters of Chesapeake Bay: Roles of benthic and planktonic respiration and physical exchange processes. *Marine Ecology Progress Series* **85**: 137-152.
- Kempe, S., Liebezeit, G., Diercks, A.R. and Asper, V. (1990) Water balance in the Black Sea. *Nature* **346**: 419.
- Klump, J.V. and Martens, C.S. (1987) Biogeochemical cycling in an organic-rich coastal marine basin. 5. Sedimentary nitrogen and phosphorus budgets upon kinetic models, mass balance and the stoichiometry of nutrient regeneration. *Geochimica et Cosmochimica Acta* **51**: 1161-1173.
- Klump, J.V. and Martens, C.S. (1989) The seasonality of nutrient regeneration in an organic-rich coastal sediment: Kinetic modeling of changing pore-water nutrient and sulfate distributions. *Limnology and Oceanography* **34**: 559-577.
- Konovalov, S.M. (1995) Anthropogenic impact and ecosystems of the Black Sea. *Bulletin de l'Institut Oceanographique, Monaco* **15**: 53-83.
- Kostka, J.E. and Luther, G.W. (1994) Partitioning and speciation of solid phase iron in saltmarsh sediments. *Geochimica et Cosmochimica Acta* **58**: 1701-1710.
- Kostka, J.E., Thamdrup, B., Glud, R.N. and Canfield, D.E. (1999) Rates and pathways of carbon oxidation in permanently cold Arctic sediments. *Marine Ecology Progress Series* **180**: 7-21.
- Kristensen, E., Ahmed, S.I. and Devol, A.H. (1995) Aerobic and anaerobic decomposition of organic matter: which is fastest? *Limnology and Oceanography* **40**: 1430-1437.
- Krustalev, Y., Chernousov, S.Y. and Denisov, V.I. (1990) Some distinctive features and laws of sedimentogenesis in the northwestern Black Sea (the material composition and distribution of the suspensions). *Oceanology* **30**: 212-216.
- Lampitt, R.S. and Antia, A.N. (1997) Particle flux in deep seas: regional characteristics and temporal variability. *Deep-Sea Research I* **44**: 1377-1403.
- Lampitt, R.S., Raine, R.C.T., Billett, D.S.M. and Rice, A.L. (1995) Material supply to the European continental slope: a budget based on benthic oxygen demand and organic supply. *Deep-Sea Research I* **42**: 1865-1880.
- Landing, W.M. and Bruland, K.W. (1987) The contrasting biogeochemistry of iron and manganese in the Pacific Ocean. *Geochimica et Cosmochimica Acta* **51**: 29-43.
- Lasker, R. (1966) Feeding, growth, respiration, and carbon utilization of a euphausiid crustacean. *Journal of the Fisheries Research Board of Canada* **23**: 1291-1317.
- Leppäkoski, E. and Mihnea, P.E. (1996) Enclosed seas under man-induced change: A comparison between the Baltic and Black Seas. *Ambio* **25**: 380-389.
- Leventhal, J.S. (1983) An interpretation of carbon and sulfur relationships in Black Sea sediments as indicators of environmental deposition. *Geochimica et Cosmochimica Acta* **47**: 133-137.
- Leventhal, J.S. and Taylor, C. (1990) Comparison of methods to determine degree of pyritization. *Geochimica et Cosmochimica Acta* **54**: 2621-2625.
- Lewis, B.L. and Landing, W.M. (1991) The biochemistry of manganese and iron in the Black Sea. *Deep-Sea Research* **38**: S773-S803.
- Li, Y.H. and Gregory, S. (1974) Diffusion of ions in sea water and in deep-sea sediments. *Geochimica et Cosmochimica Acta* **88**: 703-714.
- Lin, S. and Morse, J.W. (1991) Sulfate reduction and iron sulfide mineral formation in Gulf of Mexico anoxic sediments. *American Journal of Science* **291**: 55-89.
- Lohse, L., Epping, E.H.G., Helder, W. and Van Raaphorst, W. (1996) Oxygen pore water profiles in continental shelf sediments of the North Sea: turbulent versus molecular diffusion. *Marine Ecology Progress Series* **145**: 63-75.
- Lopez, G.R. and Levinton, J.S. (1987) Ecology of deposit-feeding animals in marine sediments. *Quarterly Review of Biology* **62**: 235-260.

- Lovley, D.R. and Phillips, E.J.P. (1987) Rapid assay for microbially reducible ferric iron in aquatic sediments. *Applied and Environmental Microbiology* **53**: 1536-1540.
- Luther, G.W. (1991) Pyrite synthesis via polysulfide compounds. *Geochimica et Cosmochimica Acta* **55**: 2839-2849.
- Luther, G.W., Church, T.M. and Powell, D. (1991) Sulfur speciation and sulfide oxidation in the water column of the Black Sea. *Deep-Sea Research* **38**: S1121-S1137.
- Lyons, T.W. (1997) Sulfur isotopic trends and pathways of iron sulfide formation in upper Holocene sediments of the anoxic Black Sea. *Geochimica et Cosmochimica Acta* **61**: 3367-3382.
- Lyons, T.W. and Berner, R.A. (1992) Carbon-sulfur-iron systematics of the uppermost deep-water sediments of the Black Sea. *Chemical Geology* **99**: 1-27.
- Lyons, T.W., Berner, R.A. and Anderson, R.F. (1993) Evidence for large pre-industrial perturbations of the Black Sea chemocline. *Nature* **365**: 538-540.
- Mackin, J.E. and Swider, K.T. (1989) Organic matter decomposition pathways and oxygen consumption in coastal marine sediments. *Journal of Marine Research* **47**: 681-716.
- Mahaut, M.L., Sibuet, M. and Shirayama, Y. (1995) Weight-dependent respiration rates in deep-sea organisms. *Deep-Sea Research* **42**: 1575-1582.
- Martin, J.H. (1990) Glacial - interglacial CO<sub>2</sub> change: the iron hypothesis. *Paleoceanography* **5**: 1-13.
- Martin, J.H., Knauer, G.A., Karl, D.M. and Broenkow, W.H. (1987) VERTEX: carbon cycling in the northeast Pacific. *Deep-Sea Research* **34**: 267-285.
- Martin, J.M. and Windom, H.L. (1991) Present and future roles of ocean margins in regulating marine biogeochemical cycles of trace elements. In: Mantoura, R.F.C., et al. (Eds.), *Ocean margin processes in global change*. John Wiley & Sons Ltd. pp. 45-67.
- May, E.B. (1973) Extensive oxygen depletion in Mobile Bay, Alabama. *Limnology and Oceanography* **18**: 353-366.
- Mee, L.D. (1992) The Black Sea in crisis: a need for concerted international action. *Ambio* **21**: 278-286.
- Meyers, C.R. and Nealson, K.H. (1988) Microbial reduction of manganese oxides: Interactions with iron and sulfur. *Geochimica et Cosmochimica Acta* **52**: 2727-2732.
- Middelburg, J.J. (1989) A simple rate model for organic matter decomposition in marine sediments. *Geochimica et Cosmochimica Acta* **53**: 1577-1581.
- Middelburg, J.J. (1991) Organic carbon, sulphur, and iron in recent semi-euxinic sediments of Kau Bay, Indonesia. *Geochimica et Cosmochimica Acta* **55**: 815-828.
- Middelburg, J.J., Calvert, S.E. and Karlin, R.E. (1991) Organic-rich transitional facies in silled basins: Response to sea-level change. *Geology* **19**: 679-682.
- Middelburg, J.J., Klaver, G., Nieuwenhuize, J., Wielemaker, A., De Haas, W. and Van Der Nat, F.J.W.A. (1996a) Organic matter mineralization in intertidal sediments along an estuarine gradient. *Marine Ecology Progress Series* **132**: 157-168.
- Middelburg, J.J., Soetaert, K. and Herman, P.M.J. (1997) Empirical relationships for use in global diagenetic models. *Deep-Sea Research* **44**: 327-344.
- Middelburg, J.J., Soetaert, K., Herman, P.M.J. and Heip, C.H.R. (1996b) Denitrification in marine sediments: A model study. *Global Biogeochemical Cycles* **10**: 661-673.
- Middelburg, J.J., Vlug, T. and Van Der Nat, F.J.W.A. (1993) Organic matter mineralization in marine systems. *Global and Planetary Change* **8**: 47-58.
- Mihnea, P.E. (1997) Major shifts in the phytoplankton community (1980-1994) in the Romanian Black Sea. *Oceanologica Acta* **20**: 119-129.
- Miller-Way, T., Boland, G.S., Rowe, G.T. and Twilley, R.R. (1994) Sediment oxygen consumption and benthic nutrient fluxes on the Louisiana continental shelf: A methodological comparison. *Estuaries* **17**: 809-815.

- Millero, F.J. (1986) The thermodynamics and kinetics of the hydrogen sulfide system in natural waters. *Marine Chemistry* **18**: 121-147.
- Millero, F.J., Sotolongo, S. and Izaguirre, M. (1987) The oxidation kinetics of Fe(II) in seawater. *Geochimica et Cosmochimica Acta* **51**: 793-801.
- Moodley, L., Heip, C.H.R. and Middelburg, J.J. (1998) Benthic activity in sediments of the northwestern Adriatic Sea: Sediment oxygen consumption, macro-and meiofauna dynamics. *Journal of Sea Research* **40**: 263-280.
- Mook, W.G. and Tan, F.C. (1991) Stable carbon isotopes in rivers and estuaries. In: Degens, E.T., et al. (Eds.), *Biogeochemistry of major world rivers*. Chichester, John Wiley & Sons. pp. 245-264.
- Muramoto, J.A., Honjo, S., Fry, B., Hay, B.J., Howarth, R.W. and Cisne, J.L. (1991) Sulfur, iron and organic carbon fluxes in the Black Sea - sulfur isotopic evidence for origin of sulfur fluxes. *Deep-Sea Research* **38**: S1151-S1187.
- Murray, J.W., Jannasch, H.W., Honjo, S., Anderson, R.F., Reeburgh, W.S., Top, Z., Friederich, G.E., Codispoti, L.A. and Izdar, E. (1989) Unexpected changes in the oxic/anoxic interface in the Black Sea. *Nature* **338**: 411-413.
- Murray, J.W. and Kuivila, K.M. (1990) Organic matter diagenesis in the northeast Pacific: transition from aerobic red clay to suboxic hemipelagic sediments. *Deep-Sea Research* **37**: 59-80.
- Mutlu, E., Bingel, F., Gücü, A.C., Melnikov, V.V., Niermann, U., Ostr, N.A. and Zaika, V.E. (1994) Distribution of the new invader *Mnemiopsis* sp. and the resident *Aurelia aurita* and *Pleurobrachia pileus* populations in the Black Sea in the years 1991-1993. *ICES Journal of Marine Science* **51**: 407-421.
- Najjar, R.G., Sarmiento, J.L. and Toggweiler, J.R. (1999) Downward transport and fate of organic matter in the ocean: simulations with a general circulation model. *Global Biogeochemical Cycles* **6**: 45-76.
- Neretin, N., Böttcher, M.E. and Volkov, I.I. (1998) The stable sulfur isotopic composition of sulfur species in the Black Sea water column. *Mineralogical Magazine* **62A**: 1075-1076.
- Neretin, N., Volkov, I.I., Böttcher, M.E. and Grinenko, V.A. (2000) The biogeochemical sulfur cycle in the Black Sea anoxic zone: a mass balance model with special regards to sulfur isotopes. *Deep-Sea Research* (In Press).
- Niermann, U., Bingel, F., Gorban, A., Gordina, A.D., Gücü, A.C., Kideys, A.E., Konsulov, A., Radu, G., Subbotin, A.A. and Zaika, V.E. (1994) Distribution of anchovy eggs and larvae (*Engraulis encrasicolus* Cuv.) in the Black Sea in 1991-1992. *ICES Journal of Marine Science* **51**: 395-406.
- Nieuwenhuize, J., Maas, Y.E.M. and Middelburg, J.J. (1994) Rapid analysis of organic carbon and nitrogen in particulate materials. *Marine Chemistry* **45**: 217-224.
- Nieuwenhuize, J., Poley-Vos, C.H., Van Den Akker, A.H. and Van Delft, W. (1991) Comparison of microwave and conventional extraction techniques for the determination of metals in soil, sediment and sludge samples by atomic spectrometry. *Analyst* **116**: 347-351.
- Oguz, T. and Malanotte-Rizzoli, P. (1996) Seasonal variability of wind and thermohaline-driven circulation in the Black Sea: modeling studies. *Journal of Geophysical Research* **101**: 16,551-16,569.
- Pamatmat, M.M. (1971) Oxygen consumption by the seabed. IV. Shipboard and laboratory experiments. *Limnology and Oceanography* **16**: 536-550.
- Parsons, T.R., Maita, Y. and Lalli, C.M. (1984) *A manual of chemical and biological methods for seawater*. Oxford, Pergamon Press Ltd, 173 p.
- Passier, H., Middelburg, J.J., De Lange, G.J. and Böttcher, M.E. (1999) Modes of sapropel formation in the eastern Mediterranean: some constraints based on pyrite properties. *Marine Geology* **153**: 199-219.
- Passier, H., Middelburg, J.J., Van Os, B.J.H. and De Lange, G.J. (1996) Diagenetic pyritisation under eastern Mediterranean sapropels caused by downward sulphide diffusion. *Geochimica et Cosmochimica Acta* **60**: 751-763.

- Pearson, T.H. and Rosenberg, R. (1978) Macrobenthic succession in relation to organic enrichment and pollution of the marine environment. *Oceanography and Marine Biology: an Annual Review* **16**: 229-311.
- Peet, R.K. (1974) The measurement of species diversity. *Annual Review of Ecology and Systematics* **5** : 285-397.
- Phillips, E.J.P. and Lovley, D.R. (1987) Determination of Fe(III) and Fe(II) in oxalate extracts of sediment. *Soil Science Society of America Journal* **51**: 938-941.
- Piepenburg, D., Blackburn, T.H., Von Dorrien, C.F., Gutt, J., Hall, P.O.J., Hulth, S., Kendall, M.A., Opalinski, K.W., Rachor, E. and Schmid, M.K. (1995) Partitioning of benthic community respiration in the Arctic (Northwestern Barents Sea). *Marine Ecology Progress Series* **118**: 199-213.
- Popa, A. (1993) Liquid and sediment inputs of the Danube river into the north-western Black Sea. *Mitteilungen aus dem Geologisch-Paleontologischen Institut der Universität Hamburg* **74**: 137-149.
- Porumb, F. (1992) On the development of *Noctiluca scintillans* under eutrophication of Romanian Black Sea waters. In: Vollenweider, R.A. (Ed.), *Science of the Total Environment*. Amsterdam, Elsevier Sci. Publ. pp. 907-920.
- Press, W.H., Teukolsky, S.A., Vetterling, W.T. and Flannery, B.P. (1994) *Numerical Recipes in FORTRAN: The Art of Scientific Computing*. Cambridge, University Press, 963 p.
- Price, F.T. and Shieh, Y.N. (1979) Fractionation of sulfur isotopes during laboratory synthesis of pyrite at low temperatures. *Chemical Geology* **27**: 245-253.
- Rabouille, C. and Gaillard, J.F. (1991a) A coupled model representing the deep-sea organic carbon mineralization and oxygen consumption in surficial sediments. *Journal of Geophysical Research* **96**: 2761-2776.
- Rabouille, C. and Gaillard, J.F. (1991b) Towards the EDGE: Early diagenetic global explanation. A model depicting the early diagenesis of organic matter, O<sub>2</sub>, NO<sub>3</sub>, Mn, and PO<sub>4</sub>. *Geochimica et Cosmochimica Acta* **55**: 2511-2525.
- Raiswell, R. (1997) A geochemical framework for the application of stable sulfur isotopes to fossil pyritization. *Journal of the Geological Society, London* **154**: 343-357.
- Raiswell, R. and Berner, R.A. (1985) Pyrite formation in euxinic and semi-euxinic sediments. *American Journal of Science* **285**: 710-724.
- Raiswell, R., Buckley, F., Berner, R.A. and Anderson, T.F. (1988) Degree of pyritization of iron as a paleoenvironmental indicator of bottom-water oxygenation. *Journal of Sedimentary Petrology* **58**: 812-819.
- Raiswell, R. and Canfield, D.E. (1998) Sources of iron for pyrite formation in marine sediments. *American Journal of Science* **298**: 219-245.
- Raiswell, R., Canfield, D.E. and Berner, R.A. (1994) A comparison of iron extraction methods for the determination of degree of pyritisation and the recognition of iron-limited pyrite formation. *Chemical Geology* **111**: 101-110.
- Reimers, C.E., Jahnke, R.A. and McCorkle, D.C. (1992) Carbon fluxes and burial rates over the continental slope and rise off central California with implications for the global carbon cycle. *Global Biogeochemical Cycles* **6**: 199-224.
- Revsbech, N.P., Sørensen, J., Blackburn, T.H. and Lomholt, J.P. (1980a) distribution of oxygen in marine sediments measured with microelectrodes. *Limnology and Oceanography* **25** : 403-411.
- Revsbech, N.P., Jørgensen, B.B. and Blackburn, T.H. (1980b) Oxygen in the sea bottom measured with a microelectrode. *Science* **207**: 1355-1356.
- Rhoads, D.C., Boesch, D.K., Zhican, T., Fengshan, X., Liqiang, H. and Nilsen, K.J. (1985) Macrobenthos and sedimentary facies on the Changjiang delta platform and adjacent continental shelf, East China Sea. *Continental Shelf Research* **4**: 189-213.

- Rice, D.L. and Tenore, K.R. (1981) Dynamics of carbon and nitrogen during the decomposition of detritus derived from estuarine macrophytes. *Estuarine, Coastal and Shelf Science* **13**: 681-690.
- Rickard, D.T. (1975) Kinetics and mechanism of pyrite formation at low temperatures. *American Journal of Science* **275**: 636-652.
- Rickard, D.T. (1995) Kinetics of FeS precipitation: Part 1. Competing reaction mechanisms. *Geochimica et Cosmochimica Acta* **59**: 4367-4379.
- Rickard, D.T. (1997a) Kinetics of pyrite formation by the H<sub>2</sub>S oxidation of iron (II) monosulfide in aqueous solutions between 25 and 125°C: The mechanism. *Geochimica et Cosmochimica Acta* **61**: 135-147.
- Rickard, D.T. (1997b) Kinetics of pyrite formation by the H<sub>2</sub>S oxidation of iron (II) monosulfide in aqueous solutions between 25 and 125°C: The rate equation. *Geochimica et Cosmochimica Acta* **61**: 115-134.
- Rosenberg, R. (1995) Benthic marine fauna structured by hydrodynamic processes and food availability. *Netherlands Journal of Sea Research* **34**: 303-317.
- Rowe, G.T., Sibuet, M., Deming, J., Khripounoff, A., Tietjen, J., Macko, S. and Theroux, R. (1991) 'Total' sediment biomass and preliminary estimates of organic carbon residence time in deep-sea benthos. *Marine Ecology Progress Series* **79**: 99-114.
- Rowe, G.T. (1983) Biomass and production of deep-sea macrobenthos. In: Rowe, G.T. (Ed.), *Deep-sea biology*. New York, John Wiley & Sons. pp. 97-121.
- Rowe, G.T., Boland, G.S., Escobar, B., Cruz-Kaegi, M.E., Newton, A., Piepenburg, D., Walsh, I. and Deming, J. (1997) Sediment community biomass and respiration in the Northeast Water Polynya, Greenland: a numerical simulation of benthic lander and spade core data. *Journal of Marine Systems* **10**: 497-515.
- Rumohr, H., Brey, T. and Ankar, S. (1987) *A compilation of biometric conversion factors for benthic invertebrates of the Baltic Sea*. Stockholm, Askö Laboratory, 56 p.
- Ryan, W.B.F., Pittman, I.I.I., Major, C.O., Shimkus, K., Moskalenko, V., Jones, G.A., Dimitrov, P., Gorür, N., Sakinç, M. and Yüce, H. (1997) An abrupt drowning of the Black Sea shelf. *Marine Geology* **138**: 119-126.
- Saager, P.M., De Baar, H.J.W. and Burkill, P.H. (1989) Manganese and iron in Indian Ocean waters. *Geochimica et Cosmochimica Acta* **53**: 2259-2267.
- Sapozhnikov, V.V. (1992) Biohydrochemical causes of the changes of Black Sea ecosystem and its present condition. *Geo Journal* **27**: 149-157.
- Schoeman, V., De Baar, H.J.W., De Jong, J.T.M. and Lancelot, C. (1998) Effects of phytoplankton blooms on the cycling of manganese and iron in coastal waters. *Limnology and Oceanography* **43**: 1427-1441.
- Shaffer, G. (1986) Phosphate pumps and shuttles in the Black Sea. *Nature* **321**: 515-517.
- Sinninghe, D. and De Leeuw, J.W. (1990) Analysis, structure and geochemical significance of organically-bound sulphur in the geosphere: state of the art and future research. *Organic Geochemistry* **16**: 1077-1101.
- Slomp, C.P., Malschaert, J.F.P., Lohse, L. and Van Raaphorst, W. (1997) Iron and manganese cycling in different sedimentary environments on the North Sea continental margin. *Continental Shelf Research* **17**: 1083-1117.
- Smith, C.R., Pope, R.H., DeMaster, D.J. and Magaard, L. (1993) Age-dependent mixing of deep-sea sediments. *Geochimica et Cosmochimica Acta* **57**: 1473-1488.
- Smith, K.L. (1978) Benthic community respiration in the N.W. Atlantic Ocean: *in situ* measurements from 40 to 5200 m. *Marine Biology* **47**: 337-347.
- Smith, K.L. (1987) Food energy supply and demand: A discrepancy between particulate organic carbon flux and sediment community oxygen consumption in the deep ocean. *Limnology and Oceanography* **32**: 201-220.

- Snelgrove, P.V.R. and Butman, C.A. (1994) Animal-sediment relationships revisited: Cause versus effect. *Oceanography and Marine Biology: an Annual Review* **32**: 111-177.
- Soetaert, K., Heip, C.H.R. and Vincx, M. (1991) Diversity of nematode assemblages along a Mediterranean deep-sea transect. *Marine Ecology Progress Series* **75**: 275-282.
- Soetaert, K. and Herman, P.M.J. (1995) Carbon flows in the Westerschelde estuary (The Netherlands) evaluated by means of an ecosystem model (MOSES). *Hydrobiologia* **311**: 247-266.
- Soetaert, K., Herman, P.M.J. and Middelburg, J.J. (1996a) A model of early diagenetic processes from the shelf to abyssal depths. *Geochimica et Cosmochimica Acta* **60**: 1019-1040.
- Soetaert, K., Herman, P.M.J. and Middelburg, J.J. (1996b) Dynamic response of deep-sea sediments to seasonal variations: A model. *Limnology and Oceanography* **41**: 1651-1668.
- Soetaert, K., Herman, P.M.J., Middelburg, J.J. and Heip, C.H.R. (1998) Assessing organic matter mineralization, degradability and mixing rate in an ocean margin sediment (Northeast Atlantic) by diagenetic modeling. *Journal of Marine Research* **56**: 519-534.
- Soetaert, K., Herman, P.M.J., Middelburg, J.J., Heip, C.H.R., Stigter, H.S.D., Van Weering, T.C.E., Epping, E.H.G. and Helder, W. (1996c) Modeling  $^{210}\text{Pb}$ -derived mixing activity in ocean margin sediments: Diffusive versus nonlocal mixing. *Journal of Marine Research* **54**: 1207-1227.
- Soetaert, K., Middelburg, J.J., Herman, P.M.J. and Buijs, K. (2000) On the coupling of benthic and pelagic biogeochemical models. *Earth-Science Reviews* **51**: 173-201.
- Soetaert, K., Vanaverbeke, J., Heip, C.H.R., Herman, P.M.J., Middelburg, J.J., Sandee, A.J.J. and Duineveld, G.C.A. (1997) Nematode distribution in ocean margin sediments of the Goban Spur (northeast Atlantic) in relation to sediment geochemistry. *Deep-Sea Research* **44**: 9-10.
- Sokal, R.S. and Rohlf, F.J. (1995) *Biometry. The principles and practice of statistics in biological research*. New York, Freeman, 887 p.
- Sorokin, Y.I. (1983) The Black Sea. In: Ketchum, B.H. (Ed.), *Estuaries and enclosed seas*. New York, Elsevier. pp. 253-292.
- Stanev, E. (1990) On the mechanisms of the Black Sea circulation. *Earth-Science Reviews* **28**: 285-319.
- Steeffel, C.I. and MacQuarrie, K.T.B. (1996) Approaches to modeling of reactive transport in porous media. In: Lichtener, P.C., et al. (Eds.), *Reactive Transport in Porous Media*. Washington, The Mineralogical Society of America. pp. 83-129.
- Stookey, L.L. (1970) Ferrozine - A new spectrophotometric reagent for iron. *Analytical Chemistry* **42**: 779-781.
- Suess, E. (1980) Particulate organic carbon flux in the oceans - surface productivity and oxygen utilization. *Nature* **288**: 260-263.
- Suits, N.L. and Wilkin, R.T. (1998) Pyrite formation in the water column and sediments of a meromictic lake. *Geology* **26**: 1099-1102.
- Sun, M.Y., Aller, R.C. and Lee, C. (1991) Early diagenesis of chlorophyll-*a* in Long Island Sound sediments: A measure of carbon flux and particle reworking. *Journal of Marine Research* **49**: 379-401.
- Sun, M.Y., Aller, R.C. and Lee, C. (1994) Spatial and temporal distributions of sedimentary chloropigments as indicators of benthic processes in Long Island Sound. *Journal of Marine Research* **52**: 176.
- Sun, M.Y., Lee, C. and Aller, R.C. (1993) Laboratory studies of oxic and anoxic degradation of chlorophyll-*a* in Long Island Sound. *Geochimica et Cosmochimica Acta* **57**: 147-157.
- Sweeney, R.E. and Kaplan, I.R. (1980) Stable isotope composition of dissolved sulfate and hydrogen sulfide in the Black Sea. *Marine Chemistry* **9**: 145-152.
- Tahey, T.M., Duineveld, G.C.A., Berghuis, E.M. and Helder, W. (1994) Relation between sediment-water fluxes of oxygen and silicate and faunal abundance at continental shelf, slope and deep-water stations in the Northwest Mediterranean. *Marine Ecology Progress Series* **104**: 119-130.



- Tahey, T.M., Duineveld, G.C.A., De Wilde, P.A.W.J., Berghuis, E.M. and Kok, A. (1996) Sediment O<sub>2</sub> demand, density and biomass of the benthos and phytopigments along the northwestern Adriatic coast: The extent of Po enrichment. *Oceanologica Acta* **19**: 117-130.
- Teague, K.G., Madden, C.J. and Day, J.W. (1988) Sediment-water oxygen and nutrient fluxes in a river-dominated estuary. *Estuaries* **11**: 1-9.
- Ter Braak, C.J.F. (1988) *CANOCO - a FORTRAN program for canonical community ordination by (partial) (detrended) (canonical) correspondence analysis, principal components analysis and redundancy analysis (version 2.1)*. Wageningen, Agricultural Mathematics Group
- Ter Braak, C.J.F. (1990) *Update notes: CANOCO version 3.10*. Wageningen, Agricultural Mathematics Group
- Thamdrup, B. and Canfield, D.E. (1996) Pathways of carbon oxidation in continental margin sediments off central Chile. *Limnology and Oceanography* **41**: 1629-1650.
- Therkildsen, M.S. and Lomstein, B.A. (1993) Seasonal variation in net benthic C-mineralization in a shallow estuary. *FEMS Microbiology Ecology* **12**: 131-142.
- Thornton, S.F. and McManus, J. (1994) Application of organic carbon and nitrogen stable isotope and C/N ratios as source indicators of organic matter provenance in estuarine systems: evidence from the Tay Estuary, Scotland. *Estuarine, Coastal and Shelf Science* **38**: 219-233.
- Tolmazin, D. (1985b) Changing coastal oceanography of the Black Sea. I: northwestern shelf. *Progress in Oceanography* **15**: 217-276.
- Tolmazin, D. (1985a) Economic impact on the riverine-estuarine environment of the USSR: the Black Sea basin. *Geo Journal* **11**: 137-152.
- Ullman, W.J. and Aller, R.C. (1982) Diffusion coefficients in nearshore marine sediments. *Limnology and Oceanography* **27**: 552-556.
- Van Cappellen, P., Gaillard, J.F. and Rabouille, C. (1993) Biogeochemical transformations in sediments: Kinetic models of early diagenesis. In: Wollast, R., et al. (Eds.), *Interactions of C, N, P and S Biogeochemical Cycles and Global Change*. Berlin, Springer-Verlag. pp. 401-445.
- Van Cappellen, P. and Wang, Y. (1995) Metal cycling in surface sediments: Modeling the interplay of transport and reaction. In: Allen, H.E. (Ed.), *Metal Contaminated Sediments*. Chelsea, MI, Ann Arbor Press. pp. 21-64.
- Van Cappellen, P. and Wang, Y. (1996) Cycling of iron and manganese in surface sediments: A general theory for the coupled transport and reaction of carbon, oxygen, nitrogen, sulfur, iron and manganese. *American Journal of Science* **296**: 197-243.
- Van Eeckhout, D. and Lancelot, C. (1997) Modelling the functioning of the North-western Black Sea ecosystem from 1960 to present. In: Özsoy, E., et al. (Eds.), *Sensitivity of North Sea, Baltic Sea and Black Sea to Anthropogenic and Climate changes*. pp. 455-468.
- Vaynshteyn, M.B., Tokarev, V.G., Shakola, V.A., Lein, A.Y. and Ivanov, M.V. (1986) The geochemical activity of sulfate-reducing bacteria in sediments in the western part of the Black Sea. *Geochemistry International* **23**: 110-122.
- Wang, Y. and Van Cappellen, P. (1996) A multicomponent reactive transport model of early diagenesis: Application to redox cycling in coastal marine sediments. *Geochimica et Cosmochimica Acta* **60**: 2993-3014.
- Warren, F. and Kamykowski, D. (1984) Benthic nutrient regeneration in South Texas coastal waters. *Estuarine, Coastal and Shelf Science* **18**: 221-230.
- Wells, R.M.G. (1980) *Invertebrate respiration*. London, Edward Arnold, 72 p.
- Weston, D.P. (1990) Quantitative examination of macrobenthic community changes along an organic enrichment gradient. *Marine Ecology Progress Series* **61**: 233-244.
- Westrich, J.T. and Berner, R.A. (1984) The role of sedimentary organic matter in bacterial sulfate reduction: The G model tested. *Limnology and Oceanography* **29**: 236-249.

- Wijsman, J.W.M., Herman, P.M.J. and Gomoiu, M.T. (1999) Spatial distribution in sediment characteristics and benthic activity on the northwestern Black Sea shelf. *Marine Ecology Progress Series* **181**: 25-39.
- Wilke, C.R. and Chang, P. (1955) Correlation of diffusion coefficients in dilute solutions. *American Institute of Chemical Engineers Journal* **1**: 264-270.
- Wilkin, R.T., Arthur, M.A. and Dean, W.E. (1997) History of water-column anoxia in the Black Sea indicated by pyrite framboid size distributions. *Earth and Planetary Science Letters* **148**: 517-525.
- Wollast, R. (1998) Evaluation and comparison of the global cycle in the coastal zone and in the open ocean. In: Brink, K.H., et al. (Eds.), *The Sea*. New York, John Wiley & Sons. pp. 213-252.
- Zaitsev, Y.P. (1993) Impacts of eutrophication on the Black Sea fauna. In: *Fisheries Council for the Mediterranean. Studies and Reviews* Rome, FAO. pp. 63-86.
- Zaitsev, Y.P. and Mamaev, V. (1997) *Biological Diversity in the Black Sea: A Study of Change and Decline*. New York, United Nations Publications, 208 p.
- Zhabina, N.N. and Volkov, I.I. (1978) A method of determination of various sulfur compounds in sea sediments and rocks. In: Krumbein, W.E. (Ed.), *Methods, Metals and Assessment*. MI, Ann Arbor Sci. Publ. pp. 735-746.
- Zhang, J.-Z. and Millero, F.J. (1993) The products from the oxidation of H<sub>2</sub>S in seawater. *Geochimica et Cosmochimica Acta* **57**: 1705-1718.
- Ziebis, W., Huettel, M. and Forster, S. (1996) Impact of biogenic sediment topography on oxygen fluxes in permeable seabeds. *Marine Ecology Progress Series* **140**: 227-237.

# Curriculum Vitae

Jeroen Wijsman was born on December 17, 1967 in Zierikzee, the Netherlands. He followed the secondary school (H.A.V.O. followed by V.W.O.) at the R.S.G. “Professor Zeeman” in Zierikzee, where he graduated in 1987. In the same year he started his study Biology, orientation Population/Ecosystems at the Wageningen Agricultural University (WAU). As part of this study he conducted research projects at the departments of Theoretical Production Ecology and Fish Culture and Fisheries of the WAU. His practical period was fulfilled in Sri Lanka, where he joined a project in fisheries management. From 1994 to 1999 he worked as a Ph.D. student at the Netherlands Institute of Ecology, Centre for Estuarine and Coastal Ecology in Yerseke, on the research that is presented in this thesis. Jeroen is presently working as a marine ecologist at WL | Delft Hydraulics.

## List of publications

- Friedrich, J., Dinkel, C., Friedl, G., Pimenov, N.V., Wijsman, J.W.M., Gomoiu, M.T., Cociasu, A.M., Popa, A. and Wehrli, B. Benthic nutrient cycling and diagenetic pathways in the northwestern Black Sea. *Estuarine, Coastal and Shelf Science*, in press.
- Pet, J.S., Wijsman, J.W.M., Mous, P.J. and Machiels, M.A.M. (1995) Characteristics of a Sri Lankan reservoir fishery and consequences for the estimation of annual yield. *Fisheries Research* **24**: 9-33.
- Soetaert, K., Wijsman, J.W.M., Middelburg, J.J. Herman, P.M.J. and Heip, C.H.R. Ocean margin early diagenetic processes and models. Background paper for Hanse workshop ocean margin systems, Belmenhorst, 13-23 November 2000.
- Wijsman, J.W.M., Herman, P.M.J. and Gomoiu, M.T. (1999) Spatial distribution in sediment characteristics and benthic activity on the northwestern Black Sea shelf. *Marine Ecology Progress Series* **181**: 25-39.
- Wijsman, J.W.M., Herman, P.M.J., Middelburg, J.J. and Soetaert, K. A model for early diagenetic processes in sediments of the continental shelf of the Black Sea. *Estuarine, Coastal and Shelf Science*, in press.
- Wijsman, J.W.M., Middelburg, J.J. and Heip, C.H.R. Reactive iron in Black Sea sediments: implications for iron cycling. *Marine Geology*, in press.
- Wijsman, J.W.M., Middelburg, J.J., Herman, P.M.J., Böttcher, M.E. and Heip, C.H.R. Sulfur and iron cycling in sediments along the northwestern margin of the Black Sea. Submitted for publication to *Marine Chemistry*.
- Wijsman, J.W.M., Middelburg, J.J., Soetaert, K. and Herman, P.M.J. Benthic mineralization in marine environments. Manuscript in preparation.